



**UNIWERSYTET MARIII CURIE-SKŁODOWSKIEJ
W LUBLINIE**

Wydział Chemii

Instytut Nauk Chemicznych

mgr Magdalena Szaniawska

**BADANIE WŁAŚCIWOŚCI ADSORPCYJNYCH
I OBJĘTOŚCIOWYCH NIEJONOWYCH
SURFAKTANTÓW TYPU KOLLIPHOR I ICH
MIESZANIN Z BERBERYNA**

Rozprawa doktorska
wykonana w Katedrze Zjawisk Międzyfazowych
pod kierunkiem dr hab. Katarzyny Szymczyk, prof. UMCS

Lublin 2023

*„Trzeba mieć wytrwałość i wiarę w siebie. Trzeba wierzyć,
że człowiek jest do czegoś zdolny
i osiągnąć to za wszelką cenę.”*

Maria Skłodowska-Curie

Składam podziękowania

Pani Promotor dr hab. Katarzynie Szymczyk, prof. UMCS
za cenne uwagi, pomoc w przygotowaniu rozprawy doktorskiej,
poświęcony czas oraz wyrozumiałość.

Dziękuję mojej Siostrze Sylwii oraz Przyjaciołom
za wiarę w moje możliwości nawet wtedy, gdy sama w nie wątpiłam.

Bez Nich nie osiągnęłabym tego.

*Pamięci Moich Rodziców
Janiny i Arkadiusza*

SPIS TREŚCI

1. STRESZCZENIE.....	5
2. STRESZCZENIE W JĘZYKU ANGIELSKIM	6
3. WYKAZ PUBLIKACJI NAUKOWYCH STANOWIĄCYCH PODSTAWĘ POSTĘPOWANIA DOKTORSKIEGO	7
4. WYKAZ STOSOWANYCH SYMBOLI	9
5. WPROWADZENIE I CEL ROZPRAWY DOKTORSKIEJ.....	11
6. OMÓWIENIE WYNIKÓW.....	19
6.1. Właściwości fizykochemiczne ELP, RH40 i Ber.....	19
6.2. Właściwości adsorpcyjne i objętościowe dwuskładnikowych mieszanin ELP+RH40.....	23
6.3. Właściwości adsorpcyjne i objętościowe ELP + Ber, RH40 + Ber i ELP + RH40 + Ber.....	27
7. WNIOSKI.....	35
8. LITERATURA.....	37
9. PODSUMOWANIE DOROBKU NAUKOWEGO.....	48
9.1. Publikacje naukowe.....	48
9.2. Konferencje naukowe.....	51
9.3. Projekty badawcze, konkursy.....	58
9.4. Aktywność organizacyjna i członkostwo naukowe.....	59
9.5. Nagrody i wyróżnienia.....	60
10. ZAŁĄCZNIKI.....	61

1. STRESZCZENIE

Tematyka rozprawy doktorskiej obejmuje badanie właściwości adsorpcyjnych i objętościowych dwóch surfaktantów niejonowych z grupy Kolliphor: Kolliphoru ELP (ELP) i Kolliphoru RH40 (RH40), a także ich dwuskładnikowych mieszanin o różnym ułamku molowym w środowisku wodnym bez i w obecności naturalnego alkaloidu berberyny (Ber) w szerokim zakresie stężenia surfaktantów i różnych temperaturach. Zastosowany do badań alkaloid, berberyna, to substancja, która od wielu lat cieszy się zainteresowaniem naukowym ze względu na swoją bardzo szeroką aktywność biologiczną. Jednym z głównych problemów związanych z jej zastosowaniem jest słaba rozpuszczalność w wodzie, a więc także biodostępność. W związku z tym poszukuje się sposobów zwiększenia biodostępności berberyny np. przy użyciu surfaktantów.

W przedstawionej rozprawie doktorskiej za pomocą pomiarów kąta zwilżania ELP i RH40 na powierzchni modelowych ciał stałych oraz kątów zwilżania wody, formamidu i dijdometanu na sprasowanej berberynie wyznaczono składowe i parametry napięcia powierzchniowego ELP, RH40 i Ber oraz przeanalizowano je w aspekcie adsorpcji na granicy faz woda-powietrze. Następnie określono właściwości adsorpcyjne i objętościowe dwuskładnikowych mieszanin ELP i RH40 o ułamku molowym w fazie objętościowej α równym 0,2; 0,4; 0,6; i 0,8 celem wyboru do dalszych badań z Ber mieszaniny surfaktantów, dla której istnieje efekt synergetyczny w redukcji napięcia powierzchniowego i procesie tworzenia micel. Kończącym etapem badań była ścisła charakterystyka fizykochemiczna mieszanin Ber z ELP, RH40, a także ELP+RH40 o ułamku molowym ELP w fazie objętościowej równym 0,8 w szerokim zakresie stężeń surfaktantów ($1 \cdot 10^{-6}$ - $1 \cdot 10^{-2}$ mol/dm³) i temperatur (293-313 K). Na podstawie otrzymanych wyników określono zachowanie się berberyny w środowisku wodnym bez i w obecności surfaktantów. Stan równowagi pomiędzy roztworem monomerycznym a micelarnym surfaktantów, ich dwuskładnikowych mieszanin, a także mieszanin z Ber poddano ścisłej analizie termodynamicznej w oparciu o otrzymane rezultaty.

2. STRESZCZENIE W JĘZYKU ANGIELSKIM

The subject of the doctoral dissertation includes the study of adsorption and volumetric properties of two nonionic surfactants from the Kolliphor group: Kolliphor ELP (ELP) and Kolliphor RH40 (RH40), as well as their binary mixtures with different mole fractions in aqueous environment without and with the presence of natural alkaloid - berberine (Ber) in a wide range of surfactant concentrations and different temperatures. The alkaloid used for research, berberine, is a substance that has been of scientific interest for many years due to its very broad biological activity. One of the main problems associated with its use is poor solubility in water, and thus also bioavailability. Therefore, ways to increase the bioavailability of berberine are sought, e.g. using surfactants.

In the presented doctoral dissertation, using the measurements of the contact angle ELP and RH40 on the surface of model solids and the contact angles of water, formamide and diiodomethane on compressed berberine, the components and parameters of the surface tension of ELP, RH40 and Ber were determined and analyzed in terms of adsorption at the interface between water and air. Then, the adsorption and volumetric properties of binary mixtures of ELP and RH40 with a mole fraction in the volumetric phase equal to 0.2; 0.4; 0.6 and 0.8 were determined in order to select a mixture of surfactants for further research with Ber, for which there is a synergistic effect in the reduction of surface tension and the process of micelle formation. The final stage of the research was the direct physicochemical characterization of mixtures of Ber with ELP, RH40, and ELP + RH40, where the ELP mole fraction in the volumetric phase was equal to 0.8, in a wide range of surfactant concentrations ($1 \cdot 10^{-6}$ – $1 \cdot 10^{-2}$ mol/dm³) and temperatures (293-313 K). Based on the obtained results, the behavior of berberine in the aqueous environment without and in the presence of surfactants was determined. The equilibrium state between the monomeric and micellar solutions of surfactants, their binary mixtures, as well as mixtures with Ber subjected to thermodynamic analysis based on the obtained results.

3. WYKAZ PUBLIKACJI NAUKOWYCH STANOWIĄCYCH PODSTAWĘ POSTĘPOWANIA DOKTORSKIEGO

Cykl powiązanych tematycznie **4 artykułów naukowych** wchodzących w skład rozprawy doktorskiej, opublikowanych w latach 2019-2023 w recenzowanych czasopismach naukowych, znajdujących się w aktualnym wykazie czasopism sporządzonym zgodnie z przepisami wydanymi na podstawie art. 267 ust. 2 pkt 2 Ustawy z dnia 20 lipca 2018 roku – Prawo o szkolnictwie wyższym i nauce (Dz. U. z 2018 poz. 1668 z późn. zm.), oznaczono numerami **D1, D2, D3, D4**. Symbolami **SM2, SM3 i SM4** oznaczono materiał uzupełniający (ang. *Supplementary Material*) do oryginalnych artykułów naukowych. Dodatkowo umieszczono informacje naukometryczne: wskaźnik wpływu (ang. *Impact Factor, IF*) publikacji zgodnie z rokiem opublikowania i na przestrzeni ostatnich pięciu lat (IF_{5-letni}) oraz punktację wg Ministerstwa Edukacji i Nauki (MEiN). Prowadzenie korespondencji z Redakcją Czasopisma oznaczono symbolem „*”.

Dysertacja ma formę zbioru spójnie powiązanych tematycznie następujących oryginalnych artykułów naukowych:

[D1] K. Szymczyk, **M. Szaniawska**, K. Terpiłowski*, Determination of acoustical parameters of aqueous solution of Kolliphors binary mixtures using density, speed of sound, viscosity and surface tension measurements, *Journal of Surfactants and Detergents*, 2019, 22(5), 1163–1174

IF₂₀₁₉/IF_{5-letni}: 1,654/1,822

MEiN₂₀₂₃: 40 pkt/40pkt

Mój wkład w powstanie tej pracy polegał na tworzeniu koncepcji artykułu, zaplanowaniu badań, wyborze technik badawczych, wykonaniu wszystkich badań eksperymentalnych i ich wizualizacji, analizie i interpretacji otrzymanych danych i ich przygotowaniu do publikacji, wykonaniu części obliczeń, przygotowaniu wstępnej wersji publikacji.

[D2] K. Szymczyk*, **M. Szaniawska**, J. Krawczyk, Temperature effect on the adsorption and volumetric properties of aqueous solutions of Kolliphor ELP®, *Molecules*, 2020, 25(3), 743

IF₂₀₂₀/IF_{5-letni}: 4,411/5,110

MEiN₂₀₂₃: 140 pkt/140 pkt

Mój wkład w powstanie tej pracy polegał na tworzeniu koncepcji artykułu, zaplanowaniu badań, wyborze technik badawczych, wykonaniu wszystkich badań eksperymentalnych i ich wizualizacji, analizie i interpretacji otrzymanych danych i ich przygotowaniu do publikacji, wykonaniu części obliczeń, przygotowaniu wstępnej wersji publikacji.

[D3] M. Szaniawska, K. Szymczyk, A. Zdziennicka, B. Jańczuk*, Adsorption properties and composition of binary Kolliphor mixtures at the air-water interface at different temperatures, *Molecules*, 2022, 27(3), 877

IF₂₀₂₂/IF_{5-letni}: 4,927/5,110

MEiN₂₀₂₃: 140 pkt/140 pkt

Mój wkład w powstanie tej pracy polegał na tworzeniu koncepcji artykułu, zaplanowaniu badań, wyborze technik badawczych, wykonaniu wszystkich badań eksperymentalnych i ich wizualizacji, analizie i interpretacji otrzymanych danych i ich przygotowaniu do publikacji, wykonaniu części obliczeń, przygotowaniu wstępnej wersji publikacji.

[D4] M. Szaniawska, K. Szymczyk*, A. Zdziennicka, B. Jańczuk, Thermodynamic parameters of berberine with Kolliphor mixtures adsorption and micellization, *Molecules*, 2023, 28(7), 3115

IF₂₀₂₃/IF_{5-letni}: 4,927/5,110

MEiN₂₀₂₃: 140 pkt/140 pkt

Mój wkład w powstanie tej pracy polegał na tworzeniu koncepcji artykułu, zaplanowaniu badań, wyborze technik badawczych, wykonaniu wszystkich badań eksperymentalnych i ich wizualizacji, analizie i interpretacji otrzymanych danych i ich przygotowaniu do publikacji, wykonaniu części obliczeń, przygotowaniu wstępnej wersji publikacji.

Sumaryczna liczba punktów przypisanych czasopismom przez

MEiN₂₀₂₃: 460/ 460pkt

Sumaryczna wartość wskaźnika IF/IF_{5-letni} prac w cyklu: 15,919/17,152

4. WYKAZ STOSOWANYCH SYMBOLI I SKRÓTÓW

ELP	Kolliphor ELP
RH40	Kolliphor RH40
Ber	berberyna
PTFE	politetrafluoroetylen
PMMA	poli(metakrylan metylu)
CMC	krytyczne stężenie micelizacji
γ_{LV}	napięcie powierzchniowe
γ^{LW}	składowa napięcia powierzchniowego wynikająca z oddziaływań Liftshitz-a-van der Waalsa
γ^{AB}	składowa napięcia powierzchniowego wynikająca z oddziaływań kwasowo- zasadowych w ujęciu Lewisa
γ^+	parametr elektronowo - akceptorowy składowej kwasowo - zasadowej napięcia powierzchniowego
γ^-	parametr elektronowo - donorowy składowej kwasowo - zasadowej napięcia powierzchniowego
Γ^{max}	maksymalne nadmiarowe stężenie powierzchniowe Gibbsa
ΔG_{ads}^0	standardowa swobodna energia Gibbsa procesu adsorpcji
β^M	parametr oddziaływań międzycząsteczkowych w mieszanej miceli
Π_{CMC}	różnica między napięciem powierzchniowym rozpuszczalnika i substancji rozpuszczonej w CMC
ΔG_{mic}^0	standardowa swobodna energia Gibbsa procesu micelizacji
ΔG_{min}^S	energia swobodna na granicy faz woda - powietrze
g^M	nadmiarowa energia Gibbsa mieszanej miceli
ε^M	energia wymiany cząsteczek w mieszanej miceli
π_i	ciśnienie wewnętrzne

A_1, A_2, t_1, t_2, y^0	stałe w funkcji wykładniczej stosowanej do opisu izoterm napięcia powierzchniowego
L_f	odległość międzycząsteczkowa
ΔS_{ads}^0	standardowa entropia procesu adsorpcji
ΔH_{ads}^0	standardowa entalpia procesu adsorpcji
γ_{WT}	napięcie międzyfazowe woda – ogon surfaktantu
γ_{WB}	napięcie powierzchniowe woda – Ber
γ_{BT}	napięcie międzyfazowe Ber – ogon surfaktantu
W_a^{BT}	praca adhezji w układzie Ber – woda – ogon surfaktantu
α	ułamek molowy
γ_0	napięcie powierzchniowe rozpuszczalnika
Z	impedancja akustyczna
π	ciśnienie powierzchniowe surfaktantów

5. WPROWADZENIE I CEL ROZPRAWY DOKTORSKIEJ

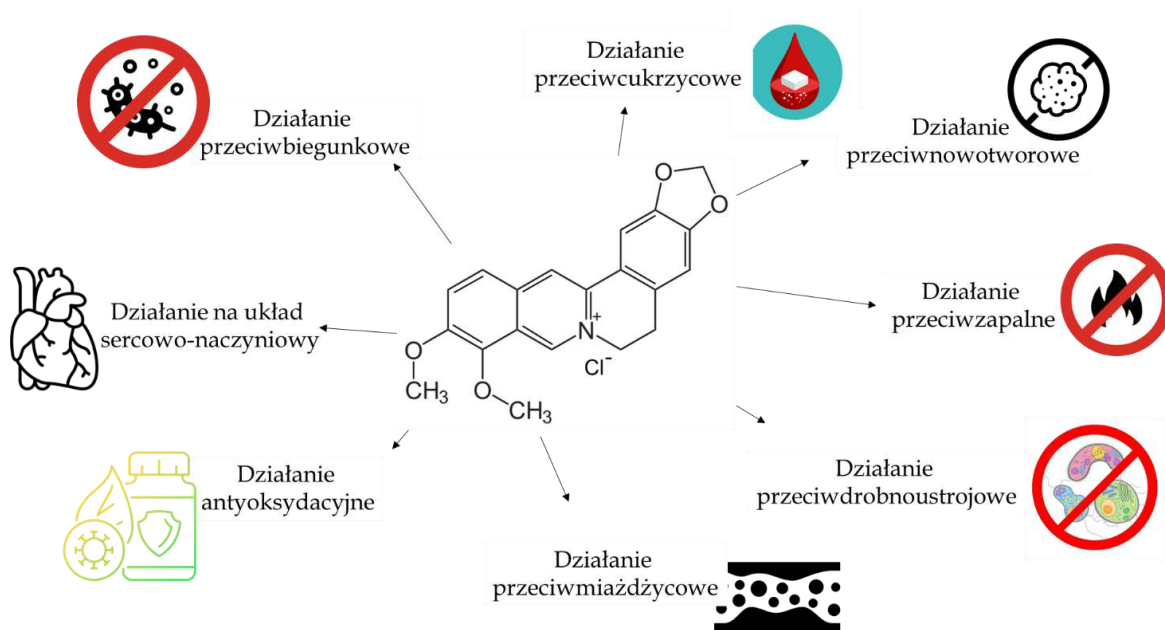
Berberyna (Ber, $C_{20}H_{18}NO_4^+$) ze względu na budowę chemiczną zaliczana jest do grupy alkaloidów, pochodnych izochinoliny. Jest to żółty bezzapachowy proszek o gorzkim smaku [1-4].



Rys. 1 Główne źródła berberyny (opracowanie własne)

Nazwa berberyny wywodzi się od rośliny, z której najczęściej jest otrzymywana. Substancja ta występuje w kłęczach, korzeniach i łodygach roślin stosowanych w tradycyjnej medycynie chińskiej, takich jak berberys zwyczajny (*Berberis vulgaris*), berberys indyjski (*Berberis aristata*) czy cynowód chiński (*Coptis chinensis*) (Rys. 1) [5-8]. Zawartość berberyny w tych roślinach wynosi od 0,05 mg/g do 96,10 mg/g [9,10]. Berberyna wykazuje bardzo szeroką aktywność biologiczną (Rys. 2), a pierwsze wzmianki na temat medycznego wykorzystania berberyny zawartej w *Rhizoma coptidis* sięgają roku 200 [11,12]. W szerokim spektrum jej działania można wyróżnić działanie przeciwcukrzycowe, przeciwnowotworowe, przeciwbiegunkowe, antyoksydacyjne, przeciwzapalne, przeciwwirusowe (m.in. w leczeniu SARS-CoV-2), a także wspomagające układ sercowo - naczyniowy oraz obniżające poziom lipidów [13-24]. Zaletą stosowania berberyny jest także fakt, że

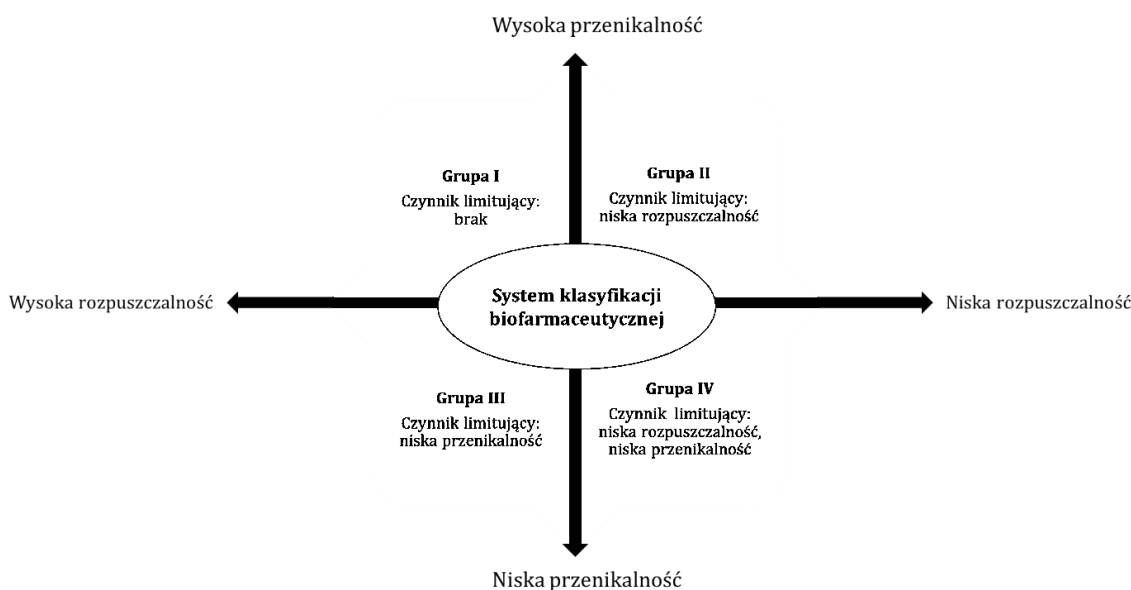
powoduje znikome efekty uboczne i ma niską toksyczność, dzięki czemu może być stosowana jako potencjalny lek [25].



Rys. 2 Aktywność biologiczna berberyny [13-24] (opracowanie własne)

Pomimo szeregu pozytywnych właściwości, stosowanie berberyny jest ograniczone, głównie ze względu na jej niską rozpuszczalność w wodzie ($5,27 \pm 0,29$ i $8,50 \pm 0,40$ mmol/dm³, odpowiednio w temperaturze 298 i 310 K), jak również w buforze fosforanowym o pH=7 ($4,05 \pm 0,09$ i $9,69 \pm 0,37$ mmol/dm³ w tych samych temperaturach) [26-28]. Wynika to głównie z obecności w jej strukturze czwartorzędowego kationu amoniowego, a także ze sztywnej i płaskiej struktury berberyny [29]. Konsekwencją słabej rozpuszczalności berberyny w wodzie jest jej niska biodostępność, np. w pracy Chena i wsp. wynosi ona 0,68 [30], według Liu i wsp. 0,36 [31], podobnie w badaniach Fenga i wsp. – 0,37 [32]. Według danych literaturowych biodostępność berberyny jest mniejsza niż 1% [33-34]. Tak niska wartość tego parametru związana jest głównie z bardzo intensywnym metabolizmem, któremu podlega berberyna w jelicie cienkim i wątrobie [35], jak również wartość $pK_a \approx 15$, co oznacza, że w warunkach fizjologicznych występuje głównie w formie zjonizowanej [36]. Do wad tego związku zaliczyć można także czułość na światło i wysoką temperaturę, które prowadzą do jej degradacji [37]. W systemie klasyfikacji leków berberyna zaliczana jest do III klasy związków (Rys.

3), charakteryzujących się bardzo słabą przenikalnością [38]. System ten klasyfikuje substancje lecznicze pod względem ich właściwości biofarmaceutycznych, tj. przenikalności przez bariery biologiczne i rozpuszczalności. Substancje klasyfikuje się sprawdzając, czy dawka przewidziana rozpuszcza się w 250 cm³ wody (w zakresie pH od 1 do 7,5), a także określając przenikalność tej substancji przez bariery biologiczne (np. warstwę komórek w hodowli *in vitro*) [39].



Rys. 3 System klasyfikacji biofarmaceutycznej (opracowanie własne)

Głównym wyzwaniem w zastosowaniu berberyny jako substancji leczniczej jest więc poprawa jej rozpuszczalności, a co za tym idzie biodostępności za pomocą różnych metod. W literaturze można znaleźć informacje o wykorzystywaniu do tego celu wielu technik, m.in. tworzenia nowych pochodnych berberyny [40], mikro- i nanoemulsji [41,42], stałych lipidowych nanocząstek [43] czy liposomów [44]. Należy mieć na uwadze, że metody te poza zaletami mają także wady i ograniczenia. W metodzie współrozpuszczania stosuje się organiczne, toksyczne rozpuszczalniki, a substancja rozpuszczana może mieć mniejszą stabilność, co w późniejszym etapie po procesie może niekorzystnie wpływać na wchłanianie [45]. Z kolei tworzenie mikroemulsji jest procesem skomplikowanym i trudnym do walidacji. Stosowanie roztworów olejowych może spowodować, że dany preparat nie może być podany dożylnie. W przypadku mikroemulsji efekt terapeutyczny często jest uzależniony od oddziaływań substancji leczniczej ze związkiem

chemicznym tworzącym micidele czy liposomy [46,47]. Tworzenie soli także nie jest metodą odpowiednią dla każdego rodzaju związków [48]. Jedną z wad tworzenia soli jest to, że zastosowanie przeciwjonu o dużej masie cząsteczkowej z lekiem o niskiej aktywności może spowodować, że wymagana jest wyższa dawka. Kolejnym problemem jest tendencja do tworzenia hydratów i odmian polimorficznych. Istnieją również przypadki, w których sole mocnych kwasów lub zasad są dobrze rozpuszczalne w wodzie, będąc jednocześnie bardzo higroskopijne, co prowadzi do niestabilności formulacji [49]. Poszukiwanie prostych i skutecznych metod jest zatem pożądane i w pełni uzasadnione.

Stosunkowo nowym rozwiązaniem jest wykorzystanie związków powierzchniowo czynnych (surfaktantów) do ekstrakcji aktywnych składników pochodzenia roślinnego o wysokim stężeniu [50]. Zastosowanie surfaktantów do poprawy rozpuszczalności w wodzie niektórych substancji jest obecnie przedmiotem badań wielu naukowców np. Krstonošić i wsp. zastosowali Poloxamer 407 i Brij 20 do ekstrakcji kwasu chlorogenowego [51], Giacomo i wsp. użyli Tritonu X-114 oraz Genapolu X-080 do ekstrakcji micelarnej papainy [52], Shestopalova z zespołem zastosowali Triton X-100 w celu poprawy rozpuszczalności azorubiny [53], a Wu i wsp. wykorzystali Span 20 do zwiększenia rozpuszczalności rytonawiru [54]. Rozwiązanie to wydaje się jak najbardziej uzasadnione, gdyż od dawna przemysł spożywczy, kosmetyczny i farmaceutyczny wykorzystuje związki powierzchniowo czynne (surfaktanty) do tworzenia różnych układów np. emulsji lub pian [55]. Surfaktanty są substancjami bardzo często stosowanymi w przemyśle kosmetycznym i farmaceutycznym, ze względu na swoje właściwości [56-58], zdolność gromadzenia się na granicy faz przy bardzo niskich stężeniach oraz wpływ na właściwości powierzchniowe cieczy, w której są rozpuszczone [59]. Są to substancje o budowie asymetrycznej, składają się z części hydrofilowej (jonowej lub niejonowej) oraz hydrofobowej. Po przekroczeniu granicznego stężenia nazywanego krytycznym stężeniem micelizacji (CMC), cząsteczki surfaktantów łączą się w agregaty nazywane micelami. Micidele są wykorzystywane w zastosowaniach biologicznych ze względu na ich unikalne właściwości, takie jak biokompatybilność i zdolność do ochrony leków oraz

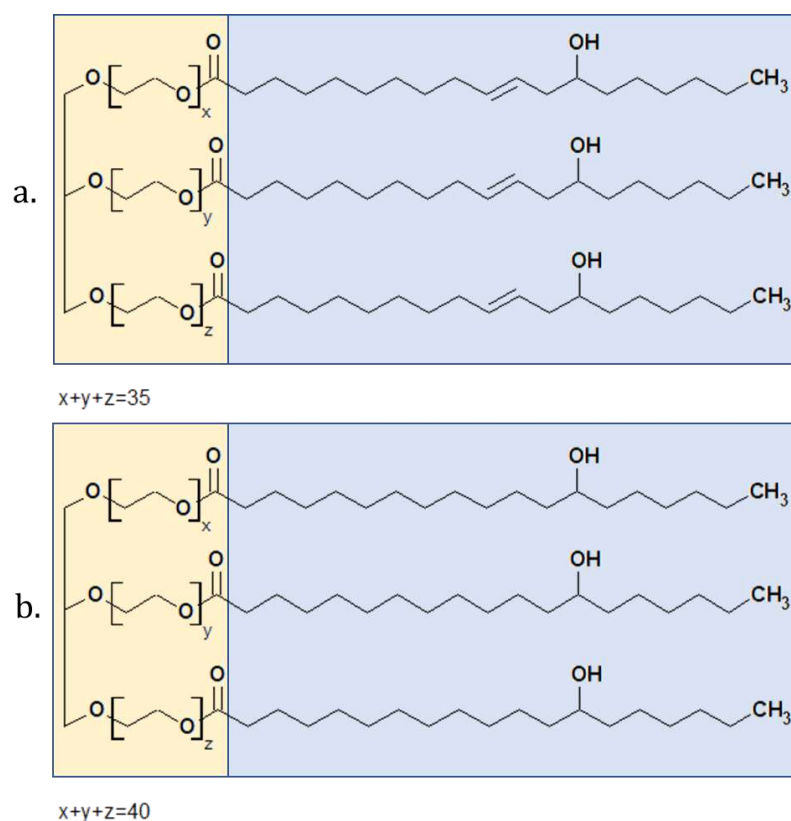
ukierunkowanego ich dostarczania [60]. O ogromną zaletą miceli jest umiejętność do solubilizowania w ich rdzeniu słabo rozpuszczalnych w wodzie lub hydrofobowych leków, co zwiększa ich biodostępność [61].

Surfaktanty mogą być stosowane pojedynczo lub w mieszaninach o różnym ułamku molowym. Od charakteru chemicznego składników zależą oddziaływania poszczególnych składników, a więc synergetyczne i antagonistyczne działanie. Kiedy oddziaływania międzycząsteczkowe są mocniejsze w mieszaninie niż w roztworach pojedynczych składników, zjawisko takie nazywa się synergetyzmem [59,62]. Powszechnie w przemyśle farmaceutycznym i kosmetycznym stosuje się mieszaniny surfaktantów o działaniu synergetycznym, ponieważ są one skuteczne w znacznie niższych stężeniach niż pojedyncze składniki [63]. Efekt taki często jest rozważany w oparciu o teorie roztworów nieidealnych, np. przybliżoną teorię roztworów rzeczywistych (ang. *regular solution approximation*), szczególnie za pomocą parametru oddziaływań międzycząsteczkowych, β^M [64].

W formulacjach farmaceutycznych wykorzystuje się surfaktanty o nazwie handlowej Kolliphor. Ich rola w takich układach związana jest głównie z hamowaniem aktywności P-glikoproteiny, dzięki czemu poprawia się rozpuszczalność substancji, a co za tym idzie wzrasta biodostępność i skuteczność [65]. Są to związki zatwierdzone przez amerykańską Agencję Żywności i Leków (FDA) do doustnego, domięśniowego i dożylnego stosowania w formulacjach farmaceutycznych leków [66].

Najpopularniejszym z tej grupy związków jest Kolliphor ELP (oczyszczona forma Kolliphoru EL, Cremophor ELP, etoksylogowany kwas (R)-12-hydroksy-*cis*-9-oktadekenowy). Surfaktant ten otrzymywany jest w reakcji kwasu (R)-12-hydroksy-*cis*-9-oktadekenowego z tlenkiem etylenu w stosunku molowym 1:35 [94]. Głównym składnikiem tego związku jest rycynooleinian glikolu polietylenowego i glicerolu, który razem z estrami tłuszczowymi glikolu polietylenowego tworzy grupę hydrofobową tego surfaktantu (Rys. 4a).

Kolliphor ELP (ELP) jest stosowany jako środek wspomagający przenikalność i biodostępność wielu leków i substancji biologicznie aktywnych [95,96]. W literaturze znaleźć można wiele prac, w których wykorzystywano ten surfaktant do poprawy biodostępności i rozpuszczalności, m.in. wardenafilu [67], pochodnych artemizyny [68], cyklosporyny [69], diazepam, propofolu [70], paklitakselu [71], symwastatyny [72], czy indirubiny [73]. Jest także składnikiem szczepionek mRNA przeciw COVID-19 firm Pfizer BioNTech i Moderna [74].



Rys. 4 Struktury Kolliphoru ELP (a) i RH40 (b)

Kolejny surfaktant z tej grupy, Kolliphor RH40, (RH40) (Rys. 4b) (uwodorniony kwas (R)-12-hydroksy-*cis*-9-oktadekenowy), jest związkiem chemicznym otrzymywanym w wyniku reakcji 1 mola uwodornionego kwasu (R)-12-hydroksy-*cis*-9-oktadekenowego z 40 molami tlenku etylenu [94]. Kolliphor RH40 wykorzystywany również jest jako solubilizator i środek poprawiający biodostępność substancji [75,76]. Kolliphor RH40 z powodzeniem jest stosowany jako składnik samoemulgujących systemów dostarczania leków (ang. Self-Emulsifying Drug Delivery Systems, SEDDS), m. in. w formulacjach zawierających

skwalen [77] czy sildenafil [78]. Kolliphor RH40 jest stosowany także jako środek poprawiający biodostępność kamptotecyny [79], itrakonazolu [80], karwedilolu [81], czy celekoksybu [82].

Mimo, że w literaturze występuje wiele danych dotyczących surfaktantów typu Kolliphor [83-92], to trudno jednak doszukać się informacji dotyczących ich współdziałania z berberyną. Istnieją badania dotyczące mieszanin berberyny np. z surfaktantami, Brij-S20 [93], SLS czy Tween 80 [26]. Brak jest jednak kompleksowej analizy tego typu układów w szerokim zakresie stężeń i temperatur. Dodatkowo właściwości fizykochemiczne samej berberyny, jak również ELP i RH40 nie zostały dotychczas jednoznacznie zbadane. Zatem z praktycznego i teoretycznego punktu widzenia poznanie właściwości adsorpcyjnych i objętościowych ELP, RH40 i Ber, a także ich mieszanin w środowisku wodnym jest jak najbardziej uzasadnione i stało się celem przedstawionej rozprawy doktorskiej [D1-D4]. W pierwszej kolejności za pomocą pomiarów napięcia powierzchniowego przeprowadzono badania wodnych roztworów Ber ($1 \cdot 10^{-5}$ mol/dm³ - $1 \cdot 10^{-4}$ mol/dm³) w temperaturach 293-313 K oraz ELP i RH40 w szerokim zakresie ich stężenia ($1 \cdot 10^{-6}$ - $1 \cdot 10^{-2}$ mol/dm³) i w różnych temperaturach ($T = 293 - 318$ K). Zmierzono także kąty zwilżania na powierzchni modelowych ciał stałych jakimi są apolarny politetrafluoroetylen (PTFE) oraz monopolarny poli(metakrylan metylu) (PMMA) (293 K). Uzyskane wyniki umożliwiły przeprowadzenie termodynamicznej analizy procesu adsorpcji składników mieszanin na granicy faz woda-powietrze, ale również ciało stałe-woda i ciało stałe-powietrze, ustalenie relacji pomiędzy ich adsorpcją na tych granicach faz oraz określenie składu mieszanych monowarstw adsorpcyjnych. Następnie, stosując dodatkowo pomiary gęstości, lepkości, prędkości dźwięku określono właściwości adsorpcyjne i objętościowe dwuskładnikowych mieszanin ELP i RH40 o ułamku molowym w fazie objętościowej $\alpha = 0,2; 0,4; 0,6; 0,8$ w zakresie stężeń $1 \cdot 10^{-6} - 1 \cdot 10^{-2}$ mol/dm³ i temperaturach 293-318 K celem wyboru do dalszych badań z Ber mieszaniny surfaktantów, dla której istnieje efekt synergetyczny w redukcji napięcia powierzchniowego i procesie tworzenia micel. Zmierzono także kąty zwilżania wody, formamidu i dijdometanu na sprasowanej Ber w celu

wyznaczenia składowych i parametrów napięcia powierzchniowego Ber. Kończącym etapem badań była ścisła charakterystyka fizykochemiczna mieszanin Ber z surfaktantami ELP, RH40, a także ELP + RH40 na podstawie pomiarów napięcia powierzchniowego, przewodności właściwej, gęstości, widm emisyjnych Ber w wodnych roztworach ELP i RH40 oraz ELP + RH40 w szerokim zakresie stężeń surfaktantów ($1 \cdot 10^{-6}$ - $1 \cdot 10^{-2}$ mol/dm³) i temperatur (293-313 K). Na podstawie otrzymanych wyników określono zachowanie się berberyny w środowisku wodnym bez i w obecności surfaktantów. Stan równowagi pomiędzy roztworem monomerycznym a micelarnym surfaktantów, ich dwuskładnikowych mieszanin, a także mieszanin z Ber poddano analizie termodynamicznej w oparciu o otrzymane rezultaty.

6. OMÓWIENIE WYNIKÓW

6.1. Właściwości fizykochemiczne ELP, RH40 i Ber

Zachowanie się surfaktantów, ich mieszanin, a także mieszanin surfaktantów z innymi związkami organicznymi w środowisku wodnym zależy nie tylko od rodzaju grup chemicznych obecnych w cząsteczkach tych związków, ale również od ich liczby i polarności. Na właściwości adsorpcyjne i agregacyjne tego typu roztworów szczególny wpływ ma wielkość i powierzchnia kontaktu części hydrofilowej i hydrofobowej surfaktantów i dodatków z innymi cząsteczkami, a także składowe i parametry ich napięcia powierzchniowego.

Według van Ossa i wsp. [97-100] napięcie powierzchniowe cieczy i ciał stałych można podzielić na dwie składowe. Pierwszą, która stanowi napięcie powierzchniowe każdej cieczy lub ciała stałego wynika z oddziaływań międzycząsteczkowych Lifshitz - van der Waalsa (γ^{LW}) i drugą, która wynika z oddziaływań kwasowo - zasadowych (γ^{AB}). Składowa kwasowo-zasadowa zależy od parametrów elektronowo-akceptorowego (γ^+) i elektronowo - donorowego (γ^-). Ponieważ van Oss i wsp. sugerują, że udział oddziaływań dipol-dipol i dipol-dipol indukowany w składowej Lifshitz-van der Waalsa napięcia powierzchniowego jest mniejszy niż 2%, wynika z tego, iż składowa γ^{LW} napięcia powierzchniowego ciała stałego i cieczy zależy tylko od dyspersyjnych oddziaływań międzycząsteczkowych.

Fowkes [101] stwierdził, że dyspersyjne oddziaływania międzycząsteczkowe na granicy faz można wywnioskować na podstawie oddziaływań jednego elementu/fragmentu z dwunastoma jego sąsiadami oraz odległości pomiędzy nimi. W przypadku wodnych roztworów ELP i RH40 na granicy faz roztwór-powietrze można wyróżnić cząsteczki wody oraz grupy $-CH_3$, $-CH_2-$, $=CH-$, $=CO$ i $-OH$. Ponieważ oddziaływania Lifshitz - van der Waalsa w pierwszym przybliżeniu są równe oddziaływaniom dyspersyjnym, to zależą one od rodzaju grup funkcyjnych znajdujących się w cząsteczce surfaktantu i napięcie powierzchniowe surfaktantu jest związane z orientacją jego cząsteczek na danej

granicy faz. Biorąc pod uwagę ten fakt van Oss i Constanzo [98] stwierdzili, że napięcie powierzchniowe surfaktantu jest różne w zależności od orientacji jego cząsteczek na granicy faz surfaktant-powietrze. Stąd też napięcie powierzchniowe związku powierzchniowo czynnego, którego cząsteczki są zorientowane grupą hydrofobową (ogonem) w kierunku fazy gazowej można nazwać napięciem powierzchniowym ogona surfaktantu (γ_T , T - tail). Dla surfaktantu, którego cząsteczki są zorientowane w stronę fazy gazowej grupami hydrofilowymi (głową), jego napięcie powierzchniowe to napięcie powierzchniowe głowy surfaktantu (γ_H , H - head).

Ze względu na bardzo silne oddziaływania hydrofobowe pomiędzy ogonami cząsteczek ELP i RH40 ich zmierzone napięcie powierzchniowe można traktować jako napięcie powierzchniowe głowy [D4]. W związku z tym prawdopodobieństwo orientacji cząsteczek ELP i RH40 na granicy faz surfaktant-powietrze głowami skierowanymi w stronę fazy gazowej jest najbardziej realne. Biorąc to po uwagę wyznaczono składowe i parametry napięcia powierzchniowego głowy ELP i RH40 w temperaturze 293K poprzez pomiary ich kąta zwilżania na powierzchni modelowych ciał stałych, politetrafluoroetylen (PTFE) i poli(metakrylanu) metylu (PMMA) [D4]. Okazało się, że wyznaczone w ten sposób składowe napięcia powierzchniowego ELP i RH40 (Tab. 1, [D4]) są zbliżone do składowych napięcia powierzchniowego głowy Tritonu X-165 (TX165) [102], co potwierdza założenie, że cząsteczki ELP i RH40 na granicy faz woda-powietrze są skierowane głowami w stronę fazy gazowej.

W cząsteczce berberyny (Ber), w przeciwieństwie do ELP i RH40, trudno jest wyróżnić część hydrofobową i hydrofilową, dlatego też należy oczekiwać, że cząsteczki Ber na granicy faz woda-powietrze będą ułożone równolegle. Napięcie powierzchniowe berberyny (Ber) określono na podstawie kąta zwilżania zmierzonego dla wody (56,2°), formamidu (38,4°) i dijdometanu (46,1°) na sprasowanej berberynie metodą van Ossa i wsp. [97-99]. Znając składową Lifshitz - van der Waalsa (γ^{LW}) napięcia powierzchniowego wody, formamidu i dijdometanu oraz parametry elektronowo - akceptorowe (γ^+) i elektronowo -

donorowe (γ^-) tego napięcia [103], otrzymano napięcie powierzchniowe Ber (46,52 mN/m), składową γ^{LW} (36,42 mN/m) oraz parametry γ^+ (1,56 mN/m) i γ^- (16,38 mN/m) tego napięcia [D4]. Z przeprowadzonych obliczeń wynika, że napięcie powierzchniowe Ber niewiele różni się od tego dla np. TX165 [104], jeśli cząsteczki TX165 skierowane są grupą hydrofilową w stronę fazy gazowej. Należy jednak podkreślić, że udział składowej γ^{LW} w napięciu powierzchniowym Ber jest mniejszy, a γ^{AB} większy od tego dla TX165. Dodatkowo, udział składnika γ^{LW} w napięciu powierzchniowym Ber wynosi 78% i to powoduje słabą rozpuszczalność berberyny w wodzie [D4]. Należy podkreślić, że berberyna w niewielkim stopniu obniża napięcie powierzchniowe wody (Rys. 1, [D4]), a maksymalne obniżenie odpowiada stężeniu Ber w wodzie bliskiemu $1 \cdot 10^{-4}$ mol/dm³. Przy większym stężeniu Ber w roztworze wodnym napięcie powierzchniowe roztworu jest stałe, jednak punktu przegięcia izotermy napięcia powierzchniowego wodnego roztworu berberyny nie można traktować jako CMC [D4].

Rozpuszczalność związków organicznych w wodzie zależy nie tylko od ich napięcia powierzchniowego i wielkości γ^{LW} oraz γ^{AB} , ale także od wielkości i powierzchni kontaktu grup hydrofilowych i hydrofobowych ich cząsteczek. Wielkość cząsteczek ELP, RH40 i Ber obliczono na podstawie długości wiązań, kąta pomiędzy wiązaniami i odległości między cząsteczkami [D4]. Wykazano, że objętość jednej cząsteczki ELP, RH40 i Ber można określić na podstawie objętości sześciątów, w które można wpisać poszczególne fragmenty danej cząsteczki. Objętość otrzymanych w ten sposób cząsteczek ELP, RH40 i Ber wyniosła odpowiednio 4378,64 i 4825,21 i 428,25 Å³. Biorąc pod uwagę otrzymane w ten sposób wielkości badanych cząsteczek wyznaczono ich powierzchnie kontaktu z cząsteczkami wody. Powierzchnia ta wyniosła odpowiednio 3779,9 Å² dla ELP, 4210,2 Å² dla RH40 i 277,45 Å² dla Ber. Pamiętając, że powierzchnia kontaktu cząsteczek wody jest równa 10 Å² [105], teoretycznie wykazano, że 378 cząsteczek wody może kontaktować się z ELP, 421 z RH40 a 28 z Ber [D4]. Ponieważ powierzchnia kontaktu ogona cząsteczek ELP i RH40 wynosi 967,7 Å² [D3], jednocześnie może kontaktować się z nim 97 cząsteczek wody. Z drugiej jednak strony z danych literaturowych wynika, że grupa oksyetylenowa w cząsteczce

związku powierzchniowo czynnego może być połączona silnymi wiązaniami wodorowymi z dwiema cząsteczkami wody oraz słabymi wiązaniami z trzema cząsteczkami [D4, 106, 107]. Biorąc to pod uwagę wykazano, że w zależności od konfiguracji łańcuchy oksyetylenowe w cząsteczce ELP mogą być otoczone najwyżej około 245 cząsteczkami wody, a łańcuchy RH40 około 280 cząsteczkami, przy czym silnymi wiązaniami wodorowymi z atomami tlenu, z wyjątkiem tego w grupie $-OH$, z ELP połączone jest 82 cząsteczki wody, a 92 z RH40 [D3]. Obliczenia te są zgodne z wartościami liczb hydratacji ELP i RH40 wyznaczonymi na podstawie pomiarów prędkości dźwięku i gęstości [D1]. Dodatkowo znaczącą hydratację grup hydrofilowych ELP przy jego stężeniu w roztworze mniejszym niż CMC i w temperaturze 293K wykazano na podstawie pomiarów lepkości i zarejestrowanych widm emisyjnych pirenu [D2]. Udowodniono także, że hydratacja ta w tym zakresie stężeń istotnie wpływa na konformację i zwartą strukturę łańcuchów ELP.

Liczba cząsteczek wody otaczających grupy hydrofilowe związków powierzchniowo czynnych sprawia, że są one w dużej mierze rozpuszczalne w wodzie. Z drugiej jednak strony liczba cząsteczek wody otaczających grupy hydrofobowe cząsteczek ELP i RH40 jest siłą napędową ich adsorpcji na granicy faz woda-powietrze i procesu micelizacji. Siła ta zależy od składowych i parametrów napięcia powierzchniowego wody i surfaktantów, a także od wielkości powierzchni kontaktu. Wyznaczona powierzchnia kontaktu cząsteczek ELP i RH40 przez fazę wodną wynosi odpowiednio 951,62 i 1054,58 Å² [D4]. Powierzchnia kontaktu pomiędzy dwiema cząsteczkami Ber wynosi 108,96 Å² i jest mniejsza od maksymalnej powierzchni kontaktu pomiędzy ogonami dwóch cząsteczek ELP i RH40, która równa jest 324,71 Å² [D4].

Duży rozmiar głowy cząsteczek ELP i RH40 gwarantuje dobrą rozpuszczalność tych związków w wodzie, natomiast ogona - powoduje dobrą aktywność powierzchniową i skłonność do tworzenia miceli w środowisku wodnym [D2, D4]. Przykładowo maksymalne nadmiarowe stężenie powierzchniowe Gibbsa ELP i RH40 w temperaturze 293 K jest większe od tego dla np. Tritonów, zaś proces

tworzenia micel ELP i RH40 rozpoczyna się przy stężeniach mniejszych niż dla Tritonów [D2, D3, 108]. Warto podkreślić, że nadmiarowe stężenie powierzchniowe Gibbsa berberyny na granicy faz woda-powietrze wynosi odpowiednio $1,5 \cdot 10^{-6}$, $1,48 \cdot 10^{-6}$ i $1,46 \cdot 10^{-6}$ mol/dm³ w temperaturze 293, 303 i 313 K, a obliczona na podstawie tych wartości minimalna powierzchnia zajmowana przez cząsteczkę Ber na tej granicy faz jest zbliżona do powierzchni kontaktu berberyny w przypadku jej równoległej orientacji [D4].

6.2. Właściwości adsorpcyjne i objętościowe dwuskładnikowych mieszanin ELP+RH40

Przeprowadzone pomiary napięcia powierzchniowego γ_{LV} wodnych roztworów dwuskładnikowych mieszanin ELP i RH40 o ułamku molowym ELP w fazie objętościowej $\alpha = 0,2; 0,4; 0,6; 0,8$ wykazały, że przy danym stężeniu mieszaniny napięcie to w większości przypadków maleje niemal liniowo w funkcji temperatury [Rys. 1, D3]. Świadczy to o tym, że w badanym zakresie temperatur (293-318 K) dehydratacja RH40 i ELP w mieszaninie jest nieznaczna. Z drugiej jednak strony brak jest liniowej zależności pomiędzy napięciem powierzchniowym wodnego roztworu mieszaniny RH40 i ELP przy danym stężeniu w funkcji jej składu (Rys. 4, [D3]) - obserwuje się dodatnie i ujemne odchylenia wartości γ_{LV} od zależności liniowej. Świadczy to o możliwości wystąpienia zmian liczby hydratacji grupy hydrofilowej surfaktantów i/lub zmian w upakowaniu cząsteczek surfaktantów w wyniku zmiany ich konfiguracji. Z danych literaturowych jasno wynika, że możliwość tworzenia się różnych konfiguracji surfaktantów o dużych i rozgałęzionych cząsteczkach, typu ELP i RH40, jest większa niż w przypadku klasycznych surfaktantów liniowych [109, 110]. Zjawisko to jest szczególnie widoczne w przypadku surfaktantów zawierających w swoich cząsteczkach grupy oksyetylenowe [111, 112].

Z przeprowadzonych pomiarów wynika, że izotermy napięcia powierzchniowego wodnych roztworów mieszanin ELP i RH40 o danym składzie w różnych temperaturach są prawie równoległe (Rys. 1b-e, [D3]). Wykazano, że wszystkie te izotermy można opisać funkcją wykładniczą drugiego rzędu (Rys. S1-

S6, [SM3]), a stałe w równaniu tej funkcji powiązać ze składowymi i parametrami napięcia powierzchniowego głowy i ogona ELP oraz RH40. Wniosek ten dotyczy zwłaszcza stałej y_0 , której wartości dla wszystkich mieszanin i badanych temperatur są zbliżone do minimalnych wartości γ_{LV} danej mieszaniny. Ponieważ minimalne wartości γ_{LV} zależą od napięcia powierzchniowego ogona surfaktantu, można stwierdzić, że y_0 jest również związana z napięciem powierzchniowym grupy hydrofobowej surfaktantu [D3].

Wyznaczone eksperymentalnie izotermy napięcia powierzchniowego mieszanin ELP i RH40 opisano także za pomocą równania Szyszkowskiego i przeprowadzono próbę ich obliczenia teoretycznego na podstawie wartości napięcia powierzchniowego ELP i RH40, przy założeniu, że badane mieszaniny zachowują się jak roztwory idealne. Wykazano, że przy takim samym stężeniu ELP i RH40 dla wszystkich badanych mieszanin obliczone przy takim założeniu wartości γ_{LV} są większe od zmierzonych (Rys. S2-S5, [SM3]). Różnica jednak pomiędzy zmierzonymi a obliczonymi wartościami γ_{LV} zależy od składu mieszaniny i np. w przypadku mieszaniny ELP i RH40 o ułamku molowym ELP w fazie objętościowej równym 0,6, obliczone wartości γ_{LV} są prawie identyczne z wartościami zmierzonymi (Rys. S4, [SM3]). Dodatkowo dla mieszaniny o danym składzie różnica pomiędzy obliczoną a zmierzoną wartością γ_{LV} praktycznie nie zmienia się w funkcji temperatury. Stosując równanie Fainermana i Millera [113-114] również teoretycznie wyznaczono izotermy napięcia powierzchniowego mieszanin ELP i RH40 [D3]. Równanie to oparte na izotermach napięcia powierzchniowego roztworów pojedynczych składników mieszanin pozwala na przewidywanie izoterm napięcia powierzchniowego prostych mieszanin dwuskładnikowych o stałym składzie a różnym stężeniu, dla których powierzchnie zajmowane przez jeden mol indywidualnych składników są do siebie zbliżone. Wykazano, że równanie Fainermana i Millera z powodzeniem można zastosować dla badanych mieszanin w zakresie ich stężenia w fazie objętościowej stężeń od 0 do CMC.

Różnica pomiędzy wyznaczonymi eksperymentalnie a obliczonymi teoretycznie wartościami γ_{LV} świadczy o tym, że roztwory mieszaniny ELP i RH40 nie zachowują się jak roztwory idealne. Potwierdzeniem tego wniosku są np. wartości standardowej swobodnej energii Gibbsa procesu adsorpcji, ΔG_{ads}^0 (Tab. S2, [D3]) i maksymalnego nadmiarowego stężenia powierzchniowego Gibbsa (Γ^{max}) zastosowane do obliczeń γ_{LV} za pomocą równania Szyszkowskiego [D3]. Wartości Γ^{max} nie zmieniają się liniowo w funkcji składu mieszaniny surfaktantów (Rys. S13, [SM3]) i mieszczą się w przedziale od $2,44 \cdot 10^{-6}$ do $3,12 \cdot 10^{-6}$ mol/m². Odpowiadają także minimalnej powierzchni zajmowanej przez jedną cząsteczkę na granicy faz, która mieści się w przedziale od 53,2 do 68 Å². Świadczy to zatem o istnieniu zależnego od składu mieszaniny efektu synergetycznego w redukcji napięcia powierzchniowego wody. Dla badanych mieszanin efekt ten został oszacowany za pomocą wartości parametru oddziaływań międzycząsteczkowych β^M obliczonego na podstawie modelu Hua i Rosena [64]. W badanym zakresie stężeń i temperatur wyznaczony parametr β^M przyjmuje zarówno wartości ujemne (efekt synergetyczny), jak i dodatnie (efekt antagonistyczny) (Tab. S1, [SM3]).

W przypadku mieszaniny ELP i RH40 o ułamku molowym ELP w fazie objętościowej równym 0,6 wszystkie wartości β^M są dodatnie i istnieje niemal liniowa zależność pomiędzy β^M a napięciem powierzchniowym roztworów i temperaturą (Rys. S16d, [SM3]). Wskazuje to na brak efektu synergetycznego tej mieszaniny w redukcji napięcia powierzchniowego wody. Dla pozostałych badanych mieszanin RH40 i ELP efekt ten występował, ale nie w każdej zastosowanej w badaniach temperaturze. Interesującym jest, że w przypadku mieszaniny o ułamku molowym ELP w fazie objętościowej równym 0,8 wraz ze wzrostem stężenia i spadkiem napięcia powierzchniowego wartości β^M maleją (Tab. S1, [SM3]). Ujemne w całym zakresie temperatur wartości parametru β zaobserwowano dla tej mieszaniny przy $\gamma_{LV} = 45$ mN/m, a więc w pobliżu CMC [D3]. Wykazano, że w przypadku badanych mieszanin ELP i RH40 efekt synergetyczny w redukcji napięcia powierzchniowego wody wynika prawdopodobnie ze zmian konfiguracji cząsteczek ELP i RH40 w mieszanej monowarstwie adsorpcyjnej w porównaniu z monowarstwą utworzoną przez

pojedyncze surfaktanty i/lub zmiany liczby wiązań wodorowych na skutek dehydratacji grup hydrofilowych i hydrofobowych surfaktantów.

Istnienie tego efektu jest ściśle związane ze zmianami składu i stężenia mieszanej monowarstwy adsorpcyjnej na granicy faz woda-powietrze w funkcji stężenia mieszaniny i temperatury przy stałym składzie w fazie objętościowej. Skład mieszanej monowarstwy adsorpcyjnej utworzonej przez mieszaniny ELP i RH40 obliczono na podstawie modelu Hua i Rosena (Tab. S1, [SM3]) oraz wartości ciśnienia powierzchniowego surfaktantów (π). Wykazano, że dla danego stężenia i temperatury wartości te są zbliżone, a w zakresie stężeń mieszaniny w fazie objętościowej odpowiadającym nienasyconej monowarstwie adsorpcyjnej, tj. od zera do $1 \cdot 10^{-6}$ mol/dm³ występuje niezależna adsorpcja ELP i RH40 i ułamek molowy ELP w monowarstwie jest mniejszy od tego w fazie objętościowej (Tab. S1, [SM3]). Przy stężeniach odpowiadających nasyconej monowarstwie adsorpcyjnej ułamek molowy ELP jest zbliżony lub większy od α [D3].

Wyznaczone na podstawie izoterm napięcia powierzchniowego w temperaturze 293K wartości krytycznego stężenia micelizacji CMC , Π_{CMC} (różnicy między napięciem powierzchniowym rozpuszczalnika γ_0 i napięciem powierzchniowym substancji rozpuszczonej γ w punkcie CMC), ΔG_{mic}^0 (standardowa swobodna energia Gibbsa procesu micelizacji), ΔG_{min}^S (energia swobodna na granicy faz woda - powietrze), β^M (parametr oddziaływań międzycząsteczkowych w mieszanej miceli), g^M (nadmiarowa energia Gibbsa mieszanej miceli) i ε^M (energia wymiany cząsteczek w mieszanej miceli) potwierdziły także istnienie efektu synergetycznego w procesie tworzenia mieszanych micel mieszaniny ELP i RH40 o ułamku molowym ELP w fazie objętościowej równym 0,8 (Tab. 1, [D1]). Również wzrost obliczonych na podstawie pomiarów gęstości, lepkości i prędkości dźwięku roztworów tej mieszaniny wartości impedancji akustycznej (Z) i ciśnienia wewnętrznego (π_i) powyżej stężenia 10^{-3} mol/dm³ (Rys. 1-Rys. 4, [D1]) wskazały na silne oddziaływania pomiędzy składnikami badanych binarnych roztworów micelarnych. Warto podkreślić, że te oddziaływania międzycząsteczkowe, jak również gęstsze upakowanie surfaktantów w mieszanych micelach ELP i RH40

przy ułamku molowym ELP w fazie objętościowej równym 0,8 powyżej $C = 10^{-3}$ mol/dm³, stwierdzono również na podstawie wartości odległości międzycząsteczkowej (*molecular free length, L_f*) obliczonych z modelu Chauhana i Sharmy [107]. Wartości L_f , czyli odległości pomiędzy powierzchniami dwóch cząsteczek, zależą zarówno od oddziaływań międzycząsteczkowych, jak i wewnątrzcząsteczkowych pomiędzy składnikami roztworu i maleją znacznie powyżej CMC mieszaniny, potwierdzając istnienie efektu synergetycznego w procesie tworzenia mieszanych micel. Jest to bardzo istotny wniosek, który połączony z rozważaniami na temat zmiany liczby hydratacji czy stopnia wiązania wody z micelami ELP, RH40 i ich mieszaniny [D1-D3] ma duże znaczenie w wyjaśnieniu oddziaływań surfaktant - berberyna i może decydować o potencjalnym praktycznym zastosowaniu tego typu układów.

6.3. Właściwości adsorpcyjne i objętościowe ELP + Ber, RH40 + Ber i ELP + RH40 + Ber

Biorąc pod uwagę udział oddziaływań międzycząsteczkowych Lifshitz - van der Waalsa w napięciu powierzchniowym wody, ELP, RH40 i Ber, można stwierdzić, że obniżenie napięcia powierzchniowego wody na skutek adsorpcji badanych związków na granicy faz woda-powietrze zależy jedynie od redukcji składowej kwasowo-zasadowej napięcia powierzchniowego wody [D4]. Składowa γ^{LW} napięcia powierzchniowego ELP (27,51 mN/m), RH40 (27,38 mN/m) i Ber (36,42 mN/m) [D4] jest większa niż ta składowa napięcia powierzchniowego wody (26,85 mN/m). W przypadku napięcia powierzchniowego ogona ELP i RH40 składowa γ^{LW} tego napięcia jest tylko nieznacznie większa niż ta dla wody (Tab. 1, [D4]). Jak wspomniano powyżej, w cząsteczkach Ber trudno jest rozróżnić ogon i głowę, i w związku z tym w monowarstwie adsorpcyjnej na granicy faz woda-powietrze przyjmują one równoległą orientację. Wobec tego, minimalne napięcie powierzchniowe wodnego roztworu Ber nie może być mniejsze od jej napięcia powierzchniowego (46,52 mN/m) (Tab 1. [D4]).

Zakładając, że tylko napięcie powierzchniowe ogona ELP i RH40 decyduje o redukcji napięcia powierzchniowego wody, można stwierdzić, że minimalne napięcie powierzchniowe roztworu wodnego powinno być znacznie mniejsze niż w przypadku roztworu wodnego Ber. Z analizy różnic pomiędzy napięciem powierzchniowym Ber oraz ogona ELP i RH40 wynika, że jeśli na granicy faz woda-powietrze powstaje mieszana monowarstwa adsorpcyjna z roztworu zawierającego ELP, RH40 i ELP + RH40 z Ber, napięcie powierzchniowe wodnych roztworów tych mieszanin przy tym samym stężeniu ELP i RH40 oraz ELP + RH40 powinno być większe niż dla roztworu bez Ber. Izotermy napięcia powierzchniowego wodnych roztworów ELP, RH40 i ELP + RH40 w obecności i przy braku Ber w roztworze (Rys. 2 - 4, [D4]) potwierdzają, że usunięcie cząsteczek ELP lub RH40 z mieszanej monowarstwy adsorpcyjnej na granicy faz woda - powietrze przez cząsteczki Ber zwiększa napięcie powierzchniowe roztworu. Izotermy te mają prawie taki sam kształt i w danej temperaturze istnieje niemal prostoliniowa zależność pomiędzy napięciem powierzchniowym roztworu a logarytmem ze stężenia surfaktantów lub ich mieszaniny. Wykazano, że podobnie jak w przypadku izoterm ELP, RH40 i ELP+RH40 [D3], izotermy ELP, RH40 i ich mieszaniny z berberyną można opisać funkcją wykładniczą drugiego rzędu, a stałe w równaniu tej funkcji powiązać ze składowymi i parametrami napięcia powierzchniowego wszystkich składników roztworu. Dodatkowo zmiany stałych A_1, A_2, t_1 i t_2 tej funkcji ze zmianą temperatury (Rys. S2, [SM4]) są bardziej skomplikowane niż zmiany stałej y^0 (Rys. S2a, [SM4]) i są związane ze zmianami stopnia hydratacji cząsteczek ELP, RH40 i Ber i odległości pomiędzy tymi cząsteczkami i wodą. Zmiany stopnia hydratacji oraz składowych i parametrów napięcia powierzchniowego mieszaniny wpływają z kolei na stężenia i skład mieszanej monowarstwy adsorpcyjnej.

Skład mieszanej monowarstwy adsorpcyjnej utworzonej przez dwu- i trójskładnikowe mieszaniny surfaktantów w wielu przypadkach można wyznaczyć za pomocą zmodyfikowanych równań Rosena i Rubingha [59, 64, D4]. Równania te jednak można zastosować do wyznaczenia ułamka molowego mieszanej monowarstwy tylko w ograniczonym składzie mieszaniny w fazie objętościowej. Z tego względu w przypadku badanych mieszanin surfaktantów

z berberyną określono skład mieszanej monowarstwy tylko przy niewielkim stężeniu surfaktantów [D4]. Wykazano, że skład obliczonej w ten sposób mieszanej monowarstwy jest zbliżony do tego wyznaczonego na podstawie izoterm napięcia powierzchniowego wodnych roztworów poszczególnych składników mieszaniny, znacznie różni się od tego w fazie objętościowej i zależy od temperatury (Rys. S2 – S5, [SM4]). Interesującym jest, że przy dużym stężeniu ELP, RH40 lub mieszaniny ELP + RH40 ułamek molowy Ber w mieszanej monowarstwie jest większy od tego w fazie objętościowej [D4]. Sugeruje to, że cząsteczki berberyny adsorbują się na granicy faz woda-powietrze łącznie z cząsteczkami surfaktantu w wyniku silnych oddziaływań hydrofobowych między cząsteczkami Ber i surfaktantu i cząsteczki Ber w tej monowarstwie nie są zorientowane równolegle do granicy faz, lecz prostopadle lub pod pewnym kątem. Efektem tego jest wzrost stężenia Ber w mieszanej monowarstwie (Rys. S2 – S5, [SM4]).

Stężenie danego składnika mieszaniny surfaktantów czy mieszaniny surfaktantów z dodatkami można wyznaczyć pośrednio m.in. za pomocą izoterm adsorpcji Gibbsa i Frumkina [104]. Niestety w badanym zakresie stężeń mieszanin odpowiadającym nasyconej mieszanej monowarstwie na granicy faz woda-powietrze za pomocą równania izoterm adsorpcji Gibbsa nie udało się wyznaczyć maksymalnego stężenia mieszaniny ELP, RH40 i ELP + RH40 w obecności Ber. Należy podkreślić, że słaba rozpuszczalność berberyny w wodzie uniemożliwia pomiar napięcia powierzchniowego wodnych roztworów mieszaniny surfaktantu i Ber w szerokim zakresie stężenia surfaktantu. Z tego powodu stężenie danego surfaktantu w badanych pojedynczych i mieszanych monowarstwach na granicy faz woda – powietrze wyznaczono za pomocą równania Frumkina, stosując do obliczeń wkład poszczególnych składników roztworu w redukcję napięcia powierzchniowego [105, D4]. Wykazano, że dla wszystkich badanych mieszanin stężenie poszczególnych składników w mieszanej monowarstwie na granicy faz woda-powietrze jest mniejsze niż poszczególnych składników osobno (Rys. S6 – S8, [SM4]). Ponadto suma stężeń ELP + Ber, RH40 + Ber czy ELP + RH40 + Ber w mieszanej monowarstwie adsorpcyjnej jest mniejsza niż w przypadku surfaktantów lub ich mieszaniny bez berberyny (Rys. S6 – S8, [SM4]).

Prawdopodobną przyczyną tego faktu jest adsorpcja Ber łącznie z cząsteczkami surfaktantu. Cząsteczki berberyny mogą łączyć się z ogonem cząsteczki surfaktantu zmniejszając jego stopień hydratacji. W konsekwencji powstaje kompleks Ber - surfaktant o mniejszej tendencji do adsorpcji na granicy faz woda-powietrze niż pojedyncza cząsteczka ELP czy RH40. Z drugiej jednak strony zaadsorbowany kompleks cząsteczka berberyny + ogon surfaktantu w mieszanej monowarstwie adsorpcyjnej może być skierowany w stronę fazy wodnej zmieniając jej napięcie powierzchniowe. Ze względu na budowę cząsteczki Ber, która posiada ładunek dodatni, mogą pojawiać się także odpychające oddziaływania elektrostatyczne pomiędzy kompleksami Ber + ogon surfaktantu. Tego typu oddziaływania mogą zmniejszać upakowanie mieszanej monowarstwy adsorpcyjnej, zmniejszając jednocześnie stężenie surfaktantu w porównaniu do jego stężenia w roztworze bez berberyny.

Standardowa swobodna energia Gibbsa (ΔG_{ads}^0), standardowa entalpia (ΔH_{ads}^0) i entropia procesu adsorpcji (ΔS_{ads}^0) są przydatne do określenia tendencji surfaktantów do adsorpcji na różnych granicach faz i do poznania przyczyny tej tendencji [D4]. W przypadku badanych mieszanin Ber + surfaktant wartości ΔG_{ads}^0 dla ELP, RH40 i Ber, w mieszaninach ELP + Ber, RH40 + Ber, ELP + RH40 + Ber obliczono za pomocą zaproponowanego równania przy założeniu, że współczynniki aktywności są bliskie jedności [D4] i porównano z tymi obliczonymi na podstawie zmodyfikowanego równania Langmuira (Rys. S9, [SM4]). Otrzymane wyniki wskazują, że w zakresie stężeń surfaktantów, w których występują one w roztworze w postaci monomerycznej, wartości ΔG_{ads}^0 obliczone z zaproponowanego równania są praktycznie stałe i nie zmieniają się ze wzrostem T (Tab. 4, [D4]). Przy stężeniu surfaktantów większym niż CMC wartości ΔG_{ads}^0 rosną w funkcji stężenia. Należy jednak podkreślić, że cząsteczki surfaktantów adsorbują się na granicy faz woda-powietrze tylko w postaci monomerycznej, a przy stężeniu większym niż CMC ich stężenie w formie monomerycznej jest stałe. W związku z tym obliczone w ten sposób wartości ΔG_{ads}^0 dla stężeń powyżej CMC nie są rzeczywiste. Zatem na podstawie wartości ΔG_{ads}^0 , ale także ΔH_{ads}^0 można

stwierdzić, że obecność Ber zmniejsza tendencję ELP i RH40 do adsorpcji na granicy faz woda - powietrze ze względu na adsorpcję kompleksów Ber + surfaktant.

Obok adsorpcyjnych, również właściwości agregacyjne badanych układów Ber + surfaktant mogą mieć bardzo istotne znaczenie np. w procesie solubilizacji. W związku z tym zrodziło się pytanie, czy berberyna jest obecna w micelach ELP, RH40 i ich mieszaniny. W celu znalezienia odpowiedzi na to pytanie w pierwszej kolejności za pomocą pomiarów napięcia powierzchniowego, przewodnictwa, gęstości, widm emisyjnych berberyny [D1, D2, D3, D4] wyznaczono krytyczne stężenie micelizacji badanych mieszanin. Wykazano, że wartości CMC ELP, RH40 i ich mieszaniny w obecności Ber są większe od tych bez Ber (Tab. 2, [D4]). Należy pamiętać, że tworzenie micel w wodnym roztworze surfaktantów występuje na skutek oddziaływań hydrofobowych pomiędzy ogonami surfaktantów poprzez fazę wodną. Wartości tych oddziaływań są dodatnie, w przeciwieństwie do oddziaływań pomiędzy głowami surfaktantów, które są ujemne niezależnie od tego, czy micelle tworzą niejonowe, czy jonowe związki powierzchniowo czynne. Zgodnie z równaniami zaproponowanymi przez Jańczuka i wsp. [106, 107] siła oddziaływań hydrofobowych zależy od napięcia międzyfazowego woda - ogon i powierzchni kontaktu ogona surfaktantu. Biorąc pod uwagę podejście van Ossa i wsp. oraz składowe i parametry napięcia powierzchniowego wody, berberyny i surfaktantów obliczono napięcie międzyfazowe woda - ogon surfaktantu (γ_{WT}), woda-Ber (γ_{WB}) i Ber-ogon surfaktantu (γ_{BT}) [D4]. Wartości te wynoszą odpowiednio 46,0; 6,0 i 10,7 mN/m. Na ich podstawie obliczono pracę adhezji ogona surfaktantu do ogona surfaktantu, ogona surfaktantu do Ber i Ber do ogona surfaktantu przez fazę wodną. Wykazano, że praca adhezji ogona surfaktantu do ogona surfaktantu przez fazę wodną wynosi $2\gamma_{WT} = 92$ mJ/m², a Ber do Ber jest równa $\gamma_{WB} = 12$ mJ/m². Praca adhezji w układzie Ber - woda- ogon surfaktantu (W_a^{BT}) wynosi 41,3 mJ/m² [D4].

Ze względu na fakt, że napięcie międzyfazowe surfaktant - woda dla ELP i RH40 jest ujemne i bliskie -18 mJ/m², ich całkowita praca adhezji poprzez fazę wodną jest bliska 56 mJ/m². Nie istnieje więc istotna różnica w tendencji do kontaktu

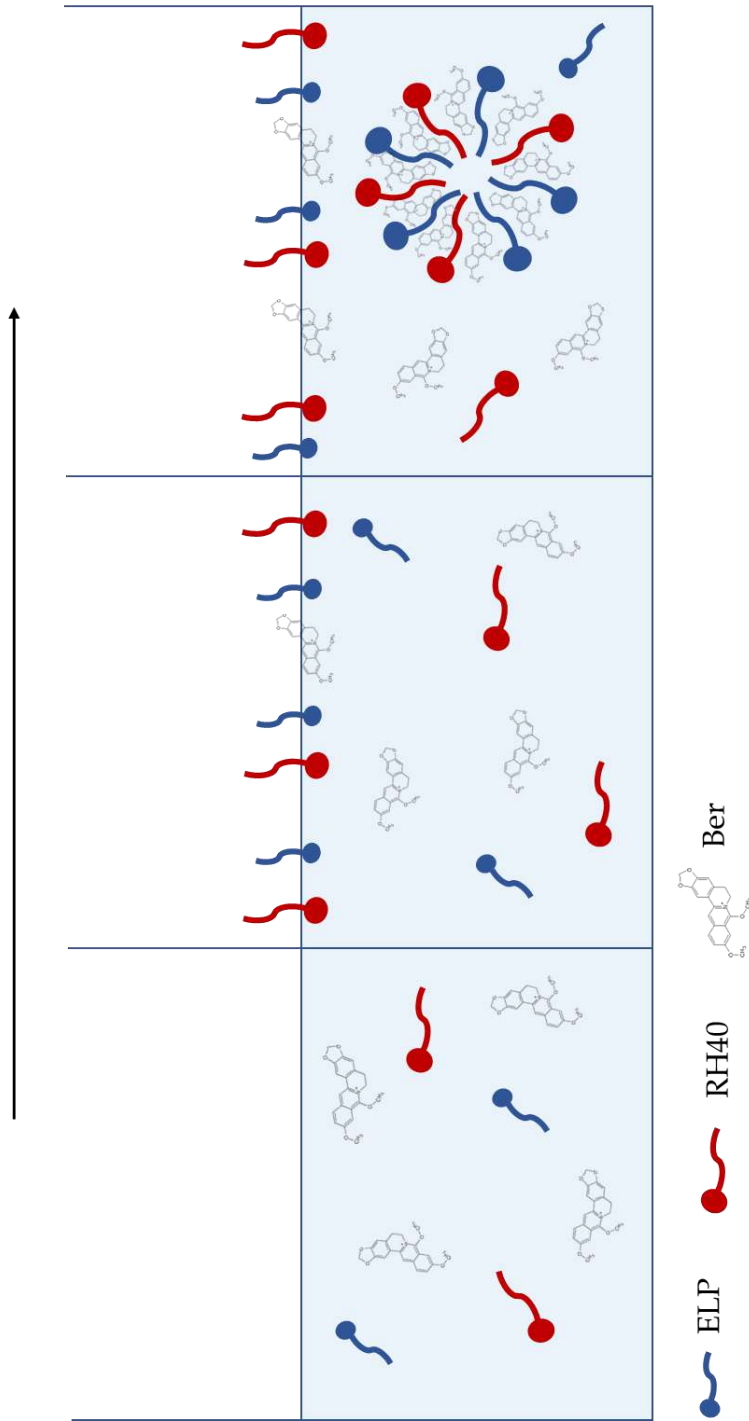
surfaktantu z drugą cząsteczką surfaktantu i surfaktantu z cząsteczką berberyny poprzez fazę wodną. Jednakże prawdopodobieństwo wiązania poprzez fazę wodną kompleksów Ber - związek powierzchniowo czynny jest mniejsze niż cząsteczek samego surfaktantu i prawdopodobnie z tego powodu CMC mieszanin ELP, RH40 i ELP + RH40 z Ber jest większe niż bez Ber (Tab. 2, [D4]). Biorąc pod uwagę powyższe obliczenia można założyć, że proces micelizacji mieszaniny badanych surfaktantów zachodzi w wyniku nie tylko łączenia się cząsteczek surfaktantów, ale także surfaktantów z cząsteczkami Ber. Wydaje się zatem, że obecność Ber w micelach ELP, RH40 i ich mieszaninie nie jest spowodowana adsorpcją czy też penetracją cząsteczek Ber w micelach, ale raczej jest wynikiem wspólnej agregacji (Rys. 5).

W przypadku mieszanych micel ELP + Ber i RH40 + Ber trudno jest określić ułamek molowy związku powierzchniowo czynnego i berberyny w micelach na podstawie ich wartości CMC. W związku z tym ułamki te wyznaczono za pomocą zmodyfikowanej koncepcji Hua i Rosena [59, 64] i wykazano, że ułamek molowy Ber nie różni się istotnie od 0,5. Świadczy to o tym, że oddziaływania kompleksów berberyna + surfaktant poprzez fazę wodną odgrywają wiodącą rolę w procesie agregacji. Stwierdzono także, że ułamek molowy poszczególnych składników mieszaniny ELP + RH40 + Ber zmienia się w niewielkim stopniu w funkcji temperatury (Tab. 3, [D4]). Należy jednak podkreślić, że zmiana wartości ułamków molowych składników mieszaniny, jak i samej wartości CMC w funkcji temperatury wynika z jednej strony ze zmiany energii kinetycznej, a z drugiej strony ze zmiany stopnia hydratacji, zwłaszcza części hydrofilowej surfaktantu. Dodatkowo wpływać może także zmiana konfiguracji cząsteczek surfaktantu.

Wpływ wymienionych czynników na skład i wielkość badanych micel znajduje także odzwierciedlenie w wartościach parametru oddziaływań międzycząsteczkowych (β^M). Ponieważ Ber nie tworzy samoistnie micel, nie było możliwe określenie parametru oddziaływań pomiędzy cząsteczkami Ber i surfaktantów w micelach mieszanin ELP + Ber i RH40 + Ber bezpośrednio z równania zaproponowanego przez Rosena i Hua [59]. W związku z tym założono,

że kompleks ELP + Ber i RH40 + Ber to pojedynczy związek i wyznaczono za pomocą tej koncepcji β^M (Ber + ELP) - RH40 i (Ber + RH40) - ELP w mieszanych micelach ELP + RH40 + Ber (Tab. 3, [D4]). Z przeprowadzonych obliczeń wynika, że parametr β^M obliczony na podstawie wartości CMC wyznaczonego z pomiarów napięcia powierzchniowego jest ujemny dla kompleksu RH40 + Ber w każdej temperaturze (−0,4159 w 293 K, −1,5256 w 303 K i −1,1598 w 318 K), ale dla kompleksu ELP + Ber tylko w T = 293 K (−5,0834). Podobny przebieg zmian zaobserwowano w przypadku wartości nadmiarowej energii Gibbsa tworzenia miceli przypadającej na mol mieszaniny surfaktantów (G^M) (Tab. 3, [D4]). Ujemna wartość parametru β^M sugeruje, że istnieje efekt synergetyczny w procesie tworzenia micel. Niestety jednak, w przypadku badanych mieszanin niemożliwe było potwierdzenie tej sugestii za pomocą drugiego warunku istnienia synergetyzmu określonego przez Rosena i Hua [D4].

C_{Ber} stałe, $C_{ELP+RH40}$ rośnie



Rys. 5 Schemat przedstawiający zmiany na granicy faz woda-powietrze w obecności mieszanin surfaktantów: ELP i RH40 i berberyny; Do wizualizacji wykorzystano stałe stężenie berberyny oraz rosnące stężenie związków powierzchniowo czynnych: (a) współwystępowanie molekul surfaktantów i cząsteczek berberyny w roztworze, (b) orientowanie molekul surfaktantów na granicy faz woda-powietrze wraz ze wzrostem ich stężenia - równoległe do granicy faz ułożenie cząsteczek berberyny, (c) po przekroczeniu krytycznego stężenia micelizacji i wysycenia granicy międzyfazowej tworzenie mieszanych miceli surfaktantów i berberyny.

7. WNIOSKI

Na podstawie wyników uzyskanych z przeprowadzonych badań oraz ich termodynamicznej analizy stwierdzono m.in., że:

1. Berberyna w niewielkim stopniu redukuje napięcie powierzchniowe wody a jej maksymalne nadmiarowe stężenie Gibbsa w warstwie powierzchniowej w temperaturze 293K jest zdecydowanie mniejsze od tego dla ELP i RH40.
2. Napięcie powierzchniowe berberyny wynika zarówno ze składowej Lifshitzavan der Waalsa, jak i kwasowo - zasadowej, jednak udział składowej Lifshitzavan der Waalsa jest dużo większy wpływając na słabą rozpuszczalność berberyny w wodzie.
3. Adsorpcja cząsteczek ELP i RH40 na granicy faz woda-powietrze powoduje redukcję składowej Lifshitzavan der Waalsa napięcia powierzchniowego wody.
4. Składowe Lifshitzavan der Waalsa napięcia powierzchniowego Ber oraz ogona ELP i RH40, a także stopień hydratacji cząsteczek Ber oraz ogona i głowy cząsteczek ELP i RH40 w największym stopniu decydują o stężeniu i składzie nasyconej monowarstwy adsorpcyjnej na granicy faz woda-powietrze.
5. Stężenie poszczególnych składników w mieszanej monowarstwie adsorpcyjnej na granicy faz woda-powietrze dla wszystkich badanych mieszanin z Ber jest mniejsze od tego dla roztworów pojedynczych związków.
6. Przy dużych stężeniach ELP, RH40 lub mieszaniny ELP + RH40 ułamek molowy Ber w mieszanej monowarstwie jest większy od tego w fazie objętościowej.
7. Stężenie berberyny w mieszanych micelach jest większe niż w fazie objętościowej, co wskazuje, że tendencja Ber do solubilizacji w micelach ELP, RH40 i ELP + RH40 jest większa niż jej tendencja do adsorpcji na granicy faz woda-powietrze.
8. Skład mieszanej monowarstwy adsorpcyjnej ELP +RH40 na granicy faz woda-powietrze można określić na podstawie wkładu poszczególnych składników

mieszaniny w redukcję napięcia powierzchniowego wody i jest on bliski temu obliczonemu za pomocą koncepcji Rosena i Hua.

9. Istnieje efekt synergetyczny w procesie tworzenia mieszanych micel ELP+RH40. Efekt ten wykazano za pomocą wartości parametru oddziaływań międzycząsteczkowych obliczonych z pomiarów napięcia powierzchniowego roztworów, a także parametrów akustycznych wyznaczonych z pomiarów gęstości i prędkości dźwięku.

10. Biorąc pod uwagę wartości nadmiarowego stężenia powierzchniowego Gibbsa Ber w mieszaninie ELP i RH40, współczynniki aktywności tych związków w warstwie adsorpcyjnej na granicy faz woda-powietrze i w micelach obliczone metodą Rosena i Hua i wkład Ber, ELP i RH40 w redukcję napięcia powierzchniowego wody, można za pomocą zaproponowanych równań określić energię Gibbsa oddziaływań Ber z ELP i RH40 poprzez fazę wodną.

8. LITERATURA

- [D1] K. Szymczyk, **M. Szaniawska**, K. Terpiłowski*, Determination of acoustical parameters of aqueous solution of Kolliphors binary mixtures using density, speed of sound, viscosity and surface tension measurements. *Journal of Surfactants and Detergents*, 2019, 22(5), 1163–1174.
- [D2] K. Szymczyk*, **M. Szaniawska**, J. Krawczyk, Temperature effect on the adsorption and volumetric properties of aqueous solutions of Kolliphor ELP®. *Molecules*, 2020, 25(3), 743.
- [D3] **M. Szaniawska**, K. Szymczyk, A. Zdziennicka, B. Jańczuk*, Adsorption properties and composition of binary Kolliphor mixtures at the air-water interface at different temperatures, *Molecules*, 2022, 27(3), 877.
- [D4] **M. Szaniawska**, K. Szymczyk*, A. Zdziennicka, B. Jańczuk, Thermodynamic parameters of berberine with Kolliphor mixtures adsorption and micellization, *Molecules*, 2023, 28(7), 3115.
1. J. Fan, K. Zhang, Y. Jin, B. Li, S. Gao i wsp., *Pharmacological effects of berberine on mood disorders*, J. Cell. Mol. Med., 2019, 23: 21-28.
 2. A. Kumar, E.K. Chopra, M. Mukherjee, R. Pottabathini, D.K. Dhull, *Current knowledge and pharmacological profile of berberine: an update*, Eur. J. Pharmacol., 2015, 761, 288-297.
 3. S. Palai, *Chapter 21 – Berberine*, Nutraceuticals and Health Care, 2022, 359-368.
 4. A. Kołodziejczyk, *Naturalne związki organiczne*, Wydawnictwo Naukowe PWN, 2013, ISBN 9788301173470.
 5. I.P. Singh, S. Mahajah, *Berberine and its derivatives: a patent review (2009-2012)*, Expert Opin. Ther. Patients, 2013, 23(2), 215-231.
 6. M. Imenshahidi, H. Hosseinzadeh, *Berberine and barberry (Berberis vulgaris): A clinical review*, Phytother. Res., 2019, 33(3), 504-523.
 7. S. Ahmad, A. Hussain, A. Hussain, I. Abdullah, M.S. Ali i wsp., *Quantification of berberine in Berberis vulgaris L. root extract and its curative and prophylactic role in cisplatin-induced in vivo toxicity and in vitro cytotoxicity*, Antioxidants, 2019, 8(6), 185.

8. M.M. Ali, A.M. Habban, A.M. Sarfaraz, A.M. Daud, H. Afzal, *An updated review on therapeutic and recent advances in drug delivery of berberine: current status and future prospects*, *Curr. Pharm. Biotechnol.*, 2022, 23(1), 60-71.
9. L. Wang, B. Xu, G. Sagada, K. Chen, J. Zhang i wsp., *Dietary berberine regulates lipid metabolism in muscle and liver of black sea bream (*Acanthopagrus schlegelii*) fed normal or high-lipid diets*, *Br. J. Nutr.*, 2021, 125, 481-493.
10. L. Wang, G. Sagada, C. Wang, C. Gao, B. Wang i wsp., *Berberine in fish nutrition: Impact on hepatocellular health, antioxidative and immune status*, *Front. Mar. Sci.*, 2022, 9:967748.
11. A. Och, R. Podgórski, R. Nowak, *Biological activity of berberine – a summary update*, *Toxins*, 2020, 12, 713.
12. X. Feng, A. Sureda, S. Jafari, Z. Memariani, D. Tewari i wsp., *Berberine in Cardiovascular and metabolic diseases: from mechanism to therapeutics*, *Theranostics*, 2019, 9, 1923-1951.
13. K. Rajasekhar, S. Samanta, V. Bagoband, A.A. Murugan, T. Govindaraju, *Antioxidant berberine-derivative inhibits multifaceted amyloid toxicity*, *iScience*, 2020, 23(4), 101005.
14. A.O. Babalghith, H.M. Al-Kuraishy, A.I. Al-Gareeb, M. De Waard, S.M. Al-Hamash i wsp., *The role of berberine in Covid-19: potential adjunct therapy*, *Inflammopharmacology*, 2022, 30, 2003-2016.
15. A. Pizzorno, B. Padey, J. Dubois, T. Julien, A. Traversier i wsp., *In vitro evaluation of antiviral activity of single and combined repurposable drugs against SARS-CoV-2*, *Antiviral Res.*, 2020, 181, 1-6.
16. Y. Wang, Y. Liu, X. Du, H. Ma, J. Yao, *The anti-cancer mechanisms of berberine: a review*, *Cancer Manag. Res.*, 2020, 12, 695-702.
17. A. Rauf, T. Abu-Izneid, A.A. Khalil, M. Imran, Z.A. Shah i wsp., *Berberine as a potential anticancer agent: a comprehensive review*, *Molecules*, 2021, 26(23), 7368.
18. W. Xie, F. Su, G. Wang, Z. Peng, Y. Xu i wsp., *Glucose-lowering effect of berberine on type 2 diabetes: a systematic review and meta-analysis*, *Front. Pharmacol.*, 2022, 13, 1015045.

19. X. Xu, L. Zhang, Y. Zhao, B. Xu, W. Qin i wsp., *Anti-inflammatory mechanism of berberine on lipopolysaccharide-induced IEC-18 models based on comparative transcriptomics*, *Mol. Med. Res.*, 2020, 22, 5163-5180.
20. R. Azadi, S.E. Mousavi, N.M. Kazemi, H. Yousefi-Manesh, S.M. Rezayat i wsp., *Anti-inflammatory efficacy of berberine nanomicelle for improvement of cerebral ischemia: formulation, characterization and evaluation in bilateral common carotid artery occlusion rat model*, *BMC Pharmacol. Toxicol.*, 2021, 22, 54.
21. R. Rui, H. Yang, Y. Liu, Y. Zhou, X. Xu i wsp., *Effects of berberine on atherosclerosis*, *Front. Pharmacol.*, 2021, 12, 764175.
22. A. Fatahian, S.M. Haftcheshmeh, S. Azhdari, H.K. Farshchi. B. Nikfar i wsp., *Promising anti-atherosclerotic effect of berberine: evidence from in vitro, in vivo and clinical studies*, *Rev. Physiol. Biochem. Pharmacol.*, 2020, 178, 83-110.
23. J. Tan, J. Wang, C. Yang, C. Zhu, J. Tang i wsp., *Antimicrobial characteristics of berberine against prosthetic joint infection-related Staphylococcus aureus of different multi-locus sequence types*, *BMC Complement. Altern. Med.*, 2019, 19, 218.
24. S. Xia, L. Ma, G. Wang, J. Yang, M. Zhang i wsp., *In vitro antimicrobial activity and the mechanism of berberine against methicillin-resistant Staphylococcus aureus isolated from bloodstream infection patients*, *Infection and Drug Resistance*, 2022, 15, 1933-1944.
25. C. Chen, Z. Yu, Y. Li, J. Fichna, M. Storr, *Effects of berberine in the gastrointestinal tract – a review of actions and therapeutic implications*, *Am. J. Chin. Med.*, 2014, 42, 1053-1070.
26. S.K. Battu, M.A. Repka, S. Maddineni, A.G. Chittiboyina, M.A. Avery, S. Majumdar, *Physicochemical characterization of berberine chloride: a perspective in the development of a solution dosage form for oral delivery*, *AAPS Pharm. Sci. Tech.*, 2010, 11(3), 1466-1475.
27. P. Patel, *A bird's eye view on a therapeutically `wonder molecule`: Berberine*, *Phytomedicine Plus* 1, 2021, 100070.
28. L. Pan, H. Yu, J. Fu, J. Hu, Z. Zhang i wsp., *Berberine ameliorates chronic kidney disease through inhibiting the production of gut-derived uremic toxins in the gut microbiota*, *Acta Pharm. Sin. B.*, 2022, DOI:10.1016/j.apsb.2022.12.010.

29. C. Godugu, A.R. Patel, R. Doddapaneni, J. Somagoni, M. Singh, *Approaches to improve the oral bioavailability of novel anticancer drugs berberine and betulinic acid*, PLoS One, 2014, 9(3), e89919.
30. W. Chen, Y.Q. Miao, D.J. Fan, S.S. Yang, X. Lin i wsp., *Bioavailability of berberine and the enhancing effects of TPGS on intestinal absorption in rats*, AAPS Pharm. Sci. Tech., 2011, 12, 705-711.
31. Y.T. Liu, H.P. Hao, H.G. Xie, L. Lai, Q. Wang i wsp., *Extensive intestinal first-pass elimination and predominant hepatic distribution of berberine explain its low plasma levels in rats*, Drug Metab. Dispos., 2010, 38(10), 1779-1784.
32. R. Feng, J.W. Shou, Z.X. Zhao, C.Y. He, C. Ma i wsp., *Transforming berberine into its intestine-absorbable form by the gut microbiota*, Sci. Rep., 2015, 5, 12155.
33. F.A. Younis, S.R. Saleh, S.S. Abd El-Rahman, A.A. Newairy, M.A. El-Demellawy, D.A. Ghareeb, *Preparation, physicochemical characterization and bioactivity evaluation of berberine-entrapped albumin nanoparticles*, Sci. Rep., 2022, 12, 17431.
34. M. Xue, M. Yang, W. Zhang, X. Li, D. Gao i wsp., *Characterization, pharmacokinetics and hypoglycemic effect of berberine loaded solid lipid nanoparticles*, Int. J. Nanomedicine, 2013, 8, 4677-4687.
35. W. Feng, S. Kuang, C. Tu, Z. Ma, J. Pang i wsp., *Natural products berberine and curcumin exhibited better ameliorative effects on rats with non-alcohol fatty liver disease than lovastatin*, Biomed. Pharmacother., 2018, 99, 325-333.
36. S. Spinuzzi, C. Colliva, C. Camborata, M. Roberti, C. Ianni i wsp., *Berberine and its metabolites: relationships between physicochemical properties and plasma levels after administration to human subjects*, J. Nat. Prod., 2014, 77(4), 766-772.
37. M.A. Neag, A. Mocan, J. Echeverria, R.M. Pop, C.I. Bocsan i wsp., *Berberine: botanical occurrence, traditional uses, extraction methods and relevance in cardiovascular, metabolic, hepatic and renal disorders*, Front. Pharmacol., 2018, 9, 557.
38. M.J. Iqbal, C. Quispe, Z. Javed, H. Sadia, Q.R. Qadri, S. Raza i wsp., *Nanotechnology-based strategies for berberine delivery system in cancer treatment: pulling strings to keep berberine in power*, Front. Mol. Biosci., 2021, 7, 624494.

39. R. Samineni, J. Chinakurthy, S. Konidala, *Emerging role of Biopharmaceutical Classification and Biopharmaceutical drug disposition system in dosage form development: A systematic review*, Turk. J. Pharm. Sci., 2022, 19(6), 706-713.
40. J.M. Moon, K.M. Ratliff, A.M. Hagele, R.A. Stecker, P.W. Mumford i wsp., *Absorption kinetics of berberine and dihydroberberine and their impact on glycemia: a randomized, controlled, crossover pilot trial*, Nutrients, 2022, 14(1), 124.
41. S.Y. Gui, L. Wu, D.Y. Peng, Q.Y. Liu, B.P. Yin i wsp., *Preparation and evaluation of a microemulsion for oral delivery of berberine*, Die Pharmazie, 2008, 63(7), 516-519.
42. M. Marino, C. Gardana, A. Scialpi, G. Giorgini, P. Simonetti i wsp., *An in vitro approach to study the absorption of a new oral formulation of berberine*, PharmaNutrition, 2021, 18, 100279.
43. G.U. Sailor, V.D. Ramani, N. Shah, G.R. Parmar, D. Gohil i wsp., *Design of experiment approach based formulation optimization of berberine solid lipid nanoparticle for antihyperlipidemic activity*, Indian J. Pharm. Sci., 2021, 83(2), 204-218.
44. T.T. Duong, T.T.H. Yen, L.T. Nguyen, T.D. Nguyen, T.Q.T. Nguyen i wsp., *Berberine-loaded liposomes for oral delivery: preparation, physicochemical characterization and in vivo evaluation in an endogenous hyperlipidemic animal model*, Int. J. Pharm., 2022, 616, 121525.
45. S.S. Solanki, L.K. Soni, R.K. Maheshwari, *Study of mixed solvency concept in formulation development of aqueous injection of poorly water soluble drug*, J. Pharm. (Cairo), 2013, 678132.
46. J.M. Lee, K.M. Park, S.J. Lim, M.K. Lee, C.K. Kim, *Microemulsion formulation of clonixic acid; solubility enhancement and pain reduction*, J. Pharm. Pharmacol., 2002, 54, 43-49.
47. A.A. Date, M.S. Nagarsenker, *Parenteral microemulsions: an overview*, Int. J. Pharm., 2008, 355, 19-30.
48. A. Sakamoto, K. Sugano, *Dissolution profiles of poorly soluble drug salts in bicarbonate buffer*, Pharm. Res., 2023, 40, 989-998.
49. P. Makary, *Principles of salt formation*, UK J. Pharm. & Biosci., 2014, 2(4), 2.
50. Y. Yamini, N. Feizi, M. Morandi, *Surfactant-based extracion systems*, Liquid-Phase Extraction, Chapter 7, 2020, 209-239.

51. M. A. Krstonošić, D. Sazdanić, D. Ćirin, N. Maravić, M. Mikulić i wsp., *Aqueous solutions of non-ionic surfactant mixtures as mediums for green extraction of polyphenols from red grape pomace*, *Sust. Chem. and Pharm.*, 2023, 33, 101069.
52. M. Giacomo, F.A. Bertoni, M.V. Rocha, B.B. Nerli, F. Rodríguez, *Cloud point extraction based on non-ionic surfactants: An ecofriendly tool for recovering papain from papaya latex*, *J. Environ. Chem. Eng.*, 2022, 10, 108762.
53. N.B. Shestopalova, Y.A. Fomina, R.K. Chernova, *Spectrophotometric Determination of Azorubine and Ponceau 4R in pharmaceutical preparations using micellar extraction*, *J. Anal. Chem.*, 2022, 77, 1073–1081.
54. H. Wu, Z. Wang, Y. Zhao, Y. Gao, H. Zhang i wsp., *Effect of Span 20 feeding zone in the twin screw extruder on the properties of amorphous solid dispersion of ritonavir*, *Pharmaceutics*, 2023, 15, 441.
55. D. Möbius, R. Miller, V.B. Fainerman, *Surfactants: chemistry, interfacial properties and applications*, 1st Edition, 2001, ISBN 9780080542133, Elsevier.
56. F. Mustan, N. Politova-Brinkova, Z. Vinarov, D. Rosetti, P. Rayment i wsp., *Interplay between bulk aggregates, surface properties and foam stability of nonionic surfactants*, *Ad. Colloid Interface Sci.*, 2022, 302, 102618.
57. R. Kurpanik, A. Lechowska-Liszka, J. Mastalska-Popławska, M. Nocuń, A. Rapacz-Kmita i wsp., *Effect of ionic and non-ionic surfactant on bovine serum albumin encapsulation and biological properties of emulsion-electrospun fibers*, *Molecules*, 2022, 27, 3232.
58. M. Basu, P.A. Hassan, S. B. Shelar, *Modulation of surfactants self-assembly in deep eutectic solvents and its relevance to drug delivery- A review*, *J. Mol. Liq.*, 2023, 375, 121301.
59. J.M. Rosen, *Surfactants and Interfacial Phenomena*, 3rd Edition, Wiley Interscience, 2004, New York.
60. S. Perumal, R. Atchudan, W. Lee, *A review of polymeric micelles and their applications*, *Polymers*, 2022, 14(12), 2510.
61. A.M. Ihaveri, V.P. Torchilin, *Multifunctional polymeric micelles for delivery of drugs and siRNA*, *Front. Pharmacol.*, 2014, 5.

62. B. Jańczuk, A. Zdziennicka, K. Szymczyk, M.L. Gonzalez-Martin, *Prediction of aqueous solution surface tension of some surfactant mixtures and composition of their monolayers at the solution-air interface*, *Colloids Interfaces*, 2021, 5(4), 53.
63. J. Zawała, A. Wiertel-Pochopień, P.B. Kowalczyk, *Critical synergetic concentration of binary surfactant mixtures*, *Minerals*, 2020, 10(2), 192.
64. M.J. Rosen, X.Y. Hua, *Surface concentration and molecular interactions in binary mixtures of surfactants*, *J. Coll. Int. Sci.*, 1982, 86(1), 164-172.
65. E.D. Hugger, B.L. Novak, P.S. Burton, K.L. Audus, R.T. Borchardt, *A comparison of commonly used polyetoxylated pharmaceutical excipients on their ability to inhibit P-glycoprotein activity in vitro*, *J. Pharm. Sci.*, 2002, 91(9), 1991-2002.
66. R.A. Petros, J.M. DeSimonne, *Strategies in the design of nanoparticles for therapeutic applications*, *Nat. Rev. Drug Discov.*, 2010, 9, 615-627.
67. K.I. Parikh, K.K. Sawant, *Solubilization of vardenafil HCl in lipid-based formulations enhances its oral bioavailability in vivo: a comparative study using Tween 20 and Cremophor EL*, *J. Mol. Liq.*, 2019, 277, 189-199.
68. P.B. Memvanga, V. Preat, *Formulation design and in vivo antimalarial evaluation of lipid-based drug delivery systems for oral delivery of β -arteether*, *Eur. J. Biopharm.*, 2012, 82(1), 112-119.
69. H. Kang, K.H. Cha, W. Cho, J. Park, H.J. Park i wsp., *Cyclosporine amellar delivery systems for dry eyes*, *Int. J. Nanomedicine*, 2016, 11, 2921-2933.
70. T.R. Buggins, P.A. Dickinson, G. Taylor, *The effects of pharmaceutical excipients on drug disposition*, *Adv. Drug Deliv. Rev.*, 2007, 59, 1482-1503.
71. Y. Li, N. Chen, M. Palmisano, S. Zhou, *Pharmacologic sensitivity of paclitaxel to its delivery vehicles drives distinct clinical outcomes of paclitaxel formulations*, *Mol. Pharm.*, 2015, 12(4), 308-317.
72. F. Gustaman, K. Idacahyati, W.T. Wulandari, F. Setiawan, I. Indra, *Improvement of the dissolution profile of simvastatin tablets with the addition of Cremophor EL using wet granulation method*, *Int. J. App. Pharm.*, 2021, 13(4), 244-246.
73. S.H. Seo, E. Kim, Y. Joo, J. Lee, K.T. Oh i wsp., *A mixed micellar formulation for the transdermal delivery of an indirubin analog*, *Pharmaceutics*, 2020, 12(2), 175.

74. L.A. Alenazy, K. Hinthner, F. AlMuhizi, M. Fein, C. Tsoukas i wsp., *Tolerance of the mRNA COVID-19 vaccines in patients with reported taxane reactions*, *J. Allergy Clin. Immunol. Pract.*, 2022, 10(8), 2169-2171.
75. T. Li, R.V. Lalla, D.J. Burgess, *Enhanced drug loading of in situ forming gels for oral mucositis pain control*, *Int. J. Pharm.*, 2021, 595, 120225.
76. S. Treesinchai, S. Puttipipatkachorn, T. Pitakssuteepong, S. Sungthongjeen, *Development of curcumin floating beads with low density materials and solubilizers*, *J. Drug Deliv. Sci. Tech.*, 2019, 51, 542-551.
77. G.E. Chae, D.W. Kim, H.E. Jin, *Development of squalene-based oil-in-water emulsion adjuvants using a self-emulsifying drug delivery systems for enhanced antigen-specific antibody titers*, *Int. J. Nanomedicine*, 2022, 17.
78. S. Jain, N. Kumar, R. Sharma, R. Ghadi, T. Date i wsp., *Self-nanoemulsifying formulation for oral delivery of sildenafil: effect on physicochemical attributes and in vivo pharmacokinetics*, *Drug Del. and Transl. Res.*, 2023, 13, 839-851.
79. S.T. Galatage, R. Trivedi, D.A. Bhagwat, *Oral self-emulsifying nanoemulsion systems for enhancing dissolution, bioavailability and anticancer effects of camptothecin*, *J. Drug Deliv. Sci. Tech.*, 2022, 78, 103929.
80. B. Lang, J.W. McGinity, R.O. Williams, *Dissolution enhancement of itraconazole by hot-melt extrusion alone and the combination of hot-melt extrusion and rapid freezing-effect of formulation and processing variables*, *Mol. Pharm.*, 2014, 11, 186-196.
81. V.M. Krishna, V.B. Kumar, N. Dudhipala, *In-situ intestinal absorption and pharmacokinetic investigations of carvedilol loaded supersaturated self-emulsifying drug systems*, *Pharm. Nanotech.*, 2020, 8(3), 207-224.
82. H.J. Kwon, E.J. Heo, Y.H. Kim, S. Kim, Y.H. Hwang i wsp., *Development and evaluation of poorly water-soluble celecoxib as solid dispersions containing nonionic surfactants using fluidized-bed granulation*, *Pharmaceutics*, 2019, 11(3), 136.
83. F. Liu, Y. Zhou, L. Liu, H. Pan, H. Liu, *Effect of 2-ethylbutyric acid on thermodynamics stability of various nonionic surfactants tanshione-loaded micelles*, *J. Mol. Liq.*, 2022, 362, 119775.

84. E.V. Akhlyustina, G A Meerovich, I.G. Tiganova, E.A. Makarova, N.I. Philipova i wsp., *New cationic photosensitizers: photophysical properties and results of preliminary studies of antibacterial efficacy*, J. Phys., 2019, 1189, 012033.
85. N.M. Cortés, G. Lorenzo, A.N. Califano, *Food grade microemulsion systems: Sunflower oil/castor oil derivative-ethanol/water. Rheological and physicochemical analysis*, Food Res. Int., 2018, 107, 41-47.
86. S.L. Childs, P. Kandi, S.R. Lingireddy, *Formulation of a danazol supersaturation plays an essential role in improving bioavailability*, Mol. Pharm., 2013, 10, 8, 3112-3127.
87. L.K. Yeo, T.O.B. Olunsanya, C.S. Chaw, A.A. Elkordy, *Brief effect of a small hydrophobic drug (cinnarizine) on the physicochemical characterisation of niosomes produced by thin-film hydration and microfluidic methods*, Pharmaceutics, 2018, 10(4), 185.
88. I. Matsaridou, P. Barmpalexis, A. Salis, I. Nikolakakis, *The influence of surfactant HLB and oil/surfactant ratio on the formation and properties of self-emulsifying pellets and microemulsion reconstitution*, AAPS Pharm. Sci. Tech., 2012, 13, 1319-1330.
89. A.P. Krawczyk-Santos, R.N. Marreto, A. Concheiro, C. Alvarez-Lorenzo, Stephânia F. Taveira, *Poly(pseudo)rotaxanes formed by mixed micelles and α -cyclodextrin enhance terbinafine nail permeation to deeper layers*, Int. J. Pharm., 2022, 4, 100118.
90. M.A. Khan, K. Ullah, N. ur Rahman, A. Mahmood, A. Müllertz i wsp., *Formulation, characterization and in-vitro evaluation of self-nanoemulsifying drug delivery system containing rhamnolipid biosurfactant*, J. Drug Deliv. Sci. Technol., 2022, 75, 103673.
91. G.E. Chae, D.W. Kim, H.E. Jin, *Development of squalene-based oil-in-water emulsion adjuvants using a self-emulsifying drug delivery systems for enhanced antigen-specific antibody titers*, Int. J. Nanomed., 2022, 17, 6221-6231.
92. Y. Ma, J. Yang, Y. Zhang, C. Zheng, Z. Liang i wsp., *Development of a naringenin microemulsion as a prospective ophthalmic delivery system for the treatment of corneal neovascularization: in vitro and in vivo evaluation*, Drug Deliv., 2022, 29, 111-127.

93. X. Wei, S. Wei, L. Ke Gang, Z.Z. Feng, C.W. San i wsp., *Dual-functional Brij S20 modified nanocrystal formulation enhances the intestinal transport and oral bioavailability of berberine*, *Int. J. Nanomedicine*, 2018, 13, 3781-3793.
94. R. Berthelsen, R. Holm, J. Jacobsen, J. Kristensen, B. Abrahamsson i wsp., *Kolliphor surfactants affect solubilization and bioavailability of fenofibrate. Studies of in vitro digestion and absorption in rats*, *Mol. Pharm.*, 2015, 12, 1062-1071.
95. A. Christensen, T. Backensfeld, W. Weitschies, *Effect of nonionic surfactants on in vitro triglyceride digestion and their susceptibility to digestion by pancreatic enzymes*, *J. Pharm. Sci.*, 2010, 41(2), 376-382.
96. H. Gelderblom, J. Verweij, K. Nooter, A. Sparreboom, *A Cremophor EL: the drawbacks and advantages of vehicle selection for drug formulation*, *Eur. J. Cancer*, 2001, 37(13), 1590-1598.
97. C.J. van Oss, *Interfacial forces in aqueous media*, 1994, Marcel Dekker, New York.
98. C.J. van Oss, P.M. Constanzo, *Adhesion of nonionic surfactants to polymer surfaces and low energy materials*, *J. Adhes. Sci. Technol.*, 1992, 4, 477-487.
99. C.J. van Oss, R.I. Good, *Surface tension and the solubility of polymers and biopolymers: The role of polar and apolar interfacial free energies*, *J. Macromol. Sci. Chem.*, 1989, 26, 1183-1203.
100. C.I. van Oss, M.K. Chaundhury, R.I. Good, *Monopolar surfaces*, *Adv. Coll. Inteface Sci.*, 1987, 28, 35-64.
101. F.M. Fowkes, *Attractive forces at interfaces*, *Ind. Eng. Chem.*, 1964, 56, 40-52.
102. A. Zdziennicka, K. Szymczyk, J. Krawczyk, B. Jańczuk, *Critical micelle concentration of some surfactants and thermodynamic parameters of their micellization*, *Fluid Phase Eq.*, 2012, 322-323, 126-134.
103. A. Zdziennicka, K. Szymczyk, J. Krawczyk, B. Jańczuk, *Some remarks on the solid surface tension determination from contact angle measurements*, *Appl. Surf. Sci.*, 2017, 405, 88-101.
104. W. Adamson, A.P. Gast, *Physical chemistry of surfaces*, 6th Edition, Wiley Interscience, New York, 1997.

105. K. Szymczyk, A. Lewandowski, A. Zdziennicka, M. Szaniawska, B. Jańczuk, *Behavior of Auramine O in the aqueous solution of the Kolliphors and their mixture*, *Molecules*, 2022, 27, 8493.
106. B. Jańczuk, J.A. Mendez-Sierra, M.L. Gonzalez-Martin, J.M. Bruque, W. Wójcik, *Properties of decylammonium chloride and cesium perfluorooctanate at interfaces and standard free energy of their adsorption*, *J. Colloid Interface Sci.*, 1997, 192, 408-414.
107. S. Chauhan, K. Sharma, *Extended studies on molecular interactions of SDBS and DTAB in aqueous solutions of amino acid at T=293,15 – 313,5K*, *J. Mol. Liq.*, 2015, 211, 675-685.

9. PODSUMOWANIE DOROBKU NAUKOWEGO

9.1. Publikacje naukowe

Lista publikacji naukowych stanowiących podstawę postępowania doktorskiego:

[D1] K. Szymczyk, **M. Szaniawska**, K. Terpiłowski*, Determination of acoustical parameters of aqueous solution of Kolliphors binary mixtures using density, speed of sound, viscosity and surface tension measurements. *Journal of Surfactants and Detergents*, 2019, 22(5), 1163–1174.

[D2] K. Szymczyk*, **M. Szaniawska**, J. Krawczyk, Temperature effect on the adsorption and volumetric properties of aqueous solutions of Kolliphor ELP®. *Molecules*, 2020, 25(3), 743.

[D3] **M. Szaniawska**, K. Szymczyk, A. Zdziennicka, B. Jańczuk*, Adsorption properties and composition of binary Kolliphor mixtures at the air-water interface at different temperatures, *Molecules*, 2022, 27(3), 877.

[D4] **M. Szaniawska**, K. Szymczyk*, A. Zdziennicka, B. Jańczuk, Thermodynamic parameters of berberine with Kolliphor mixtures adsorption and micellization, *Molecules*, 2023, 28(7), 3115.

Inne publikacje naukowe:

1. K. Szymczyk, **M. Szaniawska**, A. Taraba, *Micellar parameters of aqueous solutions of Tween 20 and 60 at different temperatures: volumetric and viscometric study*, *Colloids and Interfaces*, 2018, 2, 34.
2. K. Terpiłowski, **M. Szaniawska**, Surface properties of graphene and graphene/diamond composites located at a substrate with tungsten carbide doped by metals composites, *Adsorption*, 2019, 25(3), 513-520.
3. K. Szymczyk, A. Taraba, **M. Szaniawska**, *Interactions of Tween 20, 60 and 80 with dye molecules: Spectroscopic analysis*, *Journal of Molecular Liquids*, 2019, 290, 111227.
4. P. Wojtoń, **M. Szaniawska**, L. Hołysz, R. Miller, A. Szcześ, *Surface activity of natural surfactants extracted from Sapindus mukorossi and Sapindus trifoliatus soapnuts*, *Colloids and interfaces*, 2021, 5(1), 7.

5. K. Szymczyk, A. Lewandowski, A. Zdziennicka, **M. Szaniawska**, B. Jańczuk, *Behavior of Auramine O in the Aqueous Solution of Two Kolliphors and Their Mixture*, *Molecules*, 2022, 27(23), 8493.
6. **M. Szaniawska**, *Strategies in poorly soluble drug delivery systems*, *Annales Universitatis Mariae Curie-Skłodowska Lublin Polonia, Sectio AA*, 2018, 73 (1), 81-98.
7. **M. Szaniawska**, A. Taraba, K. Szymczyk, *Budowa, właściwości i zastosowanie antocyjanów*, *Nauki Inżynierskie i Technologie*, 2015, 2(17).
8. A. Taraba, **M. Szaniawska**, K. Szymczyk, *Polifenole – charakterystyka i prozdrowotne zastosowania*, *Zagadnienia aktualnie poruszane przez młodych naukowców 3, Tom I*, 2015, ISBN: 978-83-63058-50-0, Wyd. Creative, 253–256.
9. A. Taraba, **M. Szaniawska**, K. Szymczyk, *Wygaszanie fluorescencji pirenu w roztworach surfaktantu niejonowego*, *Fundacja na rzecz nauki TYGIEL, Wybrane zagadnienia inżynierii produkcji w zastosowaniach medycznych*, Edytorzy: R. Karpiński, J. Zubrzycki, J. Maksymiuk, 2015, ISBN 978-83-65272-04-1, 55–65.
10. **M. Szaniawska**, A. Taraba, K. Szymczyk, *Piren a spektroskopia fluorescencyjna*, *IV Wrocławska Konferencja Studentów Nauk Technicznych i Ścisłych Puzzel 2015*, Edytor: Oskar Uchański, 2015, ISBN 978-83-937278-2-7, 59–63.
11. **M. Szaniawska**, A. Taraba, *Zastosowanie surfaktantów w procesie ekstrakcji do fazy ciekłej*, *Badania i rozwój młodych naukowców w Polsce, Nauki przyrodnicze, część I*, Redakcja: Monika Panfil, Poznań 2017, ISBN 978-83-65677-79-2, 129–134.
12. **M. Szaniawska**, A. Taraba, *Spektroskopia fluorescencyjna jako metoda wyznaczenia krytycznego stężenia micelizacji Tweenu 20*, *Badania i rozwój młodych naukowców w Polsce, Nauki przyrodnicze, część I*, Redakcja: Monika Panfil, Poznań 2017, ISBN 978-83-65677-79-2, 135–140.
13. A. Taraba, **M. Szaniawska**, *Metody identyfikacji metabolitów flawonoidów i ich aktywność biologiczna*, *Badania i rozwój młodych naukowców w Polsce, Nauki przyrodnicze, część I*, Redakcja: Monika Panfil, Poznań 2017, ISBN 978-83-65677-79-2, 141–146.
14. A. Taraba, **M. Szaniawska**, *Absorpcja jako jeden z mechanizmów regulujących bioaktywność flawonoidów*, *Badania i rozwój młodych naukowców w Polsce*,

- Nauki przyrodnicze, część I, Redakcja: Monika Panfil, Poznań 2017, ISBN 978-83-65677-79-2, 147–152.
15. **M. Szaniawska**, A. Taraba, K. Szymczyk, *Determination of CMC values of the surfactant solutions*, EYEC Monograph 6th European Young Engineers Conference, Editors: Bartosz Nowak, Łukasz Werner, Patrycja Wierzba, Warsaw University of Technology, 2017, ISBN 978-83-936575-4-4, 186–193.
 16. A. Taraba, **M. Szaniawska**, *Polyphenols – description and preliminary study of alcohol extraction*, EYEC Monograph 6th European Young Engineers Conference, Editors: Bartosz Nowak, Łukasz Werner, Patrycja Wierzba, Warsaw University of Technology, 2017, ISBN 978-83-936575-4-4, 194–201.
 17. A. Taraba, **M. Szaniawska**, *Metody pomiaru aktywności przeciwutleniającej polifenoli*, Badania i rozwój młodych naukowców w Polsce, Nauki przyrodnicze, część IV, Redakcja: Jędrzej Nyckowiak, Jacek Leśny, Poznań 2017, ISBN 978-83-65917-16-4, 109–114.
 18. A. Taraba, **M. Szaniawska**, *Terpenoidy – naturalne związki organiczne*, Badania i rozwój młodych naukowców w Polsce, Nauki przyrodnicze, część IV, Redakcja: Jędrzej Nyckowiak, Jacek Leśny, Poznań 2017, ISBN 978-83-65917-16-4, 115–120.
 19. M. Chodkowski, **M. Szaniawska**, A. Taraba, *Wettability of the plasma-activated glass plates with deposited 3-bromopyruvic acid*, EYEC Monograph 7th European Young Engineers Conference, Editor: Bartosz Nowak, Warsaw University of Technology, 2018, ISBN 978-83-936575-1, 67–78.
 20. M. Chodkowski, **M. Szaniawska**, A. Taraba, *Effect of the plasma treatment on wettability and surface free energy of paper composites*, EYEC Monograph 7th European Young Engineers Conference, Editor: Bartosz Nowak, Warsaw University of Technology, 2018, ISBN 978-83-936575-1, 79–94.
 21. **M. Szaniawska**, *Alkaloidy – budowa, właściwości i zastosowania*, Badania i rozwój młodych naukowców w Polsce, Nauki przyrodnicze, część II, Redakcja: Jędrzej Nyckowiak, Jacek Leśny, Poznań 2020, ISBN 978-83-66743-01-4, str. 144-150.
 22. **M. Szaniawska**, *Surfaktanty – właściwości i zastosowanie układów micelarnych*, Badania i rozwój młodych naukowców w Polsce, Nauki

przyrodnicze, część II, Redakcja: Jędrzej Nyckowiak, Jacek Leśny, Poznań 2020, ISBN 978-83-66743-01-4, str. 136-143.

23. **M. Szaniawska**, *Characterization of alkaloids – secondary plant metabolites*, QUAERE (vol.X), Published by MAGNANIMITAS, Czech Republic, 2020, str. 515-521, ISBN 978-80-87952-32-0.

9.2. Konferencje naukowe

Osiągnięcia naukowo-badawcze, w ramach których propagowano zagadnienia oraz tematykę badawczą związaną z cyklem postępowania doktorskiego, od momentu przyjęcia na studia doktoranckie, przedstawiłam na 37 konferencjach, 18 ogólnopolskich oraz 19 międzynarodowych.

Na konferencjach naukowych wygłosiłam 16 komunikatów ustnych oraz przedstawiłam 50 posterów naukowych.

Wystąpienia ustne

1. **M. Szaniawska**, A. Taraba, *O antocyjanach słów kilka*, VI Kongres Młodych Ludzi Nauki - wizja, nauka, postęp, 25.02.2017, Kraków.
2. **M. Szaniawska**, A. Taraba, K. Szymczyk, *Oznaczanie zawartości polifenoli w owocach*, VI Wroclawska Konferencja Studentów Nauk Technicznych i Ścisłych „PUZZEL”, 1-2.04.2017, Wrocław.
3. **M. Szaniawska**, *Absorption and emission spectra of pyrene in surfactant solutions*, 49. Symposium on Catalysis, 6-7.11.2017, Praga, Czechy.
4. **M. Szaniawska**, A. Taraba, K. Szymczyk, *Właściwości adsorpcyjne i objętościowe surfaktantów niejonowych z grupy Tween*, The International Conference of Natural and Medical Sciences: Young Scientists, PhD Students and Students, 1-3.12.2017, Lublin.
5. **M. Szaniawska**, A. Taraba, K. Szymczyk, *Oznaczanie polifenoli w herbatach metodą Folina-Ciocalteu*, The International Conference of Natural and Medical Sciences: Young Scientists, PhD Students and Students, 1-3.12.2017, Lublin.

6. **M. Szaniawska**, A. Taraba, K. Szymczyk, *Adsorption and volumetric properties of surfactants used in extraction process*, 16th Young Researchers Conference Materials Science and Engineering, 6-8.12.2017, Belgrad, Serbia.
7. **M. Szaniawska**, A. Taraba, K. Szymczyk, *Właściwości adsorpcyjne i objętościowe surfaktantów niejonowych stosowanych w przemyśle farmaceutycznym*, VII Ogólnopolska Konferencja Naukowa Młodzi Naukowcy w Polsce - Badania i Rozwój, 11.05.2018, Lublin.
8. **M. Szaniawska**, A. Taraba, K. Szymczyk, *Anthocyanins – structure, properties and applications*, 7th International Young Scientist Conference “Human-Nutrition-Environment”, 4-5.06.2018, Rzeszów.
9. **M. Szaniawska**, A. Taraba, K. Szymczyk, *Tween surfactants – adsorption and volumetric properties*, XII Copernican International Young Scientists Conference, 28-29.06.2018, Toruń.
10. **M. Szaniawska**, K. Szymczyk, *Badanie właściwości objętościowych surfaktantów niejonowych typu Kolliphor*, Młodzi Naukowcy w Polsce – Badania i rozwój, 23.11.2018, Lublin.
11. **M. Szaniawska**, *Badanie właściwości objętościowych surfaktantów niejonowych typu Kolliphor*, IX Ogólnokrajowa Konferencja Naukowa Młodzi Naukowcy w Polsce – Badania i Rozwój, 5.04.2019, Lublin.
12. **M. Szaniawska**, K. Szymczyk, *Dwuskładnikowe mieszaniny surfaktantów niejonowych typu Kolliphor – właściwości adsorpcyjne i objętościowe*, Ogólnopolska Konferencja Fizykochemia granic faz – metody instrumentalne, 13-17.05.2019, Lublin.
13. **M. Szaniawska**, *Właściwości surfaktantów stosowanych w procesie solubilizacji*, Wirtualna Konferencja Młodych Przyrodników, 24-29.06.2019, online.
14. **M. Szaniawska**, *Badania spektroskopowe surfaktantów niejonowych i ich dwuskładnikowych mieszanin*, Wirtualna Konferencja Młodych Przyrodników, 30.12.2019-5.01.2020, online.
15. **M. Szaniawska**, *Characterization of alkaloids – secondary plant metabolites*, Interdisciplinary Scientific Conference for PhD. students and assistants, 22.06-26.06.2020, Czechy, online.

16. **M. Szaniawska**, K. Szymczyk, Właściwości adsorpcyjne i objętościowe dwuskładnikowych mieszanin surfaktantów niejonowych, Kopernikańskie e-seminarium Doktoranckie, 7.09.2020, Toruń, online.

Postery naukowe

1. **M. Szaniawska**, A. Taraba, K. Szymczyk, *Effect of surfactant and temperature on the emission spectra of pyrene*, 15th Ukrainian - Polish Symposia on Theoretical and Experimental Studies of Interfacial Phenomena and their Technological Applications, 12-15.09.2016, Lwów, Ukraina.
2. **M. Szaniawska**, A. Taraba, K. Szymczyk, *UV-Vis study of pyrene in nonionic surfactant solutions*, 15th Ukrainian - Polish Symposia on Theoretical and Experimental Studies of Interfacial Phenomena and their Technological Applications, 12-15.09.2016, Lwów, Ukraina.
3. **M. Szaniawska**, A. Taraba, K. Szymczyk, B. Jańczuk, *Krytyczne stężenie micelizacji surfaktantów niejonowych, pochodnych D-sorbitu*, 59 Ogólnopolski Zjazd Naukowy Polskiego Towarzystwa Chemicznego, 19-23.09.2016, Poznań.
4. **M. Szaniawska**, A. Taraba, K. Szymczyk, B. Jańczuk, *Piren jako znacznik fluorescencyjny w roztworach surfaktantów niejonowych, pochodnych D-sorbitu*, 59 Ogólnopolski Zjazd Naukowy Polskiego Towarzystwa Chemicznego, 19-23.09.2016, Poznań.
5. **M. Szaniawska**, A. Taraba, K. Szymczyk, M. Chodkowski, *Antyoksydanty w żywności*, Zjazd Zimowy Sekcji Studenckiej PTChem, 17.12.2016, Lublin.
6. **M. Szaniawska**, A. Taraba, K. Szymczyk, *Wpływ temperatury na wartość współczynnika dyfuzji surfaktantów niejonowych, pochodnych D-sorbitu*, I Ogólnopolska Konferencja Fizykochemia granic faz- metody instrumentalne, 23-26.04.2017, Lublin.
7. **M. Szaniawska**, A. Taraba, K. Szymczyk, *Badania spektroskopowe wodnych roztworów surfaktantów typu Tween*, I Ogólnopolska Konferencja Fizykochemia granic faz- metody instrumentalne, 23-26.04.2017, Lublin.

8. **M. Szaniawska**, A. Taraba, K. Szymczyk, *Determination of CMC values of the surfactant solutions*, 6th European Young Engineers Conference, 24-26.04.2017, Warszawa.
9. **M. Szaniawska**, A. Taraba, K. Szymczyk, *Metody spektroskopowe w analizie wodnych roztworów surfaktantu*, V Ogólnopolskie Sympozjum Nauka i przemysł - lubelskie spotkania studenckie, 20.06.2017, Lublin.
10. **M. Szaniawska**, A. Taraba, K. Szymczyk, *The effect of temperature on values of diffusion coefficients of nonionic Tween surfactants*, 31st Conference of The European Colloid and Interface Society, 3-8.09.2017, Madryt, Hiszpania.
11. **M. Szaniawska**, A. Taraba, K. Szymczyk, *Spectroscopic study of aqueous solutions of nonionic surfactants, derivatives of D-sorbitol*, 31st Conference of The European Colloid and Interface Society, 3-8.09.2017, Madryt, Hiszpania.
12. **M. Szaniawska**, A. Taraba, K. Szymczyk, *Porównanie wartości współczynnika dyfuzji surfaktantów typu Tween*, 60 Zjazd Polskiego Towarzystwa Chemicznego, 17-21.09.2017, Wrocław.
13. **M. Szaniawska**, A. Taraba, K. Szymczyk, *Folin-Ciocalteu method in determination of polyphenols in tea extracts*, 7th European Young Engineers Conference, 23-25.04.2018, Warszawa.
14. **M. Szaniawska**, A. Taraba, K. Szymczyk, *Determination of antioxidant activity of coffee and tea extracts by DPPH method*, 7th European Young Engineers Conference, 23-25.04.2018, Warszawa.
15. **M. Szaniawska**, A. Taraba, K. Szymczyk, *Determination of critical micelle concentration of Kolliphor surfactants from the absorption and emission spectra of pyrene*, 7th European Young Engineers Conference, 23-25.04.2018, Warszawa.
16. **M. Szaniawska**, A. Taraba, K. Szymczyk, *Antioxidant properties of tea extracts*, 7th International Young Scientist Conference Human-Nutrition-Environment, 4-5.06.2018, Rzeszów.
17. **M. Szaniawska**, A. Taraba, K. Szymczyk, M. Chodkowski, *Metody spektroskopowe w analizie surfaktantu typu Kolliphor*, Nauka i Przemysł -lubelskie spotkania studenckie, 25.06.2018, Lublin.

18. **M. Szaniawska**, A. Taraba, K. Szymczyk, *Critical Micelle Concentration of Kolliphor Surfactants – spectroscopic methods*, XII Copernican International Young Scientists Conference, 28-29.06.2018, Toruń.
19. **M. Szaniawska**, A. Taraba, K. Szymczyk, *Density and viscosity study in Kolliphor surfactants*, XVI Polish – Ukrainian Symposium Theoretical and Experimental Studies of Interfacial Phenomena and Their Technological Applications, 28-31.08.2018, Lublin.
20. **M. Szaniawska**, A. Taraba, K. Szymczyk, *UV-Vis study of pyrene in Kolliphor surfactant solutions*, XVI Polish – Ukrainian Symposium Theoretical and Experimental Studies of Interfacial Phenomena and Their Technological Applications, 28-31.08.2018, Lublin.
21. **M. Szaniawska**, A. Taraba, K. Szymczyk, *Effect of temperature on the emission spectra of pyrene in Kolliphor ELP solutions*, XVI Polish – Ukrainian Symposium Theoretical and Experimental Studies of Interfacial Phenomena and Their Technological Applications, 28-31.08.2018, Lublin.
22. **M. Szaniawska**, A. Taraba, K. Szymczyk, *Spectroscopic study of aqueous solutions of Kolliphor surfactants*, Tenth International Symposium Surface Heterogeneity Effects in Adsorption, Catalysis and Related Phenomena, ISSHAC-10, 27-31.08. 2018, Lublin.
23. **M. Szaniawska**, A. Taraba, K. Szymczyk, *Adsorption properties of Kolliphor surfactants*, Tenth International Symposium Surface Heterogeneity Effects in Adsorption, Catalysis and Related Phenomena, ISSHAC-10, 27-31.08. 2018 Lublin.
24. **M. Szaniawska**, K. Szymczyk, *Sweeteners in food industry*, 8th European Young Engineers Conference, 8-10.04.2019, Warszawa.
25. **M. Szaniawska**, K. Szymczyk, *Kolliphor surfactants – adsorption properties*, 8th European Young Engineers Conference, 8-10.04.2019, Warszawa.
26. **M. Szaniawska**, *Metoda Folina-Ciocalteu – wyznaczenie zawartości polifenoli w herbatach*, Dokonania Naukowe Doktorantów VII Edycja, 14.04.2019, Warszawa,

27. **M. Szaniawska**, *Krytyczne stężenie micelizacji surfaktantów typu Kolliphor – metody spektroskopowe*, *Dokonania Naukowe Doktorantów VII Edycja*, 14.04.2019, Warszawa.
28. **M. Szaniawska**, *Właściwości adsorpcyjne surfaktantów niejonowych typu Kolliphor*, *Dokonania Naukowe Doktorantów VII Edycja*, 14.04.2019, Warszawa.
29. **M. Szaniawska**, K. Szymczyk, *Badania gęstości i lepkości surfaktantów niejonowych stosowanych w przemyśle farmaceutycznym*, *Ogólnopolska Konferencja Fizykochemia granic faz- metody instrumentalne*, 13-17.05.2019, Lublin.
30. **M. Szaniawska**, K. Szymczyk, *Micropolarity and microviscosity study of binary mixtures of Kolliphor surfactants*, *European Student Colloid Conference*, 18-22.06.2019, Warna, Bułgaria.
31. **M. Szaniawska**, *Berberyna – alkaloid o prozdrowotnych właściwościach*, *Wirtualna Konferencja Młodych Przyrodników*, 24-29.06.2019, online.
32. **M. Szaniawska**, K. Szymczyk, *Badania właściwości surfaktantów niejonowych typu Kolliphor i ich mieszanin z berberyną*, 62. Zjazd Polskiego Towarzystwa Chemicznego, 2-6.09.2019, Warszawa.
33. **M. Szaniawska**, K. Szymczyk, *Badania spektroskopowe surfaktantów niejonowych z grupy Kolliphor i ich mieszanin z berberyną*, 62. Zjazd Polskiego Towarzystwa Chemicznego, 2-6.09.2019, Warszawa.
34. **M. Szaniawska**, K. Szymczyk, *Interactions in alkaloid-surfactant systems. Part 1*, 7th International Conference „Nanotechnologies and nanomaterials” NANO 2019, 27-30.2019, Lwów, Ukraina.
35. **M. Szaniawska**, K. Szymczyk, *Interactions in alkaloid-surfactant systems. Part 2*, 7th International Conference „Nanotechnologies and nanomaterials” NANO 2019, 27-30.2019, Lwów, Ukraina.
36. **M. Szaniawska**, K. Szymczyk, *Adsorption and volumetric properties of surfactants and their binary mixtures used in pharmaceutical industry. Part 1*, 7th International Conference „Nanotechnologies and nanomaterials” NANO 2019, 27-30.2019, Lwów, Ukraina.
37. **M. Szaniawska**, K. Szymczyk, *Adsorption and volumetric properties of surfactants and their binary mixtures used in pharmaceutical industry. Part 2*, 7th International

- Conference „Nanotechnologies and nanomaterials” NANO 2019, 27-30.2019, Lwów, Ukraina.
38. **M. Szaniawska**, K. Szymczyk, *Mixtures of berberine and nonionic surfactants – spectroscopic studies*, 6th International Conference and Workshop Plant-the source of research material, 10-12.09. 2019, Nałęczów.
 39. **M. Szaniawska**, K. Szymczyk, *Temperature influence on volumetric and adsorption properties of nonionic surfactants mixtures with berberine*, 6th International Conference and Workshop Plant-the source of research material, 10-12.09.2019, Nałęczów.
 40. **M. Szaniawska**, *Badanie oddziaływań w układzie alkaloid-surfaktant*, Wirtualna Konferencja Młodych Przyrodników, 30.12.2019-5.01.2020, online.
 41. **M. Szaniawska**, *Properties of nonionic Kolliphor surfactants*, 1st Virtual Festival of Life and Earth Sciences, 20-26.07.2020, online.
 42. **M. Szaniawska**, *Properties of Tween surfactants – spectroscopic studies*, 1st Virtual Festival of Life and Earth Sciences, 20-26.07.2020, online.
 43. **M. Szaniawska**, *Adsorption properties in alkaloid-surfactant systems*, 1st Virtual Festival of Life and Earth Sciences, 20-26.07.2020, online.
 44. **M. Szaniawska**, *Microenvironmental properties of binary mixtures of Kolliphor*, 1st Virtual Festival of Life and Earth Sciences, 20-26.07.2020, online.
 45. **M. Szaniawska**, K. Szymczyk, *Properties of Tween surfactants – spectroscopic studies. Part 1 – Pyrene*, 8th International Conference 'Nanotechnologies and Nanomaterials' NANO 2020, 26.08-29.08.2020, Lwów, online.
 46. **M. Szaniawska**, K. Szymczyk, *Properties of Tween surfactants – spectroscopic studies. Part 2 – ANS and Pyronin Y*, 8th International Conference 'Nanotechnologies and Nanomaterials' NANO 2020, 26.08-29.08.2020, Lwów, online.
 47. **M. Szaniawska**, K. Szymczyk, *Properties of nonionic surfactant Kolliphor ELP*, 8th International Conference 'Nanotechnologies and Nanomaterials' NANO 2020, 26.08-29.08.2020, Lwów, online.

48. **M. Szaniawska**, K. Szymczyk, *Surfaktanty niejonowe typu Kolliphor – badania gęstości i lepkości*, Kopernikańskie e-seminarium Doktoranckie, 7.09.2020, Toruń, online.
49. **M. Szaniawska**, K. Szymczyk, *Wpływ temperatury na adsorpcyjne i objętościowe właściwości wodnych roztworów Kolliphoru ELP*, Fizykochemia granic faz – metody instrumentalne, 22-26.08.2021, Lublin.
50. **M. Szaniawska**, K. Szymczyk, *Temperature effect on the properties of aqueous solutions of Kolliphor ELP*, 35th Conference of the European Colloid and Interface Society, 5-10.09.2021, Ateny, Grecja.

9.3. Projekty badawcze, konkursy

1. Dotacja celowa na prowadzenie badań naukowych lub prac rozwojowych oraz zadań z nimi związanych, służących rozwojowi młodych naukowców oraz uczestników studiów doktoranckich na Wydziale Chemii UMCS (tzw. „Grant dla młodych naukowców”), Uniwersytet Marii Curie-Skłodowskiej w Lublinie (środki MNiSW) pt.: „Badanie właściwości objętościowych surfaktantów niejonowych typu Kolliphor” (rok 2017/18).
2. PROM – międzynarodowa wymiana stypendialna doktorantów i kadry akademickiej (nr. PPI/PRO/2019/1/00007), Narodowa Agencja Wymiany Akademickiej - 25-dniowy staż na Uniwersytecie w Vigo, pod opieką prof. Carlosa Bravo - Diaz oraz Soni Losady - Barreiro (12.07 - 5.08.2021)
3. Projekt konkursowy polegający na doskonaleniu umiejętności naukowo-dydaktycznych służących rozwojowi uczestników studiów doktoranckich na Uniwersytecie Marii Curie-Skłodowskiej w Lublinie – szkoła zimowa dla doktorantów „Rozwój jako lokata”, 9-14.01.2017r., Zakopane.
4. Projekt konkursowy polegający na doskonaleniu umiejętności naukowo-dydaktycznych służących rozwojowi uczestników studiów doktoranckich na Uniwersytecie Marii Curie-Skłodowskiej w Lublinie – szkoła letnia dla doktorantów „Lokata Rozwoju”, 14-20.08.2017r., Zakopane.

5. Projekt konkursowy polegający na doskonaleniu umiejętności naukowo-dydaktycznych służących rozwojowi uczestników studiów doktoranckich na Uniwersytecie Marii Curie-Skłodowskiej w Lublinie – szkoła zimowa dla doktorantów „Lokata Rozwoju”, 9-15.01.2018r., Zakopane.

9.4. Aktywność organizacyjna i członkostwo naukowe

- Przedstawiciel doktorantów do Uczelnianej Rady Samorządu Doktorantów UMCS (2019/2020).
- Przewodnicząca Wydziałowej Rady Samorządu Doktorantów Wydziału Chemii UMCS (2018/2019, 2019/2020).
- Przedstawiciel doktorantów do Rady Wydziału Chemii UMCS (2016/2017, 2017/2018, 2018/2019).
- Przedstawiciel doktorantów do Kolegium Dziekańskiego (2019/2020, 2020/2021)
- Przedstawiciel doktorantów do Senatu UMCS (2018/2019)
- Przedstawiciel doktorantów do Wydziałowej Komisji Stypendialnej UMCS (2018/2019, 2019/2020)
- Przedstawiciel doktorantów do Senackiej Komisji Rozwoju Kadry Naukowej (2018/2019)
- Przedstawiciel doktorantów do Senackiej Odwoławczej Komisji Dyscyplinarnej dla Doktorantów (2018/2019)
- Współorganizator XVI Polish – Ukrainian Symposium Theoretical and Experimental Studies of Interfacial Phenomena and Their Technological Applications oraz Tenth International Symposium Surface Heterogeneity Effects in Adsorption, Catalysis and Related Phenomena, ISSHAC-10 (27-31.08. 2018, Lublin)
- Członek Wydziałowej Rady Samorządu Doktorantów Wydziału Chemii UMCS (2014/2015, 2015/2016, 2016/2017, 2017/2018)
- Organizacja 60 Zjazdu Naukowego Polskiego Towarzystwa Chemicznego (17-21.09.2017, Wrocław)
- Członek Polskiego Towarzystwa Chemicznego (2015 – do chwili obecnej)

- Lubelski Festiwal Nauki 2019 - projekt „Oszukać czas – kawa versus wolne rodniki”

9.5. Nagrody i wyróżnienia

- Zwiększenie stypendium doktoranckiego z dotacji podmiotowej na dofinansowanie zadań projakościowych (2017/2018, 2018/2019, 2019/2020, 2020/2021).
- Stypendium Rektora UMCS dla Najlepszych Doktorantów (2016/2017, 2017/2018, 2018/2019, 2019/2020, 2020/2021).
- Stypendium naukowe z Własnego Funduszu Stypendialnego UMCS dla najlepszych doktorantów (2019/2020).
- Stypendium naukowe w ramach Miejskiego Programu Stypendialnego dla Studentów i Doktorantów realizowanego przez Miasto Lublin przyznawane przez Prezydenta Miasta Lublin dr. Krzysztofa Żuka (2020/2021).
- Nagroda za najlepszy poster przedstawiony podczas Zjazdu Zimowego Sekcji Studenckiej PTChem, 17.12.2016, Lublin.
- Nagroda za najlepszy poster przedstawiony podczas I Ogólnopolskiej Konferencji Fizykochemia granic faz- metody instrumentalne, 23-26.04.2017, Lublin.

10. ZAŁĄCZNIKI

ZAŁĄCZNIK 1

PUBLIKACJA [D1]

K. Szymczyk, M. Szaniawska, K. Terpiłowski*, Determination of acoustical parameters of aqueous solution of Kolliphors binary mixtures using density, speed of sound, viscosity and surface tension measurements. *Journal of Surfactants and Detergents*, 2019, 22(5), 1163-1174.

Determination of Acoustical Parameters of Aqueous Solution of Kolliphors Binary Mixtures Using Density, Speed of Sound, Viscosity, and Surface Tension Measurements

Katarzyna Szymczyk¹ · Magdalena Szaniawska¹ · Konrad Terpiłowski¹ 

Received: 15 October 2018 / Revised: 14 June 2019 / Accepted: 10 July 2019
© 2019 AOCS

Abstract Measurements of density, speed of sound, and surface tension as well as viscosity of aqueous Kolliphor[®] ELP (ELP) and Kolliphor[®] RH 40 (RH40) solutions as well as binary mixtures at different surfactant mole fractions were made at 293 K to investigate their aggregation behavior. The free volume, internal pressure, and molar cohesive energy were calculated and compared to the specific acoustic impedance and intermolecular free length to obtain qualitative information about the character of interactions between the surfactant molecules in the mixture through the water phase.

Keywords Kolliphor[®] ELP · Kolliphor[®] RH 40 · Internal pressure · Free volume · Cohesive energy

J Surfact Deterg (2019).

Introduction

Micellar systems are widely applied in chemical, biochemical, and pharmaceutical areas as solubilizing agents and also constitute a basis for drug delivery or solvent systems in separation processes. Moreover, some aqueous solutions with nonionic surfactants can be applied in extraction processes being of significant importance in biotechnological product purification (Ingram et al., 2012; Lam et al., 2005). In pharmacy, nonionic Kolliphors (known before as Cremophors)

find application in lipid-based delivery aimed at improving poorly water-soluble drugs (Berthelsen et al., 2015; Gelderblom et al., 2001). The tricinoleate ester of ethoxylated glycerol is the main constituent of Kolliphors. Polyethylene glycol ricinoleate and the corresponding free glycols are the other constituents (Christiansen et al., 2010). Kolliphor EL (EL), the most common of all Kolliphors, can be used as a solubilization vehicle for some hydrophobic drugs including cyclosporin A, diazepam, propofol, and paclitaxel (Bakonyia et al., 2018; Bali et al., 2011; Chen et al., 2008; Constantinides and Wasan, 2007; Cuié et al., 2008; Gao et al., 2003; Sadurni et al., 2005; Seelig and Gerebtzoff, 2006; Wang et al., 2004). Moreover, mixed micelles of non-ionic surfactants are common in industry (Rosen, 2004). Interactions between *individual surfactants* can result in lower critical micelle concentration (CMC) of the binary surfactant mixture *vs.* either individual surfactant or a thermodynamically more stable one. Thus, better knowledge about the origin of nonideal and synergistic behavior contributes to more efficient surfactant mixture design so as to reduce the amount of surfactant in a formulation. Determination of volumetric and viscometric properties of aqueous solutions of binary Kolliphor[®] ELP (ELP), purified grade of EL, and Kolliphor[®] RH 40 mixtures from the measurements of density, viscosity, speed of sound, and surface tension at 293 K was the aim of this article. These data were used to obtain information about the nature of the solute–solute, solute–solvent, and solvent–solvent interactions.

Experimental

Kolliphor[®] ELP (ELP) (Cremophor[®] ELP, Polyoxyl 35 Hydrogenated Castor oil, and Polyoxyl-35 castor oil)

✉ Konrad Terpiłowski
terpil@poczta.umcs.lublin.pl

¹ Department of Interfacial Phenomena, Faculty of Chemistry, Maria Curie-Skłodowska University, Maria Curie-Skłodowska Sq. 3, 20-031 Lublin, Poland

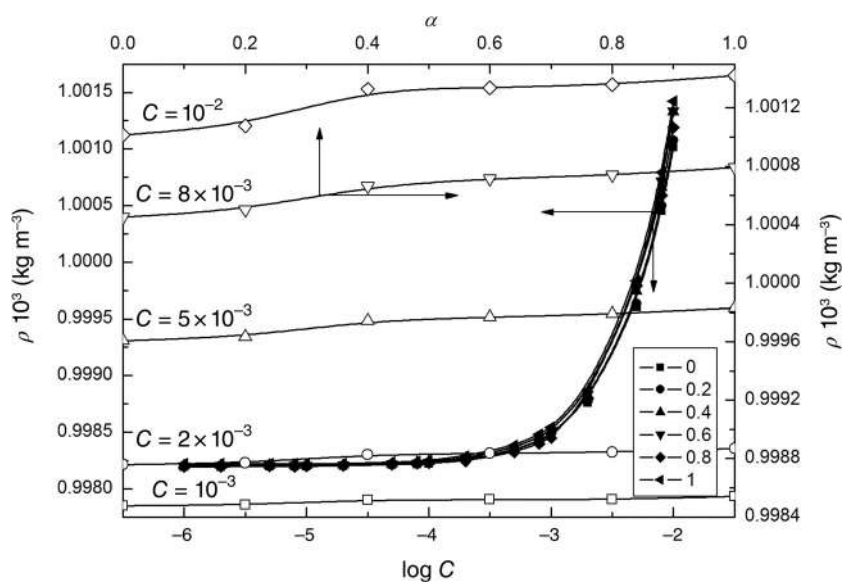


Fig. 1 A plot of the values of ρ of the aqueous solutions of RH40, ELP, and their binary mixtures at the mole fraction of ELP equal to 0.2, 0.4, 0.6, and 0.8 at $T = 293$ K vs. $\log C$ as well as the values of ρ of the studied solutions at $C = 10^{-3}$, 2×10^{-3} , 5×10^{-3} , 8×10^{-3} , and 10^{-2} M vs. α

and Kolliphor® RH 40 (RH40) (Cremophor® RH 40, Macroglycerol hydroxystearate, PEG-40 castor oil, and Polyoxyl 40 hydrogenated castor oil) were provided by Sigma (Poznań, Poland) and used without further purification. RH40 is mainly composed of trihydroxystearate ester of ethoxylated glycerol with a smaller amount of polyethylene glycol trihydroxystearate as well as the corresponding free glycols. ELP is a nonuniform product without a single well-defined structure (Shaukat, 2011). Tricinoleate esters of ethoxylated glycerols, polyethylene glycol ricinoleates

as well as their derivatives with polyethoxylated 12-hydroxy ricinoleic acid residues are the main components of ELP. Thus, ELP can be treated as a mixture. Furthermore, as the double bond at C-9 in ELP molecules is cis and C-12 atoms of the fatty acid chains are achiral or racemic, the proportions of both (R) and (S) enantiomers are equal (Shaukat, 2011). Doubly distilled and deionized water used for preparation of the aqueous solutions of individual surfactants and their mixtures with the bulk phase mole fraction of ELP (α) equal to 0.2, 0.4, 0.6, and 0.8 at

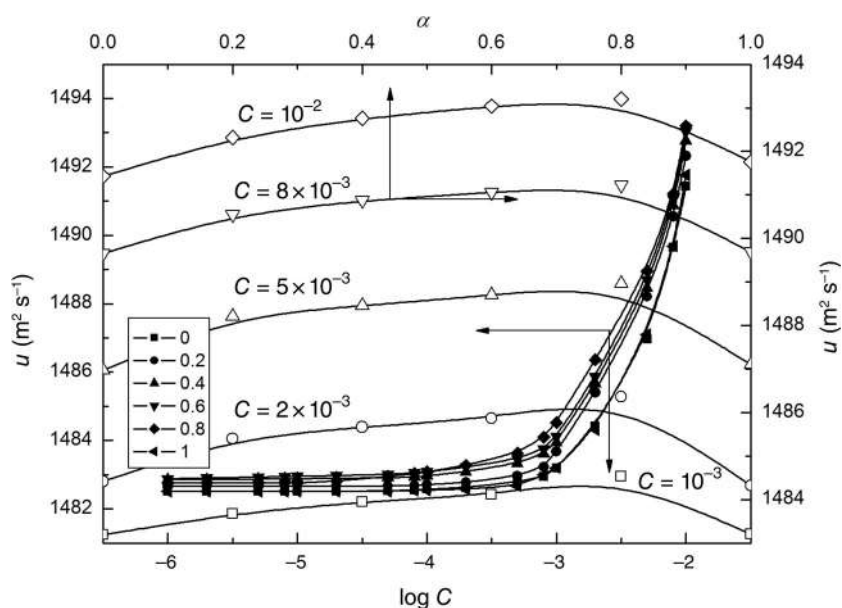


Fig. 2 A plot of the values of u of the aqueous solutions of RH40, ELP, and their binary mixtures at the mole fraction of ELP equal to 0.2, 0.4, 0.6, and 0.8 at $T = 293$ K vs. $\log C$ as well as the values of u of the studied solutions at $C = 10^{-3}$, 2×10^{-3} , 5×10^{-3} , 8×10^{-3} , and 10^{-2} M vs. α

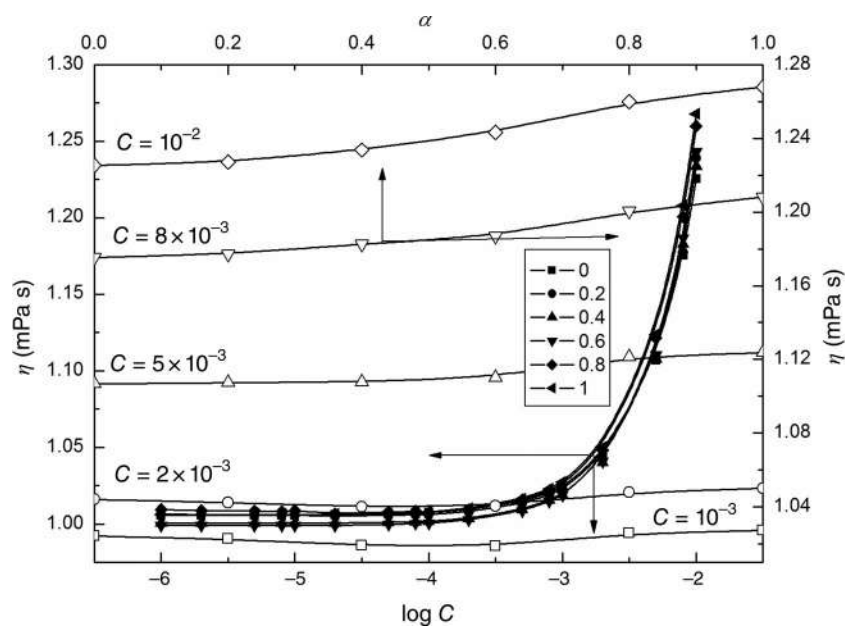


Fig. 3 A plot of the values of η of the aqueous solutions of RH40, ELP, and their binary mixtures at the mole fraction of ELP equal to 0.2, 0.4, 0.6, and 0.8 at $T = 293$ K vs. $\log C$ as well as the values of η of the studied solutions at $C = 10^{-3}$, 2×10^{-3} , 5×10^{-3} , 8×10^{-3} , and 10^{-2} M vs. α

the concentration from 10^{-6} to 10^{-2} M was obtained from a Destamat Bi18E distiller (Heraeus, Germany).

Speed of sound and densities of various solutions were measured using a vibrating tube densitometer and the speed of sound analyzer (Anton Paar DSA 5000M) equipped with the automatic viscosity correction and two integrated Pt 100 thermometers. Temperature was maintained to 0.01 K using a temperature controller. The analyzer was calibrated

with triple-distilled water and dry air. The standard density measurement uncertainties were $\pm 2 \times 10^{-3}$ kg m^{-3} and those of speed of sound were ± 0.1 m s^{-1} . An Anton Paar viscometer (AMVn) at $T = 293$ K ± 0.01 K with a precision of 0.0001 mPa s and uncertainty 0.3% was used for viscosity measurements of aqueous solutions.

Surface tension measurements were made with a Krüss K100C tensiometer under atmospheric pressure using the

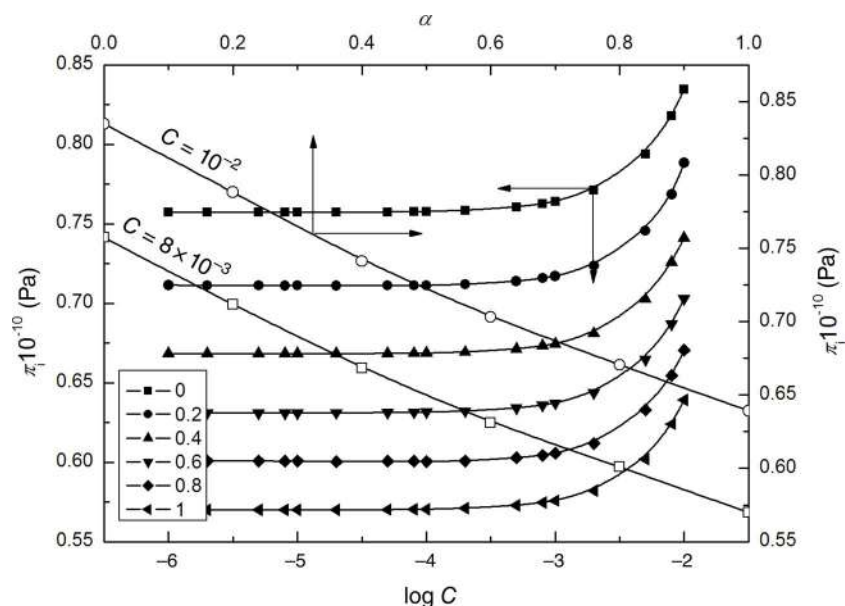


Fig. 4 A plot of the values of π_i of the aqueous solutions of RH40, ELP and their binary mixtures at the mole fraction of ELP equal to 0.2, 0.4, 0.6, and 0.8 at $T = 293$ K vs. $\log C$ as well as the values of π_i of the studied solutions at $C = 8 \times 10^{-3}$ and 10^{-2} M vs. α

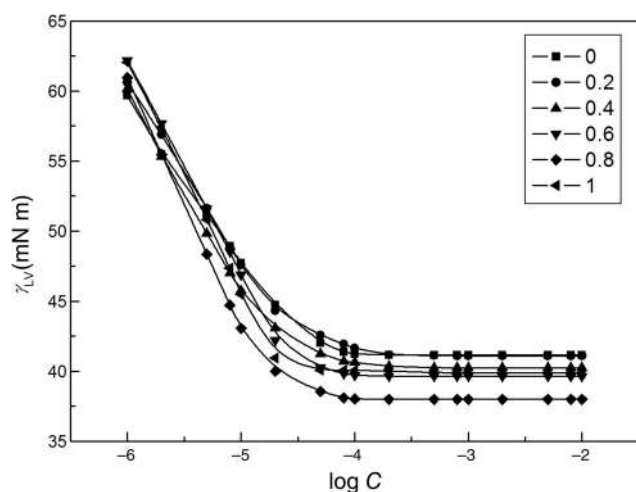


Fig. 5 A plot of the values of γ_{LV} of the aqueous solutions of RH40, ELP, and their binary mixtures at the mole fraction of ELP equal to 0.2, 0.4, 0.6, and 0.8 at $T = 293$ K vs. $\log C$

ring method. Measurements of the surface tension of pure water at 293 ± 0.1 K were performed to calibrate the tensiometer and to check the cleanliness of the glassware. In all cases, more than 10 measurements were made and the standard deviation did not exceed ± 0.2 mN m^{-1} .

Results and Discussion

The internal pressure, π_i , was calculated from the values of density (Fig. 1), speed of sound (Fig. 2), and viscosity (Fig. 3) of ELP, RH40 aqueous solutions, and their binary mixtures. The internal pressure is a measure of total dispersion, ionic, and dipolar forces for a liquid and includes all attractive and repulsive forces. The calculation of the

internal pressure is made from the following equation (Chauhan et al., 2013b; Kumar et al., 2012):

$$\pi_i = \frac{bRT(K'\eta/u)^{1/2}\rho^{2/3}}{M^{7/6}} \quad (1)$$

where ρ is the density, u is the speed of sound, η is the viscosity, R is the gas constant, T is the temperature, M is the molar mass, b is the packing factor that is assumed to be equal to 2 in the liquid system and $K' = 4.28 \times 10^9$ is the constant regardless of the liquid. An increase of π_i is found with increasing concentration of both individual surfactants and their mixtures (Fig. 4) indicating that intermolecular interactions increase as a result of formation of solvent molecule aggregates around the solute affecting the structural arrangement of the solvent system. On the other hand at high concentration of surfactants in the solution, it can be associated with the changes of the size and/or shape of the Kolliphor micelles.

The surface tension (γ_{LV}) of the surfactant aqueous solutions (Fig. 5) was used to determine the CMC , Π_{CMC} (the difference between the surface tension of the solvent, γ_0 , and the solute at the CMC , γ_{CMC}), ΔG_{mic}^0 (the standard Gibbs energy of micellization) (Szymczyk, 2011), and ΔG_{min}^S (the free energy at the water-air interface) (Sugihara et al., 2003), γ_0/γ_{CMC} as well as X_1^M (the mole fraction of surfactant in the mixed micelle), β^M (molecular interaction parameter), f_1^M and f_2^M (the activity coefficients of surfactants 1 and 2 in the mixed micelle), g^M (the excess Gibbs energy of the mixed micelle), and ϵ^M (the molecule exchange energy in the mixed micelle) based on the Rubingh and Rosen theory (Hua and Rosen, 1982; Rosen, 2004; Rubingh, 1979; Wang et al., 2005). The calculated parameters are presented in Table 1. Values of CMC , Π_{CMC} , ΔG_{mic}^0 , ΔG_{min}^S , β^M , g^M , and ϵ^M for the mixture with the mole fraction of ELP (α) in the bulk phase equal to 0.8

Table 1 Values of CMC , Π_{CMC} , ΔG_{mic}^0 , ΔG_{min}^S , γ_0/γ_{CMC} , X_1^M , β^M , f_1^M , f_2^M , g^M , and ϵ^M for the aqueous solutions of RH40, ELP, and their binary mixtures at the mole fraction of ELP (α) equal to 0.2, 0.4, 0.6, and 0.8 at $T = 293$ K

	RH40	$\alpha = 0.2$	$\alpha = 0.4$	$\alpha = 0.6$	$\alpha = 0.8$	ELP
CMC (mol dm^{-3})	6.64×10^{-5}	3.94×10^{-5}	2.88×10^{-5}	2.45×10^{-5}	1.92×10^{-5}	2.14×10^{-5}
Π_{CMC} (mN m^{-1})	31.64	31.70	32.55	33.16	34.8	32.91
ΔG_{mic}^0 (kJ mol^{-1})	-23.44	-24.71	-25.47	-25.86	-26.46	-26.19
ΔG_{min}^S (kJ mol^{-1})	21.56	19.16	15.30	13.82	11.99	12.59
γ_0/γ_{CMC}	1.77	1.77	1.81	1.84	1.92	1.82
X_1^M	—	0.452	0.620	0.79	0.895	—
β^M	—	-0.694	-0.980	-0.342	-2.097	—
f_1^M	—	0.867	0.686	0.807	0.186	—
f_2^M	—	0.812	0.868	0.985	0.977	—
g^M (kJ mol^{-1})	—	-0.434	-0.700	-0.422	-3.338	—
ϵ^M (kJ mol^{-1})	—	-0.282	-0.398	-0.139	-0.851	—

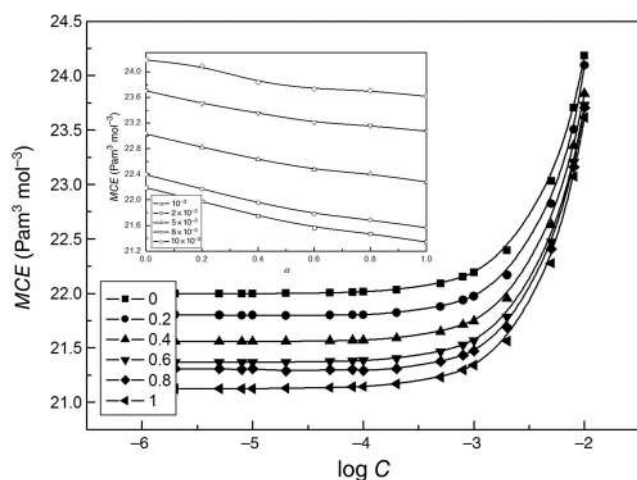


Fig. 6 A plot of the values of MCE of the aqueous solutions of RH40, ELP and their binary mixtures at the mole fraction of ELP equal to 0.2, 0.4, 0.6, and 0.8 at $T = 293$ K vs. $\log C$ as well as the values of MCE of the studied solutions at $C = 10^{-3}$, 2×10^{-3} , 5×10^{-3} , 8×10^{-3} , and 10^{-2} M vs. α

clearly indicate that at the studied temperature, synergism in mixed micelle formation causes a significantly stronger driving force for micellization. This mixture shows the smallest value of ΔG_{\min}^S , which is regarded as the free energy change accompanied by the transition from the bulk phase to the surface phase for all solution components and the biggest value of the γ_0/γ_{CMC} parameter, which is connected with the solvophobic effect (Rodríguez et al., 2008; Sachin et al., 2019). On the other hand, the measure of

attraction between different solution components is the molar cohesive energy (MCE), which can be calculated from the relation:

$$MCE = \pi_1 V_m \quad (2)$$

where V_m is the molar volume (Chauhan et al., 2013a). Figure 6 shows that MCE values increase for all solutions when C is higher than 10^{-3} M due to formation of micelles. Values of MCE for RH40 molecules are larger consistent with smaller viscous relaxation time (τ) evaluated based on (Chauhan et al., 2018):

$$\tau = \frac{4\eta}{3u^2\rho} \quad (3)$$

Figure 7 shows that the τ values increase with the increasing surfactant concentration and ELP mole fraction at the studied temperature. Smaller values of τ are found for RH40 solutions as the viscous relaxation time is proportional to the solution viscosity (Fig. 3). However, at high concentrations, much larger than CMC determined from the surface tension measurements, a linear increase of τ values with the mole fraction of ELP is not observed thus suggesting the presence of synergetic intermolecular interactions in the molecules of ELP and RH40 in the mixture.

This observation is consistent with the acoustic impedance (Z), which are possible to be calculated from the relation (Hua and Rosen, 1982):

$$Z = u\rho \quad (4)$$

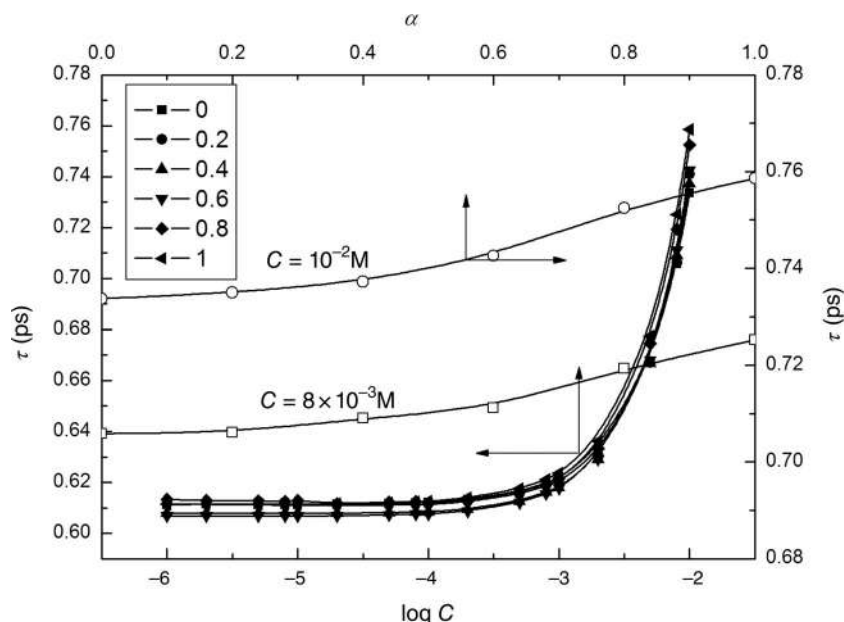


Fig. 7 A plot of the values of τ of the aqueous solutions of RH40, ELP and their binary mixtures at the mole fraction of ELP equal to 0.2, 0.4, 0.6, and 0.8 at $T = 293$ K vs. $\log C$ as well as the values of τ of the studied solutions at $C = 8 \times 10^{-3}$ and 10^{-2} M vs. α

Table 2 Values of κ_S , L_f , Z , V_a , and R_a for the aqueous solutions of RH40, ELP, and their binary mixtures at the mole fraction of ELP (α) equal to 0.2, 0.4, 0.6, and 0.8 at $T = 293$ K

	C	κ_S ($10^{-10} \text{ m}^2 \text{ N}^{-1}$)	L_f (10^{-10} m)	Z ($10^6 \text{ kg m}^{-2} \text{ s}^{-1}$)	V_a ($10^{-6} \text{ m}^3 \text{ mol}^{-1}$)	R_a ($10^{-4} \text{ m}^{10/3} \text{ s}^{-1/3} \text{ mol}^{-1}$)
RH40	10^{-6}	4.5582	0.435003	1.4798	29.4256	45.6813
	2×10^{-6}	4.5582	0.435003	1.4798	29.4256	45.6813
	5×10^{-6}	4.5582	0.435003	1.4798	29.4256	45.6812
	8×10^{-6}	4.5581	0.435003	1.4798	29.4255	45.6812
	10^{-5}	4.5581	0.435002	1.4798	29.4255	45.6811
	2×10^{-5}	4.5581	0.435000	1.4799	29.4246	45.6809
	5×10^{-5}	4.5579	0.434993	1.4799	29.4197	45.6807
	8×10^{-5}	4.5578	0.434986	1.4799	29.4149	45.6806
	10^{-4}	4.5576	0.434977	1.4799	29.4075	45.6807
	2×10^{-4}	4.5572	0.434958	1.4800	29.3964	45.6798
	5×10^{-4}	4.5557	0.434888	1.4803	29.3496	45.6777
	8×10^{-4}	4.5545	0.434828	1.4806	29.3113	45.6753
	10^{-3}	4.5527	0.434743	1.4809	29.2476	45.6753
	2×10^{-3}	4.5439	0.434321	1.4826	28.9309	45.6751
	5×10^{-3}	4.5245	0.433392	1.4864	28.2686	45.6624
	8×10^{-3}	4.5044	0.432429	1.4903	27.5750	45.6513
$\alpha = 0.2$	10^{-2}	4.4911	0.431792	1.4929	27.1150	45.6437
	10^{-6}	4.5572	0.434958	1.4800	29.3879	45.6826
	2×10^{-6}	4.5572	0.434958	1.4800	29.3879	45.6826
	5×10^{-6}	4.5572	0.434958	1.4800	29.3879	45.6826
	8×10^{-6}	4.5572	0.434957	1.4800	29.3867	45.6827
	10^{-5}	4.5572	0.434955	1.4800	29.3859	45.6826
	2×10^{-5}	4.5571	0.434954	1.4800	29.3852	45.6824
	5×10^{-5}	4.5571	0.434952	1.4800	29.3845	45.6821
	8×10^{-5}	4.5570	0.434948	1.4800	29.3823	45.6819
	10^{-4}	4.5568	0.434937	1.4801	29.3743	45.6820
	2×10^{-4}	4.5563	0.434914	1.4802	29.3588	45.6812
	5×10^{-4}	4.5547	0.434838	1.4805	29.3071	45.6793
	8×10^{-4}	4.5527	0.434742	1.4809	29.2385	45.6781
	10^{-3}	4.5497	0.434599	1.4814	29.1255	45.6800
	2×10^{-3}	4.5378	0.434032	1.4836	28.6853	45.6846
	5×10^{-3}	4.5168	0.433025	1.4877	27.9577	45.6739
8×10^{-3}	4.4987	0.432158	1.4913	27.3488	45.6582	
$\alpha = 0.4$	10^{-2}	4.4855	0.431521	1.4939	26.8910	45.6499
	10^{-6}	4.5560	0.434899	1.4802	29.3385	45.6844
	2×10^{-6}	4.5560	0.434899	1.4802	29.3385	45.6843
	5×10^{-6}	4.5559	0.434895	1.4802	29.3355	45.6844
	8×10^{-6}	4.5558	0.434891	1.4802	29.3318	45.6845
	10^{-5}	4.5558	0.434891	1.4802	29.3318	45.6845
	2×10^{-5}	4.5557	0.434886	1.4802	29.3280	45.6845
	5×10^{-5}	4.5556	0.434880	1.4803	29.3247	45.6842
	8×10^{-5}	4.5554	0.434872	1.4803	29.3192	45.6839
	10^{-4}	4.5551	0.434858	1.4804	29.3091	45.6839
	2×10^{-4}	4.5543	0.434817	1.4805	29.2782	45.6838
	5×10^{-4}	4.5524	0.434726	1.4809	29.2154	45.6820
	8×10^{-4}	4.5502	0.434621	1.4813	29.1403	45.6807
	10^{-3}	4.5478	0.434511	1.4817	29.0556	45.6813

(Continues)

Table 2 Continued

	C	$\kappa_S (10^{-10} \text{ m}^2 \text{ N}^{-1})$	$L_r (10^{-10} \text{ m})$	$Z (10^6 \text{ kgm}^{-2} \text{ s}^{-1})$	$V_a (10^{-6} \text{ m}^3 \text{ mol}^{-1})$	$R_a (10^{-4} \text{ m}^{10/3} \text{ s}^{-1/3} \text{ mol}^{-1})$	
$\alpha = 0.6$	2×10^{-3}	4.5359	0.433940	1.4839	28.6161	45.6848	
	5×10^{-3}	4.5148	0.432930	1.4881	27.8934	45.6714	
	8×10^{-3}	4.4961	0.432030	1.4919	27.2644	45.6540	
	10^{-2}	4.4817	0.431340	1.4947	26.7744	45.6430	
	10^{-6}	4.5558	0.434893	1.4802	29.3325	45.6848	
	2×10^{-6}	4.5557	0.434886	1.4802	29.3271	45.6849	
	5×10^{-6}	4.5555	0.434877	1.4803	29.3196	45.6852	
	8×10^{-6}	4.5554	0.434873	1.4803	29.3157	45.6854	
	10^{-5}	4.5554	0.434871	1.4803	29.3140	45.6854	
	2×10^{-5}	4.5552	0.434862	1.4803	29.3076	45.6854	
	5×10^{-5}	4.5550	0.434851	1.4804	29.2997	45.6853	
	8×10^{-5}	4.5547	0.434838	1.4804	29.2895	45.6854	
	10^{-4}	4.5544	0.434824	1.4805	29.2792	45.6854	
	2×10^{-4}	4.5535	0.434779	1.4806	29.2460	45.6852	
	5×10^{-4}	4.5516	0.434689	1.4810	29.1829	45.6835	
	8×10^{-4}	4.5493	0.434580	1.4815	29.1050	45.6822	
	10^{-3}	4.5469	0.434464	1.4819	29.0155	45.6829	
	2×10^{-3}	4.5347	0.433880	1.4841	28.5658	45.6864	
	5×10^{-3}	4.5132	0.432854	1.4884	27.8322	45.6727	
	8×10^{-3}	4.4947	0.431964	1.4921	27.2155	45.6536	
$\alpha = 0.8$	10^{-2}	4.4800	0.431257	1.4950	26.7043	45.6454	
	10^{-6}	4.5566	0.434930	1.4801	29.3630	45.6838	
	2×10^{-6}	4.5566	0.434929	1.4801	29.3630	45.6838	
	5×10^{-6}	4.5566	0.434929	1.4801	29.3629	45.6837	
	8×10^{-6}	4.5566	0.434929	1.4801	29.3630	45.6838	
	10^{-5}	4.5566	0.434929	1.4801	29.3629	45.6837	
	2×10^{-5}	4.5562	0.434911	1.4802	29.3487	45.6839	
	5×10^{-5}	4.5554	0.434870	1.4803	29.3148	45.6849	
	8×10^{-5}	4.5548	0.434842	1.4804	29.2921	45.6855	
	10^{-4}	4.5545	0.434829	1.4804	29.2820	45.6857	
	2×10^{-4}	4.5532	0.434768	1.4807	29.2328	45.6869	
	5×10^{-4}	4.5507	0.434647	1.4811	29.1414	45.6870	
	8×10^{-4}	4.5475	0.434493	1.4817	29.0215	45.6883	
	10^{-3}	4.5446	0.434357	1.4822	28.9132	45.6903	
	2×10^{-3}	4.5318	0.433745	1.4846	28.4441	45.6931	
	5×10^{-3}	4.5115	0.432773	1.4886	27.7658	45.6744	
	8×10^{-3}	4.4943	0.431944	1.4921	27.1790	45.6610	
	10^{-2}	4.4797	0.431242	1.4950	26.6683	45.6538	
	ELP	10^{-6}	4.5580	0.434998	1.4799	29.4249	45.6801
		2×10^{-6}	4.5580	0.434998	1.4799	29.4249	45.6801
5×10^{-6}		4.5580	0.434998	1.4799	29.4249	45.6801	
8×10^{-6}		4.5580	0.434998	1.4799	29.4249	45.6801	
10^{-5}		4.5580	0.434997	1.4799	29.4248	45.6801	
2×10^{-5}		4.5580	0.434997	1.4799	29.4248	45.6800	
5×10^{-5}		4.5579	0.434991	1.4799	29.4219	45.6795	
8×10^{-5}		4.5578	0.434984	1.4799	29.4167	45.6795	
10^{-4}		4.5577	0.434979	1.4800	29.4139	45.6791	
2×10^{-4}		4.5573	0.434962	1.4800	29.4053	45.6777	

(Continues)

Table 2 Continued

C	$\kappa_S (10^{-10} \text{ m}^2 \text{ N}^{-1})$	$L_f (10^{-10} \text{ m})$	$Z (10^6 \text{ kgm}^{-2} \text{ s}^{-1})$	$V_a (10^{-6} \text{ m}^3 \text{ mol}^{-1})$	$R_a (10^{-4} \text{ m}^{10/3} \text{ s}^{-1/3} \text{ mol}^{-1})$
5×10^{-4}	4.5563	0.434916	1.4803	29.3801	45.6744
8×10^{-4}	4.5539	0.434800	1.4807	29.2971	45.6732
10^{-3}	4.5523	0.434725	1.4810	29.2427	45.6725
2×10^{-3}	4.5440	0.434326	1.4826	28.9527	45.6690
5×10^{-3}	4.5226	0.433305	1.4869	28.2297	45.6535
8×10^{-3}	4.5026	0.432344	1.4909	27.5557	45.6362
10^{-2}	4.4873	0.431609	1.4939	27.0216	45.6286

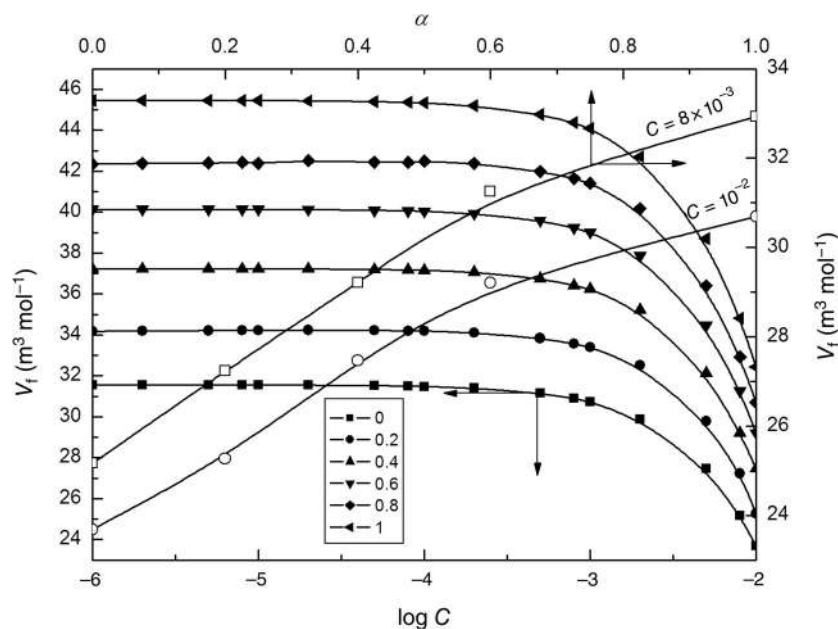


Fig. 8 A plot of the values of V_f of the aqueous solutions of RH40, ELP, and their binary mixtures at the mole fraction of ELP equal to 0.2, 0.4, 0.6, and 0.8 at $T = 293 \text{ K}$ vs. $\log C$ as well as the values of V_f of the studied solutions at $C = 8 \times 10^{-3}$ and 10^{-2} M vs. α

The acoustic impedance probes cohesive forces between the surfactant molecules in solution enabling explanation of molecular interactions. Table 2 shows that Z values of the aqueous solutions of surfactant mixtures are greater than those for a single surfactant at a given concentration. Acoustic impedance, density, and speed of sound increase with increasing surfactant concentration in mixtures indicating possible strong molecular interactions among the mixture components. E.J.A. Suys showed that the diameter of EL aggregates measured by DLS and SAXS was 12–15 nm with little micellar growth observed on increasing EL concentration (Suys et al., 2019). For characterization of aggregation, the distance between the surfaces of two molecules *i.e.* molecular free length, L_f can be determined. L_f values depend on both intermolecular and intramolecular interactions among the solution components and can be calculated from (Chauhan and Sharma, 2015):

$$L_f = K\sqrt{\kappa_S} \quad (5)$$

where $K = [(93.875 + 0.375)T \times 10^{-8}]$ and κ_S is the isentropic compressibility possible to be determined from the speed of sound (u) and density (ρ) from the Newton-Laplace equation (Kiełek and Marczak, 2010):

$$\kappa_S = \frac{1}{\rho u^2} \quad (6)$$

Values of L_f and κ_S were calculated based on those of u and ρ of the aqueous solutions of ELP, RH40, and their mixtures (Figs 1 and 2) and are presented in Table 2 along with the values of available volume (V_a) and molar sound velocity (R_a) (Sannaningannavar et al., 2013), which were calculated from:

$$V_a = \frac{1-u}{u_\infty} V_m \quad (7)$$

$$R_a = V_m u^{1/3} \quad (8)$$

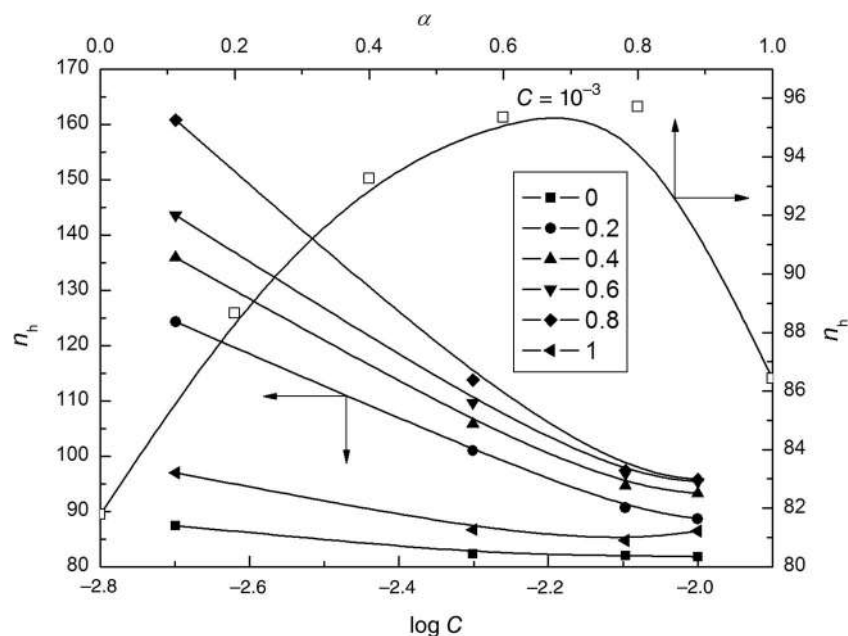


Fig. 9 A plot of the values of n_h of the aqueous solutions of RH40, ELP, and their binary mixtures at the mole fraction of ELP equal to 0.2, 0.4, 0.6, and 0.8 at C from 2×10^{-3} to 10^{-2} M and $T = 293$ K vs. $\log C$ as well as the values of n_h of the studied solutions at $C = 10^{-2}$ M vs. α

where $u_\infty = 1600 \text{ ms}^{-1}$ and V_m is the molar volume. L_f values decrease significantly at the value of C higher than 10^{-3} M for all solutions indicating closer molecular packing and is a result of specific intermolecular interactions among the molecules of surfactants in micelles. The synergistic effect between different surfactant molecules is evidenced by the smaller values of L_f at a given concentration for all mixtures compared to that of single surfactants. Comparison of the distance between two molecules (L_f) and available volume of surfactant molecule in the solution (V_a) (Table 2) with the values of free volume (V_f), that is the average volume in which a single molecule can move inside a hypothetical shell due to surrounding molecules repulsion seemed worthwhile (Chauchan et al., 2018). The free volume also referred to as a void space between molecules caused by irregular molecular packing, and can be calculated using the formula (Chauchan et al., 2018; Chauhan and Sharma, 2015):

$$V_f = \left[\frac{Mu}{K'\eta} \right]^{3/2} \quad (9)$$

where $K' = 4.28 \times 10^9$ is a constant independent of liquid nature. Figure 8 shows that V_f values decrease with concentration at high concentration of surfactants, and the addition of more ELP mixture increases V_f . A free volume increase results in greater liquid disorder due to increasing molecular mobility (Agnihorti and Adgaonkar, 1989) and V_f is dependent on the relative strength of contractive and expansive forces. Thus, V_f increases with increasing ELP fraction

may be a result of dispersion forces, steric hindrance as well as unfavorable geometric fitting. V_f increase can also be caused by more disorder of water molecules around surfactant molecules as well as decrease in oxyethylene chain hydration. Ultrasonic can be used to obtain the primary hydration number, n_h , from the expression (Burakowski and Gliński, 2007; Singh and Kumar, 2011):

$$n_h = \frac{n_w}{n_s} \left(1 - \frac{\kappa_s}{\kappa_{s,0}} \right) \quad (10)$$

where n_w and n_s are the numbers of moles of water and solute, respectively, and $\kappa_{s,0}$ is the pure water isentropic compressibility. n_h is the number of water molecules near the solute the properties of which are changed compared to those of the bulk solvent. Water molecules in this shell can be considered to be incompressible due to being tightly trapped. Figure 9 shows that the calculated values of n_h for mixtures at C more than 10^{-3} M are higher than those for single surfactants indicating that mixtures have more structured water molecules, which results in lower compressibilities. With surfactant aggregate formation, highly structured and low compressibility water molecules released from the vicinity of the hydrophobic part of surfactant become bulk water. The water molecules are highly structured around the hydrophobic part being of a rather low compressibility compared to the bulk water (Duboué-Dijon and Laage, n. d.; Desai and Dixit, 1996; El Eini et al., 1976).

The viscosity B coefficient obtained by fitting the experimental viscosity data with the Jones–Dole equation based

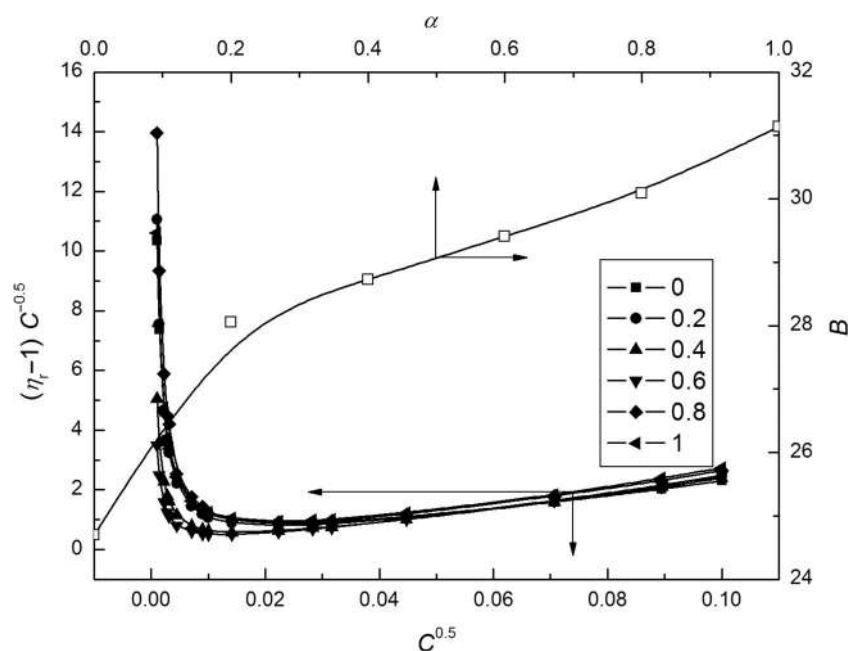


Fig. 10 A plot of the values of $(\eta_r - 1)C^{-0.5}$ of the aqueous solutions of RH40, ELP and their binary mixtures at the mole fraction of ELP equal to 0.2, 0.4, 0.6, and 0.8 at $T = 293$ K vs. $C^{0.5}$ as well as B -coefficients determined from the Jones–Dole equation vs. α

on the $(\eta_r - 1)C^{-0.5}$ plots against $C^{0.5}$ where η_r is the relative viscosity and C is the molar concentration is regarded as a measure of solute molecules size and shape as well as structural ramifications of the solute-solvent interactions (Ali et al., 2005; Jones and Dole, 1929). Figure 10 shows that B was linear with the mole fraction of ELP for the post micellar region. Moreover, B values obtained based on this equation were positive consistent with the water–water structure-breaking character of surfactant molecules. The greater kosmotropic effect in aqueous solutions of surfactant mixtures as well as more intensive solute-solvent interactions for the mixtures and ELP solutions are indicated by the higher positive values of B for ELP and mixtures with RH40.

Conclusions

Stronger interactions between ELP and RH40 in the mixture than in the single-surfactant solutions as well as the synergetic effect are indicated by the calculated acoustical parameters, especially molecular free length and free volume, and molecular interaction parameter. Moreover, more conversion to bulk water of the structured water molecules is found for the mixtures, which results in lower compressibilities and higher values of hydration numbers. The positive values of the Jones–Dole coefficient B for the studied mixtures determined from the viscosity measurements are

also of significant importance as they indicate the water–water structure breaking character of surfactant molecules.

Conflict of Interest The authors declare that they have no conflict of interest.

References

- Agnihorti, P. K., & Adgaonkar, C. S. (1989) Theoretical evaluation of ultrasonic velocity in binary liquid mixtures. *Ultrasonics*, **27**: 248–251.
- Ali, A., Hyder, S., & Akhtar, Y. (2005) Viscometric studies of amino acid in aqueous NaCl and MgCl₂ at 303 K. *Indian Journal of Physics*, **79**:157–160.
- Bakonyia, M., Berkócs, S., Kovács, A., Budai-Szűcsa, M., Kisa, N., Erős, G., ... Csányi, E. (2018) Application of quality by design principles in the development and evaluation of semisolid drug carrier systems for the transdermal delivery of lidocaine. *Journal of Drug Delivery Science and Technology*, **44**:136–145.
- Bali, V., Ali, M., & Ali, J. (2011) Nanocarrier for the enhanced bioavailability of a cardiovascular agent: In vitro, pharmacodynamic, pharmacokinetic and stability assessment. *International Journal of Pharmaceutics*, **403**:46–56.
- Berthelsen, R., Holm, R., Jacobsen, J., Kristensen, J., Abrahamsson, B., & Müllertz, A. (2015) Kolliphor surfactants affect solubilization and bioavailability of fenofibrate. Studies of in vitro digestion and absorption in rats. *Molecular Pharmaceutics*, **12**:1062–1071.
- Burakowski, A., & Gliński, J. (2007) Hydration numbers of non-electrolytes – Application of the acoustic method of Pasynski. *Chemical Physics*, **332**:336–340.
- Chauchan, S., Sharma, V., Kaur, M., & Chaudhary, P. (2018) Temperature-dependent aggregation of bio-surfactant in aqueous

- solutions of galactose and lactose: Volumetric and viscometric approach. *Chinese Journal of Chemical Engineering*, **26**: 1119–1131.
- Chauhan, S., Chaudhary, P., Sharma, K., & Kumar, K. K. (2013a) Temperature-dependent volumetric and viscometric properties of amino acids in aqueous solutions of an antibiotic drug. *Chemical Papers*, **67**:1442–1452.
- Chauhan, S., Kumar, K., & Patial, B. S. (2013b) Study of acoustical parameters of proline in lecithin–ethanol mixture at varying temperature. *Indian Journal of Pure and Applied Physics*, **51**:531–541.
- Chauhan, S., & Sharma, K. (2015) Extended studies on molecular interactions of SDBS and DTAB in aqueous solutions of amino acid at T = 293.15–313.15 K. *Journal of Molecular Liquids*, **211**: 675–685.
- Chen, Y., Li, G., Wu, X., Chen, Z., Hang, J., Qin, B., ... Wang, R. (2008) Self-microemulsifying drug delivery system (SMEDDS) of vinpocetine: Formulation development and in vivo assessment. *Biological & Pharmaceutical Bulletin*, **31**:118–125.
- Christiansen, A., Backensfeld, T., & Weitschies, W. (2010) Effects of nonionic surfactants on in vitro triglyceride digestion and their susceptibility to digestion by pancreatic enzymes. *European Journal of Pharmaceutical Sciences*, **41**:376–382.
- Constantinides, P. P., & Wasan, K. M. (2007) Lipid formulation strategies for enhancing intestinal transport and absorption of P-glycoprotein (P-gp) substrate drugs: In vitro/in vivo case studies. *Journal of Pharmaceutical Sciences*, **96**:235–248.
- Cuiné, J. F., McEvoy, C. L., Charman, W. N., Pouton, C. W., Edwards, G. A., Benamer, H., & Porter, C. J. (2008) Evaluation of the impact of surfactant digestion on the bioavailability of danazol after oral administration of lipidic self-emulsifying formulations to dogs. *Journal of Pharmaceutical Sciences*, **97**:995–1012.
- Desai, T. R., & Dixit, S. G. (1996) Interaction and viscous properties of aqueous solution of mixed cationic and nonionic surfactant. *Journal of Colloid and Interface Science*, **177**:471–477.
- Duboué-Dijon, E., & Laage, D. (2015) Characterization of the local structure in liquid water by various order parameters. *Journal of Physical Chemistry B*, **119**:8406–8418.
- El Eini, D. I., Barry, B. W., & Rhodes, J. (1976) Micellar size, shape, and hydration of long-chain polyoxyethylene nonionic surfactants. *Journal of Colloid and Interface Science*, **54**:348–351.
- Gao, P., Rush, B. D., Pfund, W. P., Huang, T., Bauer, J. M., Morozowich, W., ... Hageman, M. J. (2003) Development of a supersaturable SEDDS (S-SEDDS) formulation of paclitaxel with improved oral bioavailability. *Journal of Pharmaceutical Sciences*, **92**:2386–2398.
- Gelderblom, H., Verweij, J., Nooter, K., Sparreboom, A., & Cremophor, E. L. (2001) The drawbacks and advantages of vehicle selection for drug formulation. *European Journal of Cancer*, **37**: 1590–1598.
- Hua, X. Y., & Rosen, M. J. (1982) Calculation of the coefficient in the Gibbs equation for the adsorption of ionic surfactants from aqueous binary mixtures with non-ionic surfactants. *Journal of Colloid and Interface Science*, **87**:469–477.
- Ingram, T., Storm, S., Glembin, P., Bendt, S., Huber, D., Mehling, T., & Smirnova, I. (2012) Aqueous surfactant two-phase systems for the continuous countercurrent cloud point extraction. *Chemie Ingenieur Technik*, **84**:840–848.
- Jones, G., & Dole, M. (1929) The viscosity of aqueous solutions of strong electrolytes with special reference to barium chloride. *Journal of the American Chemical Society*, **51**:2950–2964.
- Kietek, K., & Marczak, W. (2010) Hydration of non-electrolytes in H₂O and D₂O investigated by Passynski's method. *International Journal of Thermodynamics*, **31**:77–84.
- Kumar, R., Mahesh, R., Shanmugapriyan, B., & Kannappan, V. (2012) Volumetric, viscometric, acoustic and refractometric studies of molecular interactions in certain binary systems of o-chlorophenol at 303.15 K. *Indian Journal of Pure and Applied Physics*, **50**:633–640.
- Lam, H., Kavvoosi, M., Haynes, C. A., Wang, D. I. C., & Blankschtein, D. (2005) Affinity-enhanced protein partitioning in decyl beta-Dglucopyranoside two-phase aqueous micellar systems. *Biotechnology and Bioengineering*, **89**:381–392.
- Rodriguez, A., del Mar, G. M., & Moya, M. L. (2008) Effects of addition of polar organic solvents on micellization. *Langmuir*, **24**: 12785–12792.
- Rosen, J. M. (2004) *Surfactants and interfacial phenomena* (3rd ed.). New York, NY: Wiley Interscience.
- Rubingh, D. N. (1979) Mixed Micelle Solutions. In K. Mittal (Ed.), *Solution chemistry of surfactants* (pp. 337–354). New York, NY: Plenum Press.
- Sachin, K. M., Karpel, S. A., Singh, M., & Bhattarai, A. (2019) Self-assembly of sodium dodecylsulfate and dodecyltrimethylammonium bromide mixed surfactants with dyes in aqueous mixtures. *Royal Society Open Science*, **6**:181979.
- Sadurni, N., Solans, C., Azemar, N., & Garcia-Celma, M. J. (2005) Studies on the formation of O/W nano-emulsions, by low-energy emulsification methods, suitable for pharmaceutical applications. *European Journal of Pharmaceutical Sciences*, **26**: 438–445.
- Sannaningannavar, F. M., Navati, B. S., & Ayachit, N. H. (2013) Studies on thermo-acoustic parameters of poly(ethylene glycol)-400 at different temperatures. *Journal of Thermal Analysis and Calorimetry*, **112**:1573–1578.
- Seelig, A., & Gerebtzoff, G. (2006) Enhancement of drug absorption by noncharged detergents through membrane and P-glycoprotein binding. *Expert Opinion on Drug Metabolism & Toxicology*, **2**: 733–752.
- Shaukat, A. (2011) Koliphor (TM) RH 40. In T. Reintjes (Ed.), *Solubility enhancement with BASF pharma polymers–solubilizer compendium* (pp. 89–94). Germany: Lamperthe, BASF SE Pharma Ingredients & Services.
- Singh, T., & Kumar, A. (2011) Thermodynamics of dilute aqueous solutions of imidazolium based ionic liquids. *The Journal of Chemical Thermodynamics*, **43**:958–965.
- Sugihara, G., Miyazono, A., Nagadome, S., Oda, T., Hayashi, Y., & Ko, J. S. (2003) Adsorption and micelle formation of mixed surfactant systems in water II: A combination of cationic gemini-type surfactant with MEGA-10. *Journal of Oleo Science*, **52**:449–461.
- Suys, E. J. A., Warren, D. B., Pham, A. C., Nowell, C. J., Clulow, A. J., Benamer, H., ... Chalmers, W. P. (2019) A non-ionic polyethylene oxide (PEO) surfactant model: Experimental and molecular dynamics studies of Kolliphor EL. *Journal of Pharmaceutical Sciences*, **108**:193–204.
- Szymczyk, K. (2011) The properties of binary mixtures of ethoxylated octyl phenols with ethoxylated fluorinated alkanols at the water/air interface. *Journal of Surfactants and Detergents*, **14**:415–423.
- Wang, S. W., Monagle, J., McNulty, C., Putnam, D., & Chen, H. (2004) Determination of P-glycoprotein inhibition by excipients and their combinations using an integrated high-throughput process. *Journal of Pharmaceutical Sciences*, **93**:2755–2767.
- Wang, Z. H., Li, G. Z., Zhang, G. Y., Diao, Z. Y., Chen, L. S., & Wang, Z. W. (2005) Molecular interaction in binary surfactant mixtures containing alkyl polyglycoside. *Journal of Colloid and Interface Science*, **290**:598–602.

Biographies

Katarzyna Szymczyk studied Chemistry at Maria Curie Skłodowska University in Lublin, Poland from 1997 to 2002. Then after graduation, she was employed in the Department of Interfacial Phenomena,

Faculty of Chemistry, UMCS in Lublin where she obtained her degrees (M.Sc. 2002, Ph.D. 2007, Assistant Professor 2015). She has published over 60 original articles in professional journals and books. Her research areas are interfacial phenomena at the solid–liquid, solid–gas, and liquid–liquid interfaces, adsorption, wettability, adhesion, and surface as well as volumetric properties of surfactants and their mixtures with the active substances of plant origin.

Magdalena Szaniawska is a doctoral course student in the Department of Interfacial Phenomena, Maria Curie-Skłodowska University

in Lublin (Poland). Her main research interests are the volumetric and adsorption properties of aqueous solution of nonionic surfactants and their mixtures with biologically active compounds at different temperatures.

Konrad Terpiłowski was born in Poland in 1979. He studied chemistry at Maria Curie-Skłodowska University in Lublin and graduated in 2003. At present, he is an assistant professor in the Department of Interfacial Phenomena UMCS Lublin. His research work concerns apparent surface free energy of solids and stability of dispersed systems.

ZAŁĄCZNIK 2

PUBLIKACJA [D2]

K. Szymczyk*, M. Szaniawska, J. Krawczyk, Temperature effect on the adsorption and volumetric properties of aqueous solutions of Kolliphor ELP. *Molecules*, 2020, 25(3), 743.

Article

Temperature Effect on the Adsorption and Volumetric Properties of Aqueous Solutions of Kolliphor[®] ELP

Katarzyna Szymczyk *, Magdalena Szaniawska and Joanna Krawczyk

Department of Interfacial Phenomena, Institute of Chemical Sciences, Faculty of Chemistry,
Maria Curie-Skłodowska University in Lublin, Maria Curie-Skłodowska Sq. 3, 20-031 Lublin, Poland;
magdalena.szaniawska@poczta.umcs.lublin.pl (M.S.); j.krawczyk@poczta.umcs.lublin.pl (J.K.)

* Correspondence: katarzyna.szymczyk@poczta.umcs.lublin.pl; Tel.: +48-81-537-5538; Fax: +48-81-533-3348

Received: 10 January 2020; Accepted: 6 February 2020; Published: 9 February 2020



Abstract: Density, viscosity and surface tension of Kolliphor[®] ELP, the nonionic surfactant aqueous solutions were measured at temperature $T = 293\text{--}318\text{ K}$ and at 5K interval. Steady-state fluorescence measurements have been also made using pyrene as a probe. On the basis of the obtained results, a number of thermodynamic, thermo-acoustic and anharmonic parameters of the studied surfactant have been evaluated and interpreted in terms of structural effects and solute–solvent interactions. The results suggest that the molecules of studied surfactant at concentrations higher than the critical micelle concentration act as structure makers of the water structure.

Keywords: Kolliphor[®] ELP; volume expansivity; thermo-acoustic parameters; Gruneisen parameter; fractional free volume; coiling and micropolarity index

1. Introduction

Considering the landscape of current drug development, it can be stated, that 40% of NCE (new chemical entities) are characterized by poor water solubility [1]. Therefore, there is a need for excipients to solubilize such candidates in both the early preclinical and clinical evaluation, as well as for the development of the marketed drug dosage forms. Solubilization is the process of drug uptake through complex formation into, e.g., oligomers of dextrose and fatty acids, through the cosolvent systems (such as ethanol, polyethyleneglycol and glycerol), or through the surfactant systems [2]. Contrary to the expectation that pharmaceutical excipients are pharmacologically inactive, there is abundant evidence that they can influence drug metabolism and efflux transport [3–5]. Some surfactants, particularly nonionic Kolliphors which were known earlier as Cremophors, find application in pharmaceutical formulations as the forms of solid dosage and delivery systems based on lipids aimed at improvement of poorly water-soluble drugs bioavailability [2,6]. The tricinoleate ester of ethoxylated glycerol is the main component of Kolliphors. The others are polyethylene glycol ricinolates, as well as the corresponding free glycols [7]. Kolliphor[®] EL (EL), being the most often used Kolliphor, was applied as a vehicle in the case of solubilization of some hydrophobic drugs, including cyclosporin A, diazepam, propofol and paclitaxel [8]. However, some researchers stated that EL is not an inert vehicle but exerts a range of biological effects, some of which have important clinical implications. Its use was associated with severe anaphylactoid hypersensitivity reactions, hyperlipidemia, abnormal lipoprotein patterns, aggregation of erythrocytes and peripheral neuropathy. The pharmacokinetic behavior of EL is dose-independent, although its clearance is highly influenced by the duration of the infusion [9,10]. This is particularly important since EL can affect the disposition of various drugs by changing the unbound drug concentration through micellar encapsulation. From this point of view, a clear understanding of the biological and pharmacological role of surfactants is essential to help oncologists avoid side-effects associated with the use of paclitaxel or other agents. On the other

hand to describe the behavior of surfactants in relation to two non-miscible phases and the range of temperatures at which they are active, some adsorption and volumetric properties of the solution of such surfactants are needed. Thus, the purpose of the presented studies was to determine some adsorption, volumetric, thermo-acoustic as well as anharmonic properties of aqueous solutions of Kolliphor® ELP (ELP), a purified grade of EL, by surface tension, density and viscosity measurements at $T = 293\text{--}318\text{ K}$ with 5 K interval. Moreover, the properties of the solutions were studied by means of steady-state fluorescence measurements. Based on the results, the analysis was applied to study different molecular interactions in the solutions taking into account the change of these properties depending on concentration and temperature.

2. Results and Discussion

Table 1 presents the calculated different parameters determining the surface and bulk properties of aqueous solutions of ELP based on the values of their surface tension (γ_{LV}) (Figure 1). These parameters include: CMC (critical micelle concentration), surfactant efficiency for water surface tension reduction, which means the concentration of the surfactant for 20 mN/m reduction of the surface tension (C_{20}), preference of the surfactant for adsorption in relation to the micelle formation with the pointer indicating possible reduction of water surface tension due to the surfactant presence (CMC/C_{20}), the surface pressure at the CMC (Π_{CMC}), the surface excess concentration at the surface saturation (Γ_m), the minimum surface area per molecule (A_m), as well as the standard free enthalpy (ΔG_{mic}^0 and ΔG_{ad}^0), enthalpy (ΔH_{mic}^0 and ΔH_{ad}^0) and entropy (ΔS_{mic}^0 and ΔS_{ad}^0) of micellization and adsorption [11–13]. For studied ELP solutions, Γ_m and A_m were calculated from the equations:

$$\Gamma_m = -\frac{Cd\gamma_{LV}}{RTdC} = -\frac{1}{RT} \frac{d\gamma_{LV}}{d\ln C} = -\frac{1}{2.303RT} \frac{d\gamma_{LV}}{d\log C} \quad (1)$$

$$A_m = \frac{1}{N\Gamma_m} \quad (2)$$

where C represents the concentration of surfactant, R is a gas constant, T is temperature and N is an Avogadro number [11,12]. Next, the values of ΔG_{mic}^0 and ΔG_{ad}^0 were determined:

$$\Delta G_{mic}^0 = RT \ln \frac{CMC}{\omega} \quad (3)$$

$$\Delta G_{ad}^0 = \Delta G_{mic}^0 - \left(\frac{\Pi_{CMC}}{\Gamma_m} \right) \quad (4)$$

where ω is the number of water moles in 1 dm³.

Knowing the values of ΔG^0 at different temperatures, it was possible to calculate ΔH^0 and ΔS^0 . If it is assumed that in a range of temperature, ΔH^0 is constant, then:

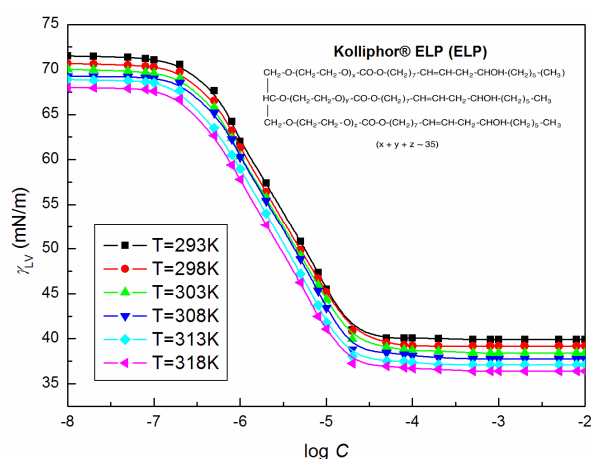
$$\frac{d(\Delta G^0)}{dT} = -\Delta S^0 \quad (5)$$

On the other hand, if ΔS^0 is constant, it is obtained [11]:

$$T^2 \frac{d\left(\frac{\Delta G^0}{T}\right)}{dT} = -\Delta H^0 \quad (6)$$

Table 1. Values of CMC , C_{20} , CMC/C_{20} , Π_{CMC} , ΔG_{mic}^0 , ΔS_{mic}^0 , ΔH_{mic}^0 , Γ_m , A_m , ΔG_{ad}^0 , ΔS_{ad}^0 and ΔH_{ad}^0 for the aqueous solutions of ELP at the temperatures from 293 to 318 K.

	T = 293K	298K	303K	308K	313K	318K
CMC (mol/dm ³)	2.14×10^{-5}	2.09×10^{-5}	2.03×10^{-5}	1.97×10^{-5}	1.91×10^{-5}	1.85×10^{-5}
C_{20} (mol/dm ³)	3.83×10^{-6}	3.82×10^{-6}	3.79×10^{-6}	3.74×10^{-6}	3.65×10^{-6}	3.53×10^{-6}
CMC/C_{20}	5.59	5.47	5.35	5.26	5.23	5.24
Π_{CMC} (mN/m)	32.91	32.82	32.72	32.59	32.43	32.29
ΔG_{mic}^0 (kJ/mol)	-26.19	-26.70	-27.22	-27.75	-28.28	-28.81
ΔS_{mic}^0 (kJ/mol K)	0.105					
ΔH_{mic}^0 (kJ/mol)	4.58	4.59	4.59	4.59	4.59	4.58
Γ_m (mol/m ²)	3.17×10^{-6}	3.11×10^{-6}	3.06×10^{-6}	3.01×10^{-6}	2.95×10^{-6}	2.90×10^{-6}
A_m (nm ²)	0.524	0.533	0.542	0.552	0.563	0.572
ΔG_{ad}^0 (kJ/mol)	-36.58	-37.23	-37.91	-38.58	-39.27	-39.93
ΔS_{ad}^0 (kJ/mol K)	0.135					
ΔH_{ad}^0 (kJ/mol)	2.98	3.00	3.00	3.00	2.99	3.00

**Figure 1.** A plot of the values of the surface tension (γ_{LV}) of the aqueous solution of Kolliphor[®] ELP (ELP) at T = 293 K, 298 K, 303 K, 308 K, 313 K and 318 K vs. the logarithm of the surfactant concentration, $\log C$.

As follows from the table, the calculated values of ΔG_{mic}^0 and ΔG_{ad}^0 are negative, indicating that the ELP molecules have a trend to adsorb at the water–air interface and to form micelles in the bulk phase, as well as the two processes are spontaneous. The adsorption free enthalpy values are more negative in comparison with the micellization values indicating greater propensity of ELP for adsorption at the interface than micelles formation in the bulk phase. The ΔG_{mic}^0 and ΔG_{ad}^0 values become more negative with the increasing temperature probable due to the greater stability of the adsorbed and micellized molecules of ELP compared to the freely dispersed in the aqueous phase. However, the positive values of ΔS_{ads}^0 show that, after adsorption and micellization, the studied solutions become more random [11].

On the other hand, ΔH_{mic}^0 and ΔH_{ads}^0 positive values indicate the predominance of bond breaking when micellization and adsorption proceed. Figure 1 shows the gradual decrease of ELP surface tension values with the increasing temperature being 293–318 K, which is similar to the Γ_m, Π_{CMC} and CMC/C_{20} values (Table 1). As follows from the data presented in Table 1, the ELP CMC values drop slightly with the temperature rise from 293 to 318 K. This indicates that temperature increase can break down the intra-hydrogen bonds between the surfactant molecules and weaken the hydration action of the hydrophilic groups, which favors the micelle formation [14].

The surface tension isotherm ($\gamma_{LV} = f(\log C)$) is known to not be the only way to determine CMC. What is more, the values of CMC for a surface-active agent very often differ depending on its determination method [15]. Considering the values of the dynamic viscosity (η) of ELP aqueous solutions (Figure 2 as an example), it is evident that the great increase of the η values take place at 293 K and the concentration exceeding 10^{-3} M.

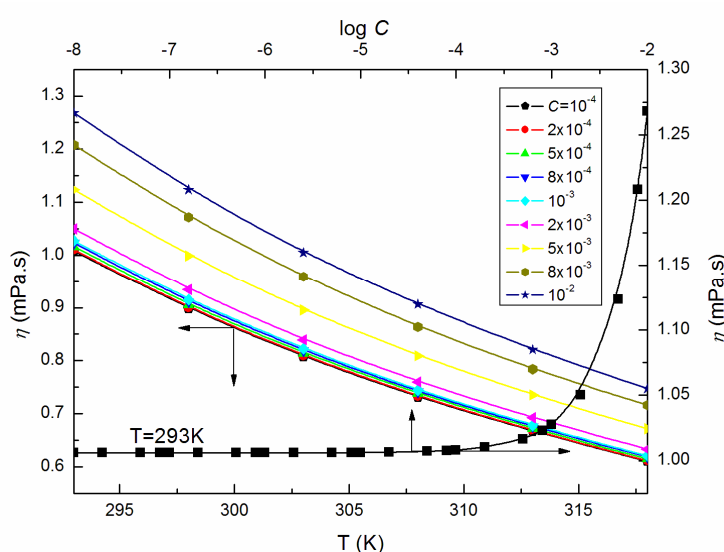


Figure 2. A plot of the values of η of aqueous solutions of ELP at C from 10^{-4} to 10^{-2} M vs. the temperature, T , as well as the values of η of the aqueous solutions of ELP at $T = 293$ K vs. $\log C$.

Based on the relations between the relative viscosity (η/η_0) and concentration C [16] of ELP at a given T (Figure 3 as an example), the CMC values are as follows: 9.87×10^{-6} M, 9.84×10^{-6} M, 9.73×10^{-6} M, 9.66×10^{-6} M, 9.52×10^{-6} M and 9.32×10^{-6} M in the temperature range 293–318 K. They are similar to the values given in Table 1. However, besides the determination of CMC from the viscosity measurements, it was attempted to relate the surface tension with viscosity [17]. Moreover, the basic equation proposed by Pelofsky is the linear relation and can be used for organic and inorganic phases of pure and mixed components [18]. It is interesting that, taking into account the measured values of γ_{LV} and η at a given temperature, and C corresponding to the saturated monolayer at the water–air interface, there is the linear dependence proposed by Pelofsky that is between $\ln \gamma_{LV}$ and $1/\eta$ for the ELP solutions (Figure 3).

On the other hand, the constant B in the relation presented by the author as a function of the molecular weight and thermal conductivity possesses a positive value at each temperature contrary to the values for n -alkanes, n -alcohols, water as well as some aqueous solutions [17]. In our opinion, the B parameter values can be better explained by conducting additional measurements for a larger amount of surfactant concentrations. Therefore, it is certain that the measured dynamic viscosity (η) of ELP solutions is greatly sensitive to changes in temperature (exemplary Figure 2) following the Arrhenius law [19,20]:

$$\eta = B \exp \frac{E_a}{RT} \quad (7)$$

where B is the pre-exponential factor and E_a is shear activation energy. The calculated from Equation (7) values of E_a (Figure 4), that is energy necessary for individual micelles motion in an environment of surrounding micelles determined on the basis of this law, increases significantly at ELP concentrations in the bulk phase higher than 10^{-3} M. Moreover, the highest value of E_a being 16.35 kJ/mol is found at $C = 10^{-2}$ M. Furthermore, the enthalpy of activation (ΔH^*) values, as well as the change in heat capacity of activation (ΔC_p^*), are affected to a great extent by temperature (exemplary Figures 5 and 6). The values of ΔH^* and ΔC_p^* were determined based on the relations proposed by Mukherjee et al. [21,22]:

$$-\frac{\Delta H^*}{RT^2} = \frac{d \ln \eta}{dT} \quad (8)$$

$$\Delta C_p^* = \frac{d\Delta H^*}{dT} \quad (9)$$

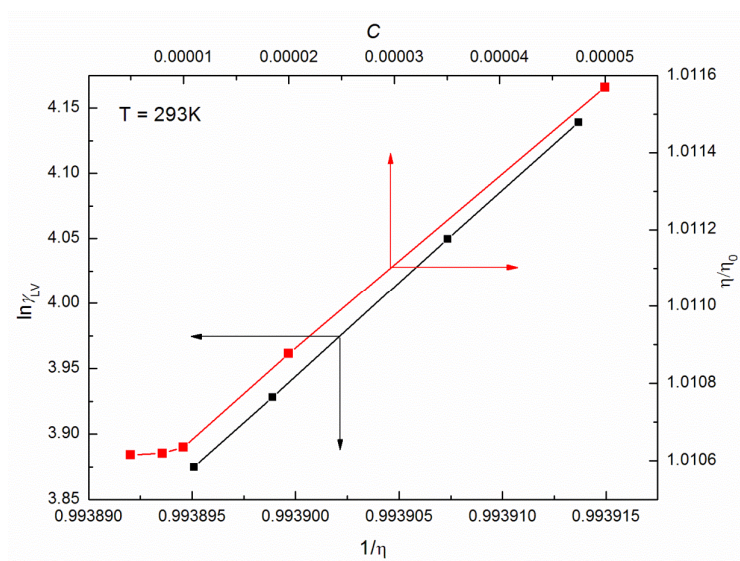


Figure 3. A plot of the values of the $\ln \gamma_{LV}$ vs. $1/\eta$ as well as η/η_0 vs. C for the aqueous solutions of ELP at $T = 293$ K.

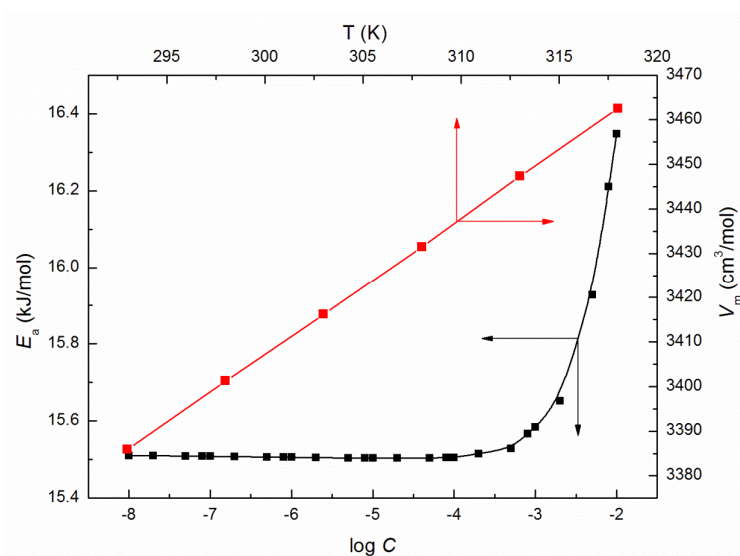


Figure 4. A plot of the values of shear activation energy (E_a) of the aqueous solutions of ELP vs. $\log C$, as well as the values of the partial molar volume (V_M) of the aqueous solutions of ELP vs. the temperature, T .

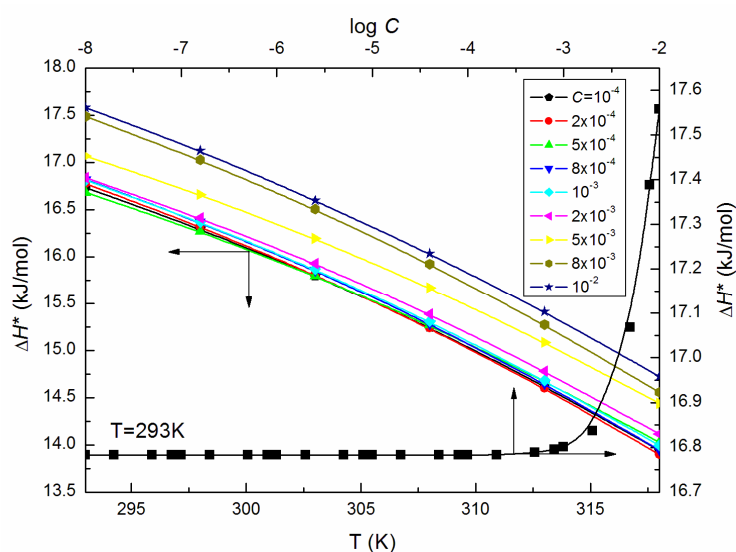


Figure 5. A plot of the values of the enthalpy of activation (ΔH^*) of the aqueous solutions of ELP at C from 10^{-4} to 10^{-2} M vs. the temperature, T , as well as the values of ΔH^* of the aqueous solutions of ELP at $T = 293$ K vs. $\log C$.

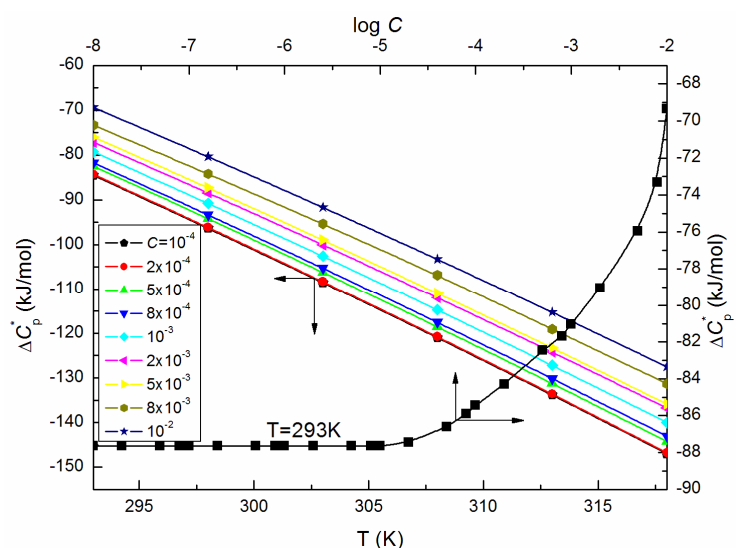


Figure 6. A plot of the values of the change in heat capacity of activation (ΔC_p^*) of the aqueous solutions of ELP at C from 10^{-4} to 10^{-2} M vs. the temperature, T , as well as the values of ΔC_p^* of the aqueous solutions of ELP at $T = 293$ K vs. $\log C$.

What is more, the ΔH^* values calculated from Equation (8) for the ELP solutions are positive and expectedly declined with increasing temperature (Figure 5) indicating that the processes are connected with the heat absorption in the solutions under considerations. From this reason, the ΔC_p^* values are negative and decrease linearly with T (Figure 6).

As the ELP molecules are strongly hydrated by water, and it is possible that the H_3O^+ ions can be associated to the oxyethylene groups, similarly to other nonionic surfactants studied by us [15,22–25], it was also interesting to analyze the viscosity data according to the Jones–Dole equation and A and B coefficients [26,27]. This equation and the relationship between $(\eta_r - 1)C^{-0.5}$ and $C^{0.5}$ (Figure 7) for C equal to and higher than 5×10^{-3} M, where η_r is the relative viscosity, were used for the determination of B coefficients values which proved to be positive (Figure 8), disclosing the water-structure-breaking nature of the ELP molecules. It is interesting that the value of dB/dT , which by some authors is designed as a better criterion for determining any solute effect on the structure of

solutions depending on temperature [28], for the studied concentrations of ELP solutions, is equal to -0.21 , and according to Hugue et al. [28], indicates that the solute is a structure maker. To solve an idea about the structure-making or breaking role of the ELP in the solution, the apparent molar volume values, ϕ_V [29,30], were determined from the density measurements (ρ) (exemplary Figures 9 and 10) and the equation which has the form:

$$\phi_V = \frac{M}{\rho_0} + \frac{1000(\rho_0 - \rho)}{C} \quad (10)$$

where M is the molecular weight of the surface-active agent and ρ_0 is the density of the “pure” solvent. The calculated values of ϕ_V were then analyzed based on the Hepler equation [31]. It proved that at C equal to and greater than 5×10^{-3} M, the values of $(\partial^2 \phi_V^0 / \partial T^2)_p$, where ϕ_V^0 is the apparent molar volume at infinite dilution, are positive, indicating the structure-making properties of the investigated surfactant.

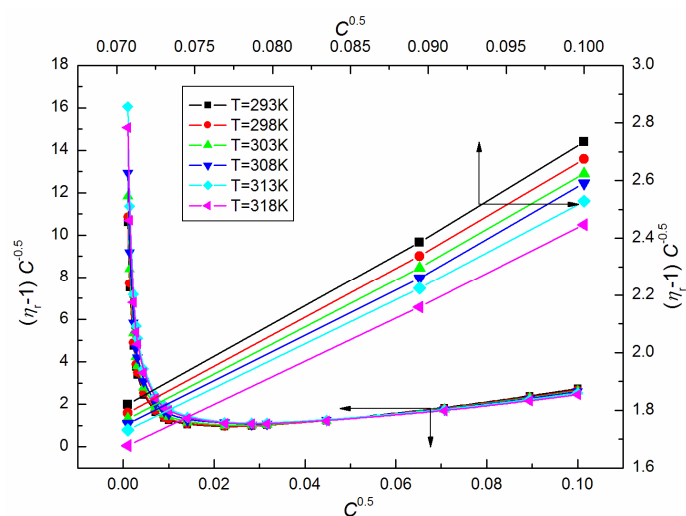


Figure 7. A plot of the values of $(\eta_r - 1)C^{-0.5}$ of the aqueous solutions of ELP at $T = 293$ K, 298 K, 303 K, 308 K, 313 K and 318 K vs. $C^{0.5}$

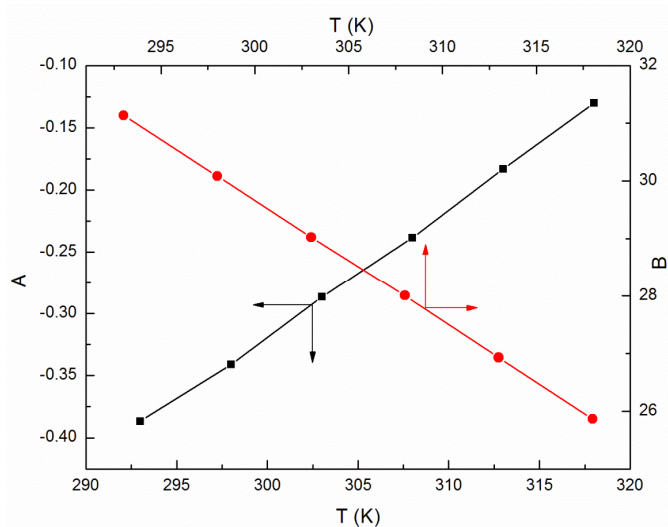


Figure 8. A plot of the values of A and B coefficients determined from the Jones–Dole equation and viscosity of the aqueous solutions of ELP vs. T .

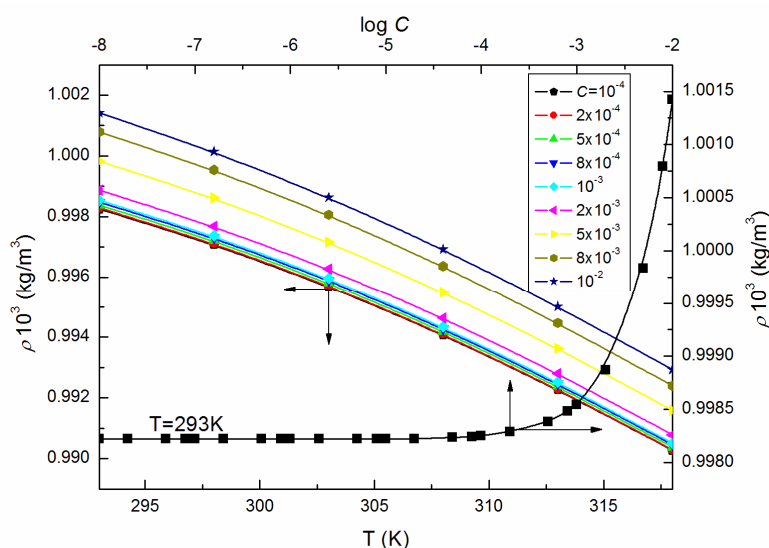


Figure 9. A plot of the values of ρ of the aqueous solutions of ELP at C from 10^{-4} to 10^{-2} M vs. the temperature, T , as well as the values of ρ of the aqueous solutions of ELP at $T = 293$ K vs. $\log C$.

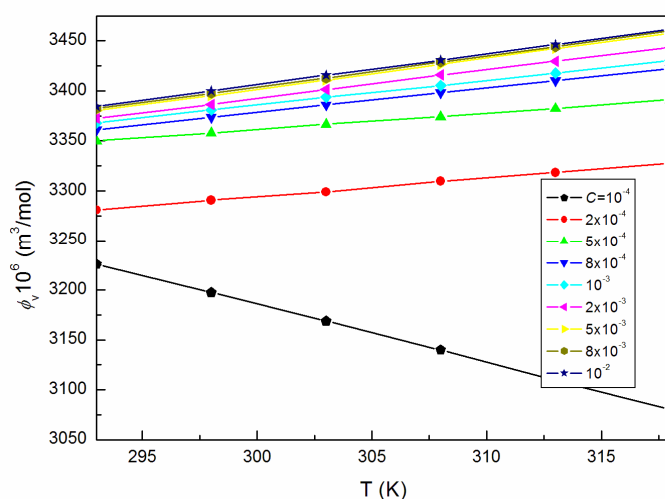


Figure 10. A plot of the values of the apparent molar volume, ϕ_V , of the aqueous solutions of ELP at C from 10^{-4} to 10^{-2} M vs. the temperature, T .

However, the changes of the ϕ_V values with T before and after $C = 10^{-4}$ M (shown in Figure 10) are different pointing out the great structural changes of ELP molecules due to the increase in temperature and/or those of intermolecular interactions between the surfactant and water. They, in turn, can be determined, among others, based on the volume expansivity values α (Figure 11), which are also regarded as the thermal expansion coefficient being a measure of volume change with the temperature and can be calculated based on the measurements of density from the equation [18,28]:

$$\alpha = \frac{1}{V_m} \left(\frac{dV_m}{dT} \right) \quad (11)$$

where V_m is the partial molar volume. It follows from Figure 11 that for ELP, the calculated values of α increase with the rise of T and C , which is consistent with the increasing tendency of V_M for studied solutions (Figure 4) at the concentrations higher than CMC of the studied surfactant determined from the surface tension measurements (Table 1).

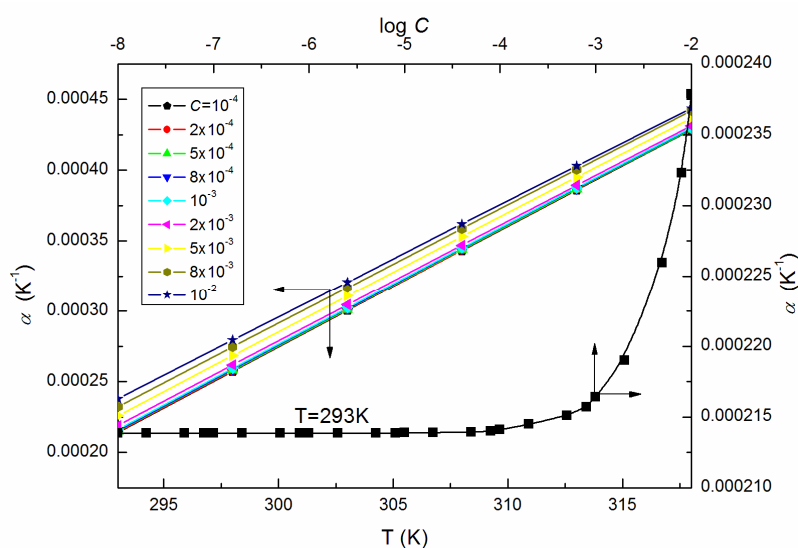


Figure 11. A plot of the volume expansivity α of the aqueous solutions of ELP at C from 10^{-4} to 10^{-2} M vs. the temperature, T , as well as the values of α of the aqueous solutions of ELP at $T = 293$ K vs. $\log C$.

Having the ELP α values at various temperatures and concentrations, there could be calculated the thermodynamic parameters such as: reduced volume (\tilde{V}), Moelwyn–Hughes parameter (C_1), reduced compressibility ($\tilde{\beta}$), isochoric temperature coefficient of internal pressure (X), Sharma parameter (S_0), Huggin’s parameter (F), isochoric temperature coefficient of volume expansivity (X'), anharmonic microscopic isothermal Gruneisen parameter (Γ), fractional free volume (f), Gruneisen parameter (Γ_p), isobaric thermo-acoustic parameter (K) and isochoric thermo-acoustic parameter (K'') [32–35]. These parameters for ELP solutions are presented in Table S1 (Supplementary Materials) and were calculated from the following equations:

$$\tilde{V} = \left\{ \frac{\left(\frac{\alpha T}{3}\right)}{1 + \alpha T} + 1 \right\}^3 \quad (12)$$

$$C_1 = \left(\frac{13}{3}\right) + \left(\frac{1}{\alpha T}\right) + \left(\frac{4\alpha T}{3}\right) \quad (13)$$

$$\tilde{\beta} = [\tilde{V}C_1]^{-1} \quad (14)$$

$$X = -\frac{2(1 + 2\alpha T)}{\tilde{V}C_1} \quad (15)$$

$$S_0 = \left(-\frac{X}{2}\right)(3 + 4\alpha T) \quad (16)$$

$$F = 2\left[1 + \left(\frac{S_0}{3 + 4\alpha T}\right)\right] - \left(3 + \frac{4\alpha T}{3}\right) \quad (17)$$

$$X' = -(1 + 2\alpha T) \quad (18)$$

$$\Gamma = \left(\frac{2}{3}\right)\alpha T + \left(\frac{2 - F + 4\alpha T}{2\alpha T}\right) \quad (19)$$

$$f = \frac{1}{(\Gamma + 1)} \quad (20)$$

$$\Gamma_p = \left(\frac{2}{3}\right)\alpha T + \left(\frac{1}{2\alpha T}\right) + 2 \quad (21)$$

$$K = \frac{1}{2} \left[1 + \frac{(1 + \frac{4\alpha T}{3})(1 + \alpha T)}{\alpha T} \right] \quad (22)$$

$$K' = \frac{1}{2} \left[3 + \frac{(1 + \frac{4\alpha T}{3})(1 + \alpha T) + X}{\alpha T} \right] \quad (23)$$

Table S1 shows the variable character of S_0 and T which differs from the suggestions given by Sharma et al. [20,36]. They stated that S_0 is the constant in any liquid or solid-state system. However, fractional free volume (f) values, which are expressed in terms of the repulsive exponent of intermolecular potential, are characterized by the non-linear rise with T pointing out that the surfactant molecules mobility results in greater liquid (surfactant + water) disorder, which is due to irregular molecular packing [35]. Simultaneously the C_1 , X' , F , Γ and Γ_p the decreasing values with the increasing temperature and concentration of the surfactant indicating the molecular ordering increase with the increasing values of T and C [37]. This is consistent with the conclusions drawn based on the viscosity measurements namely that the ELP molecules act as a structure maker at its high concentrations. One should bear in mind that ELP, as a nonionic surfactant possessing three amphiphilic chains, is a nonconventional surfactant that can be treated as a polymer. The coiling index was determined based on the pyrene fluorescence spectroscopy in order to reveal the changes of the chains' conformation. It is the ratio of the excimer intensity I_E (at ~480 nm) and the monomer, $I_M = (I_1 + I_3)/2$, where I_1 and I_3 are the intensity of the first and the third vibrionic peaks in the pyrene emission spectra [38]. The high value of I_E/I_M indicates the medium with a greater possibility of excimer formation and coiled surfactant chains. As can be seen in Figure 12, the highest coiling index values are found at the concentrations close to the ELP CMC values calculated from the surface tension measurements as well as the C values with the polarity index (I_1/I_3) characterized by a minimal value. Considering the concentration values higher than CMC, there is observed the I_E/I_M values' decrease with the increasing number of micelles providing more pyrene locations or micellar size or shape changes. At C higher than 10^{-3} M, I_E/I_M is still constant with the lowest values indicating stretching of the surfactant chains, which is consistent with the f values which increase remarkably at C greater than 10^{-3} M at a given temperature (Table S1).

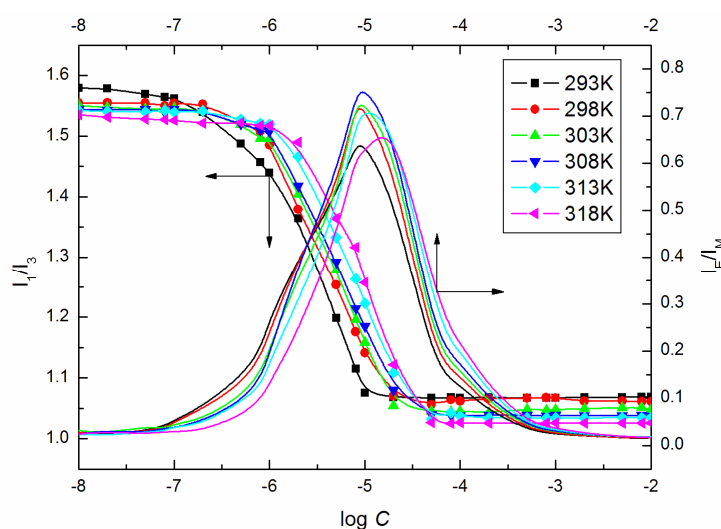


Figure 12. Plot of the values of I_E/I_M and I_1/I_3 determined from the fluorescence spectra of pyrene in the aqueous solutions of ELP vs. $\log C$.

3. Materials and Methods

Kolliphor[®] ELP (ELP) (Cremophor[®]ELP, Polyoxyl 35 Hydrogenated Castor Oil, Polyoxyl-35 Castor Oil) purchased from Sigma were used without further purification. Its aqueous solutions

were obtained at the concentrations 10^{-6} to 10^{-2} M applying the doubly distilled and deionized water provided by a Destamat Bi18E distiller. The surface tension was measured by means of a Krüss K100C tensiometer according to the platinum ring tensiometer method (du Nouy's method). The measurements of pure water surface tension at 293 K were aimed at the calibration of the tensiometer and glassware cleanliness control. There were performed ten successive measurements with the standard deviation not exceeding ± 0.2 mN/m. The controlled temperature was within ± 0.1 K. The measurements of surfactant aqueous solutions density were performed by means of a U-tube densitometer (DMA 5000 Anton Paar) at 293–318 K. The density and temperature measurement precision given by the producer was ± 0.000005 g cm $^{-3}$ and ± 0.001 K. The calculated uncertainty was 0.01%. The densitometer calibration with distilled and deionized water was regular.

The surfactant aqueous solutions viscosity was determined using the Anton Paar viscometer (AMVn) at 293–318 K ± 0.01 K. Its precision was 0.0001 mPa s and the uncertainty was 0.3%. The steady-state fluorescence was measured at 293–318 K by means of a Hitachi F-2700 Fluorescence Spectrometer where pyrene was as a luminescence probe ($C_{Py} = 4 \times 10^{-6}$ M). The fluorescence excitation for pyrene was induced at 335 nm and the range of the emission spectra recording was 350–600 nm at a scan speed of 300 nm/min. The widths of the excitation and emission slit widths were 5 nm.

4. Conclusions

In this paper, some physicochemical properties of the aqueous solutions of the nonionic surfactant, Kolliphor®ELP (ELP), are singled out, discussed and compared on the basis of the surface tension, density and viscosity measurements as well as fluorescence spectra. From the presented data and calculations, it is evident that ELP displays a greater propensity to be absorbed at the interface than form micelle in the bulk phase and that bond breaking predominates in the micellization and adsorption process. The ELP structure-making tendency at concentrations higher than 10^{-3} M was confirmed by the Hepler's theory as well as the values of viscosity B coefficients and apparent molar volume. In addition, at this concentration range and a given temperature, the stretching of the surfactant chains were proved on the basis of pyrene emission spectra and the values of fractional free volume. On the other hand, at a concentration of ELP smaller than CMC, the polar head of the surfactant is strongly hydrated resulting in very compact conformation, probably because of water-bridging, which promotes gauche conformations.

Supplementary Materials: The following are available online, Table S1: Values of \tilde{V} , C_1 , $\tilde{\beta}$, X , S_0 , F , X' , Γ , f , Γ_p , K and K'' for the aqueous solutions of ELP at the temperatures from 293 to 318 K.

Author Contributions: Conceptualization, K.S.; investigation, M.S.; project administration, K.S. and M.S.; software, J.K.; supervision, K.S. and J.K.; writing—original draft, K.S. All authors have read and agreed to the published version of the manuscript.

Conflicts of Interest: The authors declare no conflicts of interest.

References

1. Otter, M.; Oswald, S.; Siegmund, W.; Keiser, M. Effects of frequently used pharmaceutical excipients on the organic cation transporters 1–3 and peptide transporters 1/2 stably expressed in MDCKII cells. *Europ. J. Pharm. Biopharm.* **2017**, *112*, 187–195. [[CrossRef](#)] [[PubMed](#)]
2. Gelderblom, H.; Verweij, J.; Nooter, K.; Sparreboom, A. Cremophor EL: The drawbacks and advantages of vehicle selection for drug formulation. *Eur. J. Cancer* **2001**, *37*, 1590–1598. [[CrossRef](#)]
3. Shi, Y.; Porter, W.; Merdan, T.; Li, L.C. Recent advances in intravenous delivery of poorly water-soluble compounds. *Expert Opin. Drug Deliv.* **2009**, *6*, 1261–1282. [[CrossRef](#)] [[PubMed](#)]
4. Hanke, U.; May, K.; Rozehnal, V.; Nagel, S.; Siegmund, W.; Weitschies, W. Commonly used nonionic surfactants interact differently with the human efflux transporters ABCB1 (p-glycoprotein) and ABCC2 (MRP2). *Eur. J. Pharm. Biopharm.* **2010**, *76*, 260–268. [[CrossRef](#)] [[PubMed](#)]

5. Christiansen, A.; Backensfeld, T.; Denner, K.; Weitschies, W. Effects of non-ionic surfactants on cytochrome P450-mediated metabolism in vitro. *Eur. J. Pharm. Biopharm.* **2011**, *78*, 166–172. [[CrossRef](#)] [[PubMed](#)]
6. Berthelsen, R.; Holm, R.; Jacobsen, J.; Kristensen, J.; Abrahamsson, B.; Müllertz, A. Kolliphor surfactants affect solubilization and bioavailability of fenofibrate. Studies of in vitro digestion and absorption in rats. *Mol. Pharma.* **2015**, *12*, 1062–1071. [[CrossRef](#)]
7. Christiansen, A.; Backensfeld, T.; Weitschies, W. Effects of nonionic surfactants on in vitro triglyceride digestion and their susceptibility to digestion by pancreatic enzymes. *Eur. J. Pharm. Sci.* **2010**, *41*, 376–382. [[CrossRef](#)]
8. Bakonyia, M.; Berkó, S.; Kovács, A.; Budai-Szűcs, M.; Kisa, N.; Erős, G.; Csóka, I.; Csányi, E. Application of quality by design principles in the development and evaluation of semisolid drug carrier systems for the transdermal delivery of lidocaine. *J. Drug Deliv. Sci. Technol.* **2018**, *44*, 136–145. [[CrossRef](#)]
9. Buggins, T.R.; Dickinson, P.A.; Taylor, G. The effects of pharmaceutical excipients on drug disposition. *Adv. Drug Deliv. Rev.* **2007**, *59*, 1482–1503. [[CrossRef](#)]
10. Ganetsky, M.; Böhlke, M.; Pereira, L.; Williams, D.; LeDuc, B.; Guatam, S.; Salhanick, S.D. Effect of excipients on acetaminophen metabolism and its implications for prevention of liver injury. *J. Clin. Pharmacol.* **2013**, *53*, 413–420. [[CrossRef](#)]
11. Rosen, J.M. *Surfactants and Interfacial Phenomena*, 3rd ed.; Wiley Interscience: New York, NY, USA, 2004; pp. 59–167.
12. Szymczyk, K. The properties of binary mixtures of ethoxylatedoctyl phenols with ethoxylated fluorinated alkanols at the water/air interface. *J. Surf. Deterg.* **2011**, *14*, 415–423. [[CrossRef](#)]
13. Adamson, A.W.; Gast, A.P. *Physical Chemistry of Surfaces*, 3rd ed.; Wiley-Interscience: New York, NY, USA, 1997; pp. 71–77.
14. Xie, Y.; Li, J.; Sun, T.; Han, Y.; Qu, G.; Niu, R. Synthesis, surface activity, and corrosion inhibition of dentritic quaternary ammonium salt-type tetrameric surfactants. *J. Disper. Sci. Technol.* **2018**, *39*, 1153–1159. [[CrossRef](#)]
15. Szymczyk, K. Behaviour of the fluorocarbon surfactants in the monolayer at the water-air interface and in the bulk phase. *J. Fluorine Chem.* **2013**, *150*, 109–116. [[CrossRef](#)]
16. Wu, C.; Li, N.J.; Chen, K.C.; Hsu, H.-F. Determination of critical micelle concentrations of ionic and nonionic surfactants based on relative viscosity measurements by capillary electrophoresis. *Res. Chem. Int.* **2014**, *40*, 2371–2379. [[CrossRef](#)]
17. Queimada, A.J.; Marrucho, I.M.; Stenby, E.H.; Coutinho, J.A.P. Generalized relation between surface tension and viscosity: a study on pure and mixed n-alkanes. *Fluid Phase. Equilib.* **2004**, *222–223*, 161–168. [[CrossRef](#)]
18. Pelofsky, A.H. Surface tension-viscosity relation for liquids. *J. Chem. Eng. Data* **1966**, *11*, 394–397. [[CrossRef](#)]
19. Subrahmanyam, M.S.R.; Vedanayagam, H.S.; Venkateshwar, R.D.; Rajaiah, A.; Venkatacharyulu, P. Estimation of Sharma constant and thermoacoustic properties of fatty acids. *J. Am. Oil Chem. Soc.* **1995**, 1537–1540. [[CrossRef](#)]
20. Sharma, B.K. Volume dependence of thermodynamic Grüneisen parameter of fluorocarbon fluids. *Phys. Lett.* **1983**, *99*, 227–229. [[CrossRef](#)]
21. Mukherjee, I.; Manna, K.; Dinda, G.; Ghosh, S.; Moulik, S.P. Shear- and temperature-dependent viscosity behavior of two phosphonium-based ionic liquids and surfactant triton X-100 and their biocidal activities. *J. Chem. Eng. Data* **2012**, *57*, 1376–1386. [[CrossRef](#)]
22. Szymczyk, K.; Taraba, A. Aggregation behavior of Triton X-114 and Tween 80 at various temperatures and concentrations studied by density and viscosity measurements. *J. Therm. Anal. Calorim.* **2016**, *126*, 315–326. [[CrossRef](#)]
23. Szymczyk, K.; Taraba, A. Properties of aqueous solutions of nonionic surfactants, Triton X-114 and Tween 80, at temperatures from 293 to 318K: spectroscopic and ultrasonic studies. *Chem. Phys.* **2017**, *483–484*, 96–102. [[CrossRef](#)]
24. El Eini, D.I.; Barry, B.W.; Rhodes, J. Micellar size, shape, and hydration of long-chain polyoxyethylene nonionic surfactants. *J. Colloid Inter. Sci.* **1976**, *54*, 348–351. [[CrossRef](#)]
25. Desai, T.R.; Dixit, S.G. Interaction and viscous properties of aqueous solutions of mixed cationic and nonionic surfactants. *J. Colloid Inter. Sci.* **1966**, *177*, 471–477. [[CrossRef](#)]
26. Jones, G.; Dole, M. The viscosity of aqueous solutions of strong electrolytes with special reference to barium chloride. *J. Am. Chem. Soc.* **1929**, *51*, 2950–2964. [[CrossRef](#)]

27. Ali, A.; Hyder, S.; Akhtar, Y. Viscometric studies of α -amino acid in aqueous NaCl and MgCl₂ at 303 K. *Indian J. Phys.* **2005**, *79*, 157–160.
28. Huque, M.; Siddiquey, I.A.; Uddin, N. Volumetric and viscometric studies on dodecyltrimethylammonium bromide in aqueous and in aqueous amino acid solutions in premicellar region. *J. Chem. Thermodyn.* **2006**, *38*, 1474–1478. [[CrossRef](#)]
29. Gautam, P.K.; Gautam, R.K.; Rai, R.; Pandey, J.D. Thermodynamic and transport properties of sodium dodecylbenzenesulphonate (SDBS) in aqueous medium over the temperature range 298.15 K to 333.15 K. *J. Mol. Liq.* **2014**, *191*, 107–110. [[CrossRef](#)]
30. Szymczyk, K.; Jańczuk, B. The adsorption at solution-air interface and volumetric properties of mixtures of cationic and nonionic surfactants. *Coll. Surf. A* **2007**, *293*, 39–50. [[CrossRef](#)]
31. Hepler, L.G. Thermal expansion and structure in water and aqueous solutions. *Can. J. Chem.* **1969**, *47*, 4613–4617. [[CrossRef](#)]
32. SunilBabu, K.; VenkateswaraRao, A.; MadhaviLatha, D.; Pardhasaradhi, P.; Pisipati, V.G.K.M. Estimation of thermodynamic parameters in 4-(hexyloxybenzylidene)-4'-alkoxy anilines, 6O-Om liquid crystalline compounds— A densitystudy. *J. Mol. Liq.* **2016**, *220*, 999–1003.
33. VenkataRao, D.; Pardhasaradhi, P.; Pisipati, V.G.K.M.; Madhavi Latha, D.; Datta Prasad, P.V. Estimation of thermodynamic parameters in 3.Om and 3O.Om liquid crystalline compounds. *J. Mol. Liq.* **2015**, *211*, 90–95. [[CrossRef](#)]
34. Reddy, R.R.; Rama Gopal, K.; Narasimhulu, K.; Siva Sankara Reddy, L.; Raghavendra Kumar, K.; Venkatesulu, A.; Krishna Reddy, C.V. Correlations between Moelwyn–Hughes parameter, available volume and intermolecular free-lengths in liquid systems. *J. Mol. Liq.* **2008**, *140*, 48–53. [[CrossRef](#)]
35. Sannaningannavar, F.M.; Patil, S.N.; Navati, B.S.; Melavanki, R.M.; Ayachit, N.H. Studies on thermodynamic properties of purepoly(ethyleneglycol)-400 in the temperature range 299–363 K using volume expansivities. *Polym. Bull.* **2013**, *70*, 3171–3183. [[CrossRef](#)]
36. Sharma, B.K.; Reddy, R.R. Sharmaconstant and some more thermo-acousticproperties of ionic liquids. *Ind. J. Pure. Appl. Phys.* **1985**, *23*, 396–399.
37. Fakruddin, K.; Jeevan Kumar, R.; Pisipati, V.G.K.M.; MadhaviLatha, D.; Madhav, B.T.P.; Datta Prasad, P.V. Phase transitions and thermodynamic parameters of N-(p-n-octyloxybenzylidene)-p-nalkoxyanilines—A dilatometric study. *Mol. Cryst. Liq. Cryst.* **2010**, *524*, 102–118. [[CrossRef](#)]
38. Dong, D.C.; Winnik, M.A. The Py scale of solvent polarities. *Can. J. Chem.* **1984**, *62*, 2560–2565. [[CrossRef](#)]

Sample Availability: Samples of the compounds are not available from the authors.



© 2020 by the authors. Licensee MDPI, Basel, Switzerland. This article is an open access article distributed under the terms and conditions of the Creative Commons Attribution (CC BY) license (<http://creativecommons.org/licenses/by/4.0/>).

ZAŁĄCZNIK 2a

MATERIAŁ UZUPEŁNIAJĄCY [SM2]

K. Szymczyk*, M. Szaniawska, J. Krawczyk, Temperature effect on the adsorption and volumetric properties of aqueous solutions of Kolliphor ELP. *Molecules*, 2020, 25(3), 743.

SUPPLEMENTARY MATERIALS

Temperature Effect on the Adsorption and Volumetric Properties of Aqueous Solutions of Kolliphor®ELP

Katarzyna Szymczyk*, Magdalena Szaniawska and Joanna Krawczyk

Department of Interfacial Phenomena, Institute of Chemical Sciences, Faculty of Chemistry, Maria Curie-Skłodowska University in Lublin, Maria Curie-Skłodowska Sq. 3, 20-031 Lublin, Poland

Phone: (48-81) 537-5538

Fax: (48-81) 533-3348

*Correspondence: katarzyna.szymczyk@poczta.umcs.lublin.pl (K. Szymczyk)

Table S1. Values of \tilde{V} , C_1 , $\tilde{\beta}$, X , S_0 , F , X' , Γ , f , Γ_p , K and K'' for the aqueous solutions of ELP at the temperatures from 293 to 318 K.

	C	293K	298K	303K	308K	313K	318K	
\tilde{V}	10^{-5}	1.0681	1.0848	1.1026	1.1215	1.1416	1.1629	
	2×10^{-5}	1.0681	1.0848	1.1026	1.1215	1.1416	1.1629	
	5×10^{-5}	1.0681	1.0848	1.1026	1.1215	1.1416	1.1630	
	8×10^{-5}	1.0681	1.0848	1.1026	1.1215	1.1416	1.1630	
	10^{-4}	1.0682	1.0848	1.1027	1.1215	1.1417	1.1630	
	2×10^{-4}	1.0683	1.0850	1.1028	1.1216	1.1418	1.1631	
	5×10^{-4}	1.0685	1.0852	1.1030	1.1218	1.1419	1.1632	
	8×10^{-4}	1.0687	1.0854	1.1032	1.1221	1.1422	1.1634	
	10^{-3}	1.0690	1.0856	1.1034	1.1223	1.1423	1.1635	
	2×10^{-3}	1.0698	1.0865	1.1042	1.1230	1.1430	1.1642	
	5×10^{-3}	1.0723	1.0889	1.1067	1.1255	1.1455	1.1667	
	8×10^{-3}	1.0745	1.0912	1.1089	1.1278	1.1478	1.1690	
	10^{-2}	1.0764	1.0929	1.1105	1.1291	1.1488	1.1698	
	C_1	10^{-5}	20.3750	17.4834	15.4432	13.9331	12.7715	11.8545
		2×10^{-5}	20.3730	17.4822	15.4421	13.9329	12.7711	11.8543
		5×10^{-5}	20.3710	17.4809	15.4406	13.9327	12.7706	11.8538
8×10^{-5}		20.3657	17.4792	15.4399	13.9325	12.7702	11.8534	
10^{-4}		20.3583	17.4786	15.4364	13.9321	12.7688	11.8529	
2×10^{-4}		20.3303	17.4569	15.4230	13.9275	12.7625	11.8501	
5×10^{-4}		20.2835	17.4284	15.4094	13.9107	12.7575	11.8454	
8×10^{-4}		20.2410	17.4045	15.3876	13.8912	12.7446	11.8369	
10^{-3}		20.1879	17.3682	15.3695	13.8833	12.7383	11.8318	
2×10^{-3}		20.0034	17.2532	15.2946	13.8331	12.7040	11.8083	
5×10^{-3}		19.5278	16.9378	15.0743	13.6735	12.5852	11.7178	
8×10^{-3}		19.1156	16.6615	14.8801	13.5320	12.4793	11.6371	
10^{-2}		18.7756	16.4544	14.7511	13.4517	12.4308	11.6098	
$\tilde{\beta}$		10^{-5}	3.8265	4.1502	4.5198	4.9423	5.4277	5.9861
		2×10^{-5}	3.8267	4.1504	4.5200	4.9423	5.4279	5.9862
		5×10^{-5}	3.8268	4.1505	4.5204	4.9424	5.4282	5.9866
	8×10^{-5}	3.8273	4.1508	4.5205	4.9425	5.4284	5.9869	
	10^{-4}	3.8279	4.1509	4.5213	4.9426	5.4291	5.9873	
	2×10^{-4}	3.8304	4.1540	4.5244	4.9442	5.4323	5.9893	
	5×10^{-4}	3.8345	4.1582	4.5275	4.9500	5.4349	5.9928	
	8×10^{-4}	3.8383	4.1617	4.5325	4.9568	5.4414	5.9990	
	10^{-3}	3.8430	4.1670	4.5367	4.9595	5.4446	6.0028	
	2×10^{-3}	3.8597	4.1842	4.5542	4.9773	5.4624	6.0202	
	5×10^{-3}	3.9052	4.2335	4.6077	5.0353	5.5255	6.0891	
	8×10^{-3}	3.9477	4.2794	4.6574	5.0893	5.5842	6.1529	
	10^{-2}	3.9850	4.3157	4.6919	5.1211	5.6120	6.1750	
	X	10^{-5}	-0.5882	-0.5558	-0.5230	-0.4902	-0.4575	-0.4251
		2×10^{-5}	-0.5882	-0.5558	-0.5230	-0.4902	-0.4575	-0.4251

	5×10^{-5}	-0.5881	-0.5557	-0.5230	-0.4902	-0.4575	-0.4251
	8×10^{-5}	-0.5881	-0.5557	-0.5230	-0.4902	-0.4575	-0.4251
	10^{-4}	-0.5880	-0.5557	-0.5229	-0.4902	-0.4574	-0.4251
	2×10^{-4}	-0.5878	-0.5554	-0.5227	-0.4901	-0.4572	-0.4250
	5×10^{-4}	-0.5873	-0.5550	-0.5224	-0.4897	-0.4571	-0.4248
	8×10^{-4}	-0.5869	-0.5547	-0.5220	-0.4892	-0.4567	-0.4245
	10^{-3}	-0.5864	-0.5542	-0.5216	-0.4890	-0.4565	-0.4243
	2×10^{-3}	-0.5847	-0.5526	-0.5202	-0.4877	-0.4554	-0.4233
	5×10^{-3}	-0.5799	-0.5480	-0.5158	-0.4836	-0.4515	-0.4197
	8×10^{-3}	-0.5756	-0.5439	-0.5119	-0.4798	-0.4479	-0.4164
	10^{-2}	-0.5718	-0.5406	-0.5091	-0.4776	-0.4463	-0.4153
S_0	10^{-5}	0.955981	0.918851	0.879754	0.839011	0.796822	0.753574
	2×10^{-5}	0.95596	0.918832	0.879727	0.839005	0.796807	0.753567
	5×10^{-5}	0.95594	0.918811	0.879693	0.838999	0.796784	0.753554
	8×10^{-5}	0.955884	0.918784	0.879679	0.838993	0.796768	0.753519
	10^{-4}	0.955808	0.918773	0.879597	0.838979	0.796708	0.753491
	2×10^{-4}	0.955518	0.918427	0.879288	0.838834	0.796447	0.753344
	5×10^{-4}	0.95503	0.91797	0.878974	0.83883	0.796235	0.753088
	8×10^{-4}	0.954583	0.917585	0.878467	0.83768	0.795695	0.752637
	10^{-3}	0.954023	0.916997	0.878046	0.837429	0.795432	0.752362
	2×10^{-3}	0.952041	0.91511	0.876283	0.835813	0.793983	0.751097
	5×10^{-3}	0.946694	0.909743	0.870947	0.830561	0.788862	0.746152
	8×10^{-3}	0.941754	0.904795	0.866039	0.825739	0.784168	0.74163
	10^{-2}	0.937447	0.900923	0.862671	0.822931	0.78197	0.740074
	F	10^{-5}	1.5046	1.4536	1.4017	1.3493	1.2964
2×10^{-5}		1.5046	1.4536	1.4017	1.3493	1.2964	1.2435
5×10^{-5}		1.5046	1.4535	1.4016	1.3493	1.2964	1.2434
8×10^{-5}		1.5045	1.4535	1.4016	1.3493	1.2964	1.2434
10^{-4}		1.5044	1.4535	1.4015	1.3492	1.2963	1.2434
2×10^{-4}		1.5040	1.4530	1.4011	1.3490	1.2960	1.2432
5×10^{-4}		1.5033	1.4524	1.4007	1.3484	1.2957	1.2429
8×10^{-4}		1.5027	1.4519	1.4000	1.3476	1.2950	1.2423
10^{-3}		1.5019	1.4511	1.3995	1.3473	1.2947	1.2420
2×10^{-3}		1.4991	1.4485	1.3972	1.3452	1.2929	1.2405
5×10^{-3}		1.4917	1.4413	1.3902	1.3386	1.2866	1.2345
8×10^{-3}		1.4848	1.4347	1.3839	1.3325	1.2808	1.2290
10^{-2}		1.4789	1.4296	1.3795	1.3290	1.2781	1.2272
X'		10^{-5}	-1.1253	-1.1533	-1.1820	-1.2114	-1.2416
	2×10^{-5}	-1.1253	-1.1533	-1.1820	-1.2114	-1.2416	-1.2725
	5×10^{-5}	-1.1254	-1.1533	-1.1821	-1.2115	-1.2417	-1.2725
	8×10^{-5}	-1.1254	-1.1533	-1.1821	-1.2115	-1.2417	-1.2725
	10^{-4}	-1.1255	-1.1533	-1.1821	-1.2115	-1.2417	-1.2726
	2×10^{-4}	-1.1257	-1.1536	-1.1823	-1.2116	-1.2419	-1.2727
	5×10^{-4}	-1.1261	-1.1539	-1.1826	-1.2120	-1.2420	-1.2728
	8×10^{-4}	-1.1264	-1.1542	-1.1829	-1.2124	-1.2424	-1.2732
	10^{-3}	-1.1268	-1.1547	-1.1833	-1.2126	-1.2426	-1.2734
	2×10^{-3}	-1.1283	-1.1561	-1.1845	-1.2137	-1.2437	-1.2743
	5×10^{-3}	-1.1324	-1.1600	-1.1884	-1.2175	-1.2473	-1.2778
	8×10^{-3}	-1.1361	-1.1637	-1.1920	-1.2210	-1.2507	-1.2810
	10^{-2}	-1.1394	-1.1665	-1.1944	-1.2230	-1.2522	-1.2822
	Γ	10^{-5}	5.9944	5.6159	5.3479	5.1480	4.9923
2×10^{-5}		5.9941	5.6157	5.3477	5.1480	4.9923	4.8670
5×10^{-5}		5.9939	5.6155	5.3475	5.1480	4.9922	4.8670
8×10^{-5}		5.9932	5.6153	5.3475	5.1480	4.9921	4.8669
10^{-4}		5.9922	5.6152	5.3470	5.1479	4.9919	4.8668
2×10^{-4}		5.9886	5.6124	5.3452	5.1473	4.9911	4.8665
5×10^{-4}		5.9824	5.6087	5.3434	5.1450	4.9904	4.8658
8×10^{-4}		5.9769	5.6055	5.3406	5.1424	4.9887	4.8646
10^{-3}		5.9699	5.6008	5.3382	5.1414	4.9878	4.8639
2×10^{-3}		5.9458	5.5857	5.3283	5.1347	4.9832	4.8607
5×10^{-3}		5.8836	5.5443	5.2992	5.1134	4.9671	4.8481
8×10^{-3}		5.8296	5.5081	5.2736	5.0945	4.9527	4.8369
10^{-2}		5.7851	5.4809	5.2565	5.0838	4.9461	4.8331
f		10^{-5}	0.142971	0.151152	0.157533	0.162654	0.166881

	2×10^{-5}	0.142977	0.151155	0.157536	0.162654	0.166882	0.170444	
	5×10^{-5}	0.142982	0.151159	0.157541	0.162655	0.166884	0.170446	
	8×10^{-5}	0.142996	0.151164	0.157543	0.162656	0.166886	0.170447	
	10^{-4}	0.143016	0.151166	0.157555	0.162657	0.166891	0.17045	
	2×10^{-4}	0.143091	0.151231	0.157599	0.162673	0.166914	0.170461	
	5×10^{-4}	0.143217	0.151317	0.157643	0.162733	0.166934	0.17048	
	8×10^{-4}	0.143331	0.151388	0.157715	0.162802	0.166982	0.170514	
	10^{-3}	0.143474	0.151498	0.157774	0.162829	0.167006	0.170534	
	2×10^{-3}	0.143972	0.151844	0.15802	0.163007	0.167135	0.170629	
	5×10^{-3}	0.145274	0.152804	0.158749	0.163574	0.167587	0.170995	
	8×10^{-3}	0.146421	0.153655	0.159398	0.164082	0.167991	0.171323	
	10^{-2}	0.147382	0.1543	0.159833	0.164371	0.168178	0.171435	
Γ_p	10^{-5}	10.0209	8.5751	7.5549	6.7999	6.2191	5.7606	
	2×10^{-5}	10.0198	8.5744	7.5544	6.7998	6.2189	5.7605	
	5×10^{-5}	10.0188	8.5738	7.5536	6.7997	6.2186	5.7603	
	8×10^{-5}	10.0162	8.5729	7.5533	6.7996	6.2184	5.7600	
	10^{-4}	10.0125	8.5726	7.5515	6.7994	6.2177	5.7598	
	2×10^{-4}	9.9985	8.5618	7.5448	6.7971	6.2146	5.7584	
	5×10^{-4}	9.9751	8.5475	7.5381	6.7887	6.2121	5.7560	
	8×10^{-4}	9.9538	8.5356	7.5271	6.7789	6.2056	5.7518	
	10^{-3}	9.9273	8.5174	7.5181	6.7750	6.2025	5.7492	
	2×10^{-3}	9.8350	8.4599	7.4806	6.7499	6.1853	5.7375	
	5×10^{-3}	9.5973	8.3022	7.3705	6.6701	6.1259	5.6923	
	8×10^{-3}	9.3911	8.1641	7.2734	6.5993	6.0730	5.6519	
	10^{-2}	9.2211	8.0605	7.2089	6.5592	6.0487	5.6382	
	K	10^{-5}	9.6875	8.2417	7.2216	6.4666	5.8858	5.4272
		2×10^{-5}	9.6865	8.2411	7.2210	6.4665	5.8856	5.4272
		5×10^{-5}	9.6855	8.2405	7.2203	6.4664	5.8853	5.4269
8×10^{-5}		9.6828	8.2396	7.2200	6.4663	5.8851	5.4267	
10^{-4}		9.6791	8.2393	7.2182	6.4660	5.8844	5.4265	
2×10^{-4}		9.6652	8.2285	7.2115	6.4638	5.8813	5.4251	
5×10^{-4}		9.6418	8.2142	7.2047	6.4553	5.8787	5.4227	
8×10^{-4}		9.6205	8.2023	7.1938	6.4456	5.8723	5.4185	
10^{-3}		9.5940	8.1841	7.1848	6.4417	5.8692	5.4159	
2×10^{-3}		9.5017	8.1266	7.1473	6.4165	5.8520	5.4041	
5×10^{-3}		9.2639	7.9689	7.0372	6.3367	5.7926	5.3589	
8×10^{-3}		9.0578	7.8308	6.9400	6.2660	5.7397	5.3186	
10^{-2}		8.8878	7.7272	6.8756	6.2259	5.7154	5.3049	
K'		10^{-5}	-3.6931	-2.6259	-1.8737	-1.3185	-0.8934	-0.5602
		2×10^{-5}	-3.6924	-2.6254	-1.8733	-1.3185	-0.8933	-0.5601
		5×10^{-5}	-3.6916	-2.6249	-1.8727	-1.3184	-0.8931	-0.5600
	8×10^{-5}	-3.6897	-2.6243	-1.8725	-1.3183	-0.8930	-0.5598	
	10^{-4}	-3.6869	-2.6240	-1.8712	-1.3182	-0.8924	-0.5596	
	2×10^{-4}	-3.6766	-2.6161	-1.8663	-1.3165	-0.8902	-0.5586	
	5×10^{-4}	-3.6593	-2.6055	-1.8613	-1.3103	-0.8883	-0.5569	
	8×10^{-4}	-3.6436	-2.5967	-1.8532	-1.3031	-0.8836	-0.5538	
	10^{-3}	-3.6240	-2.5833	-1.8466	-1.3003	-0.8813	-0.5520	
	2×10^{-3}	-3.5559	-2.5409	-1.8190	-1.2818	-0.8688	-0.5435	
	5×10^{-3}	-3.3804	-2.4246	-1.7379	-1.2233	-0.8255	-0.5108	
	8×10^{-3}	-3.2282	-2.3227	-1.6664	-1.1715	-0.7870	-0.4817	
	10^{-2}	-3.1027	-2.2463	-1.6190	-1.1421	-0.7693	-0.4718	


ZAŁĄCZNIK 3

PUBLIKACJA [D3]

M. Szaniawska, K. Szymczyk, A. Zdziennicka, B. Jańczuk*, Adsorption properties and composition of binary Kolliphor mixtures at the air-water interface at different temperatures, *Molecules*, 2022, 27(3), 877

Article

Adsorption Properties and Composition of Binary Kolliphor Mixtures at the Water–Air Interface at Different Temperatures

Magdalena Szaniawska, Katarzyna Szymczyk, Anna Zdziennicka and Bronisław Jańczuk * 

Department of Interfacial Phenomena, Institute of Chemical Sciences, Faculty of Chemistry, Maria Curie-Skłodowska University in Lublin, Maria Curie-Skłodowska Sq. 3, 20-031 Lublin, Poland; magdalena.szaniawska@poczta.umcs.lublin.pl (M.S.); katarzyna.szymczyk@mail.umcs.pl (K.S.); anna.zdziennicka@mail.umcs.pl (A.Z.)

* Correspondence: bronislaw.janczuk@poczta.umcs.lublin.pl; Tel.: +48-81-537-5649

Abstract: The studies on the adsorption properties and composition of the adsorbed monolayer at the water–air interface of the binary Kolliphor[®] ELP (ELP) and Kolliphor[®] RH 40 (RH40) mixtures based on the measurements of the surface tension (γ_{LV}) of their aqueous solution in the temperature range from 293 to 318 K were carried out. The γ_{LV} isotherms were described by the exponential function of the second order and the Szyszkowski equation as well as predicted by Fainerman and Miller equation. The obtained γ_{LV} isotherms were analyzed using the exponential function of the second order, the Szyszkowski, Fainerman and Miller as well as independent adsorption equations. The γ_{LV} isotherms were also used for determination of the Gibbs surface excess concentration of RH40, ELP and their mixture (Γ) at the water–air interface as well as the mixed monolayer composition. Based on Γ and the constant a in the Szyszkowski equation, the standard thermodynamic functions of adsorption were considered. From the consideration dealing with the γ_{LV} isotherms obtained by us, it results, among others, that these isotherms for the non-ideal solution of macromolecular surfactants mixture can be predicted using the Fainerman and Miller equation. From this consideration, it also results that a simple method proposed by us, based on the isotherms of RH40 and ELP, allows us to predict the composition of their mixed monolayer in the whole concentration range of RH40 and ELP in the bulk phase.

Keywords: Kolliphor[®] ELP; Kolliphor[®] RH 40; adsorption; thermodynamic parameters of adsorption; monolayer composition



Citation: Szaniawska, M.; Szymczyk, K.; Zdziennicka, A.; Jańczuk, B. Adsorption Properties and Composition of Binary Kolliphor Mixtures at the Water–Air Interface at Different Temperatures. *Molecules* **2022**, *27*, 877. <https://doi.org/10.3390/molecules27030877>

Academic Editors: Patrycja Dynarowicz-Latka and Aneta D. Petelska

Received: 21 December 2021

Accepted: 25 January 2022

Published: 27 January 2022

Publisher's Note: MDPI stays neutral with regard to jurisdictional claims in published maps and institutional affiliations.



Copyright: © 2022 by the authors. Licensee MDPI, Basel, Switzerland. This article is an open access article distributed under the terms and conditions of the Creative Commons Attribution (CC BY) license (<https://creativecommons.org/licenses/by/4.0/>).

1. Introduction

The wide application of surfactants in many industrial areas, agriculture, pharmacy, medicine and everyday life results from their ability to adsorb at the solid–liquid, solid–air and liquid–air interfaces and to form micelles in the bulk phase of the solutions [1–4]. Indeed, in practice the mixtures of the surfactants, rather than the individual ones, are used [4–7]. This is due to the specific properties of the mixed adsorption layers at the different interfaces or the resulting mixed micelles that cannot be predicted on the basis of the single surfactant properties.

The properties of the adsorption layers at the interfaces depend on the kind of the surfactants, orientation of their molecules towards the interface, layers thickness and pacing [4]. In some practical applications, the flexibility of the adsorption layers at the water–air or water–oil interfaces plays an important role. It can be expected that such conditions can be satisfied by the surfactant mixtures, the molecules of which are large and branched. Such surfactants include nonionic Kolliphors (known before as Cremophors) which are represented by Kolliphor[®] ELP (ELP) and Kolliphor[®] RH 40 (RH40). These surfactants are applied, among others, in pharmacy [8,9]. Their main constituent is tricinoleate ester of ethoxylated glycerol (Scheme S1 in Supplementary Materials). Besides this constituent

the others are polyethylene glycol ricinoleate and the corresponding free glycols [10,11]. Three hydrocarbon chains with one -OH group each constitute the hydrophobic part of the RH40 and ELP molecules. One difference between the tail of RH40 and ELP is that in the hydrophobic ELP tail the double bond exists between the carbon atoms. The hydrophilic character of the molecule head results mainly from the presence of oxyethylene groups. Thus, at the first approximation the properties of the hydrophilic part of RH40 and ELP can be compared to those of Triton's [4,12,13]. However, the RH40 and ELB molecules have a more complicated structure than Triton's, and for this reason more cases of these molecule orientations are possible at the water–air interface [10,11]. These orientations can influence on the reduction in the water surface tension by the adsorbed RH40 and/or ELP molecules in the surface region. This may be the reason that the literature does not report the unambiguous opinion dealing with the influence of RH40 and ELP on the water surface tension. It is practically impossible to find description or prediction of the isotherm of the surface tension of the aqueous solution of these surfactants at different temperatures.

As it is known, in practice the mixtures of surfactants are used, but not single surfactants. Therefore, it is important to predict the surface tension isotherms, composition and packing of the mixed monolayer at the water–air interface as well as the thermodynamic parameters of the adsorption of the surfactants mixture at this interface based on the surface tension isotherms of the aqueous solution of the single surfactants being components of the mixture. This issue was the main objective of our studies. These studies were based on the surface tension measurements of the aqueous solutions of ELP and RH40 as well as their mixtures in the temperature range from 293 to 318 K. The obtained isotherms of surface tension were considered in terms of the concentration of RH40 and ELP in the mixed monolayer at the water–air interface and the composition of this monolayer. Different concepts were applied in this consideration. To explain the adsorption properties of the RH40 and ELP mixtures at the water–air interface, its thermodynamic parameters were determined and analyzed.

2. Results and Discussion

2.1. Surface Tension

The surface tension of the aqueous solution of RH40 and ELP depends on that of water, RH40 and ELP. According to van Oss et al. [14–17] the surface tension of liquids and solids can be divided into two components. One, which is present in the surface tension of each liquid or solid, results from the Lifshitz-van der Waals intermolecular interactions (γ^{LW}) and the other one results from the acid-base intermolecular interactions (γ^{AB}). The acid-base component depends on the electron-acceptor (γ^+) and electron-donor (γ^-) parameters. However, van Oss et al. [14–17] suggest that the contribution of the dipole–dipole and induced dipole–dipole interactions to the Lifshitz-van der Waals component of the surface tension is smaller than 2%. This indicates that the γ^{LW} component of the solid and liquid surface tension depends only on the dispersion intermolecular interactions.

Fowkes [18] stated that the dispersion intermolecular interactions at the interface can be deduced on the basis of the interactions of one element with twelve neighbors and the distance between particular elements. In the case of the aqueous solution of RH40 and ELP at the solution–air interface there can be highlighted such elements as follows: water molecule and $-\text{CH}_3$, $-\text{CH}_2-$, $=\text{CH}-$, $=\text{CO}$ and $-\text{OH}$ groups. As the Lifshitz-van der Waals interactions at the first approximation are equal to the dispersion ones, they depend on the type of the groups being in the surfactants molecule, hence their surface tension is related to the orientation of surfactant molecules towards the interface. Taking into account this fact van Oss and Constanzo [15] stated that the surfactant surface tension is different depending on the orientation of its molecules at the surfactant–air interface. Hence, the surface tension of surfactant whose molecules are oriented by tail towards the air phase can be called the “surfactant tail surface tension” (γ_T). In the case of the surfactant molecules orientation by the hydrophilic group towards the air, its surface tension is called the “surfactant head surface tension” (γ_H). If there are no hydrophilic groups and/or a double bond between

the carbon atoms in the tail, then the γ_T results only from the Lifshitz-van der Waals intermolecular interactions. In the case of RH40 the $-OH$ groups present in its tail and in the ELP tail apart from the $-OH$ groups also a double bond occurs between the carbon atoms. For this reason, the hydrophobic properties of tail are reduced. Unfortunately, the literature lacks the data on the surface tension of RH40 and ELP tails and heads. However, it is possible that the surface tension of both surfactants tail is the same and close to the Lifshitz-van der Waals component of fatty acids. Depending on the type of fatty acid the values of γ^{LW} are larger than the surface tension of hexadecane and smaller than 30 mN/m. The values of γ_H of RH40 and ELP can be approximately compared to that of Triton's, particularly Triton X-165 (TX165), which has 16 oxyethylene groups in one molecule. The γ^{LW} value for TX165 is equal to 27.7 mN/m at 293 K [19]. This value is insignificantly higher than that of γ^{LW} for the water surface tension (26.85 mN/m) [20], but the electron-acceptor and electron-donor parameters of TX165 acid-base component of its head surface tension differ considerably from those of water surface tension. It seems that the components and parameters of RH40 and ELP surface tension can be close to those of TX165. If so, it can be stated that the adsorption of RH40 and ELP mixture at the water–air interface decreases only the acid-base component of the water surface tension. However, it is possible that in a studied range of mixture concentration the values γ^{LW} of the surface tension of surfactant mixtures solution slightly increase as a result of their molecules tail orientation in the mixed monolayer towards the air phase, whereas the reduction in the water surface tension takes place due to the decrease in the acid-base component of its surface tension. In the other words, the number of hydrogen bonds between the water molecules decreases as a function of RH40 and ELP concentration. The greater changes of the number of hydrogen bonds take place in the range of surfactant and their mixtures concentration in which the linear dependence between the surface tension and $\log C / \log C_{12}$ is observed (C_{12} is the mixture concentration) (Figure 1 and Ref. [21]).

According to the Gibbs isotherm equation [4], the saturated mixed monolayer at the water–air interface is formed in this range of C_{12} . The question arises why such a significant decrease in solution surface tension takes place in this concentration range. Indeed, this concentration range is smaller than CMC and it is difficult to take into account the influence of the micelles on the solution surface tension. It is more probable that in the saturated monolayer the surfactant molecules change the orientation and can change the part of tail being in the air phase. This fact causes the changes of the water molecules orientation preventing them from the hydrogen bond formation. On the other hand, the concentration gradient of surfactants at the interface changes with their concentration changes in the bulk phase. As a matter of fact, the destruction of hydrogen bonds is not complete because the minimal surface tension of the aqueous solution of RH40 and ELP mixtures is considerably higher than that resulting from the surfactants tail (Figure 1b–e). The minimal values of the surface tension change as a function of the mixture composition (Figure 2). These changes are not linear and probably result from the synergetic effect of the micelle formation. It is known that only single molecules adsorb at the water–air interface and the surface tension of the surfactant aqueous solution depends largely on the concentration of surfactants in the monomeric form in the bulk phase. This concentration depends on the tendency of the surfactants and their mixture to form micelles. Unfortunately, based only on the surface tension isotherms it is difficult to explain more precisely changes in the minimum surface tension of the aqueous solutions of the RH40 and ELP mixture as a function of its composition. Additional measurements are required. However, we can state that the minimal values of the surface tension of the aqueous solution of RH40 and ELP mixtures do not differ significantly from the minimal values of the aqueous solution of TX165 at a given temperature (39.5 mN/m at 293 K) [22]. However, this value is achieved at a significantly smaller concentration than that of TX165. This indicates that the adsorption activity of RH40 and ELP as well as of their mixture is larger than that of TX165.

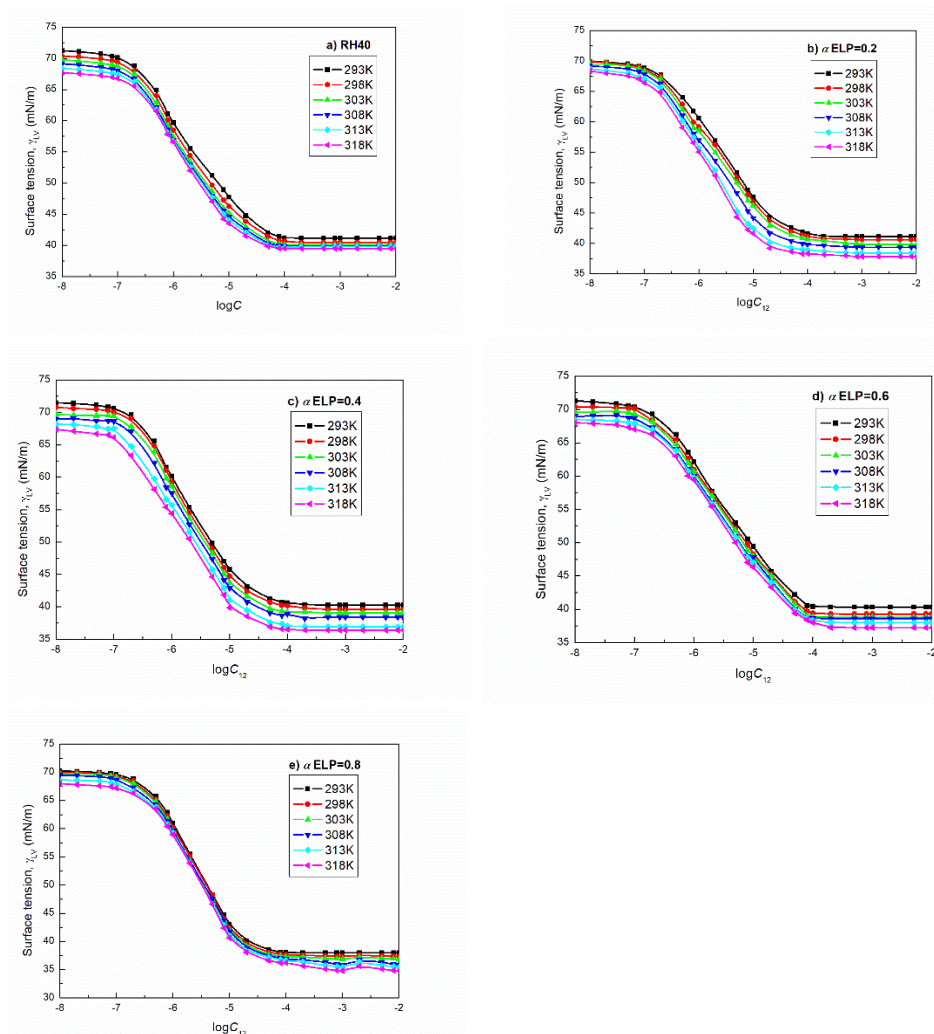


Figure 1. A plot of the surface tension (γ_{LV}) of the aqueous solutions of RH40 (a) as well as RH40 and ELP mixtures at the mole fraction of ELP in the bulk phase, α , equal to 0.2 (b), 0.4 (c), 0.6 (d) and 0.8 (e) vs. the logarithm of their concentration ($\log C$ and $\log C_{12}$) at different temperatures equal to 293, 298, 303, 308, 313 and 318 K, respectively.

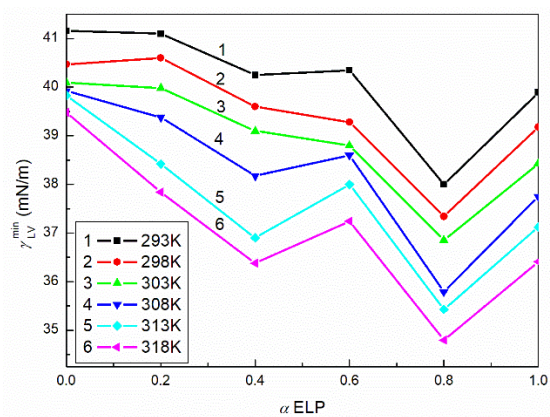


Figure 2. A plot of the minimal surface tension (γ_{LV}^{min}) of the aqueous solutions of RH40 and ELP mixtures at the temperature equal to 293 (curve 1), 298 (curve 2), 303 (curve 3), 308 (curve 4), 313 (curve 5) and 318K (curve 6) vs. the mole fraction of ELP in the bulk phase, α .

The adsorption activity of a surfactant is closely related to the hydration of tail and head of surfactant molecules. Tail hydration is the driving force for the surfactant adsorp-

tion and the head hydration is the brake. It was proved that the volume of the surfactant molecule can be approximated by cubes in which a given part of the surfactant is inscribed. Hence, taking into account the length of the bonds and angle between them as well as the distance between molecules, it is possible to establish the contactable area of RH40 and ELP tail as equal $\approx 967.7 \text{ \AA}^2$. Since the contact plane of the water molecule with a molecule of another substance can be assumed to be equal to 10 \AA^2 , theoretically about 97 water molecules can be contacted with the RH40 or ELP tail simultaneously. On the other hand, it is known that one oxygen atom in the oxyethylene group can form a strong hydrogen bond with two molecules of water [23]. Assuming that the other oxygen atoms, except the one in the $-\text{OH}$ group, can also form the hydrogen bond with two molecules of water, then the RH40 head can be hydrated by 92 molecules of water and head of ELP by 82 ones. This is in accordance with the earlier studies [24].

If, during the transfer of RH40 and ELP molecules from the bulk phase to the mixed surface layer, the head of their molecules does not exist or is poorly hydrated, then the driving forces of adsorption are large, and therefore RH40 and ELP are more surface active than Triton's [25]. It is possible that the dehydration of their head increases with the increasing temperature. On the other hand, the isotherms of the surface tension of the aqueous solutions of RH40 and ELP mixtures with different compositions obtained from the measurements are almost parallel (Figure 1b–e).

The surface tension of the aqueous solution of studied mixtures at a given concentration and composition as a function of temperature in most cases decreases almost linearly (Figure 3 as an example). This indicates that in the studied range of the temperature the dehydration of RH40 and ELP is insignificant.

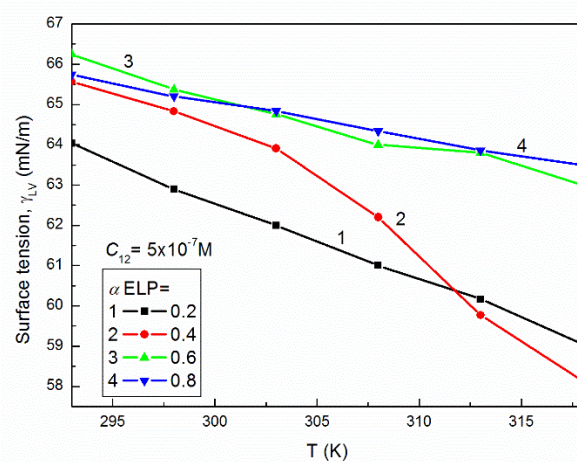


Figure 3. A plot of the surface tension (γ_{LV}) of the aqueous solutions of RH40 and ELP mixtures at the mole fraction of ELP in the bulk phase equal to 0.2 (curve 1), 0.4 (curve 2), 0.6 (curve 3) and 0.8 (curve 4) at $C_{12} = 5 \times 10^{-7} \text{ M}$ vs. the temperature, T.

On the other hand, there is not a linear dependence between the surface tension of the aqueous solution of RH40 and ELP mixture at a given concentration as a function of mixture composition (Figure 4 as an example). The positive and negative deviations of γ_{LV} values from the linear dependence were observed. This indicates that some changes in the hydration number of surfactants head can take place and/or the changes in the surfactant molecules packing as a result of their configuration variation. As follows from the literature [26,27] the possibility of forming different configuration by surfactants having large and branched molecules is greater than for the classical surfactants whose molecules are linear and not very long. It is possible that the oxyethylene and/or hydrocarbon chains are coiling. Such phenomenon was observed for other surfactants having many oxyethylene groups in their molecules [28,29].

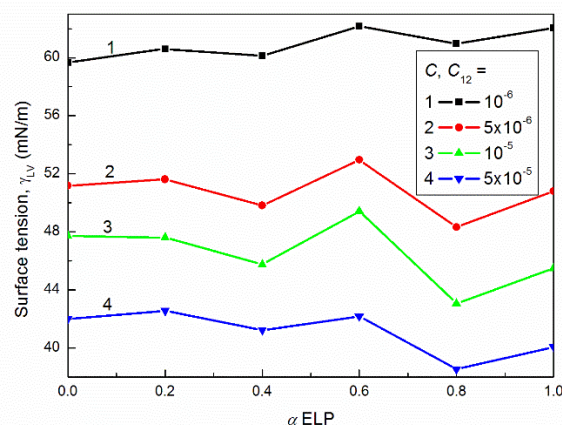


Figure 4. A plot of the surface tension (γ_{LV}) of the aqueous solutions of RH40 and ELP mixtures at temperature T equal to 293 K and C or C_{12} equal to 10^{-6} (curve 1), 5×10^{-6} (curve 2), 10^{-5} (curve 3) and 5×10^{-5} M (curve 4) vs. the mole fraction of ELP in the bulk phase, α .

From the theoretical and practical points of view it is interesting to describe and/or to predict the isotherm of the surface tension of the aqueous solution of the RH40 and ELP mixture on the basis of the isotherm of the individual component of the mixture. It appeared that all isotherms of γ_{LV} can be described by the exponential function of the second order (Figures S1–S6 in Supplementary Materials). This function has the form:

$$\gamma_{LV} = y_0 + A_1 \exp\left(\frac{-C}{t_1}\right) + A_2 \exp\left(\frac{-C}{t_2}\right), \quad (1)$$

where γ_{LV} is the surface tension of the aqueous solution of surfactant, C is the surfactant concentration, y_0 , A_1 , A_2 , t_1 and t_2 are the constants.

Unfortunately, no unequivocal dependence of the constants in Equation (1) on the physicochemical properties of surfactants has been reported so far. It was suggested that these constants are related to the components and parameters of the surfactants head and tail [30]. However, it is difficult to predict the constants in Equation (1) for the mixtures of surfactants based on the constants for individual components of the mixtures. In the case of RH40 and ELP mixtures the additional difficulties result from the fact that they can be treated not as binary but rather as multicomponent ones. However, it can be stated that the values of the y_0 constant are close to the minimal values of γ_{LV} at each temperature (Figure S7). As the minimal values of γ_{LV} depend on the surface tension of surfactant tail, it can be stated that y_0 also is related to the tail of surfactant surface tension. Although the y_0 values are close to the minimum γ_{LV} values, the y_0 values for the RH40 with ELP mixture cannot be predicted based on the y_0 values for RH40 and ELP. This results from the fact that there is no linear relationship between the y_0 values and the composition of the mixture (Figure S8). Changes of the remaining constants from Equation (1) are also non-linear as a function of the mixture composition (Figures S9–S12). Hence, it can be concluded that the isotherms of the surface tension of the aqueous solution of RH40 and ELP mixtures can be satisfactorily described but not predicted.

The changes of the surface tension of the aqueous solutions of many surfactants as a function of their concentration can be described by the Szyszkowski equation if the Gibbs surface excess concentration of the saturated monolayer at the water–air interface and the standard Gibbs free energy of adsorption are known. The Szyszkowski equation for the aqueous solution of RH40 and ELP mixtures can be expressed in the form [4]:

$$\gamma_W - \gamma_{LV} = \pi = -RT\Gamma^{max} \ln\left(\frac{C}{a} + 1\right), \quad (2)$$

where γ_W is the water surface tension, π is the monolayer at the water–air interface pressure, a is the constant, which depends on the standard Gibbs free energy of adsorption (ΔG_{ads}^0), Γ^{max} is the maximal Gibbs surface excess concentration of surfactant in the saturated monolayer at the water–air interface, T is the temperature and R is the gas constant.

The a constant in Equation (2) fulfills the expression [4]:

$$a = \omega \exp\left(\frac{\Delta G_{ads}^0}{RT}\right), \quad (3)$$

where: ω is the number of the water moles in one dm^3 .

To describe the surface tension isotherm Equation (2) can be solved numerically choosing proper values of Γ^{max} and a . For calculation of γ_{LV} from Equation (2) it was assumed that C changes from 0 to CMC. This resulted from the fact that not aggregated surfactant molecules are surface active. It appeared that at the first approximation it was possible to describe all isotherms of surface tension using the Szyszkowski equation (Equation (2)) (Figures S1–S6).

For the ideal mixture of surfactants, it is possible not only to describe but also to predict the isotherm of the aqueous solutions of this mixture at different compositions based on the data for individual surfactants. In the case of the ideal surfactant mixture the changes of the Γ^{max} , a and CMC as a function of its composition should be linear. In addition, the surface tension of the aqueous solution of ideal surfactants mixture should satisfy the equation which for the binary mixture has the form:

$$\gamma_{LV} = \gamma_{LV}^1 X_1^S + \gamma_{LV}^2 X_2^S, \quad (4)$$

where γ_{LV}^1 and γ_{LV}^2 is the surface tension of the aqueous solution of surfactants 1 and 2 at a given concentration in the bulk phase and X_1^S and X_2^S are the mole fractions of surfactants 1 and 2 in the monolayer.

As it was suggested earlier, X_1^S and X_2^S can be determined using the film pressure of surfactants 1 and 2 at their given concentration in their individual solutions. Hence, $X_1^S = \frac{\pi_1}{\pi_1 + \pi_2}$ and $X_2^S = \frac{\pi_2}{\pi_1 + \pi_2}$ (π_1 and π_2 are the layer of surfactants 1 and 2 pressure, respectively). The values of γ_{LV} calculated from Equation (4) for all studied systems are higher than the measured ones at the same RH40 and ELP concentration (Figures S2–S5). However, the difference between the measured and calculated values of γ_{LV} depends on the composition of this mixture. In the case of RH40 and ELP mixture with the mole fraction of ELP equal to 0.6, the calculated values of γ_{LV} are almost identical to those measured (Figure S4). For the aqueous solution of RH40 and ELP at a given composition the difference between the calculated from Equation (4) and measured values of γ_{LV} practically does not change as a function of temperature (Figures S2–S5).

The difference between the measured and calculated values of γ_{LV} indicates that the RH40 and ELP mixture does not behave as ideal one and the deviation from the ideal behaviour depends on the mixture composition. This conclusion is also confirmed by the Γ^{max} values used in the Szyszkowski equation (Equation (2)) for the γ_{LV} calculations. The Γ^{max} values do not change linearly as a function of mixture surfactants composition (Figure S13), and they are in the range from 2.44×10^{-6} to 3.12×10^{-6} mol/m^2 . These values correspond to the minimal area occupied by one molecule which is in the range from 53.2 to 68 \AA^2 . Thus, it can be concluded that there is a synergetic effect in the reduction in water surface tension by the RH40 and ELP mixture which depends on its composition. For this reason, for the RH40 and ELP mixture the surface tension of its aqueous solution cannot be precisely predicted based on the Γ^{max} , a and CMC for RH40 and ELP. However, this tension can be predicted using the Fainerman and Miller equation. This equation for binary mixtures has the form [31,32]:

$$\exp\Pi = \exp\Pi_1 + \exp\Pi_2 - 1, \quad (5)$$

where $\Pi = \pi\omega/RT$, $\Pi_1 = \pi_1\omega_1/RT$ and $\Pi_2 = \pi_2\omega_2/RT$ are the dimensionless pressure of the mixed monolayer at the water–air interface and individual surfactants 1 and 2, respectively, and ω_1 , ω_2 and ω are the areas occupied by one mole of surfactants 1 and 2 and mixture at the water–air interface and π , π_1 and π_2 are the differences between the surface tension of the solvent and solution of the surfactants mixture and components 1 and 2, respectively.

The calculation made using Equation (5) confirmed the above mentioned conclusion that, on the basis of the Fainerman and Miller equation, the isotherm of surface tension of RH40 and ELP mixture can be predicted (Figures S2–S5). However, at the concentration of the surfactant mixtures above their CMC the values calculated from Equation (5) are smaller than those measured. Some differences between the measured and calculated from Equation (5) γ_{LV} values are observed for the mixture with the mole fraction of ELP equal to 0.6 at the constant temperatures 313 and 318 K (Figure S4).

2.2. Concentration of Surfactants at the Water–Air Interface and Composition of the Mixed Monolayer

In most cases the concentration of surfactants and/or their mixture is determined using the Gibbs adsorption isotherm Equation [4]. As a matter of fact, this equation allows us to determine only the surface excess concentration of surfactants at the interface, but it can be treated as the total dimensional concentration because of the small surfactant concentration in the bulk phase. For the studies on the adsorption properties of surfactants their very low concentration in the aqueous solution is used. Therefore, for such solution it can be assumed that the activity coefficient of surfactants is close to unity and its mole fraction is very close to $\frac{C}{\omega}$ and ω is practically constant in the range of studied surfactant concentrations. In such case the Gibbs isotherm equation for the nonionic surfactants and their mixtures has the form [4]:

$$\Gamma = -\frac{C}{RT} \left(\frac{\partial \gamma_{LV}}{\partial C} \right)_T = -\frac{1}{2.303RT} \left(\frac{\partial \gamma_{LV}}{\partial \log C} \right)_T. \quad (6)$$

The calculated values of Γ indicate that the adsorption of RH40 and ELP and their mixtures depends on the temperature and in the case of mixtures also on their composition (Figure S14). However, for the RH40 and ELP mixtures in which the mole fraction of ELP is equal to 0.2 and 0.8, respectively, the surface excess concentration at the water–air interface decreases and increases as a function of temperature. This indicates that for these mixtures the synergetic and/or antagonistic effect in the reduction in water surface tension takes place. It is also confirmed by the fact that there is no linear dependence between Γ^{max} and composition of the RH40 and ELP mixtures. Thus, the negative and positive deviations from the linear dependence are observed. In many cases the Γ^{max} values obtained from the Gibbs isotherm equation using the linear dependence between the surface tension of the solution and the logarithm from the surfactants concentration are similar to the Γ^{max} values obtained from the Szyszkowski equation (Figure S13). As mentioned above this equation was solved against the surface tension of the aqueous solution of surfactant numerically.

The calculations of Γ from Equation (6) also indicate that in many cases the values of Γ^{max} are obtained for RH40 and ELP as well as their mixtures at the concentration equal to 1×10^{-6} mol/dm³. It was proved that in the range of the surfactants and their mixture concentrations from 0 to 1×10^{-6} mol/dm³, the independent adsorption at the water–air interface takes place (Figures S2–S5). This results from the calculation of γ_{LV} from the following expression:

$$\gamma_{LV} = \gamma_W - \pi_1 - \pi_2, \quad (7)$$

In the mentioned range of surfactants concentration, the values of γ_{LV} calculated from Equation (7) are very close to those measured (Figures S2–S5). This points out that in this range of surfactants concentration $X_1^S = \frac{\pi_1}{\pi_1 + \pi_2}$ and $X_2^S = \frac{\pi_2}{\pi_1 + \pi_2}$. The relative composition

of the surfactants saturated mixed monolayer at the water–air interface can be determined using the Hua and Rosen equation which has the form [4,33]:

$$\frac{(X_1^S)^2 \ln(\alpha C_{12}/X_1^S C_1)}{(1 - X_1^S)^2 \ln[(1 - \alpha)C_{12}/(1 - X_1^S)C_2]} = 1, \quad (8)$$

where α is the mole fraction of surfactant 1 (ELP) in the mixture in the bulk phase, and indices 1, 2 and 12 are related to surfactants 1, 2 and their mixture, respectively.

Taking into account the error in the calculation of mole fraction of surfactants in the mixed monolayer using Equation (8), it can be stated that in most cases the X_1^S and X_2^S values determined from this equation are close to those determined from π_1 and π_2 (Figure S15). Hence, the values of X_1^S and X_2^S obtained from π_1 and π_2 , at the first approximation can be treated as a mole fraction of RH40 and ELP in the mixed monolayer at the water–air interface in the whole range of RH40 and ELP mixture concentration in the bulk phase.

In the range of ELP mixture concentration corresponding to the unsaturated mixed monolayer, i.e., from zero to 1×10^{-6} mol/dm³ in the bulk phase the mutual effect of surfactants on their adsorption was not observed and for each composition of the surfactant mixtures the mole fraction of ELP in the mixed monolayer decreases in this concentration range of the mixture in the bulk phase. However, from the beginning of the saturated mixed monolayer formation at the water–air interface the X_1^S increases to the value which depends on the composition of the mixture in the bulk phase. In any case, the mole fraction of X_1^S is equal to α . However, the difference between these fractions does not yet prove the existence of synergy or antagonism in the reduction in the water surface tension by the mixture of RH40 and ELP. Hua and Rosen [33] stated that the synergy and antagonistic effects in the reduction in water surface tension by the adsorption of surfactants mixture can be determined on the basis of the parameter of intermolecular interactions (β^σ). This parameter fulfills the condition [4,34]:

$$\beta^\sigma = \frac{\ln(\alpha C_{12}/X_1^S C_1)}{(1 - X_1^S)^2}, \quad (9)$$

From the calculations of the β^σ parameter from Equation (9) it results that each value depends on the concentration and composition of the RH40 and ELP mixture as well as temperature (Figure S16). This is connected with the changes of the mixed monolayer composition at the water–air interface as a function of mixture concentration and temperature at a given constant mixture composition in the bulk phase, α . It should be noted that the values of the surfactant mole fraction in the mixed monolayer calculated from Equation (8), as mentioned above, are close to those determined on the basis of the surface tension isotherms of RH40 and ELP. The β^σ parameter can assume both the positive and negative values (Table S1 in Supplementary Materials). For the mixture of RH40 and ELP with the ELP mole fraction equal to 0.6 the values of β^σ are only positive and there is the almost linear dependence between β^σ and the surface tension of solutions and temperature (Figure S16d). This indicates the synergetic effect in the water surface tension does not occur for this mixture. For the other RH40 and ELP mixtures this effect was noted but not at each temperature applied in the studies. As mentioned above, in the case of the RH40 and ELP mixture, the synergetic effect in the reduction in water surface tension results probably from the changes of the configuration of RH40 and ELP molecules in the mixed monolayer, in comparison to the individual surfactant monolayer and/or the changes of number of hydrogen bonds as a result of dehydration of surfactants tail and head.

2.3. Thermodynamic Parameters of Adsorption

The standard Gibbs free energy (ΔG_{ads}^0), enthalpy (ΔH_{ads}^0) and entropy (ΔS_{ads}^0) of adsorption are powerful in understanding the adsorption process of the RH40 and ELP mixture at the water–air interface [4]. ΔG_{ads}^0 informs only about the surfactants tendency to

adsorb at the water–air interface. Based on this it is not possible to conclude what changes took place in the bulk phase as a result of surfactants adsorption. The ΔH_{ads}^0 value informs us about chemical reactions which occurred during the adsorption process. In other words, based on ΔH_{ads}^0 it can be stated whether more chemical bonds were broken or whether new ones were created. On the other hand, ΔS_{ads}^0 informs about the structural and orientation changes of molecules in the bulk phase during the adsorption process. ΔS_{ads}^0 is the main force of this process.

The literature reports numerous methods for determination of ΔG_{ads}^0 . Among them, those that are based on the Langmuir equation modified by de Boer are very often used. This equation has the form [35,36]:

$$\frac{A^0}{A - A^0} \exp \frac{A^0}{A - A^0} = \frac{C}{\omega} \exp \left(\frac{-\Delta G_{ads}^0}{RT} \right), \quad (10)$$

where A and A^0 are the areas occupied by one molecule in the monolayer and limiting one. ΔG_{ads}^0 can be also determined from the linear Langmuir equation [4,35]:

$$\frac{C}{\Gamma} = \frac{C}{\Gamma^{max}} + \frac{a}{\Gamma^{max}}, \quad (11)$$

where a fulfills Equation (4).

The ΔG_{ads}^0 values were determined from Equations (10) and (3). In Equation (3) there were used the values of a established from the Szyszkowski equation and obtained from the Langmuir linear equation. Hence, for each system three values of ΔG_{ads}^0 were obtained. There are small differences between the ΔG_{ads}^0 values obtained using these methods (Table S2 in Supplementary Materials). There is no linear dependence between ΔG_{ads}^0 and the composition of RH40 and ELP mixtures. The absolute values of ΔG_{ads}^0 for RH40, ELP and their mixtures are higher than those for other nonionic surfactants. This explains why, at small concentrations of RH40, ELP and their mixtures, the reduction in water surface tension by their adsorption is higher than that of other nonionic surfactants [4,22].

It is known that ΔG_{ads}^0 fulfills the expression [4,35]:

$$\Delta G_{ads}^0 = \Delta H_{ads}^0 - T \Delta S_{ads}^0, \quad (12)$$

Assuming that in the temperature range from 293 to 318 K the ΔH_{ads}^0 is constant then [4,35]:

$$\frac{\partial \Delta G_{ads}^0}{\partial T} = -\Delta S_{ads}^0, \quad (13)$$

Introducing the values of ΔS_{ads}^0 calculated from Equation (13) to Equation (12) the values of ΔH_{ads}^0 were determined.

It follows from Table 1 that the values of ΔH_{ads}^0 for the RH40 and ELP mixture with the mole fraction of 0.6 are close to zero. For this mixture no synergetic effect is observed in the reduction in water surface tension. For the mixture of different compositions, the positive and negative values of ΔH_{ads}^0 were obtained. However, the absolute value of ΔH_{ads}^0 is not large.

The nonlinear dependence between the ΔG_{ads}^0 and composition of the RH40 and ELP mixture can result from the fact that the Gibbs free energy of RH40 and ELP mixing is different from zero. In the other words, the mixed monolayer is not ideal and the coefficients of RH40 and ELP activity are different from zero (Table S1). The coefficient of surfactants activity and next the Gibbs free energy of surfactants mixing can be determined based on the parameter of the intermolecular interactions. The coefficients of surfactants activity satisfy the condition [4]:

$$\ln f_1 = \beta^\sigma (1 - X_1^\xi)^2, \quad (14)$$

and

$$\ln f_2 = \beta^\sigma (X_1^s)^2. \quad (15)$$

In turn the Gibbs free energy of surfactants mixing (G_{mix}^E) can be expressed by equation [37]:

$$G_{mix}^E = RT(X_1^s \ln f_1 + X_2^s \ln f_2), \quad (16)$$

It was proved that the absolute values of G_{mix}^E are not great. This means that there is no great difference between the ideal and real behavior of the RH40 and ELP mixtures.

Table 1. The values of the ΔH_{ads}^0 and ΔS_{ads}^0 for the RH40 and ELP as well as their binary mixtures calculated from Equations (12) and (13), respectively.

		ΔS_{ads}^0 [kJ/molK]				
	RH40	$\alpha = 0.2$	$\alpha = 0.4$	$\alpha = 0.6$	$\alpha = 0.8$	ELP
	−0.172	−0.178	−0.191	−0.146	−0.159	−0.161
		ΔH_{ads}^0 [kJ/mol]				
T [K]	RH40	$\alpha = 0.2$	$\alpha = 0.4$	$\alpha = 0.6$	$\alpha = 0.8$	ELP
293	3.344	5.034	8.984	−3.262	−0.197	0.857
298	3.403	5.123	9.140	−2.983	−0.201	0.871
303	3.473	5.221	9.305	−3.034	−0.196	0.896
308	3.292	5.069	9.101	−3.084	−0.200	0.910
313	3.352	5.037	8.977	−3.125	−0.195	0.845
318	3.411	5.116	9.123	−3.166	−0.199	0.869

3. Materials and Methods

For our studies the aqueous solution of Kolliphor® ELP (ELP) (Cremophor® ELP, Polyoxyl 35 Hydrogenated Castor oil, Polyoxyl-35 castor oil, CAS number 61791-12-6,) and Kolliphor® RH 40 (RH40) (Cremophor® RH 40, macrogolglycerol hydroxystearate, PEG-40 castor oil, Polyoxyl 40 hydrogenated castor oil, CAS number 61788-85-0,) mixture were applied. RH40 and ELP were purchased from Sigma-Aldrich (St. Louis, MO, USA) and used without additional purification. The solution concentration was in the range from 0 to the values significantly higher than the critical micelle concentration (CMC) of RH40 and ELP that is from 0 to 0.01 M (mol/dm³) and the ELP mole fraction in the surfactant mixtures in the bulk phase, α , was equal to 0.2, 0.4, 0.6 and 0.8. The water used for the solutions preparation was doubly distilled and deionized (Destamat) the surface tension of which changed from 72.8 to 68.7 mN/m in the temperature range from 293 to 318 K.

The surface tension (γ_{LV}) measurements of the aqueous solution of the RH40 and ELP mixture were made in the temperature range from 293 to 318 K using the Krüss K100 tensiometer according to the platinum ring tensiometer method (du Nouy's method) calibrated before the measurements. The calibration was made only at 293 K using water and methanol whose surface tension at this temperature was equal to 72.8 and 22.5 mN/m, respectively. The surface tension measurements for each concentration and composition of the aqueous solution of RH40 and ELP mixtures were repeated at least ten times. The standard deviation of the results obtained from the measurements was ± 0.1 mN/m, and the uncertainty was in the range from 0.3% to 0.9%.

4. Conclusions

Based on the results obtained from the surface tension measurements of the aqueous solution of RH40 and ELP mixtures and their analysis many conclusions can be drawn.

In the small concentration range of RH40 and ELP as well as their mixture in the aqueous solution the greater reduction in water surface tension takes place as a result of the adsorption at the water–air interface that due to the adsorption of other nonionic

surfactants. However, the minimal surface tension of the aqueous solution of RH40 and ELP and their mixtures which can be obtained is close to that of TX165.

There is no linear dependence between the surface tension of RH40, ELP mixtures and their composition. The isotherm of the surface tension of RH40 and ELP, as well as their mixture, can be precisely described by the exponential function of the second order. It is possible to describe the isotherm of the surface tension by the numerical solution of the Szyszkowski equation. The maximal Gibbs surface excess concentration obtained solving the Szyszkowski equation against the surface tension is comparable to that determined from the equation of the Gibbs isotherm of adsorption.

The surface tension of the aqueous solution of RH40 and ELP mixtures can be predicted using the Fainerman and Miller equation in the range of mixtures concentration from zero to CMC. In some cases, it is possible to predict the changes of the surface tension of the aqueous solution of RH40 and ELP mixtures in the whole studied range of concentration.

The synergetic effect of the RH40 and ELP mixtures in the reduction in the water surface tension but not at all their composition was found based on the intermolecular interactions parameter.

The composition of the RH40 and ELP mixed monolayer at the water–air interface can be predicted from the contribution of a particular surfactant to the reduction in water surface tension.

The calculated values of the mole fraction of RH40 and ELP in the mixed monolayer at the water–air interface, on the basis of their aqueous solution surface tension isotherms, are in most cases close to those determined based on the Rosen and Hua concept.

The values of the Gibbs free energy of adsorption for a given system calculated from the constant in the Szyszkowski equation are close to those calculated from the Langmuir equation modified by de Boer and the linear Langmuir equation.

The absolute values of the Gibbs free energy of adsorption for the studied systems are higher than those for Triton's.

The standard enthalpy of adsorption assumes negative and positive values depending on the composition of the RH40 and ELP mixture, but the absolute values of enthalpy do not differ significantly from zero.

Supplementary Materials: The following are available online, Scheme S1: The structure of the main components of ELP (a) and RH40 (b); Table S1: The values of the mole fractions of ELP (X_1^S) and RH40 (X_2^S) in the mixed monolayer at the water–air interface, parameter of intermolecular interactions (β^σ), activity coefficient of ELP (f_1) and RH40 (f_2) as well as Gibbs free energy of surfactants mixing (G_{mix}^E) (kJ/mol) for the mixtures at the mole fraction of ELP in the bulk phase, α equal to 0.2 (a), 0.4 (b), 0.6 (c) and 0.8 (d). There is also the condition for synergism or antagonism existence ($\ln(C_1/C_2)$) [4]; Table S2: The values of the standard Gibbs free energy of adsorption (ΔG_{ads}^0) calculated from Equations (3), (10) and (11); Figure S1: A plot of the surface tension (γ_{LV}) of the aqueous solutions of RH40 vs. the logarithm of its concentration ($\log C$) at different temperatures equal to 293 (a), 298 (b), 303 (c), 308 (d), 313 (e) and 318 K (f). Points 1 correspond to the measured values, curves 2 and 3 correspond to the values calculated from the Szyszkowski equation (Equation (2)) and the exponential function of the second order (Equation (1)), respectively; Figure S2: A plot of the surface tension (γ_{LV}) of the aqueous solutions of RH40 and ELP mixtures at the mole fraction of ELP in the bulk phase equal to 0.2 vs. the logarithm of their concentration ($\log C_{12}$) at different temperatures equal to 293 (a), 298 (b), 303 (c), 308 (d), 313 (e) and 318 K (f). Points 1 correspond to the measured values, curves 2–6 correspond to the values calculated from the Szyszkowski equation (Equation (2)), exponential function of the second order (Equation (1)), Fainerman and Miller equation (Equation (5)), Equation (7) and Equation (4), respectively; Figure S3: A plot of the surface tension (γ_{LV}) of the aqueous solutions of RH40 and ELP mixtures at the mole fraction of ELP in the bulk phase equal to 0.4 vs. the logarithm of their concentration ($\log C_{12}$) at different temperatures equal to 293 (a), 298 (b), 303 (c), 308 (d), 313 (e) and 318 K (f). Points 1 correspond to the measured values, curves 2–6 correspond to the values calculated from the Szyszkowski equation (Equation (2)), exponential function of the second order (Equation (1)), Fainerman and Miller equation (Equation (5)), Equation (7) and Equation (4),

respectively; Figure S4: A plot of the surface tension (γ_{LV}) of the aqueous solutions of RH40 and ELP mixtures at the mole fraction of ELP in the bulk phase equal to 0.6 vs. the logarithm of their concentration ($\log C_{12}$) at different temperatures equal to 293 (a), 298 (b), 303 (c), 308 (d), 313 (e) and 318 K (f). Points 1 correspond to the measured values, curves 2–6 correspond to the values calculated from the Szyszkowski equation (Equation (2)), exponential function of the second order (Equation (1)), Fainerman and Miller equation (Equation (5)), Equation (7) and Equation (4), respectively; Figure S5: A plot of the surface tension (γ_{LV}) of the aqueous solutions of RH40 and ELP mixtures at the mole fraction of ELP in the bulk phase equal to 0.8 vs. the logarithm of their concentration ($\log C_{12}$) at different temperatures equal to 293 (a), 298 (b), 303 (c), 308 (d), 313 (e) and 318 K (f). Points 1 correspond to the measured values, curves 2–6 correspond to the values calculated from the Szyszkowski equation (Equation (2)), exponential function of the second order (Equation (1)), Fainerman and Miller equation (Equation (5)), Equation (7) and Equation (4), respectively; Figure S6: A plot of the surface tension (γ_{LV}) of the aqueous solutions of ELP vs. the logarithm of its concentration ($\log C$) at different temperatures equal to 293 (a), 298 (b), 303 (c), 308 (d), 313 (e) and 318 K (f). Points 1 correspond to the measured values, curves 2 and 3 correspond to the values calculated from the Szyszkowski equation (Equation (2)) and the exponential function of the second order (Equation (1)), respectively; Figure S7: A plot of the values of constant y_0 in Equation (1) (curve 1) and the minimal surface tension of aqueous solution (γ_{LV}^{min}) (curve 2) vs. the temperature (T) for the RH40 and ELP mixtures at the mole fraction of ELP in the bulk phase equal to 0 (RH40 (a)), 0.2 (b), 0.4 (c), 0.6 (d), 0.8 (e) and 1 (ELP (f)), respectively; Figure S8: A plot of the values of constant y_0 in Equation (1) for studied surfactant mixtures vs. the mole fraction of ELP in the bulk phase (α) at the temperatures equal to 293 (curve 1), 298 (curve 2), 303 (curve 3), 308 (curve 4), 313 (curve 5) and 318 K (curve 6), respectively; Figure S9: A plot of the values of constant A_1 in Equation (1) for studied surfactant mixtures vs. the mole fraction of ELP in the bulk phase (α) at the temperatures equal to 293 (curve 1), 298 (curve 2), 303 (curve 3), 308 (curve 4), 313 (curve 5) and 318 K (curve 6), respectively; Figure S10: A plot of the values of constant A_2 in Equation (1) for studied surfactant mixtures vs. the mole fraction of ELP in the bulk phase (α) at the temperatures equal to 293 (curve 1), 298 (curve 2), 303 (curve 3), 308 (curve 4), 313 (curve 5) and 318 K (curve 6), respectively; Figure S11: A plot of the values of constant t_1 in Equation (1) for studied surfactant mixtures vs. the mole fraction of ELP in the bulk phase (α) at the temperatures equal to 293 (curve 1), 298 (curve 2), 303 (curve 3), 308 (curve 4), 313 (curve 5) and 318 K (curve 6), respectively; Figure S12: A plot of the values of constant t_2 in Equation (1) for studied surfactant mixtures vs. the mole fraction of ELP in the bulk phase (α) at the temperatures equal to 293 (curve 1), 298 (curve 2), 303 (curve 3), 308 (curve 4), 313 (curve 5) and 318 K (curve 6), respectively; Figure S13: The values of Γ^{max} calculated from Equations (6) and (2) for studied surfactant mixtures at the mole fraction of ELP in the bulk phase (α) equal to 0, 0.2, 0.4, 0.6, 0.8 and 1 at different temperatures equal to 293 (a), 298 (b), 303 (c), 308 (d), 313 (e) and 318 K (f), respectively; Figure S14: A plot of the values of Gibbs surface excess concentration (Γ) vs. logarithm of the concentration in the bulk phase (C or C_{12}) for the RH40 and ELP mixtures at the mole fraction of ELP in the bulk phase equal to 0 (RH40 (a)), 0.2 (b), 0.4 (c), 0.6 (d), 0.8 (e) and 1 (ELP (f)), respectively; Figure S15: The values of the mole fraction of ELP in the mixed monolayer at the water air interface (X_1^S) calculated from the relationship: $X_1^S = \frac{\pi_1}{\pi_1 + \pi_2}$ (bars 1) and from Equation (8) (bars 2) and temperature range 293–318K for mixtures at the mole fraction of ELP in the bulk phase (α) equal to 0.2 (a), 0.4 (b), 0.6 (c) and 0.8 (d). Figure S16: A plot of the values of parameter of intermolecular interactions, β^σ , for studied binary surfactant mixtures (a) at the mole fraction of ELP in the bulk phase α , equal to 0.2, 0.4, 0.6, 0.8 and $T = 293K$ vs. surface tension, (γ_{LV}), (b) at the surface tension, (γ_{LV}), equal to 65, 55, 45 mN/m and $T = 293K$ vs. mole fraction of ELP in the bulk phase α , (c) at the mole fraction of ELP in the bulk phase α , equal to 0.2, 0.4, 0.6, 0.8 and $\gamma_{LV} = 65$ mN/m vs. temperature, T, (d) at the mole fraction of ELP in the bulk phase α , equal to 0.6 and $\gamma_{LV} = 65, 55, 45$ mN/m vs. temperature, T.

Author Contributions: Conceptualization, M.S., K.S., A.Z. and B.J.; methodology, M.S. and K.S.; software, K.S.; validation, K.S., A.Z. and B.J.; formal analysis, K.S., A.Z. and B.J.; investigation, M.S. and K.S.; resources, M.S. and K.S.; data curation, K.S., A.Z. and B.J.; writing—original draft preparation, K.S., A.Z. and B.J.; writing—review and editing, K.S., A.Z. and B.J.; visualization, K.S., A.Z. and B.J.; supervision, B.J.; project administration, K.S., A.Z. and B.J.; funding acquisition, B.J. All authors have read and agreed to the published version of the manuscript.

Funding: This research received no external funding.

Institutional Review Board Statement: Not applicable.

Informed Consent Statement: Not applicable.

Data Availability Statement: The data presented in this study are available in Supplementary Materials.

Conflicts of Interest: The authors declare no conflict of interest.

Sample Availability: Samples of the compounds are not available from the authors.

References

1. Guo, J.; Xia, Y.; Liu, Y.; Liu, S.; Zhang, L.; Li, B. Microscopic adsorption behaviors of ionic surfactants on lignite surface and its effect on the wettability of lignite: A simulation and experimental study. *J. Mol. Liq.* **2022**, *345*, 117851. [[CrossRef](#)]
2. Corona, R.R.B.; Sad, C.M.S.; da Silva, M.; Lopes, D.L.; Leite, J.S.D.; de F. Viegas, G.M.; Gonçalves, G.R.; Filgueiras, P.R.; de Castro, E.V.R. Adsorption of anionic surfactant in graphite oxide: A study for treatment of laundry wastewater. *J. Environ. Chem. Eng.* **2021**, *9*, 106858. [[CrossRef](#)]
3. Reeve, J.R.; Thomas, J.R.; Penfold, J. Surface activity of ethoxylate surfactants with different hydrophobic architectures: The effect of layer substructure on surface tension and adsorption. *Langmuir* **2021**, *37*, 9269–9280. [[CrossRef](#)] [[PubMed](#)]
4. Rosen, M.J. *Surfactants and Interfacial Phenomena*, 3rd ed.; Wiley-Interscience: New York, NY, USA, 2004; pp. 34–178.
5. Kronberg, B.; Holmberg, K.; Lindman, B. *Surface Chemistry of Surfactants and Polymers*; John Wiley & Sons, Ltd.: West Sussex, UK, 2014; pp. 251–269.
6. Holland, P.M.; Rubingh, D.N. *Mixed Surfactant Systems*; ACS Symposium Series; American Chemical Society: Washington, DC, USA, 1992; Chapter 1; pp. 1–30.
7. Scamehorn, J.F. *An Overview of Phenomena Involving Surfactant Mixtures*; ACS Symposium Series; American Chemical Society: Washington, DC, USA, 1986; pp. 1–27.
8. Seo, S.H.; Kim, E.; Joo, Y.; Lee, J.; Oh, K.T.; Hwang, S.-J.; Choi, K.-Y. A mixed micellar formulation for the transdermal delivery of an indirubin analog. *Pharmaceutics* **2020**, *12*, 175. [[CrossRef](#)]
9. Shakeel, F.; Salem-Bekhit, M.M.; Haq, N.; Alshehri, S. Nanoemulsification improves the pharmaceutical properties and bioactivities of niaouli essential oil (*Melaleuca quinquenervia* L.). *Molecules* **2021**, *26*, 4750. [[CrossRef](#)]
10. Jadhav, S.R.; Bryant, G.; Mata, J.P.; Eldridge, D.S.; Palombo, E.A.; Harding, I.H.; Shah, R.M. Structural aspects of a self-emulsifying multifunctional amphiphilic excipient: Part II. The case of Cremophor EL. *J. Mol. Liq.* **2021**, *344*, 117881. [[CrossRef](#)]
11. Parikh, K.J.; Sawant, K.K. Solubilization of vardenafil HCl in lipid-based formulations enhances its oral bioavailability in vivo: A comparative study using Tween-20 and Cremophor-EL. *J. Mol. Liq.* **2019**, *277*, 189–199. [[CrossRef](#)]
12. Farsang, E.; Gaál, V.; Horváth, O.; Bárdos, E.; Horváth, K. Analysis of non-ionic surfactant Triton X-100 using hydrophilic interaction liquid chromatography and mass spectrometry. *Molecules* **2019**, *24*, 1223. [[CrossRef](#)]
13. Bandivadekar, M.; Pancholi, S.; Kaul-Ghanekar, R.; Choudhari, A.; Koppikar, S. Single non-ionic surfactant based self-nanoemulsifying drug delivery systems: Formulation, characterization, cytotoxicity and permeability enhancement study. *Drug Dev. Ind. Pharm.* **2013**, *39*, 696–703. [[CrossRef](#)]
14. van Oss, C.J. *Interfacial Forces in Aqueous Media*; Marcel Dekker: New York, NY, USA, 1994.
15. van Oss, C.J.; Constanzo, P.M. Adhesion of anionic surfactants to polymer surfaces and low-energy materials. *J. Adhes. Sci. Technol.* **1992**, *4*, 477–487. [[CrossRef](#)]
16. van Oss, C.J.; Good, R.J. Surface tension and the solubility of polymers and biopolymers: The role of polar and apolar interfacial free energies. *J. Macromol. Sci. Chem.* **1989**, *26*, 1183–1203. [[CrossRef](#)]
17. van Oss, C.J.; Chaudhury, M.K.; Good, R.J. Monopolar surfaces. *Adv. Coll. Interface Sci.* **1987**, *28*, 35–64. [[CrossRef](#)]
18. Fowkes, F.M. Attractive forces at interfaces. *Ind. Eng. Chem.* **1964**, *56*, 40–52. [[CrossRef](#)]
19. Szymczyk, K.; Zdziennicka, A.; Jańczuk, B. Properties of some nonionic fluorocarbon surfactants and their mixtures with hydrocarbon ones. *Adv. Coll. Inter. Sci.* **2021**, *292*, 102421. [[CrossRef](#)]
20. Zdziennicka, A.; Krawczyk, J.; Szymczyk, K.; Jańczuk, B. Components and parameters of liquids and some polymers surface tension at different temperature. *Coll. Surf. A* **2017**, *529*, 864–875. [[CrossRef](#)]
21. Szymczyk, K.; Szaniawska, M.; Krawczyk, J. Temperature effect on the adsorption and volumetric properties of aqueous solutions of Kolliphor® ELP. *Molecules* **2020**, *25*, 743. [[CrossRef](#)]
22. Zdziennicka, A.; Szymczyk, K.; Krawczyk, J.; Jańczuk, B. Activity and thermodynamic parameters of some surfactants adsorption at the water–air interface. *Fluid Phase Equilib.* **2012**, *318*, 25–33. [[CrossRef](#)]
23. Beyer, K. Phase structures, water binding, and molecular dynamics in liquid crystalline and frozen states of the system Triton X-100-D₂O: A deuteron and carbon NMR study. *J. Colloid Interface Sci.* **1982**, *86*, 73–89. [[CrossRef](#)]
24. Szymczyk, K.; Szaniawska, M.; Terpiłowski, K. Determination of acoustical parameters of aqueous solution of Kolliphors binary mixtures using density, speed of sound, viscosity and surface tension measurements. *J. Surfact. Deterg.* **2019**, *22*, 1163–1174. [[CrossRef](#)]
25. Zdziennicka, A.; Krawczyk, J.; Szymczyk, K.; Jańczuk, B. Macroscopic and microscopic properties of some surfactants and biosurfactants. *Int. J. Mol. Sci.* **2018**, *19*, 1934. [[CrossRef](#)]

26. Frank, C.; Frielinghaus, H.; Allgaier, J.; Prast, H. Nonionic surfactants with linear and branched hydrocarbon tails: compositional analysis, phase behavior, and film properties in bicontinuous microemulsions. *Langmuir* **2007**, *23*, 6526–6535. [[CrossRef](#)] [[PubMed](#)]
27. Adkins, S.S.; Chen, X.; Nguyen, Q.P.; Sanders, A.W.; Johnston, K.P. Effect of branching on the interfacial properties of nonionic hydrocarbon surfactants at the air-water and carbon dioxide-water interfaces. *J. Colloid Interface Sci.* **2010**, *346*, 455–463. [[CrossRef](#)] [[PubMed](#)]
28. Ghosh, S.K.; Khatua, P.K.; Bhattacharya, S.C. Aggregation of nonionic surfactant Igepal in aqueous solution: Fluorescence and light scattering studies. *Int. J. Mol. Sci.* **2003**, *4*, 562–571. [[CrossRef](#)]
29. FitzGerald, P.A.; Davey, T.W.; Warr, G.G. Micellar structure in gemini nonionic surfactants from small-angle neutron scattering. *Langmuir* **2005**, *21*, 7121–7128. [[CrossRef](#)]
30. Jańczuk, B.; Zdziennicka, A.; Szymczyk, K.; González-Martin, M.L. Prediction of aqueous solution surface tension of some surfactant mixtures and composition of their monolayers at the solution-air interface. *Colloids Interfaces* **2022**, *5*, 53. [[CrossRef](#)]
31. Fainerman, V.B.; Miller, R.; Aksenenko, E.V. Simple model for prediction of surface tension of mixed surfactant solutions. *Adv. Colloid Interface Sci.* **2002**, *96*, 339–359. [[CrossRef](#)]
32. Fainerman, V.B.; Miller, R. Simple method to estimate surface tension of mixed surfactant solutions. *J. Phys. Chem. B* **2001**, *105*, 11432–11438. [[CrossRef](#)]
33. Rosen, J.M.; Hua, X.Y. Surface concentrations and molecular interactions in binary mixtures of surfactants. *J. Colloid Interface Sci.* **1982**, *86*, 164–172. [[CrossRef](#)]
34. Rubingh, D.N. *Solution Chemistry of Surfactants*; Mittal, K.L., Ed.; Plenum Press: New York, NY, USA, 1979; Volume 3, pp. 337–354.
35. Adamson, W.; Gast, A.P. *Physical Chemistry of Surfaces*, 6th ed.; Wiley Interscience: New York, NY, USA, 1997.
36. De Boer, J.H. *The Dynamic Character of Adsorption*; Oxford University: Oxford, UK, 1953.
37. Szymczyk, K. Composition of multicomponent surfactant systems at the water–air interface. *J. Surfact. Deterg.* **2012**, *15*, 647–656. [[CrossRef](#)]

ZAŁĄCZNIK 3a

MATERIAŁ UZUPEŁNIAJĄCY [SM3]

M. Szaniawska, K. Szymczyk, A. Zdziennicka, B. Jańczuk*, Adsorption properties and composition of binary Kolliphor mixtures at the air-water interface at different temperatures, *Molecules*, 2022, 27(3), 877

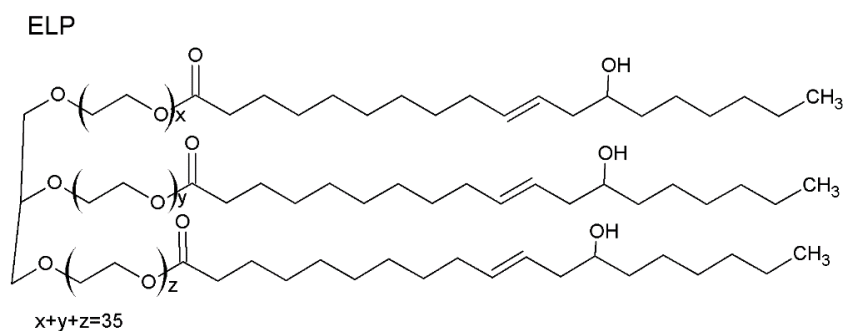
Adsorption properties and composition of binary Kolliphor mixtures at the water-air interface at different temperatures

Magdalena Szaniawska¹, Katarzyna Szymczyk¹, Anna Zdziennicka¹, and Bronisław Jańczuk^{1,*}

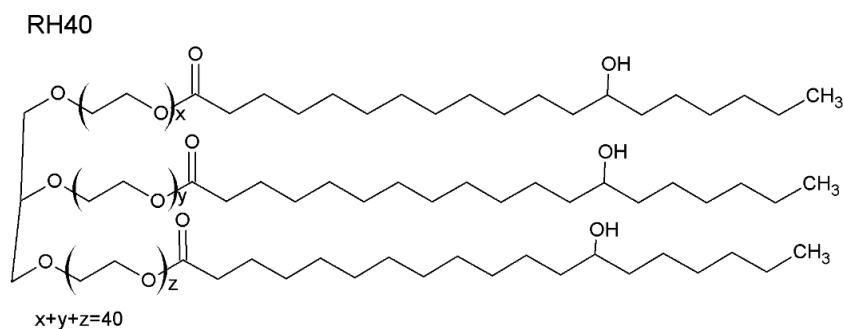
¹ Department of Interfacial Phenomena, Institute of Chemical Sciences, Faculty of Chemistry, Maria Curie-Skłodowska University in Lublin, Maria Curie-Skłodowska Sq. 3, 20-031 Lublin, Poland;

* Correspondence: bronislaw.janczuk@poczta.umcs.lublin.pl; Tel.: +48-81-537-56-49

a)



b)



Scheme S1. The structure of the main components of ELP (a) and RH40 (b).

Table S1. The values of the mole fractions of ELP (X_1^S) and RH40 (X_2^S) in the mixed monolayer at the water-air interface, parameter of intermolecular interactions (β^σ), activity coefficient of ELP (f_1) and RH40 (f_2) as well as and Gibbs free energy of surfactants mixing (G_{mix}^E) (kJ/mol) for the mixtures at the mole fraction of ELP in the bulk phase, α equal to 0.2 (a), 0.4 (b), 0.6 (c) and 0.8 (d). There is also the condition for synergism or antagonism existence ($\ln(C_1/C_2)$) [4].

a)

α ELP = 0.2, $\gamma_{LV} = 65$ mN/m							
T [K]	X_1^S	X_2^S	β^σ	$\ln(C_1/C_2)$	f_1	f_2	G_{mix}^E
293	0.2708	0.7292	-1.7006	0.3838	0.4048	0.8828	-0.8180
298	0.2603	0.7397	-1.6267	0.4380	0.4106	0.8956	-0.7760
303	0.2365	0.7635	-1.4850	0.4960	0.4208	0.9203	-0.6755
308	0.2405	0.7595	-1.4010	0.5388	0.4456	0.9222	-0.6552
313	0.2518	0.7482	-1.2870	0.3152	0.4865	0.9216	-0.6310
318	0.2673	0.7327	-1.2858	0.2217	0.5014	0.9122	-0.6658
α ELP = 0.2, $\gamma_{LV} = 55$ mN/m							
293	0.2722	0.7278	-0.8054	0.2215	0.6527	0.9421	-0.3887
298	0.2610	0.7390	-0.2582	0.3000	0.8685	0.9826	-0.1234
303	0.2400	0.7600	0.3737	0.3797	1.2409	1.0218	0.1717
308	0.2510	0.7490	0.0917	0.4241	1.0528	1.0058	0.0441
313	0.2568	0.7432	-1.2022	0.2597	0.5148	0.9238	-0.5971
318	0.2856	0.7144	-1.4203	0.1393	0.4844	0.8906	-0.7662
α ELP = 0.2, $\gamma_{LV} = 45$ mN/m							
293	0.27682	0.72318	0.27178	0.5473	1.1527	1.0210	0.1325
298	0.2680	0.7320	0.72404	0.3283	1.4740	1.0534	0.3519
303	0.2500	0.7500	2.42876	0.1432	3.9203	1.1639	1.1472
308	0.2590	0.7410	-0.20318	0.0836	0.8944	0.9865	-0.0999
313	0.3200	0.6800	-1.82648	0.1750	0.4297	0.8294	-1.0343
318	0.34357	0.65643	-1.77151	0.1837	0.4661	0.8113	-1.0563

b)

α ELP = 0.4, $\gamma_{LV} = 65$ mN/m							
T [K]	X_1^S	X_2^S	β^σ	$\ln(C_1/C_2)$	f_1	f_2	G_{mix}^E
293	0.3267	0.6733	-0.1910	0.3838	0.9171	0.9798	-0.1023
298	0.2837	0.7163	0.1910	0.4380	1.1029	1.0155	0.0962
303	0.2935	0.7065	-0.0529	0.4960	0.9739	0.9955	-0.0276
308	0.3312	0.6689	-0.7090	0.5388	0.7282	0.9252	-0.4021
313	0.3854	0.6146	-1.7359	0.3152	0.5191	0.7727	-1.0700
318	0.4333	0.5667	-2.6775	0.2217	0.4232	0.6050	-1.7382
α ELP = 0.4, $\gamma_{LV} = 55$ mN/m							
293	0.3801	0.6199	-0.5749	0.2215	0.8018	0.9203	-0.3300
298	0.3532	0.6468	-0.3420	0.3000	0.8667	0.9582	-0.1936
303	0.3334	0.6666	-0.2679	0.3797	0.8878	0.9707	-0.1500
308	0.3397	0.6603	-0.5233	0.4241	0.7960	0.9414	-0.3006
313	0.3950	0.6050	-1.1453	0.2597	0.6576	0.8363	-0.7122
318	0.4287	0.5713	-1.8049	0.1393	0.5548	0.7177	-1.1687
α ELP = 0.4, $\gamma_{LV} = 45$ mN/m							
293	0.5260	0.4740	-0.7231	0.5473	0.8501	0.8187	-0.4392
298	0.4873	0.5127	-0.7825	0.3283	0.8141	0.8304	-0.4844
303	0.4536	0.5464	-0.8350	0.1432	0.7793	0.8422	-0.5213
308	0.4437	0.5563	-0.8497	0.0836	0.7688	0.8460	-0.5370
313	0.4630	0.5370	-1.1080	0.1750	0.7265	0.7886	-0.7169
318	0.4664	0.5336	-1.2825	0.1837	0.6941	0.7566	-0.8438

c)

$\alpha \text{ ELP} = 0.6, \gamma_{LV} = 65 \text{ mN/m}$							
T [K]	X_1^S	X_2^S	β^σ	$\ln(C_1/C_2)$	f_1	f_2	G_{mix}^E
293	0.5060	0.4940	0.2101	0.3838	1.0526	1.0553	0.1279
298	0.4908	0.5092	0.2404	0.438	1.0643	1.0596	0.1489
303	0.4733	0.5267	0.3271	0.4960	1.0950	1.0760	0.2054
308	0.4679	0.5321	0.3505	0.5388	1.1043	1.0798	0.2235
313	0.5201	0.4799	0.3944	0.3152	1.0951	1.1126	0.2562
318	0.5583	0.4417	0.4225	0.2217	1.0859	1.1407	0.2755
$\alpha \text{ ELP} = 0.6, \gamma_{LV} = 55 \text{ mN/m}$							
293	0.6090	0.3910	1.1888	0.2215	1.1993	1.5541	0.6896
298	0.5933	0.4067	1.4586	0.3000	1.2729	1.6710	0.8720
303	0.5660	0.4340	1.6555	0.3797	1.3659	1.6995	1.0244
308	0.5580	0.4420	1.7510	0.4241	1.4079	1.7250	1.1059
313	0.6401	0.3599	1.8977	0.2597	1.2787	2.1761	1.1377
318	0.7400	0.2600	2.0000	0.1393	1.1448	2.9898	1.0174
$\alpha \text{ ELP} = 0.6, \gamma_{LV} = 45 \text{ mN/m}$							
293	0.6400	0.3600	1.5235	0.5473	1.2183	1.8664	0.8551
298	0.6300	0.3700	1.8585	0.3283	1.2897	2.0910	1.0553
303	0.6400	0.3600	1.9591	0.1432	1.2890	2.2310	1.1371
308	0.6500	0.3500	2.0930	0.0836	1.2923	2.4213	1.2193
313	0.7000	0.3000	2.3117	0.1750	1.2313	3.1041	1.2633
318	0.8000	0.2000	2.3452	0.1837	1.0983	4.4859	0.9921

d)

$\alpha \text{ ELP} = 0.8, \gamma_{LV} = 65 \text{ mN/m}$							
T [K]	X_1^S	X_2^S	β^σ	$\ln(C_1/C_2)$	f_1	f_2	G_{mix}^E
293	0.6783	0.3217	-0.7193	0.3838	0.9283	0.7182	-0.3823
298	0.6926	0.3074	-0.3532	0.4380	0.9672	0.8442	-0.1863
303	0.7063	0.2937	-0.0337	0.4960	0.9971	0.9833	-0.0176
308	0.6807	0.3193	0.2259	0.5388	1.0233	1.1103	0.1257
313	0.7098	0.2902	0.5465	0.3152	1.0471	1.3170	0.2929
318	0.8291	0.1709	0.6282	0.2217	1.0185	1.5400	0.2353
$\alpha \text{ ELP} = 0.8, \gamma_{LV} = 55 \text{ mN/m}$							
293	0.6831	0.3169	-1.0828	0.2215	0.8970	0.6033	-0.5710
298	0.7016	0.2984	-0.8880	0.3000	0.9240	0.6459	-0.4606
303	0.6893	0.3107	-0.5618	0.3797	0.9472	0.7657	-0.3031
308	0.6947	0.3053	-0.3522	0.4241	0.9677	0.8437	-0.1912
313	0.7883	0.2117	0.3289	0.2597	1.0148	1.2267	0.1428
318	0.9298	0.0702	1.5557	0.1393	1.0077	3.8385	0.2683
$\alpha \text{ ELP} = 0.8, \gamma_{LV} = 45 \text{ mN/m}$							
293	0.7063	0.2938	-2.5609	0.5473	0.8017	0.2788	-1.2942
298	0.6929	0.3071	-2.3356	0.3283	0.8023	0.3258	-1.2314
303	0.6925	0.3075	-1.8596	0.1432	0.8388	0.4099	-0.9975
308	0.7251	0.2749	-1.1108	0.0836	0.9195	0.5577	-0.5670
313	0.7627	0.2374	-0.7509	0.175	0.9586	0.6461	-0.3537
318	0.8254	0.1746	-0.0268	0.1837	0.9992	0.9819	-0.0102

Table S2. The values of the standard Gibbs free energy of adsorption (ΔG_{ads}^0) calculated from Eqs. (3), (10) and (11).

Temperature [K]	ΔG_{ads}^0 [kJ/mol]					
	RH40	$\alpha = 0.2$	$\alpha = 0.4$	$\alpha = 0.6$	$\alpha = 0.8$	ELP
			Eq. (3)			
293	-47.02	-47.02	-47.02	-45.99	-46.81	-46.29
298	-47.82	-47.82	-47.82	-46.44	-47.61	-47.08
303	-48.61	-48.61	-48.61	-47.22	-48.40	-47.86
308	-49.65	-49.65	-49.77	-48.00	-49.20	-48.65
313	-50.45	-50.57	-50.85	-48.77	-49.99	-49.52
318	-51.25	-51.38	-51.66	-49.54	-50.79	-50.30
			Eq. (10)			
293	-46.12	-45.41	-45.90	-45.03	-44.86	-45.00
298	-46.86	-47.08	-46.68	-45.81	-45.81	-45.72
303	-47.75	-48.06	-47.36	-46.38	-46.66	-46.53
308	-48.46	-49.19	-48.50	-47.23	-47.41	-47.05
313	-49.03	-49.76	-50.04	-47.68	-47.89	-48.33
318	-49.49	-50.90	-51.19	-48.32	-48.39	-49.14
			Eq. (11)			
293	-49.20	-48.14	-48.36	-48.21	-46.88	-47.68
298	-49.96	-51.11	-49.18	-49.15	-48.03	-48.62
303	-50.89	-52.07	-49.99	-49.85	-48.88	-49.55
308	-51.65	-53.23	-51.36	-50.85	-49.73	-50.03
313	-52.31	-53.39	-53.15	-51.38	-50.27	-51.12
318	-52.82	-54.72	-54.57	-52.01	-50.82	-52.37

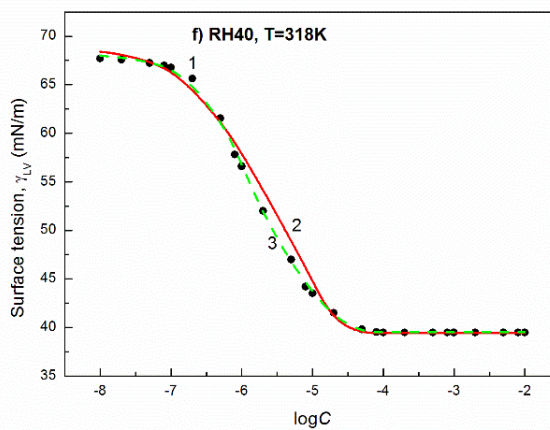
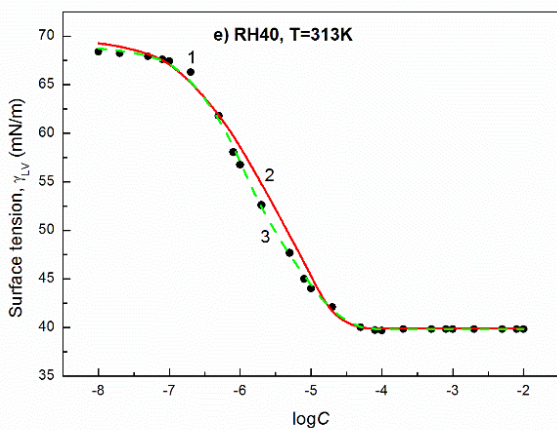
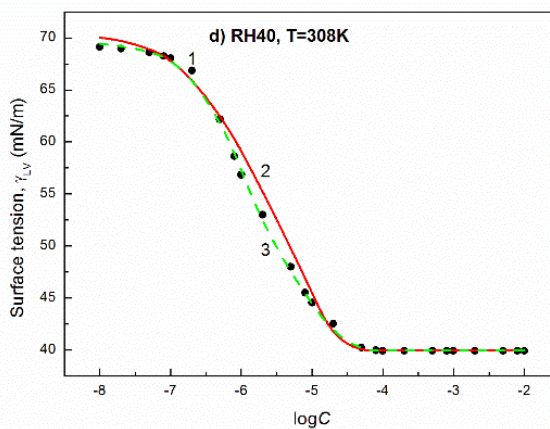
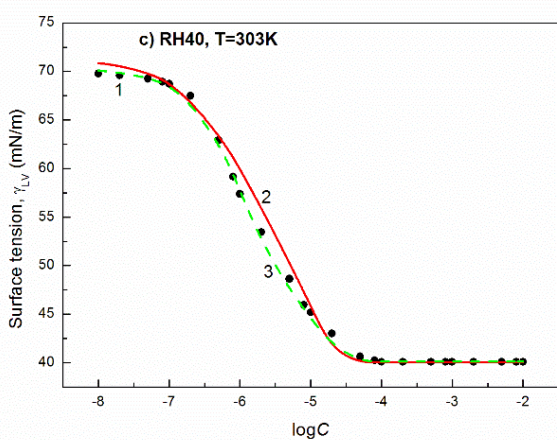
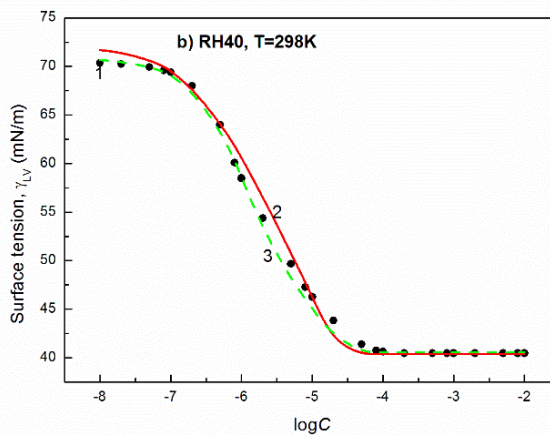
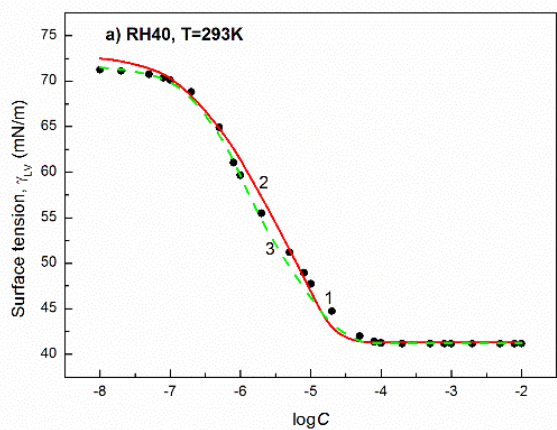


Figure S1. A plot of the surface tension (γ_{LV}) of the aqueous solutions of RH40 vs. the logarithm of its concentration ($\log C$) at different temperatures equal to 293 (a), 298 (b), 303 (c), 308 (d), 313 (e) and 318 K (f). Points 1 correspond to the measured values, curves 2 and 3 correspond to the values calculated from the Szyszkowski equation (Eq. (2)) and the exponential function of the second order (Eq. (1)), respectively.

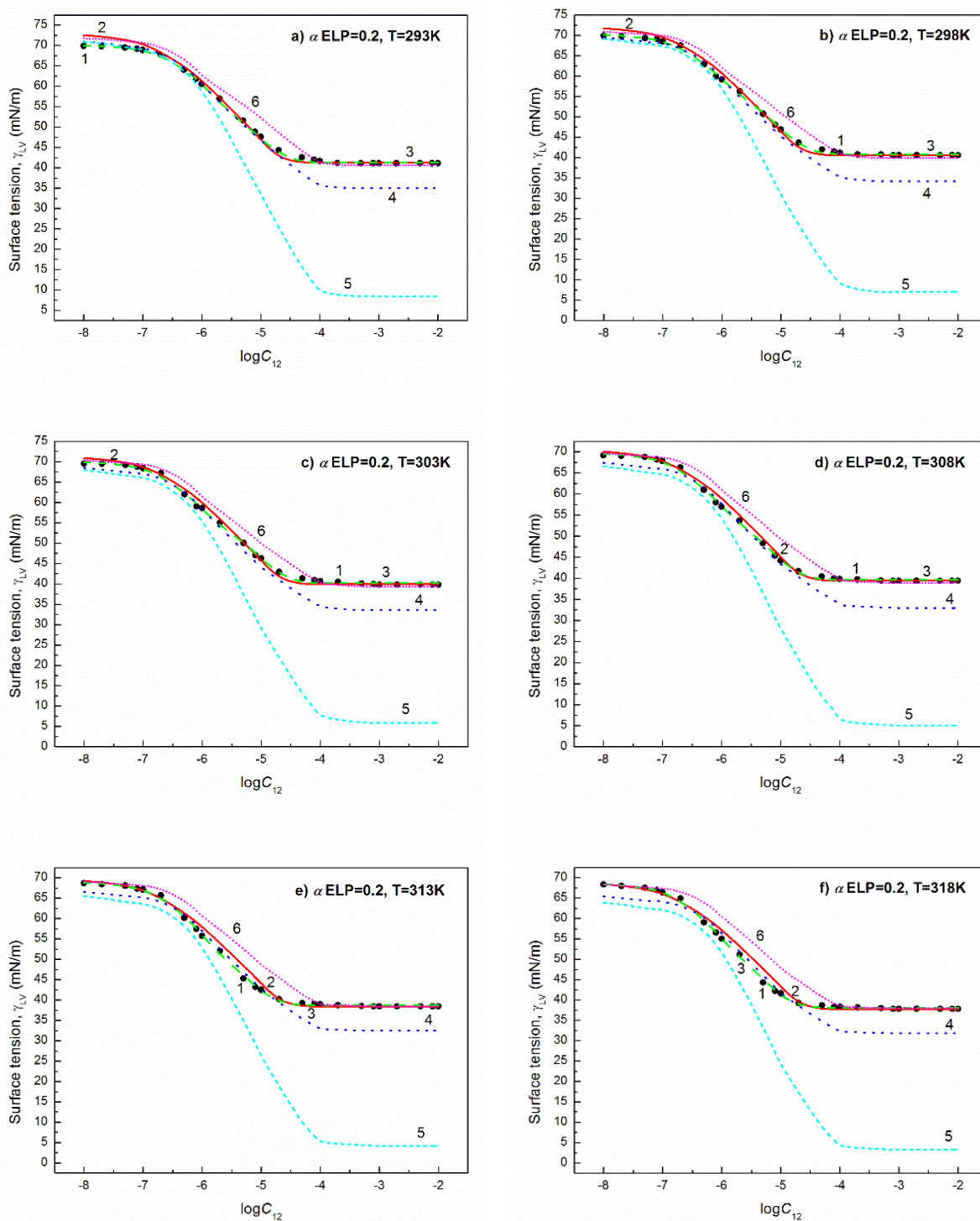


Figure S2. A plot of the surface tension (γ_{LV}) of the aqueous solutions of RH40 and ELP mixtures at the mole fraction of ELP in the bulk phase equal to 0.2 vs. the logarithm of their concentration ($\log C_{12}$) at different temperatures equal to 293 (a), 298 (b), 303 (c), 308 (d), 313 (e) and 318 K (f). Points 1 correspond to the measured values, curves 2 – 6 correspond to the values calculated from the Szyszkowski equation (Eq. (2)), exponential function of the second order (Eq. (1)), Fainerman and Miller equation (Eq. (5)), Eq. (7) and Eq. (4), respectively.

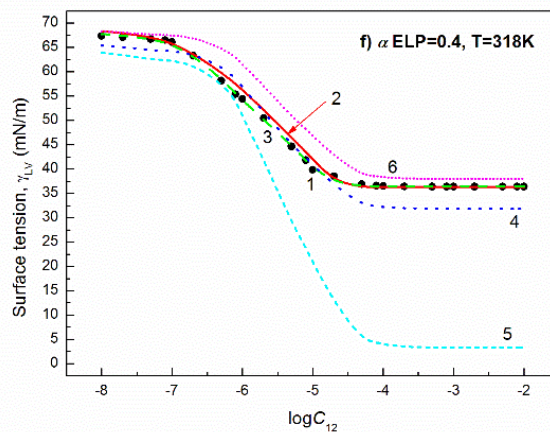
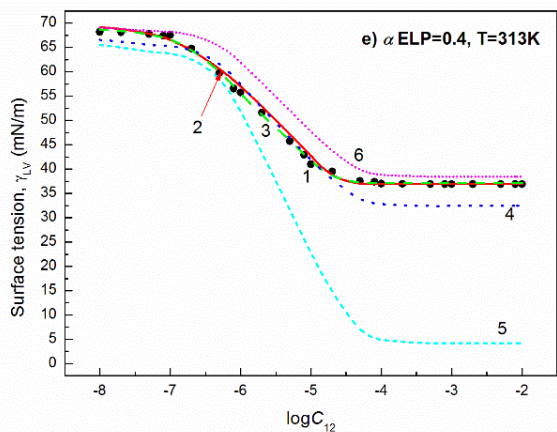
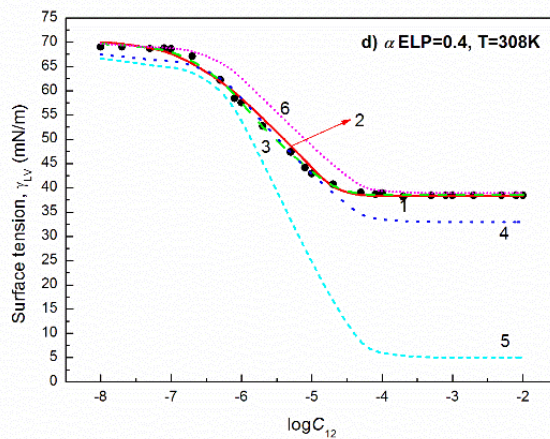
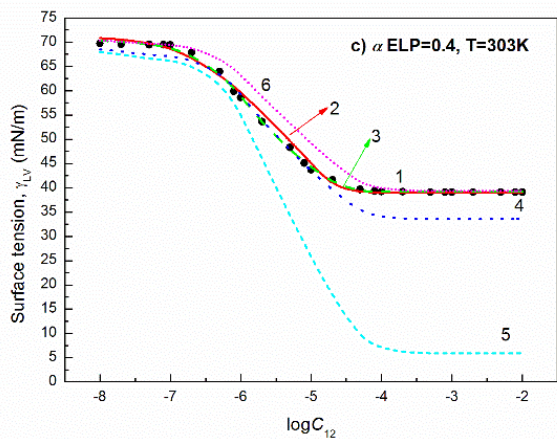
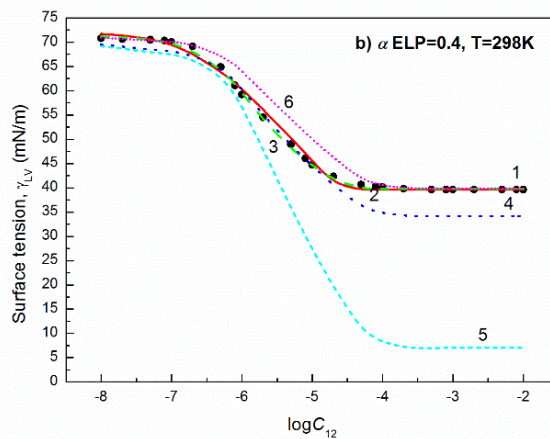
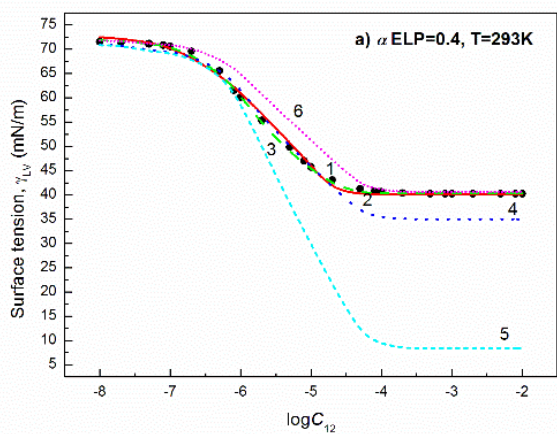


Figure S3. A plot of the surface tension (γ_{LV}) of the aqueous solutions of RH40 and ELP mixtures at the mole fraction of ELP in the bulk phase equal to 0.4 vs. the logarithm of their concentration ($\log C_{12}$) at different temperatures equal to 293 (a), 298 (b), 303 (c), 308 (d), 313 (e) and 318 K (f). Points 1 correspond to the measured values, curves 2 – 6 correspond to the values calculated from the Szyszkowski equation (Eq. (2)), exponential function of the second order (Eq. (1)), Fainerman and Miller equation (Eq. (5)), Eq. (7) and Eq. (4), respectively.

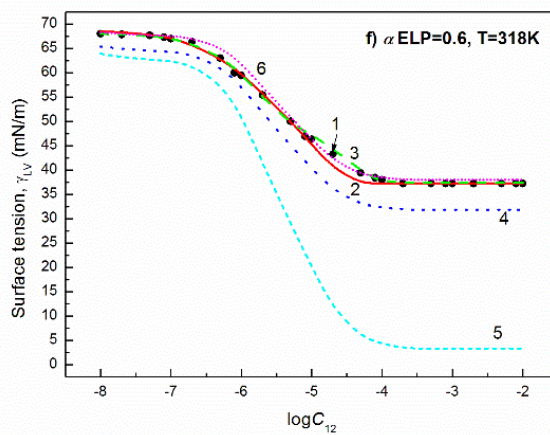
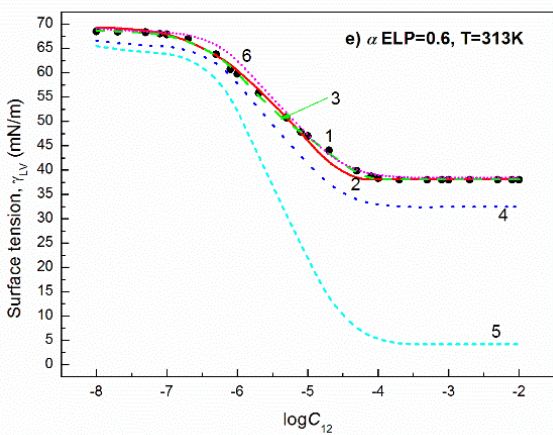
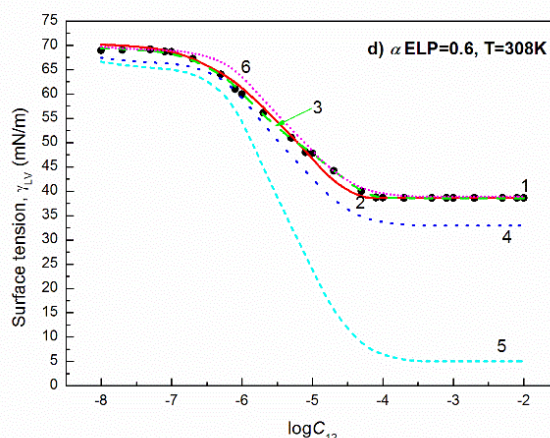
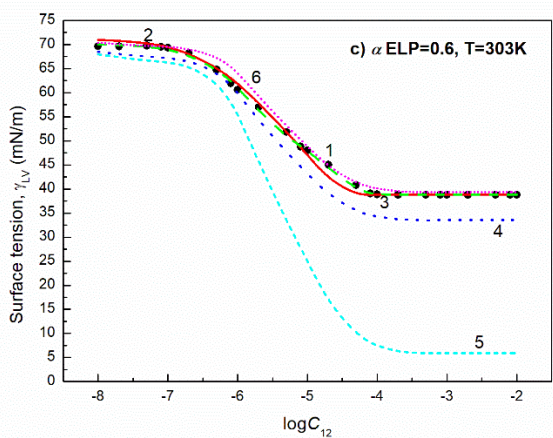
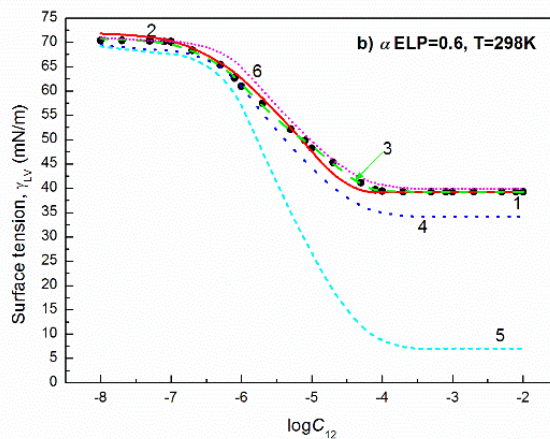
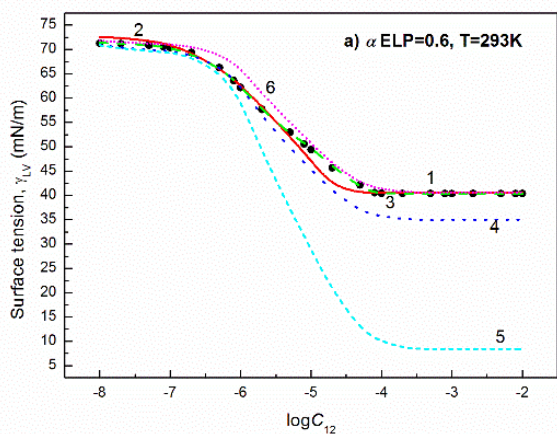


Figure S4. A plot of the surface tension (γ_{LV}) of the aqueous solutions of RH40 and ELP mixtures at the mole fraction of ELP in the bulk phase equal to 0.6 vs. the logarithm of their concentration ($\log C_{12}$) at different temperatures equal to 293 (a), 298 (b), 303 (c), 308 (d), 313 (e) and 318 K (f). Points 1 correspond to the measured values, curves 2 – 6 correspond to the values calculated from the Szyszkowski equation (Eq. (2)), exponential function of the second order (Eq. (1)), Fainerman and Miller equation (Eq. (5)), Eq. (7) and Eq. (4), respectively.

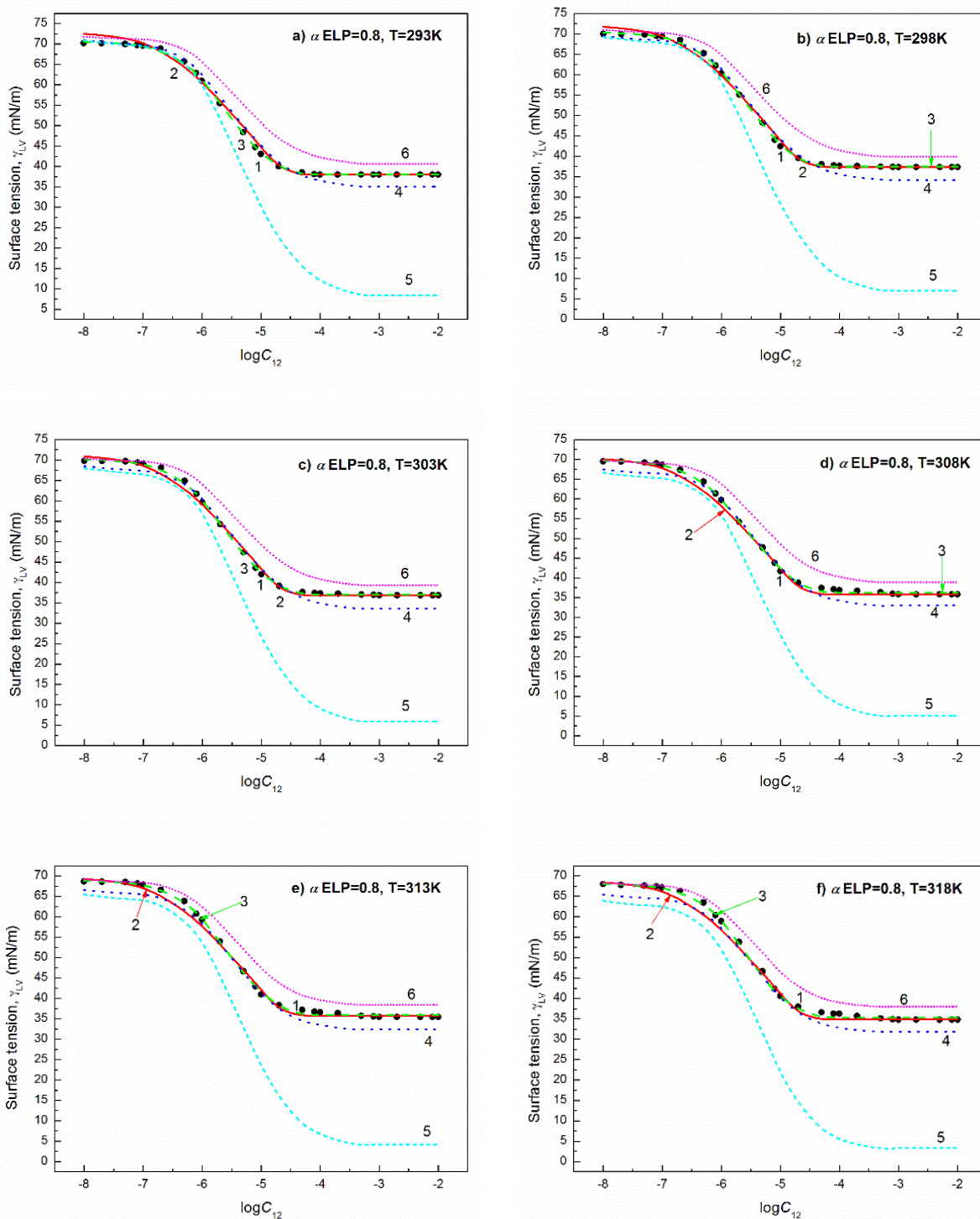


Figure S5. A plot of the surface tension (γ_{LV}) of the aqueous solutions of RH40 and ELP mixtures at the mole fraction of ELP in the bulk phase equal to 0.8 vs. the logarithm of their concentration ($\log C_{12}$) at different temperatures equal to 293 (a), 298 (b), 303 (c), 308 (d), 313 (e) and 318 K (f). Points 1 correspond to the measured values, curves 2 – 6 correspond to the values calculated from the Szyszkowski equation (Eq. (2)), exponential function of the second order (Eq. (1)), Fainerman and Miller equation (Eq. (5)), Eq. (7) and Eq. (4), respectively.

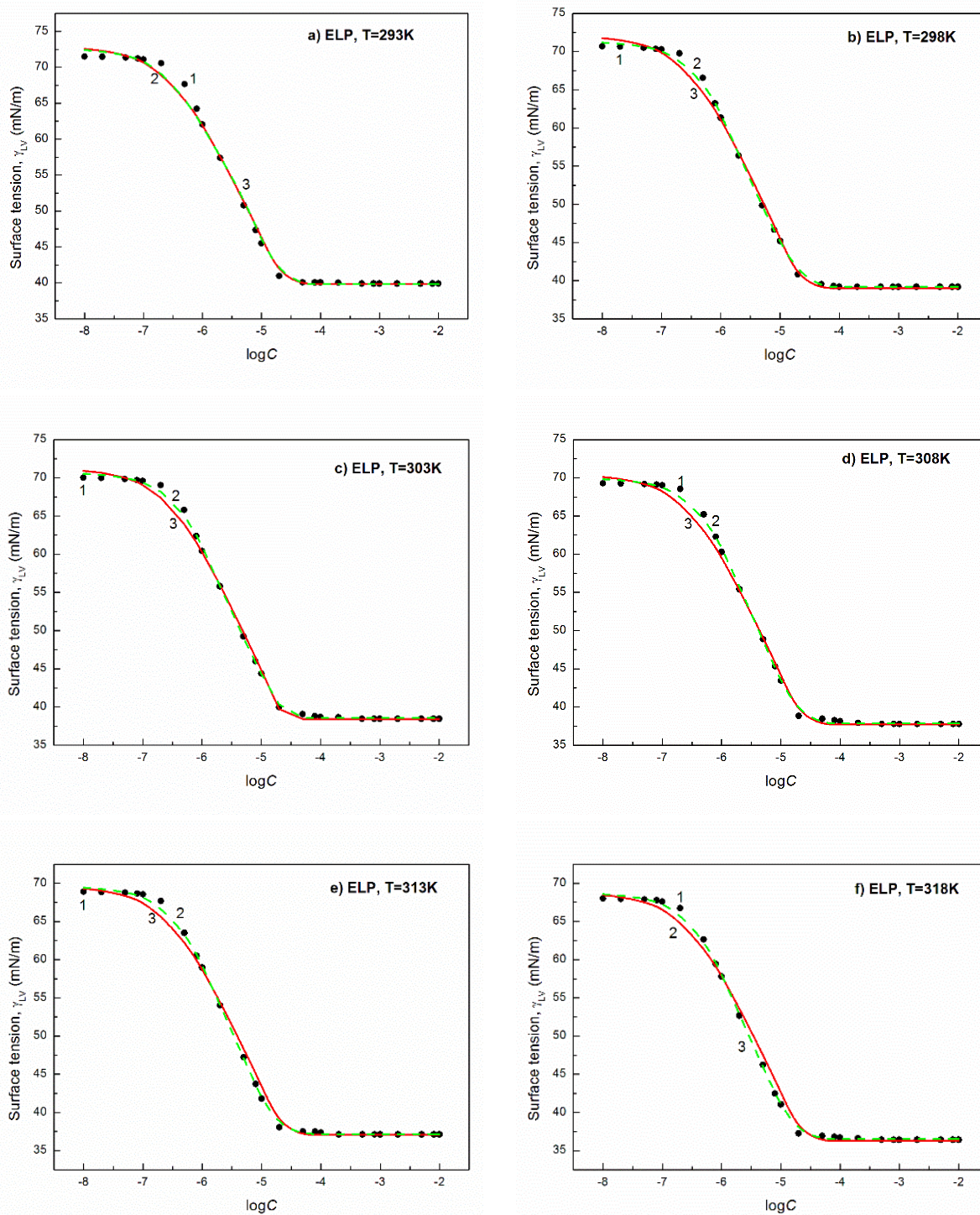


Figure S6. A plot of the surface tension (γ_{LV}) of the aqueous solutions of ELP vs. the logarithm of its concentration ($\log C$) at different temperatures equal to 293 (a), 298 (b), 303 (c), 308 (d), 313 (e) and 318 K (f). Points 1 correspond to the measured values, curves 2 and 3 correspond to the values calculated from the Szyszkowski equation (Eq. (2)) and the exponential function of the second order (Eq. (1)), respectively.

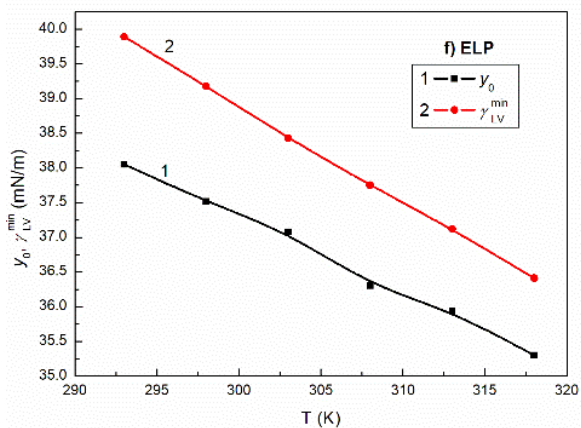
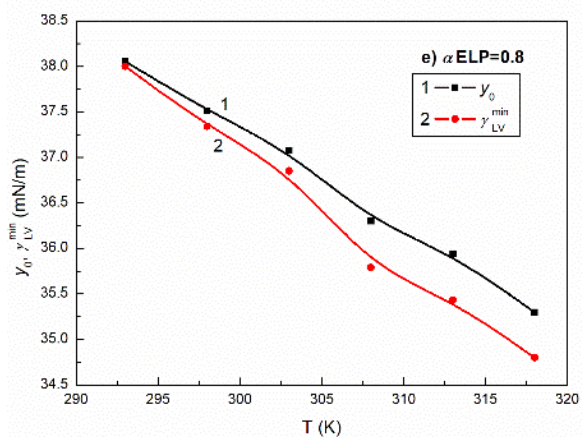
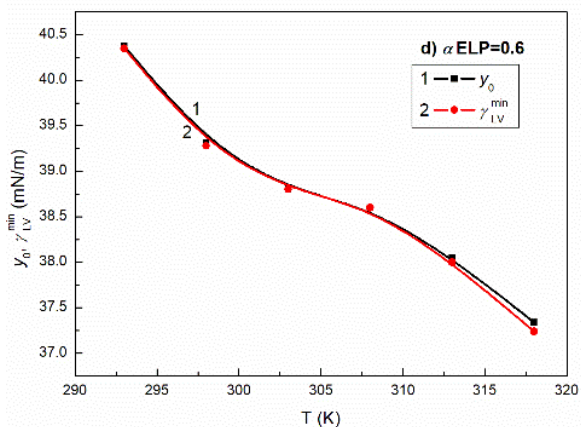
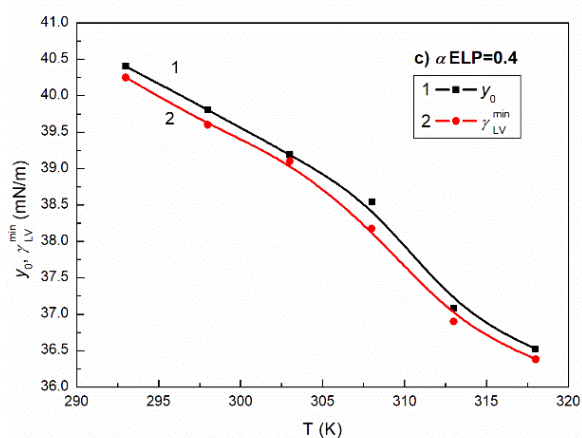
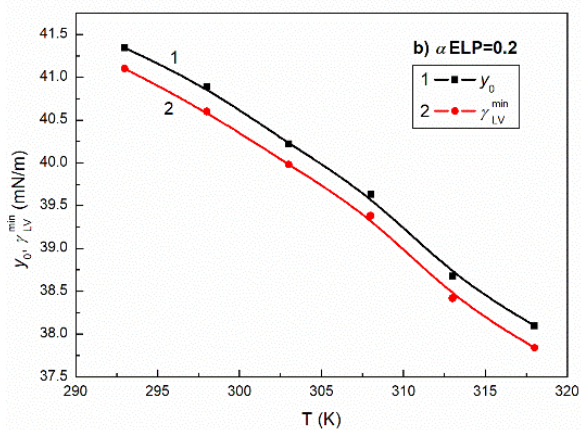
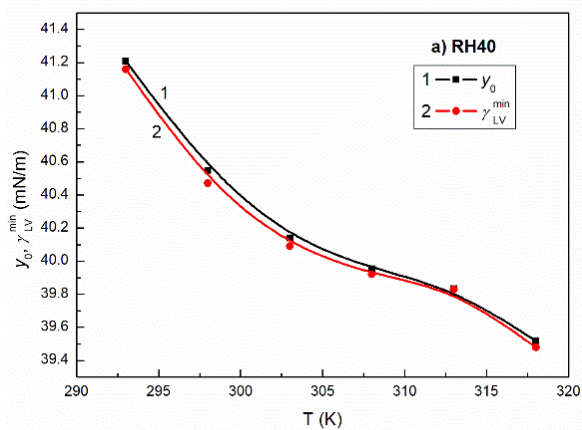


Figure S7. A plot of the values of constant y_0 in Eq. (1) (curve 1) and the minimal surface tension of aqueous solution (γ_{LV}^{min}) (curve 2) vs. the temperature (T) for the RH40 and ELP mixtures at the mole fraction of ELP in the bulk phase equal to 0 (RH40 (a)), 0.2 (b), 0.4 (c), 0.6 (d), 0.8 (e) and 1 (ELP (f)), respectively.

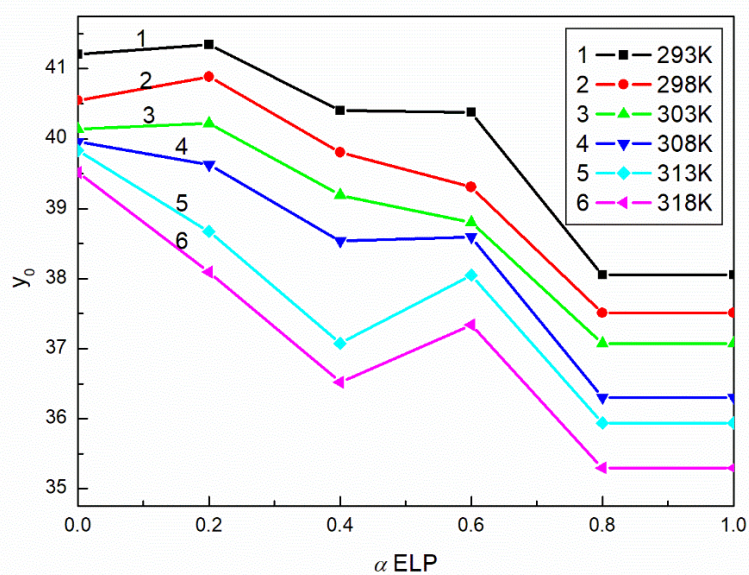


Figure S8. A plot of the values of constant y_0 in Eq. (1) for studied surfactant mixtures vs. the mole fraction of ELP in the bulk phase (α) at the temperatures equal to 293 (curve 1), 298 (curve 2), 303 (curve 3), 308 (curve 4), 313 (curve 5) and 318 K (curve 6), respectively.

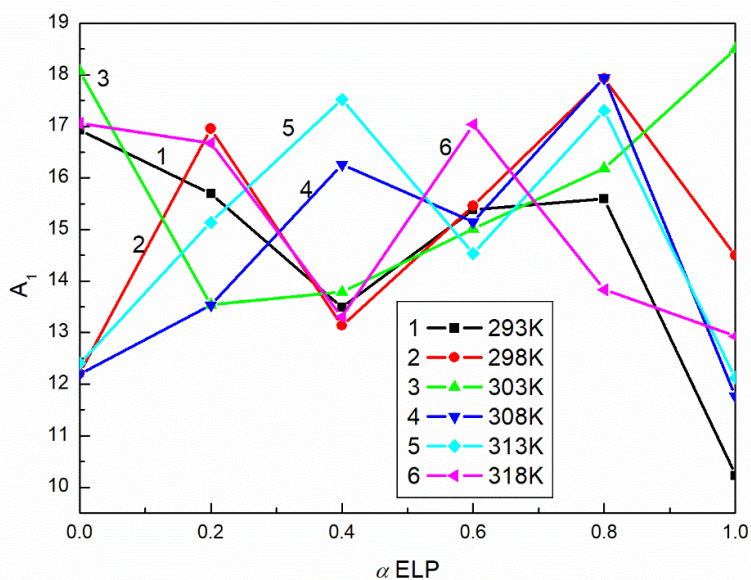


Figure S9. A plot of the values of constant A_1 in Eq. (1) for studied surfactant mixtures vs. the mole fraction of ELP in the bulk phase (α) at the temperatures equal to 293 (curve 1), 298 (curve 2), 303 (curve 3), 308 (curve 4), 313 (curve 5) and 318 K (curve 6), respectively.

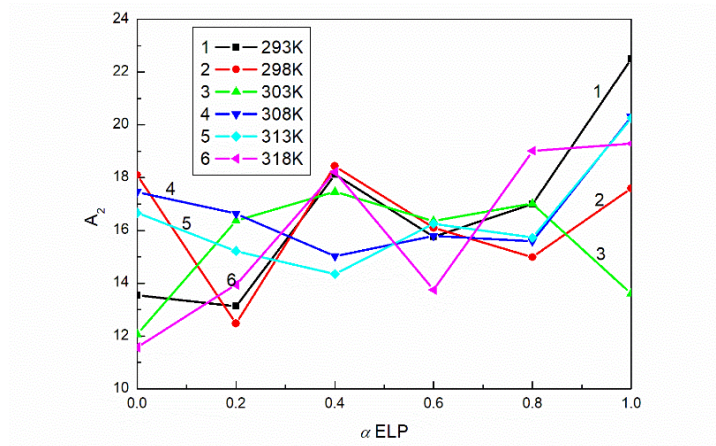


Figure S10. A plot of the values of constant A_2 in Eq. (1) for studied surfactant mixtures vs. the mole fraction of ELP in the bulk phase (α) at the temperatures equal to 293 (curve 1), 298 (curve 2), 303 (curve 3), 308 (curve 4), 313 (curve 5) and 318 K (curve 6), respectively.

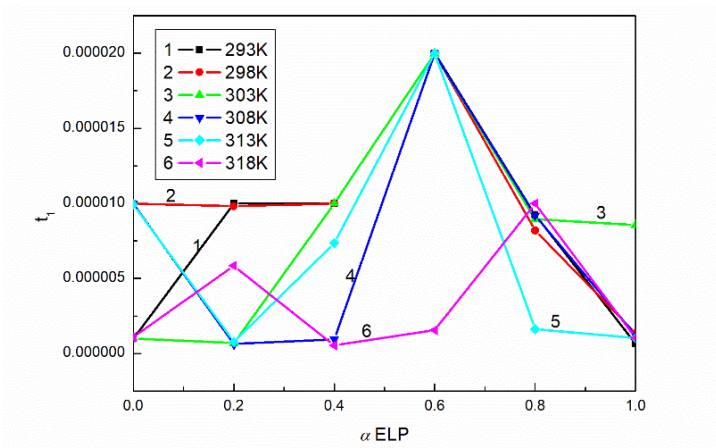


Figure S11. A plot of the values of constant t_1 in Eq. (1) for studied surfactant mixtures vs. the mole fraction of ELP in the bulk phase (α) at the temperatures equal to 293 (curve 1), 298 (curve 2), 303 (curve 3), 308 (curve 4), 313 (curve 5) and 318 K (curve 6), respectively.

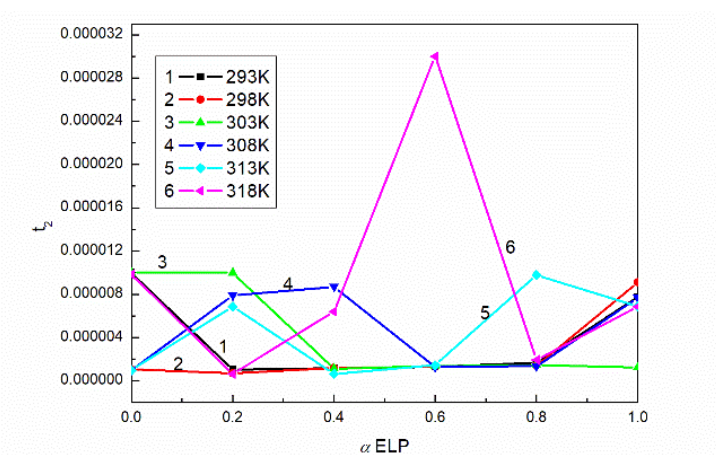


Figure S12. A plot of the values of constant t_2 in Eq. (1) for studied surfactant mixtures vs. the mole fraction of ELP in the bulk phase (α) at the temperatures equal to 293 (curve 1), 298 (curve 2), 303 (curve 3), 308 (curve 4), 313 (curve 5) and 318 K (curve 6), respectively.

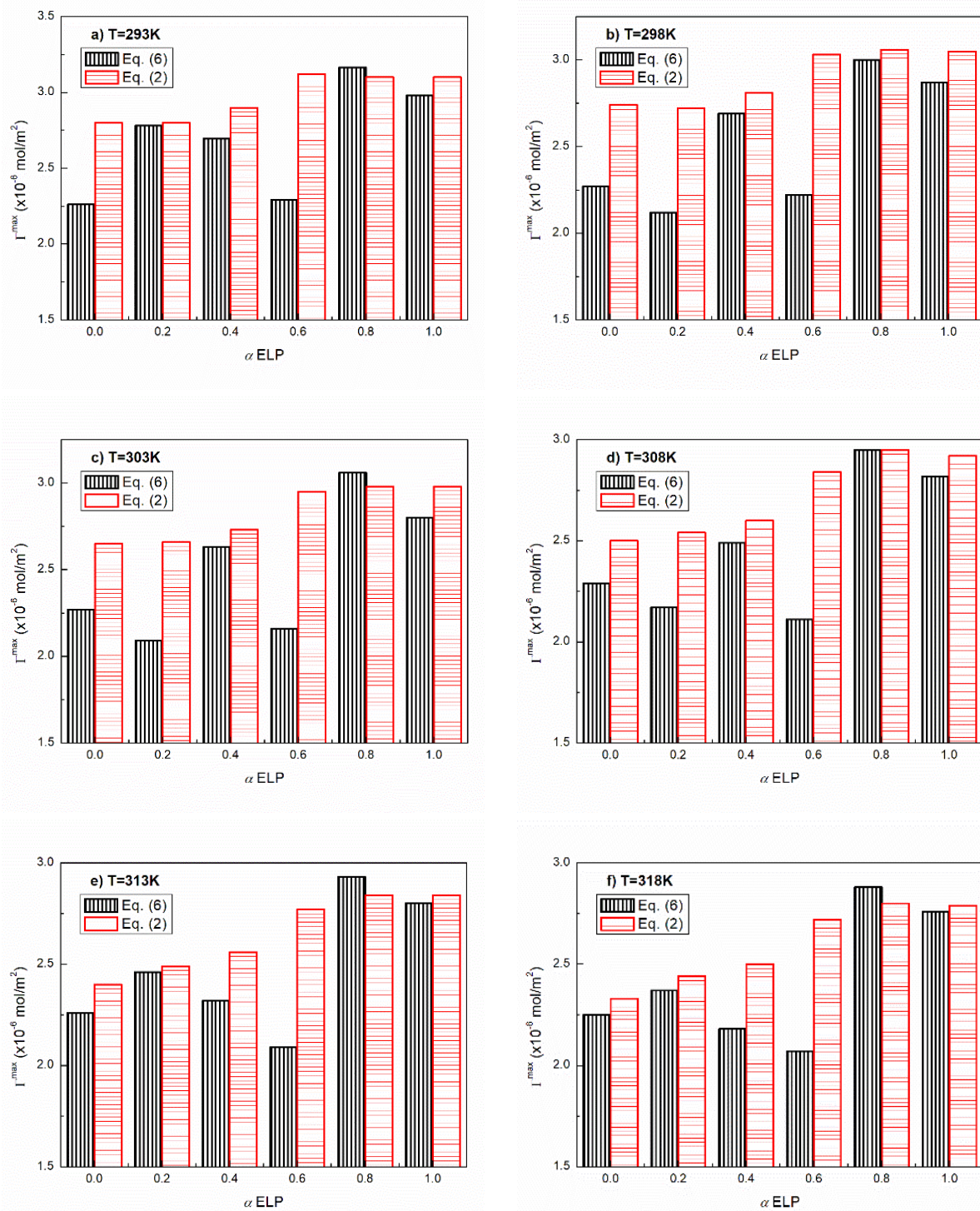


Figure S13. The values of Γ^{max} calculated from Eq. (6) and (2) for studied surfactant mixtures at the mole fraction of ELP in the bulk phase (α) equal to 0, 0.2, 0.4, 0.6, 0.8 and 1 at different temperatures equal to 293 (a), 298 (b), 303 (c), 308 (d), 313 (e) and 318 K (f), respectively.

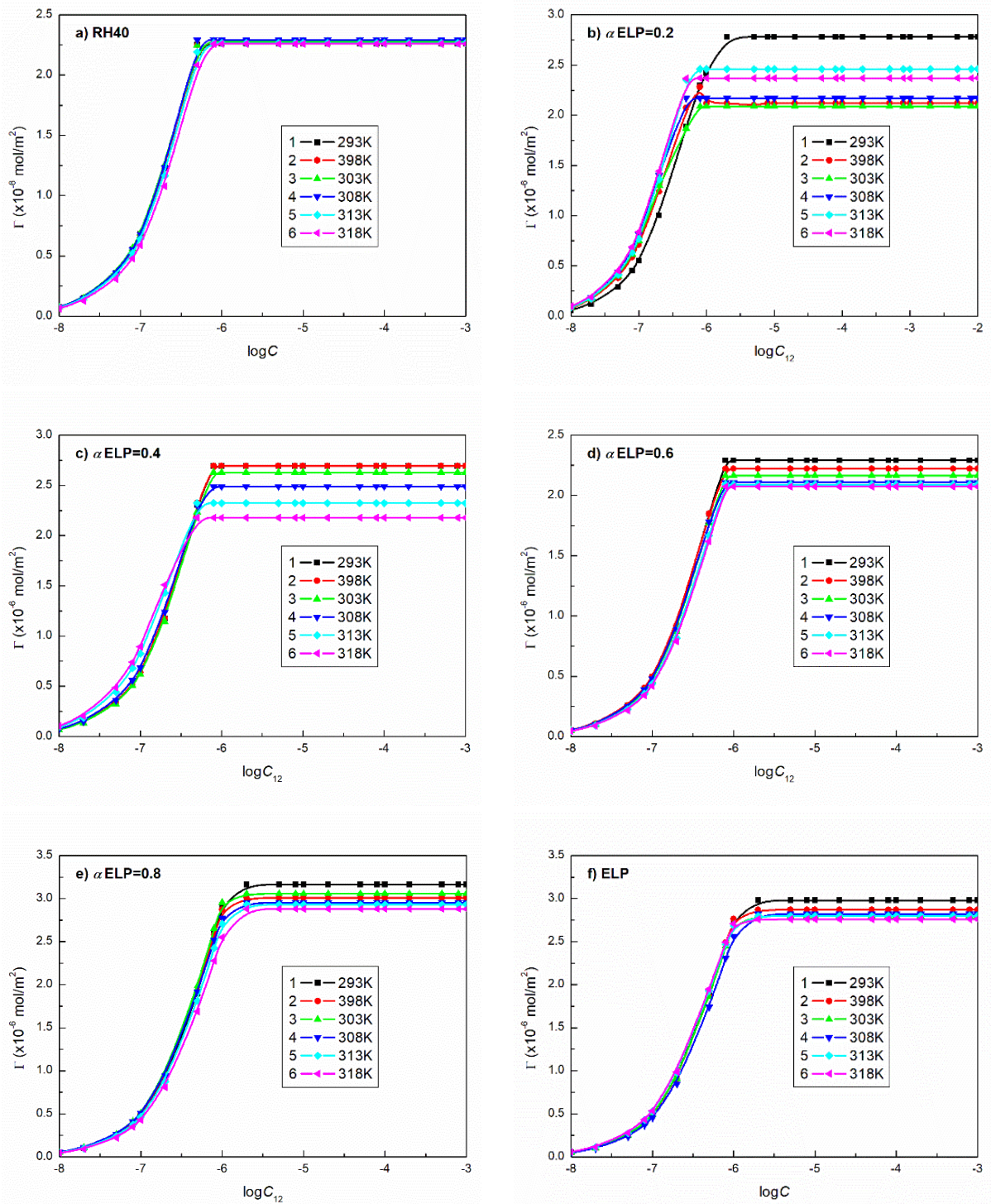


Figure S14. A plot of the values of Gibbs surface excess concentration (Γ) vs. logarithm of the concentration in the bulk phase (C or C_{12}) for the RH40 and ELP mixtures at the mole fraction of ELP in the bulk phase equal to 0 (RH40 (a)), 0.2 (b), 0.4 (c), 0.6 (d), 0.8 (e) and 1 (ELP (f)), respectively.

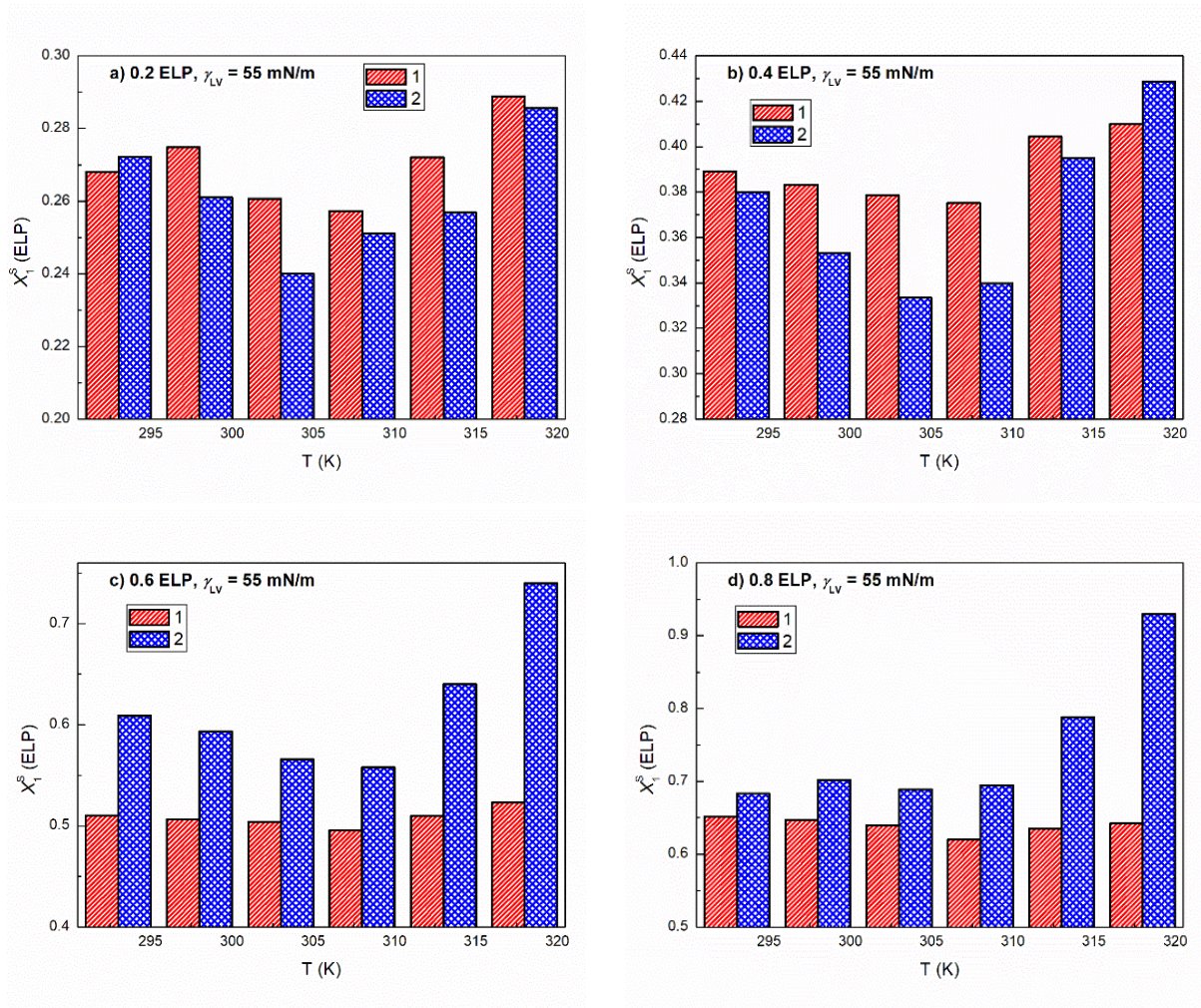


Figure S15. The values of the mole fraction of ELP in the mixed monolayer at the water air interface (X_1^S) calculated from the relationship: $X_1^S = \frac{\pi_1}{\pi_1 + \pi_2}$ (bars 1) and from Eq. (8) (bars 2) and temperature range 293-318K for mixtures at the mole fraction of ELP in the bulk phase (α) equal to 0.2 (a), 0.4 (b), 0.6 (c) and 0.8 (d).

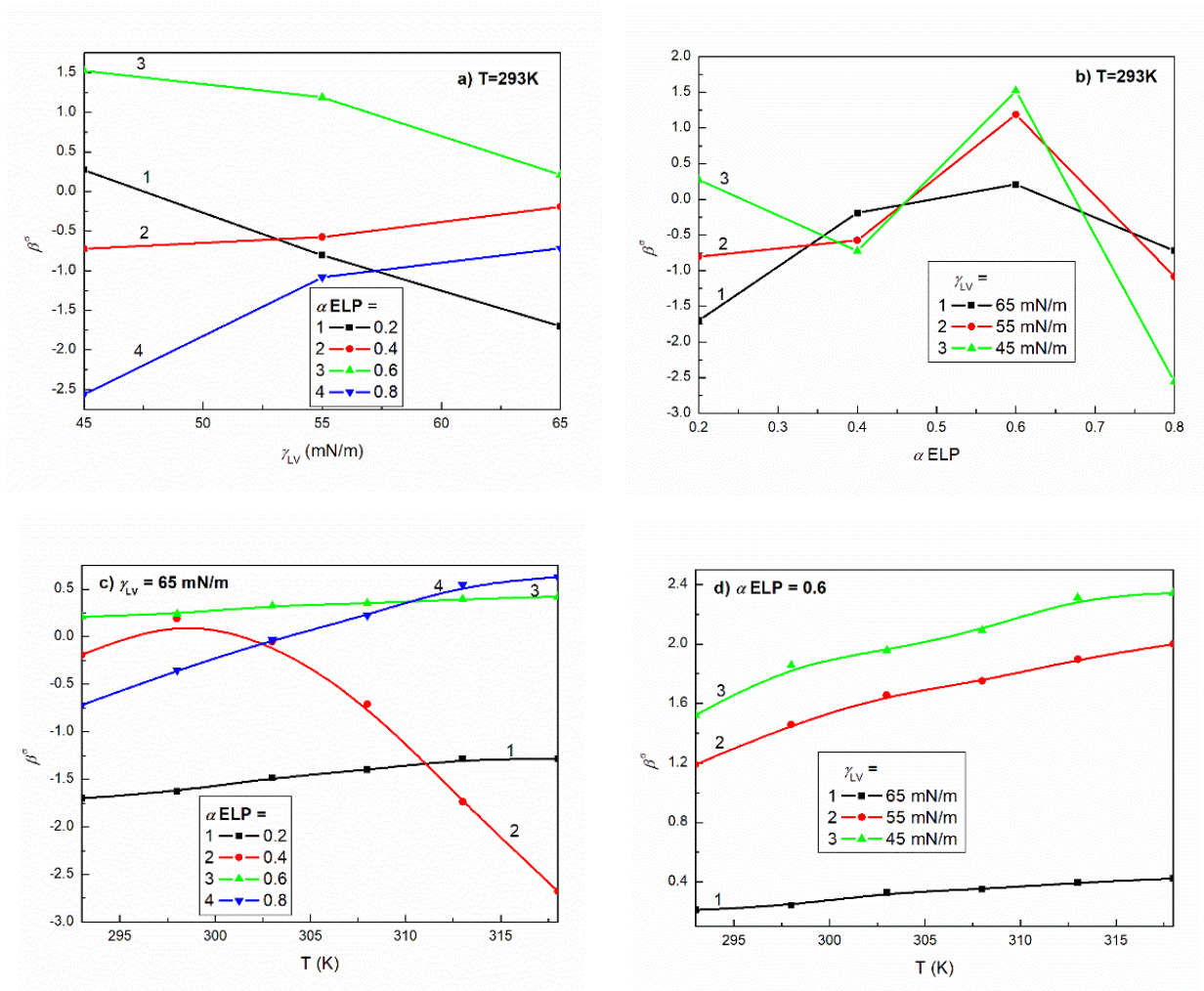


Figure S16. A plot of the values of parameter of intermolecular interactions, β^σ , for studied binary surfactant mixtures a) at the mole fraction of ELP in the bulk phase α , equal to 0.2, 0.4, 0.6, 0.8 and $T = 293\text{K}$ vs. surface tension, (γ_{LV}), b) at the surface tension, (γ_{LV}), equal to 65, 55, 45 mN/m and $T = 293\text{K}$ vs. mole fraction of ELP in the bulk phase α , c) at the mole fraction of ELP in the bulk phase α , equal to 0.2, 0.4, 0.6, 0.8 and $\gamma_{LV} = 65$ mN/m vs. temperature, T , d) at the mole fraction of ELP in the bulk phase α , equal to 0.6 and $\gamma_{LV} = 65, 55, 45$ mN/m vs. temperature, T .

ZAŁĄCZNIK 4

PUBLIKACJA [D4]

M. Szaniawska, K. Szymczyk*, A. Zdziennicka, B. Jańczuk, Thermodynamic parameters of berberine with Kolliphor mixtures adsorption and micellization, *Molecules*, 2023, 28(7), 3115

Article

Thermodynamic Parameters of Berberine with Kolliphor Mixtures Adsorption and Micellization

Magdalena Szaniawska, Katarzyna Szymczyk * , Anna Zdziennicka  and Bronisław Jańczuk 

Department of Interfacial Phenomena, Institute of Chemical Sciences, Faculty of Chemistry, Maria Curie-Skłodowska University in Lublin, Maria Curie-Skłodowska Sq. 3, 20-031 Lublin, Poland

* Correspondence: katarzyna.szymczyk@mail.umcs.pl; Tel.: +48-81-537-55-38

Abstract: The poor solubility of berberine (Ber) in water limits its practical use. Its solubility can be increased, among other ways, by the addition of surfactants. Of the surfactants, Kolliphor[®] ELP (ELP) and Kolliphor[®] RH 40 (RH40) can be very useful in this respect. The increase of Ber's solubility in water in the presence of ELP and RH40 should be reflected in the composition of the surface layers at the water-air interface and the micelles. The determined composition is reflected in the Gibbs energy of interactions of berberine with ELP and RH40 through the water phase and the standard Gibbs free energy, enthalpy, and entropy of adsorption and micellization. These energies were determined from the equations proposed by us, based on the Gibbs surface excess concentration of the Ber mixture with ELP and RH40, the activity of these compounds in the surface layer at the water-air interface and in the micelles obtained by the Hua and Rosen method, and the contributions of Ber, ELP, and RH40 to the reduction in the water surface tension. For this determination, the measurements of the surface tension of the aqueous solution of the Ber mixture with ELP or RH40 and that of the Ber mixture with these two surfactants, as well as the density and conductivity were performed. Moreover, the fluorescence emission spectra for the Ber + surfactant mixtures were recorded.

Keywords: berberine; Kolliphor[®] ELP; Kolliphor[®] RH 40; adsorption; micellization; thermodynamic parameters of adsorption and micellization



Citation: Szaniawska, M.; Szymczyk, K.; Zdziennicka, A.; Jańczuk, B. Thermodynamic Parameters of Berberine with Kolliphor Mixtures Adsorption and Micellization. *Molecules* **2023**, *28*, 3115. <https://doi.org/10.3390/molecules28073115>

Academic Editor: Vasył M. Haramus

Received: 2 March 2023

Revised: 23 March 2023

Accepted: 28 March 2023

Published: 30 March 2023



Copyright: © 2023 by the authors. Licensee MDPI, Basel, Switzerland. This article is an open access article distributed under the terms and conditions of the Creative Commons Attribution (CC BY) license (<https://creativecommons.org/licenses/by/4.0/>).

1. Introduction

Berberine (Ber), which occurs in the roots, rhizomes, stems and bark of medicinal plants is widely used in medicine [1–10]. Its molecule consists of condensed hydrocarbon rings, a ring containing oxygen atoms, and a ring with a quaternary nitrogen atom, as well as the $-\text{CH}_3\text{O}$ groups (Figure 1). The predominance of hydrophobic groups over hydrophilic ones in the berberine molecule causes its poor solubility in water [11,12], which, among others, is the reason for the limited use of berberine in practice. The solubility of Ber in water can be increased, among other ways, by mixing it with suitable surfactants. Such surfactants include Kolliphor[®] ELP (ELP) and Kolliphor[®] RH 40 (RH40). These surfactants, which are well soluble in water, are nontoxic, allowing them to be used, for example, in cosmetics and pharmaceutical products [13–16]. The good solubility of ELP and RH40 results from the presence of many oxyethylene groups, as well as $-\text{C}=\text{O}$ and $=\text{C}-\text{O}$ groups in their molecules. However, in the ELP and RH40 molecules, hydrocarbon chains containing one $-\text{OH}$ group are also present. This group decreases the hydrophobic properties of these chains to some extent.

The type and amount of the chemical groups present in the molecule determine the values of the compound surface tension and its components, as well as the number of the water molecules that can be contacted with this compound in aqueous media. According to van Oss and Constanzo [17], the surface tension of surfactants depends on their molecules' orientation toward the air phase. If they are oriented toward this phase by the hydrophobic parts of their molecules, then the surfactant surface tension is treated as its tail surface

tension. Otherwise, when the surfactant molecules are oriented by their hydrophilic part toward the air phase, then the surface tension is called the head surface tension. In turn, van Oss et al. divided the surface tension of all substances into the Lifshitz-van der Waals (LW) and acid-base (AB) components. The AB component associated with hydrogen bond formation is a function of electron-acceptor and electron-donor parameters of the surface tension [17–20]. For the condensed phases, van Oss et al. proved that the LW component results from the dispersion intermolecular interactions because the contributions of dipole-dipole and induced dipole-dipole interactions to this component are smaller than 2% [18–20].

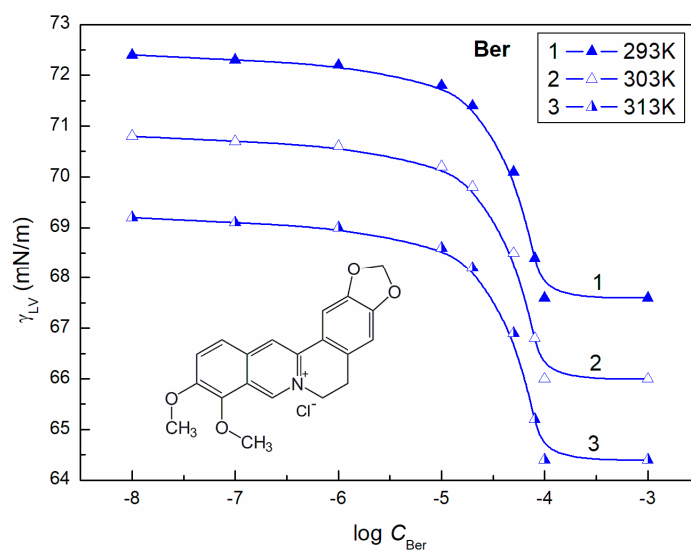


Figure 1. A plot of the surface tension (γ_{LV}) of berberine (Ber) aqueous solutions vs. the logarithm of Ber concentration ($\log C_{Ber}$) at a constant temperature equal to 293 K (curve 1), 303 K (curve 2), and 313 K (curve 3).

Knowledge of the values of the components and parameters of the surfactants' surface tension allows for the determination of the Gibbs free energy of interactions of the surfactants through the water phase. Additionally, knowing the contactable area of the hydrophobic and hydrophilic parts of the surfactants' molecules, it is possible to predict their tendency to adsorb and aggregate [21,22]. In other words, based on the components and parameters of the surfactants' tail and head surface tension, as well as their contactable area, it is possible to predict the standard Gibbs free energy of adsorption and micellization. This process is possible for single surfactants. In the case of surfactant mixtures or their mixture with additives, it is more complicated. Moreover, such considerations are rarely found in the literature. In the case of such mixtures, the standard Gibbs energy of adsorption at the water-air interface and aggregation depends on the activity of all mixture components in the surface layer and in the micelles, which has not often been considered by investigators [23,24]. In fact, the activity depends on the composition and activity coefficient.

The knowledge of the interactions between Ber and ELP, as well as RH40 molecules in aqueous media associated with the standard Gibbs free energy of adsorption and micellization, should enable understanding of the increase in Ber solubility in water, which is important from the practical point of view. As it is difficult to find such studies, the aim of our paper was to determine the relationship among the intermolecular interactions of the Ber, ELP, and RH40 through the water phase and the relationship between the composition of the mixed surface layer and mixed micelles, as well as the standard Gibbs free energy of adsorption and micellization. To solve this problem, measurements of the surface tension, conductivity, and density at temperatures of 293, 303 and 313 K of the following solutions were performed: ELP + Ber (M1), RH40 + Ber (M2), and ELP + RH40 + Ber (M3). In each

solution, the concentration of Ber was constant and equal to 1×10^{-4} mol/dm³, and the concentration of surfactants was in the range of 1×10^{-6} – 1×10^{-2} mol/dm³. In the M3 mixture, the mole fraction of ELP in the bulk phase was equal to 0.8. Moreover, the fluorescence emission spectra for the Ber + surfactant mixtures were recorded. Additionally, for the determination of the components and parameters of berberine's surface tension, the contact angles of water, diiodomethane, and formamide on pressed Ber tablets were measured.

2. Theory

The amount of the surfactants adsorbed at the water-air (W-A) interface as well as the standard Gibbs free energy of adsorption and micellization, is directly associated with the chemical potential of the surfactants in the surface layer and/or micelles, as well as in the bulk phase. It should be remembered that, at a constant temperature (T) and pressure (p), the chemical potential of i -th solution component (μ_i) is equal to the contribution of the Gibbs free energy (G_i) of this component. The adsorption and micellization processes of a single surfactant are related to the standard Gibbs free energy of these processes. In turn, the standard Gibbs free energy of adsorption (ΔG_{ads}^0) and micellization (ΔG_{mic}^0) is equal to the difference between the standard potential, which is symmetrically (μ_i^0) and asymmetrically (μ_i^*) defined. In the case of solutions of multicomponent mixture, the changes of the Gibbs free energy of the solution during the adsorption and micellization processes can be also related to the Gibbs free energy of surfactants mixing in the monolayer at the W-A interface and in the micelles.

In the case of aqueous solutions, the amount of surfactant mixture adsorbed at the W-A interface is connected to the changes in the solution surface tension (γ_{LV}), which is expressed by the Gibbs-Duhem equation [25,26]:

$$A d\gamma_{LV} + \sum_{i=1}^{j-1} n_i d\mu_i = 0, \quad (1)$$

where n_i is the number of moles of the i -th component, A is the area of the interface, and j is the number of the components.

Knowing that, in the equilibrium state, the chemical potential of i -th component in the surface layer is equal to that in the bulk phase, assuming that the activity of $j \neq i$ components is constant and that the Gibbs surface excess concentration of i -th component, Γ_i , is equal to $\frac{n_i}{A}$, the following can be written:

$$\Gamma_i = -\frac{a_i}{mRT} \left(\frac{\partial \gamma_{LV}}{\partial a_i} \right)_{a_{j \neq i}, T} = -\frac{1}{mRT} \left(\frac{\partial \gamma_{LV}}{\partial \ln a_i} \right)_{a_{j \neq i}, T}, \quad (2)$$

where the value of m depends on the type of surfactant; for example, for the ionic surfactant type 1:1 electrolyte is equal to 2, a_i is the activity, and R is the gas constant.

If the concentration of surfactants is small, then according to the asymmetrical definition of the chemical potential, its activity coefficient (f_i) is close to unity, and $a_i \cong x_i$ (x_i is the molar fraction of i -th component in the bulk phase). In such cases, $x_i \cong C_i/\omega$, where C_i is the mole concentration of the i -th component in the bulk phase, and ω is the number of the water moles in 1 dm³ of solution. Taking these assumptions into account, Equation (2) can be written as:

$$\Gamma_i = -\frac{C_i}{mRT} \left(\frac{\partial \gamma_{LV}}{\partial C_i} \right)_{C_{j \neq i}, T} = -\frac{1}{2.303mRT} \left(\frac{\partial \gamma_{LV}}{\partial \log C_i} \right)_{C_{j \neq i}, T}, \quad (3)$$

In the case of the constant composition of the multicomponent mixtures of substrates in the bulk phase, it was proved that the sum of the mixture's Gibbs surface excess concentration at the W-A interface (Γ_{sum}) can be determined from the following equation:

$$\Gamma_{sum} = -\frac{C_{sum}}{mRT} \left(\frac{\partial \gamma_{LV}}{\partial C_{sum}} \right)_T = -\frac{1}{2.303mRT} \left(\frac{\partial \gamma_{LV}}{\partial \log C_{sum}} \right)_T, \quad (4)$$

where C_{sum} is the sum of the mole concentration of all components of substrate in the solution.

Unfortunately, in the case of the mixtures in which the concentrations of all components except one in the bulk phase are constant, the Gibbs surface excess concentration at the W-A interface of the components at a constant concentration in the bulk phase changes as a function of component at variable concentration. In such cases, it is possible to determine the Gibbs surface concentration using the Frumkin equation, which for i -th component of the mixture has this form:

$$\pi_i = -RT\Gamma_i^{max} \ln\left(1 - \frac{\Gamma_i}{\Gamma_i^{max}}\right), \quad (5)$$

where π_i is the contribution of i -th component to the reduction in water surface tension (γ_w), Γ_i is the concentration of i -th component of the mixture at the W-A interface, and Γ_i^{max} is the maximal concentration of i -th mixture component at the W-A interface.

It is proved that the fraction of area occupied by the i -th component in the mixture at the W-A interface (x_i^S) is equal to $\frac{\pi_i^{ind}}{\sum_{i=1}^n \pi_i^{ind}}$, where π_i^{ind} is the film pressure at the W-A interface of the individual component of the mixture in the absence of others. Hence π_i can be determined from the following expression [21]:

$$\pi_i = x_i^S \pi = x_i^S (\gamma_w - \gamma_{LV}), \quad (6)$$

The studies of the composition of binary and ternary mixtures of surfactants have shown that the x_i^S values determined based on the contributions of particular mixture components to the reduction in water surface tension are comparable to those determined from the Hua and Rosen concept [27]. The Hua and Rosen concept, based on the non-ideal solution theory, allows for determining the composition of the binary mixture of the surfactants in the interface region [27]. However, our studies showed that it is possible to apply the Hua and Rosen concept successfully to determine the composition of the mixed monolayer of the ternary surfactants' mixture [21]. For the i -th, k -th, and l -th components of the ternary mixture, the Rosen and Hua equation can be written in this form:

$$\frac{(x_{ik}^S)^2 \ln(\alpha_{ik} C_{ikl}^0 / x_{ik}^S C_{ik}^0)}{(1 - x_{ik}^S)^2 \ln[(1 - \alpha_{ik}) C_{ikl}^0 / (1 - x_{ik}^S) C_l^0]} = 1, \quad (7)$$

and

$$\frac{(x_{kl}^S)^2 \ln(\alpha_{kl} C_{ikl}^0 / x_{kl}^S C_{kl}^0)}{(1 - x_{kl}^S)^2 \ln[(1 - \alpha_{kl}) C_{ikl}^0 / (1 - x_{kl}^S) C_l^0]} = 1, \quad (8)$$

and

$$\frac{(x_{il}^S)^2 \ln(\alpha_{il} C_{ikl}^0 / x_{il}^S C_{il}^0)}{(1 - x_{il}^S)^2 \ln[(1 - \alpha_{il}) C_{ikl}^0 / (1 - x_{il}^S) C_k^0]} = 1, \quad (9)$$

where α is the mole fraction of a given component in the surfactant mixture in the bulk phase of the solution, C^0 is the concentration of the individual component of the mixture or the sum of components' concentrations at which the water surface tension is reduced to the same value, and $\alpha_{ik} = \alpha_i + \alpha_k$, $\alpha_{il} = \alpha_i + \alpha_l$, $\alpha_{kl} = \alpha_k + \alpha_l$, $x_{ik}^S = x_i^S + x_k^S$, $x_{il}^S = x_i^S + x_l^S$, $x_{kl}^S = x_k^S + x_l^S$, $C_{ikl}^0 = C_i^0 + C_k^0 + C_l^0$, $C_{ik}^0 = C_i^0 + C_k^0$, $C_{il}^0 = C_i^0 + C_l^0$ and $C_{kl}^0 = C_k^0 + C_l^0$.

The composition of the mixed micelles of binary mixtures of the surfactants in the aqueous media can be determined using the Rubingh equation [28,29]. This equation can be successfully used for the ternary surfactant mixture in a modified way [21]. For the ternary mixtures, it can be written as:

$$\frac{(x_{ik}^M)^2 \ln(\alpha_{ik} C_{ikl}^M / x_{ik}^M C_{ik}^M)}{(1 - x_{ik}^M)^2 \ln[(1 - \alpha_{ik}) C_{ikl}^M / (1 - x_{ik}^M) C_l^M]} = 1, \quad (10)$$

and

$$\frac{(x_{kl}^M)^2 \ln(\alpha_{kl} C_{ikl}^M / x_{kl}^M C_{kl}^M)}{(1 - x_{kl}^M)^2 \ln[(1 - \alpha_{kl}) C_{ikl}^M / (1 - x_{kl}^M) C_i^M]} = 1, \quad (11)$$

and

$$\frac{(x_{il}^M)^2 \ln(\alpha_{il} C_{ikl}^M / x_{il}^M C_{il}^M)}{(1 - x_{il}^M)^2 \ln[(1 - \alpha_{il}) C_{ikl}^M / (1 - x_{il}^M) C_k^M]} = 1, \quad (12)$$

where M refers to the micelles, and the other symbols have the same meaning as above.

It is known that, for the ideal mixtures, there are direct relationships between the standard Gibbs free energy of adsorption and the mole fraction of components in the mixed monolayer and between the standard Gibbs free energy of micellization and the mole fraction of components of the mixed micelle. In the case of the non-ideal mixtures of surfactants, the activity of particular components of the mixture in the surface region and micelle should be known. The literature reports different methods for the determination of standard Gibbs free energy of adsorption (ΔG_{ads}^0) and micellization (ΔG_{mic}^0) [29]. These methods are useful for aqueous solutions of single surfactants. However, they are not quite suitable for aqueous solutions of the multicomponent surfactant mixtures [21].

In the aqueous solution of the multicomponent surfactant mixture, three regions can be distinguished: interface (S), bulk (B), and micellar (M). These regions can be treated as separate phases. The chemical potential of the i -th component of the surfactant mixture in these phases can be expressed as follows [30]:

$$\mu_i^S = \mu_i^{0,S} + RT \ln a_i^S + \pi_i \omega_i, \quad (13)$$

and

$$\mu_i^M = \mu_i^{0,M} + RT \ln a_i^M, \quad (14)$$

and

$$\mu_i^B = \mu_i^{*,B} + RT \ln a_i^B, \quad (15)$$

In the equilibrium state, the chemical potential of i -th component is the same. Hence:

$$\mu_i^{0,S} - \mu_i^{*,B} = RT \ln \frac{a_i^B}{a_i^S} - \pi_i \omega_i, \quad (16)$$

and

$$\mu_i^{0,M} - \mu_i^{*,B} = RT \ln \frac{a_i^B}{a_i^M}, \quad (17)$$

At constant T and p , $\mu_i^{0,S} - \mu_i^{*,B} = \Delta G_{ads,i}^0$ and $\mu_i^{0,M} - \mu_i^{*,B} = \Delta G_{mic,i}^0$. In the case of surfactants, their concentrations in aqueous solution are small, and it can be assumed that $a_i^B = x_i^B$ and $x_i^B \cong C_i / \omega$. Based on these assumptions the following can be written:

$$\Delta G_{ads,i}^0 = RT \ln \frac{C_i}{\omega x_i^S f_i^S} - \pi_i \omega_i, \quad (18)$$

and

$$\Delta G_{mic,i}^0 = RT \ln \frac{CMC \alpha_i^B}{\omega x_i^M f_i^M}, \quad (19)$$

where ω_i is the area occupied by one mole of surfactant, CMC is the critical micelle concentration, and f_i is the activity coefficient.

According to the thermodynamic rule, the standard Gibbs free energy of adsorption or micellization of the i -th component of the surfactant mixture (ΔG_i^0) satisfies the following equation [25,29]:

$$\Delta G_i^0 = \Delta H_i^0 - T \Delta S_i^0, \quad (20)$$

where ΔH_i^0 is the standard enthalpy of adsorption or micellization, and ΔS_i^0 is the standard entropy of adsorption or micellization.

Knowing the values of ΔG_i^0 at different temperatures and assuming that, in the given temperature range, ΔH_i^0 is constant, it is possible to determine ΔS_i^0 from the following equation [25,29]:

$$\frac{d(\Delta G_i^0)}{dT} = -\Delta S_i^0, \quad (21)$$

Indeed, knowing the ΔG_i^0 and ΔS_i^0 values, the ΔH_i^0 values can be calculated from Equation (20). The activity coefficients of the i -th component of the surfactant mixture needed for the standard Gibbs free energy of adsorption and micellization determination can be obtained, among other ways, on the basis of intermolecular interactions parameter for the mixed monolayer (β^σ) and the micelles (β^M) from the Rosen and Hua equations, which for the two-component mixtures of surfactants have the following forms [27,29]:

$$\ln f_1^S = \beta^\sigma (1 - x_1^S)^2, \quad (22)$$

and

$$\ln f_2^S = \beta^\sigma (x_1^S)^2, \quad (23)$$

and

$$\ln f_1^M = \beta^M (1 - x_1^M)^2, \quad (24)$$

and

$$\ln f_2^M = \beta^M (x_1^M)^2, \quad (25)$$

For calculations of the β^σ and β^M parameters, Rosen and Hua derived the following equations [27,29]:

$$\beta^\sigma = \frac{\ln(\alpha_1 C_{12}^0 / x_1^S C_1^0)}{(1 - x_1^S)^2}, \quad (26)$$

and

$$\beta^M = \frac{\ln(\alpha_1 C_{12}^M / x_1^M C_1^M)}{(1 - x_1^M)^2}, \quad (27)$$

Jańczuk et al. [31,32] showed that there is a relation between the Gibbs free energy of adsorption and/or micellization and the components and parameters of the surface tension of water, as well as the tail and head of surfactant surface tension. They proposed the following equation:

$$\Delta G_{ads}^0 = (\gamma_T - \gamma_{TW})A_T N + (\gamma_{WH1} - \gamma_{WH})A_H N, \quad (28)$$

where γ_T is the tail surface tension; γ_{TW} , γ_{WH} , and γ_{WH1} are the tail-water, head-water and dehydrated head-water interface tensions, respectively; A_T and A_H are the contactable areas of the tail and head; N is the Avogadro number. If during the transfer of the surfactant molecule from the bulk phase to the surface region, its head does not dehydrate, then:

$$\Delta G_{ads}^0 = (\gamma_T - \gamma_{TW})A_T N, \quad (29)$$

The proposed equation for ΔG_{mic}^0 has the following form:

$$\Delta G_{mic}^0 = -N \left[2\gamma_{WT}A_T - \left(2\gamma_{WH} - \Delta G_{int}^{EL} \right) A_H \right], \quad (30)$$

where ΔG_{int}^{EL} is the Gibbs free energy of electrostatic interactions.

For nonionic surfactants, Equation (30) assumes the following form:

$$\Delta G_{mic}^0 = -N(2\gamma_{WT}A_T - 2\gamma_{WH}A_H), \quad (31)$$

3. Results and Discussion

3.1. Some Physicochemical Properties of Ber, ELP and RH40

The behavior of surfactants and their mixtures with organic additives in aqueous media depends not only on the types of the chemical groups present in the surfactant molecules and additives but also on their number, as well as their polarity. The sizes of the contactable area of the apolar and polar parts of the surfactants and additives with other molecules and their surface tension components and parameters are responsible for the adsorption and aggregation behaviors of surfactants and their mixtures with organic additives.

The sizes of Ber, ELP, and RH40 molecules were calculated based on the bonds' lengths, the angles between the bonds, and the distance between the molecules. It was proved that the volume of one molecule each of Ber, ELP, and RH40 can be deduced based on the volumes of cubes into which particular fragments of the molecule can enter. The volumes of Ber, ELP, and RH40 molecules obtained in this way are equal 428.25, 4378.64, and 4825.21 Å³, respectively. As follows from these volumes and the Ber, ELP, and RH40 mole weights, the density of these compounds is equal to 1.3042, 0.91947, and 0.9979 g/cm³, respectively. Taking into account the molecule size of a given compound obtained in this way, it was possible to establish the contactable area of this molecule with those of water. This area is close to 277.45 Å² for Ber, 3779.9 Å² for ELP, and 4210.2 Å² for RH40. Considering the contactable area of water molecules, which is equal to 10 Å² [33], it can be stated that there can theoretically be contacted 28 water molecules with Ber, 378 with ELP, and 421 with RH40. In turn, one oxyethylene group in the surfactant molecule can be joined with two water molecules by strong hydrogen bonds and three by the weak ones [34,35]. Hence, it can be concluded that, depending on the configuration, the oxyethylene chains in the RH40 molecule can be surrounded at most by about 280 water molecules and ELP by 245. As the contactable area of ELP and RH40 tails is twice as small as the head of their molecules, approximately two times fewer water molecules surround the tails of ELP and RH40 molecules than the heads. The numbers of water molecules surrounding the heads of surfactant molecules make them largely soluble in water. On the other hand, the number of water molecules surrounding the tails of RH40 and ELP molecules is the driving force in their adsorption at the W-A interface and micellization. This driving force depends on the components and parameters of water and surfactants' surface tension, as well as on the size of the contactable area. The contactable area of the surfactant molecules through the water phase is smaller than that of the whole one. These areas for ELP and RH40 are equal to 951.616 and 1054.582 Å², respectively. In the case of Ber, its contactable area between two molecules is equal to 108.96 Å². This area is smaller than the maximal contactable area between the tails of two ELP and RH40 molecules, which is close to 324.714 Å².

The surface tension of Ber was determined based on the contact angle (θ) measured for water (56.2°), formamide (38.4°), and diiodomethane (46.1°) on pressed berberine using the van Oss et al. concept [18–20]. According to this concept and the Young equation, the following can be written:

$$\gamma_{LV}(\cos \theta + 1) = 2 \left(\sqrt{\gamma_{SV}^{LW} \gamma_{LV}^{LW}} + \sqrt{\gamma_{SV}^{+} \gamma_{LV}^{-}} + \sqrt{\gamma_{SV}^{-} \gamma_{LV}^{+}} \right), \quad (32)$$

Knowing the Lifshitz-van der Waals component (γ_{LV}^{LW}) of the water, formamide and diiodomethane surface tension, and the electron-acceptor (γ_{LV}^{+}) and electron-donor (γ_{LV}^{-}) parameters of this tension [36], it was possible to obtain from Equation (32) the Lifshitz-van der Waals component ($\gamma_{SV}^{LW} = 36.42$ mN/m) of the Ber surface tension ($\gamma_{SV} = 46.52$ mN/m), as well as its electron-acceptor ($\gamma_{SV}^{+} = 1.56$ mN/m) and electron-donor ($\gamma_{SV}^{-} = 16.38$ mN/m) parameters. From the calculations based on Equation (32), it resulted that the Ber surface tension is not much different from that of Triton X-165 (TX165) if its molecules are positioned with the hydrophilic part toward the air phase [37]. However, the contribution of the LW component to the Ber surface tension is smaller, and that of AB larger than those of TX165 surface tension. The contribution of the LW component to Ber γ_S is equal

to 78%, and it results in the poor solubility of Ber in water. Indeed, the solubility of organic substrates in water depends not only on the LWtoAB ratio and their surface tension but also on the contactable area of the hydrophobic and hydrophilic groups in their molecules. To increase the solubility of Ber in water, it is added to water in the form of an alcohol solution. Probably due to strong interactions between the hydrocarbon groups in the alcohol and in the Ber molecules, the displacement of water molecules surrounding the hydrophobic groups in the Ber molecule, as well as the orientation of the alcohol molecules with the -OH group toward the water phase, enhances the hydrophilic character of the Ber molecules. The constant concentration of ethanol used to dissolve Ber in water, equal to 1×10^{-3} mol/dm³, practically changes the water surface tension by a value comparable to the accuracy of surface tension measurements. It seems that, in such cases, all thermodynamic considerations dealing with the adsorption and micellization properties of Ber, ELP, and RH40, as well as their mixtures, are reasonable.

In the Ber molecule, in contrast to ELP and RH40, it is difficult to distinguish the hydrophobic (tail) and hydrophilic (head) parts. Therefore, it should be expected that the preferential orientation of Ber molecules at the W-A interface is parallel to this interface. On the other hand, it is possible that the hydrophilic group in the Ber molecule causes its orientation at the W-A interface in the form of an inclined plane. A greater tendency of hydrophobic chains composed of -CH₃, -CH₂- or =CH- groups for horizontal orientation than toward reorientation is suggested by the investigators on the basis of thermodynamic considerations of the adsorption processes of different compounds at the W-A interface [38–40]. Indeed, this orientation depends largely on the packing of the compound molecules being influenced by the strong intermolecular interactions in the surface region.

Berberine reduces the water surface tension to a small extent (Figure 1), and its maximal reduction corresponds to a Ber concentration close to 1×10^{-4} mol/dm³. At higher Ber concentrations in aqueous solutions, the surface tension of solution is constant. However, the inflection point on the surface tension isotherm of the berberine aqueous solution cannot be treated as the CMC. The Gibbs surface excess concentration of Ber at the W-A interface calculated from Equation (4) is equal to 1.5×10^{-6} , 1.48×10^{-6} , and 1.46×10^{-6} mol/dm³ at 293, 303, and 313 K, respectively. The minimal area occupied by one Ber molecule is close to the contactable area of berberine at its parallel orientation at the W-A interface. In contrast to berberine, the ELP and RH40 molecules in the surface layer can be oriented perpendicularly and/or at an angle to the W-A interface because their molecules are of an amphiphilic nature.

It seems that, in the case of ELP and RH40 the directly measured surface tension can be treated as the head surface tension because of very strong hydrophobic interactions between the tails of ELP and RH40 molecules. For this reason, the probability of the orientation of ELP and RH40 molecules at the surfactant-air interface with their heads directed toward the air phase is very high. If so, it is possible to determine the components and parameters of the heads of ELP and RH40 surface tension by measuring their contact angles on the PTFE and PMMA surfaces. It is known that PTFE is a modeling apolar solid, the surface tension of which results from only the Lifshitz-van der Waals intermolecular interactions [18–20]. According to Fowkes [41] and van Oss et al. [18–20], the equilibrium state of the PTFE-liquid drop-air system fulfills this equation:

$$\gamma_{LV}(\cos \theta + 1) = 2\sqrt{\gamma_{SV}^{LW}\gamma_{LV}^{LW}}, \quad (33)$$

On the basis of γ_{LV}^{LW} and the contact angle on the monopolar PMMA, the electron-acceptor parameter of ELP and RH40 head surface tension can be determined. It should be noted that PMMA is treated as a monopolar solid because its surface tension results from the LW intermolecular interactions [32]. On the other hand, PMMA can also interact with polar liquids by acid-base (AB) forces because the γ^- parameter of the PMMA surface

tension is greater than zero. The contact angle of liquids on the PMMA surface can be expressed by the following equation [18]:

$$\gamma_{LV}(\cos \theta + 1) = 2 \left(\sqrt{\gamma_{SV}^{LW} \gamma_{LV}^{LW}} + \sqrt{\gamma_{SV}^{-} \gamma_{LV}^{+}} \right), \quad (34)$$

Knowing that $\gamma_{LV}^{AB} = \gamma_{LV} - \gamma_{LV}^{LW}$, it is possible to determine all components and parameters of the ELP and RH40 head surface tension based on the measured values of γ_{LV} and θ on the PTFE and PMMA surfaces. These components and parameters determined in this way are similar to those of the head of TX165 surface tension (Table 1). This outcome confirms the assumption that ELP and RH40 molecules are oriented by their heads toward the air phase. In turn, as suggested earlier, the surface tension of the ELP and RH40 heads should be close to those of unsaturated fatty acids [22]. One –OH group in the hydrophobic single chain of ELP and RH40 molecules does not seem to have a significant effect on the value of the tail surface tension. The large size of the head of ELP and RH40 molecules guarantees good solubility of these surfactants in water, and the large size of the tail causes good surface activity and the tendency to form micelles in aqueous media. The maximal Gibbs concentration of ELP and RH40 is greater than for Tritons, and micelle formation takes place at concentrations smaller than that in the case of Tritons [42].

Table 1. The values of the contact angles of water (θ_W), formamide (θ_F), and diiodomethane (θ_D) on the pressed Ber; the contact angles (θ) of ELP and RH40 on PTFE and PMMA surfaces; and the components and parameters of the surface tension of water, Ber, ELP, ELP/RH40/TX165 head, PTFE and PMMA.

	θ_W	θ_F	θ_D	
Ber	56.2	38.4	46.1	
	θ PTFE		θ PMMA	
ELP	74			23
RH40	75			25
	γ_{LV}^{LW}	γ_{LV}^{+}	γ_{LV}^{-}	γ_{LV}
Ber	36.42	1.556	16.38	46.52
ELP head	27.51	0.460	48.95	37.00
RH40 head	27.38	0.565	44.42	37.40
Water	26.85	22.975	22.975	72.80
TX165 head	27.70	0.33	50.20	35.84
PTFE	20.24	-	-	20.24
PMMA	41.28	-	7.28	41.28

3.2. Surface Tension of the Aqueous Solution of ELP, RH40, and ELP + RH40 Mixtures with Ber; Concentration and Composition of Mixed Monolayers at the Water-Air Interface

Taking into account the contribution of the Lifshitz–van der Waals intermolecular interactions in the surface tension of water, Ber, ELP, and RH40, it can be stated that reduction in water surface tension due to their adsorption at the W-A interface depend on only the decrease in the acid-base component of the water surface tension. The LW component of Ber, ELP, and RH40 surface tension is larger than that of water's surface tension. In the case of the ELP and RH40 tail surface tension, the LW component is only insignificantly larger than that for water (Table 1) [36]. As mentioned above, in Ber molecules, it is difficult to distinguish the tail and head. Therefore, Ber molecules adsorbed in the monolayer at the W-A interface should be oriented parallel to the interface. Hence, the minimal surface tension of the aqueous solution of Ber cannot be smaller than its surface tension (46.52 mN/m) (Table 1).

Assuming that only the surface tension of the ELP and RH40 tail determines the reduction in water surface tension, it can be stated that the minimal surface tension of the aqueous solution should be considerably smaller than that of the Ber aqueous solution. From the differences between the surface tension of Ber and the tail of ELP and RH40, it results that, if the mixed monolayer is formed at the W-A interface from the solution including ELP, RH40, and ELP + RH40 with Ber, the surface tension of the aqueous solution of these mixtures should be greater than that for the solution in the absence of Ber at the same concentrations of ELP, RH40 and ELP + RH40. Removal of the ELP or RH40 molecules from the mixed monolayer at the W-A interface by Ber molecules increases the solution surface tension. This suggestion is confirmed by the isotherms of the surface tension of the aqueous solution of ELP, RH40, and ELP + RH40 mixture in the presence and absence of Ber [22] (Figures 2–4). These isotherms have almost the same shape, and at a given temperature, there is almost a linear dependence between the surface tension of the solution and the logarithm of the surfactants or their mixture concentration. The isotherms of the surface tension of the aqueous solution of ELP, RH40, and ELP + RH40 mixture in the presence of Ber, similar to those in its absence [22], can be described by the exponential function of the second order (Figure S1):

$$\gamma_{LV} = y^0 + A_1 \exp\left(\frac{-C}{t_1}\right) + A_2 \exp\left(\frac{-C}{t_2}\right), \quad (35)$$

where A_1 , A_2 , t_1 , t_2 , and y^0 are constants.

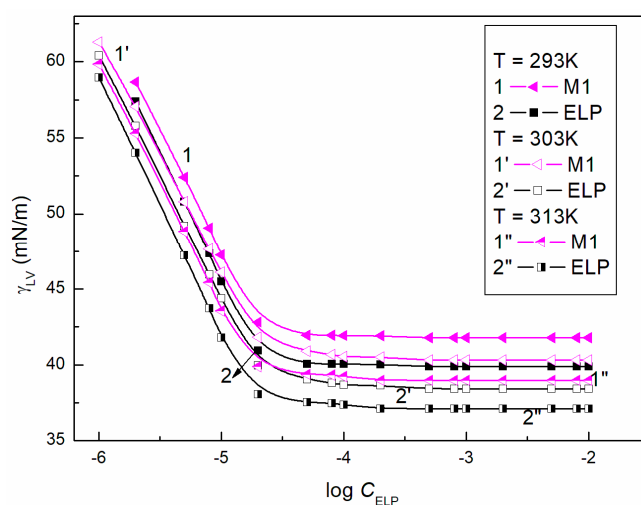


Figure 2. A plot of the surface tension (γ_{LV}) of M1 aqueous solutions (curves 1, 1' and 1'') and ELP aqueous solutions [22] (curves 2, 2' and 2'') vs. the logarithm of ELP concentration ($\log C_{ELP}$) at a constant temperature equal to 293 K (curves 1 and 2), 303 K (curves 1' and 2'), and 313 K (curves 1'' and 2'').

It was suggested earlier that the constants in Equation (35) are related to the components and parameters of the surface tension of all components of the solution, which are decisive for the interactions between these components [22]. It seems that the constant y^0 is related to the LW component of the surface tension of all compounds present in the solution and is close to the minimal surface tension of a given solution. This constant changes as a function of temperature almost linearly (Figure S2a). It is likely that the other constants in Equation (35) are closely related to the AB component of the surface tension of water and other compounds present in the aqueous solution. As a matter of fact, the changes in the hydration degree of the Ber, ELP, and RH40 molecules and the distance between these molecules and water can influence on the values of the A_1 , A_2 , t_1 , and t_2 constants. Presumably for these reasons, the changes in A_1 , A_2 , t_1 , and t_2 as a function of the temperature are more complicated than the y^0 constant (Figure S2). The LW components of the Ber, ELP, and RH40 tail surface tension as well as the degree of Ber, tail,

and head of ELP and RH40 molecule hydration, are decisive regarding the concentration and composition of the mixed monolayer at the W-A interface.

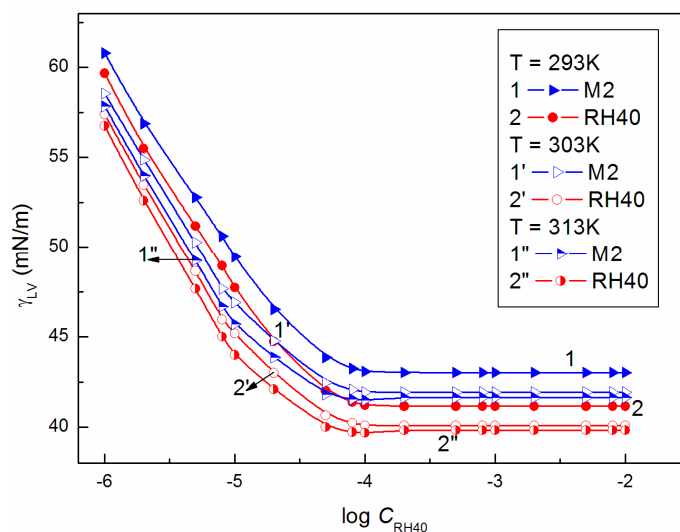


Figure 3. A plot of the surface tension (γ_{LV}) of M2 mixture aqueous solutions (curves 1, 1' and 1'') and RH40 aqueous solutions [22] (curves 2, 2' and 2'') vs. the logarithm of RH40 concentration ($\log C_{RH40}$) at a constant temperature equal to 293 K (curves 1 and 2), 303 K (curves 1' and 2'), and 313 K (curves 1'' and 2'').

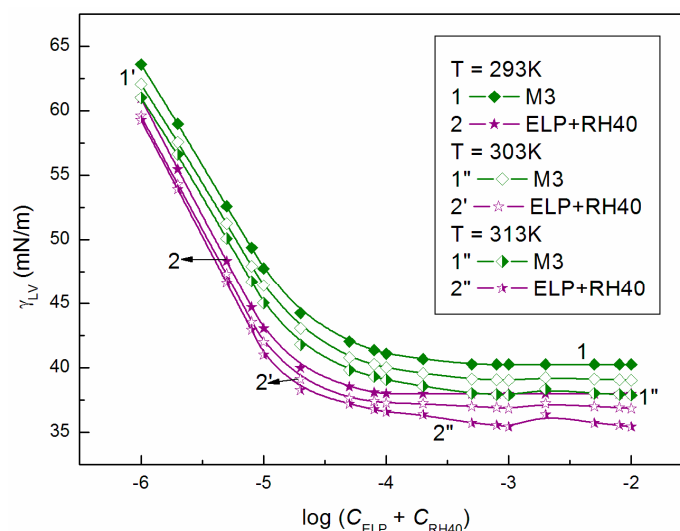


Figure 4. A plot of the surface tension (γ_{LV}) of M3 mixture aqueous solutions (curves 1, 1' and 1'') and ELP + RH40 mixture aqueous solutions at a mole fraction of ELP equal to 0.8 [22] (curves 2, 2' and 2'') vs. the logarithm of the sum of ELP and RH40 concentration ($\log (C_{ELP} + C_{RH40})$) at a constant temperature equal to 293 K (curves 1 and 2), 303 K (curves 1' and 2'), and 313 K (curves 1'' and 2'').

The concentration of a given component of the surfactant mixture and surfactant mixtures with additives can be indirectly determined, among other ways, using the Gibbs isotherm (Equation (4)) and Frumkin equation (Equation (5)). Unfortunately, in the studied concentration range, which corresponds to the saturated mixed monolayer at the W-A interface, it was possible to determine the maximal concentration of ELP, RH40, and ELP + RH40 mixture in the presence of Ber. It should be noted that the poor solubility of berberine in water will make it impossible to measure the surface tension of the aqueous solutions of the mixture of surfactant and Ber in a broad range of constant surfactant concentration. For this reason, the concentration of the particular surfactant in the single and mixed monolayers at the W-A

interface was determined using the Frumkin equation (Equation (5)). To solve this equation in the case of the mixtures, the contribution of their particular components to the reduction in the water surface tension must be known. It was found earlier that the composition of the mixed monolayer can be determined based on the γ_{LV} isotherm of the aqueous solution of the single components of the mixture [21,22]. If so, the reduction in the water surface tension by a given mixture component (π_i) can be calculated from Equation (6).

In many cases, it is possible to determine the composition of the binary and ternary mixtures of surfactants using the modified Rosen and Rubingh equations (Equations (8)–(10)) [27,29]. It is known that these equations can be used for the determination of the mole fraction of the mixed monolayer only in limited mixture compositions in the bulk phase. For this reason, it was possible to determine the composition of the mixed monolayer only at small concentrations of surfactants in the M1–M3 mixtures. It was proved that the composition of the mixed monolayer established in this way is close to that determined based on the γ_{LV} isotherm of the aqueous solutions of the individual mixture components. The mole fraction of particular components of the M1, M2, and M3 mixtures in the mixed monolayer at the W-A interface is considerably different from that in the bulk phase and depends on the temperature (Figures S3–S5). It is interesting that, at large concentrations of ELP, RH40, or the mixture of ELP + RH40, the mole fraction of Ber in the mixed monolayer is larger than in the bulk phase. This finding indicates that the Ber molecules likely adsorb at the W-A interface together with the surfactant ones. In this case, as a result of strong hydrophobic interactions between Ber and surfactant molecules, the Ber molecules in the mixed monolayer are not oriented parallel and toward the interface but perpendicularly or at a given angle to the interface. This orientation results in an increase in the Ber concentration in the mixed monolayer. In fact, if the berberine concentration in the mixed monolayer is larger than in the bulk phase, then the relation of the mole fraction of surfactants in these phase is reversed. The relation of the composition of the mixed monolayer, including ELP, RH40, and Ber, to that in the bulk phase is slightly different from that for the solutions of mixture M3. In the whole concentration range, the mole fraction of RH40 in the mixed monolayer is larger than in the bulk phase. This relation is consistent with the results for the ELP and RH40 mixture in the absence of Ber [22].

Taking into account the mole fraction of particular mixture components in the mixed monolayer at the W-A interface, the contribution of these components to the reduction in water surface tension was determined using Equation (6). Next, using the Frumkin equation, the concentration of the mixture components in the surface region was calculated. The concentration of the particular components in the mixed monolayer at the W-A interface for all studied mixtures is smaller than those of the individual components in the absence of others (Figures S6–S8). Moreover, the sum of the concentrations of Ber and the surfactant or of Ber and the ELP + RH40 mixture in the mixed surface monolayer is smaller than that of the surfactant or surfactants mixture in the absence of Ber (Figures S6–S8). What causes these phenomena? It is possible, as mentioned above, that the Ber molecules adsorb together with the surfactant ones. The berberine molecules can join the tail of surfactant molecules, decreasing the extent of hydration. As a consequence, a complex of surfactant-Ber is formed with a smaller tendency to adsorb at the W-A interface than the single molecule of ELP or RH40. On the other hand, the adsorbed berberine molecule + surfactant tail complex in the mixed monolayer can be directed toward the water phase, changing its surface tension. Due to the Ber molecule's structure, it has a positive charge; hence, repulsive electrostatic interactions between the Ber + surfactant tail complexes can appear. These interactions can reduce the packing of the mixed monolayer, decreasing the concentration of surfactant in comparison to its concentration in the absence of Ber.

3.3. CMC of ELP + Ber, RH40 + Ber and ELP + RH40 + Ber Mixtures

The ability of surfactants to form aggregates in aqueous solution is one of their characteristic and a very important property. The micellar phase plays a very important role, among others, because of its solubilization properties. We were interested in whether Ber is

present in the micelles formed by ELP, RH40, and their mixture. To consider this problem, it was first necessary to determine the CMC and the composition of the mixed micelles. In the literature, there are many methods for CMC determination, for example, based on the isotherms of the surface tension, density, and conductivity and using spectroscopic methods. Formation of micelles in aqueous media is reflected by the inflection point appearing on these isotherms [29]. However, it should be remembered that each method can be sensitive to a different size and shape of aggregates formed by surfactants. The CMC values of surfactant + Ber mixtures (M1–M3) determined from the γ_{LV} isotherms (Figures 2–4), as well as conductivity (Figure 5), density (Figure 6) measurements, and fluorescence emission spectra (Figures 7 and 8 as an example), are different even for the same mixture (Table 2). The CMC values of the surfactants or their mixture in the presence of Ber are higher than those in its absence.

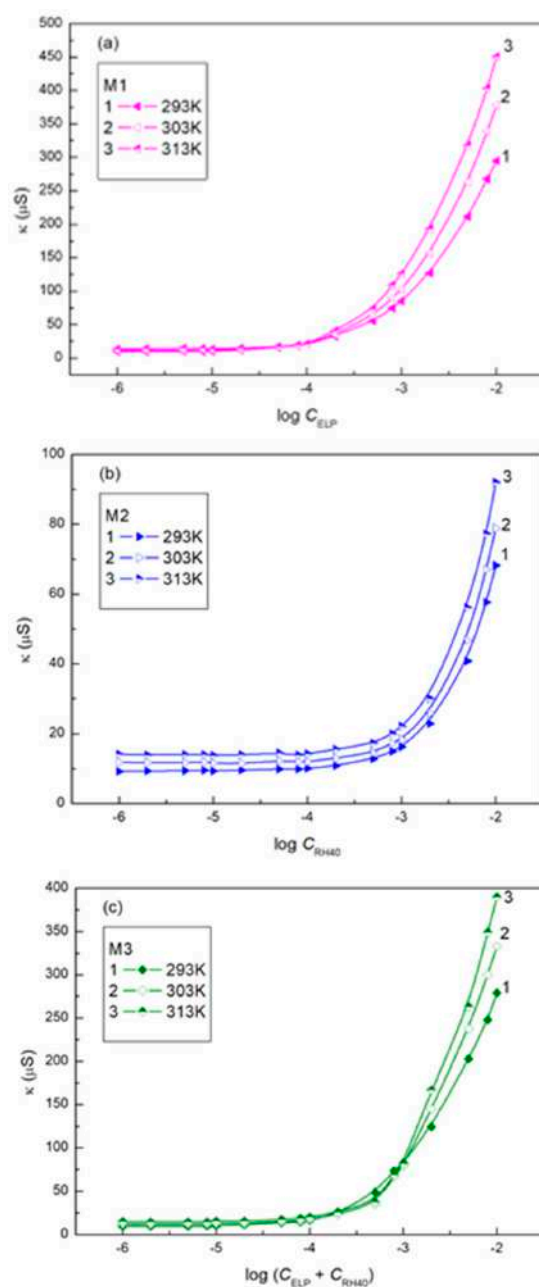


Figure 5. A plot of the specific conductivity (κ) of mixtures M1 (a), M2 (b), and M3 (c) vs. the logarithm of the surfactant or their mixture concentrations at a constant temperature equal to 293 K (curve 1), 303 K (curve 2) and 313 K (curve 3).

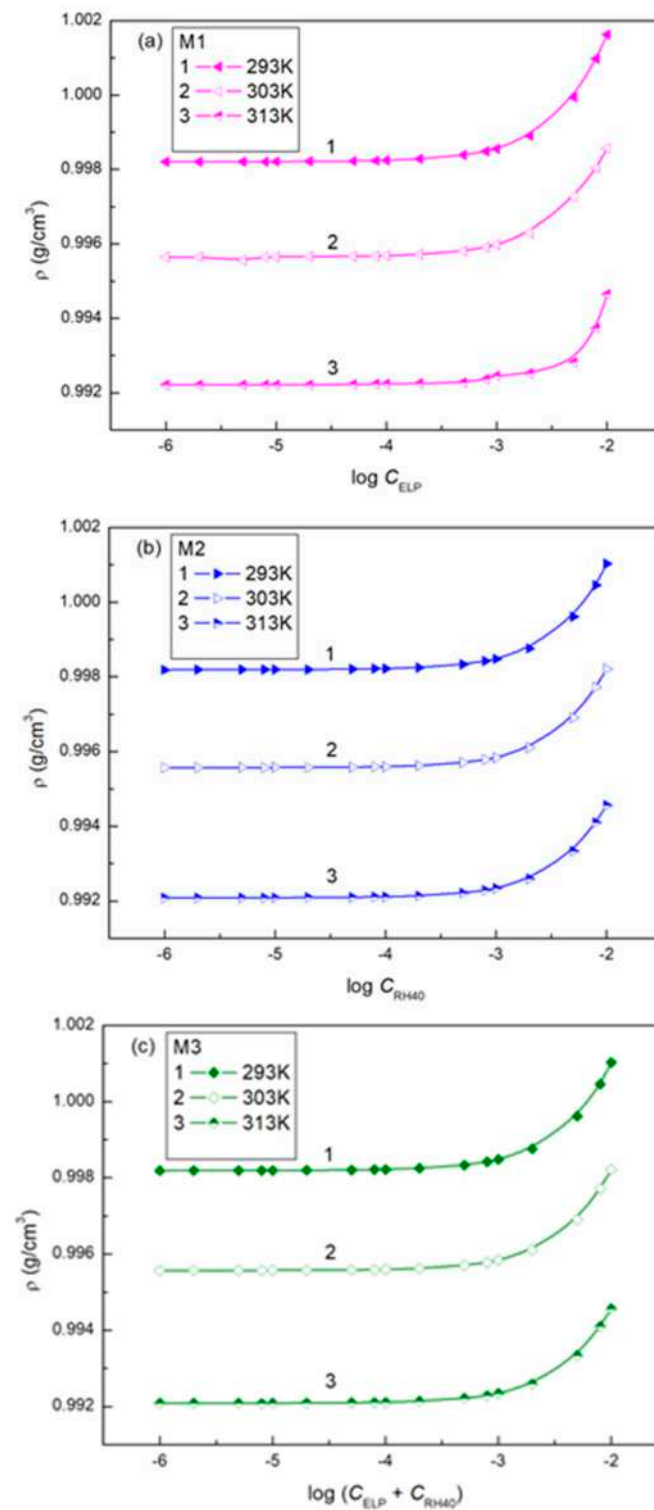


Figure 6. A plot of the density (ρ) of mixtures M1 (a), M2 (b) and M3 (c) vs. the logarithm of the surfactant or their mixture concentration at a constant temperature equal to 293 K (curve 1), 303 K (curve 2), and 313 K (curve 3).

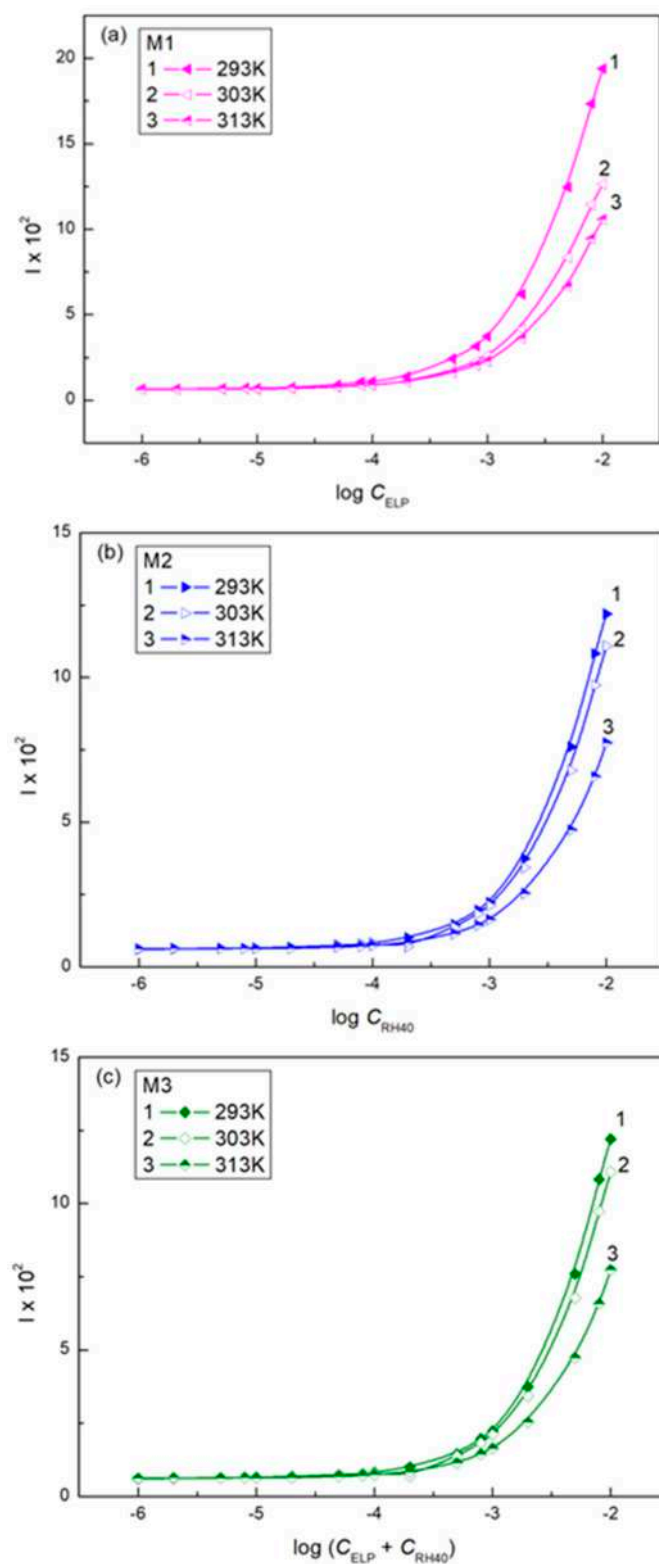


Figure 7. A plot of the fluorescence intensity (I) of mixtures M1 (a), M2 (b), and M3 (c) vs. the logarithm of the surfactant or their mixture concentration at a constant temperature equal to 293 K (curve 1), 303 K (curve 2), and 313 K (curve 3).

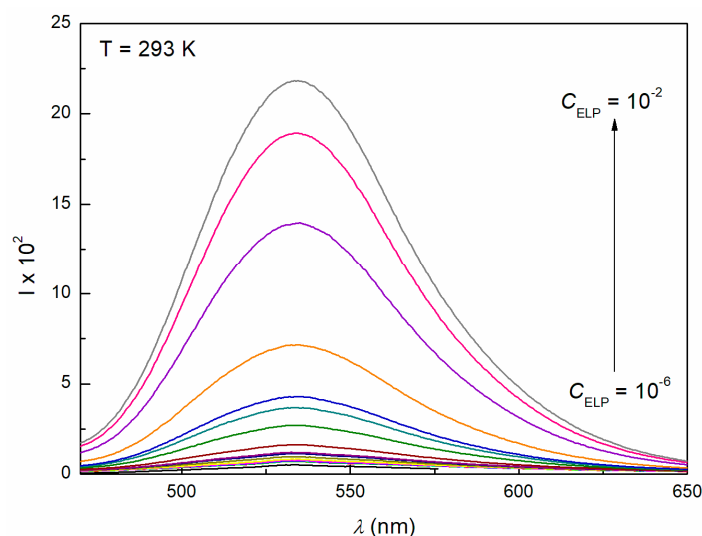


Figure 8. Fluorescence emission spectra of mixture M1 at $T = 293$ K.

Table 2. The values of the CMC (mol/dm^3) of the aqueous solutions M1, M2, and M3 mixtures as, well as ELP, RH40 and their mixture at $T = 293, 303,$ and 313 K, determined from the surface tension isotherms ($\gamma_{LV} = f(\log C)$), conductivity ($\kappa = f(1/C)$), and density ($\rho = f(1/C)$) measurements, as well as fluorescence emission spectra ($I = f(1/C)$). The values of CMC for ELP, RH40, and their mixture, determined from surface tension measurements, are taken from Ref. [22].

	T (K)	CMC from γ_{LV}	CMC from κ	CMC from ρ	CMC from I
ELP + Ber (M1)	293	2.11×10^{-5}	3.87×10^{-4}	5.92×10^{-4}	
	303	2.78×10^{-5}	4.02×10^{-4}	5.40×10^{-4}	
	313	2.72×10^{-5}	4.67×10^{-4}	5.05×10^{-4}	
ELP	293	2.14×10^{-5}		5.13×10^{-4}	6.03×10^{-4}
	303	2.03×10^{-5}		7.78×10^{-4}	4.16×10^{-4}
	313	1.91×10^{-5}		5.32×10^{-4}	3.71×10^{-4}
RH40 + Ber (M2)	293	4.24×10^{-5}	7.31×10^{-4}	4.97×10^{-4}	
	303	5.62×10^{-5}	7.70×10^{-4}	4.67×10^{-4}	
	313	5.05×10^{-5}	4.46×10^{-4}	4.16×10^{-4}	
RH40	293	6.64×10^{-5}		6.03×10^{-4}	4.97×10^{-4}
	303	2.50×10^{-5}		5.77×10^{-4}	4.67×10^{-4}
	313	2.12×10^{-5}		5.22×10^{-4}	4.42×10^{-4}
ELP + RH40 + Ber (M3)	293	3.13×10^{-5}	3.81×10^{-4}	4.74×10^{-4}	
	303	2.81×10^{-5}	4.23×10^{-4}	4.33×10^{-4}	
	313	2.80×10^{-5}	4.74×10^{-4}	4.16×10^{-4}	
ELP + RH40	293	1.92×10^{-5}		8.76×10^{-4}	4.89×10^{-4}
	303	1.84×10^{-5}		7.21×10^{-4}	4.40×10^{-4}
	313	1.70×10^{-5}		7.03×10^{-4}	3.90×10^{-4}

Formation of micelles in aqueous solution by surfactants at their given concentrations is due to hydrophobic interactions between the tails of surfactants through the water phase. The values of these interactions are positive, in contrast to the interactions of the surfactant head, which are negative independent of whether micelles are formed by nonionic or ionic

surfactants. According to Equations (30) and (31) [31,32], the power of the hydrophobic interactions depends on the tail-water interface tension and the contactable area of the tail. The interface tension can be calculated from, among others, the van Oss et al. [18–20] concept. From this concept it follows:

$$\gamma_{ij} = \gamma_i + \gamma_j - 2 \left(\sqrt{\gamma_i^{LW} \gamma_j^{LW}} + \sqrt{\gamma_i^+ \gamma_j^-} + \sqrt{\gamma_i^- \gamma_j^+} \right), \quad (36)$$

If the surface tension of at least one of the phases being in contact results from only the LW intermolecular interactions, then Equation (36) takes the following form:

$$\gamma_{ij} = \gamma_i + \gamma_j - 2 \sqrt{\gamma_i^{LW} \gamma_j^{LW}}, \quad (37)$$

Taking into account Equations (36) and (37) the components and parameters of berberine, water, and surfactant tail surface tension (Table 1), the values of the water tails of surfactants, water-Ber, and Ber-surfactant tail interface tension were calculated. The obtained values of the water-surfactant tail, water-Ber, and Ber-surfactant tail interface tension are close to 46.0, 6.0, and 10.7 mN/m, respectively. Based on these values, it was possible to determine the adhesion work of the surfactant tail to the surfactant tail, the surfactant tail to Ber, and Ber to the surfactant tail through the water phase. The adhesion work of the surfactant tail to the surfactant tail through the water phase is equal to $2\gamma_{WT} = 92 \text{ mJ/m}^2$ and that of Ber to Ber through the water phase to $\gamma_{WB} = 12 \text{ mJ/m}^2$. In the case of the Ber-water-surfactant tail system, the adhesion work (W_a^{BT}) was calculated from the following equation [25]:

$$W_a^{BT} = \gamma_{WT} + \gamma_{WB} - \gamma_{BT}, \quad (38)$$

The value of W_a^{BT} calculated from Equation (38) is equal to 41.3 mJ/m^2 .

As the surfactant head-water interface tension of both surfactants is negative and close to -18 mJ/m^2 , their total adhesion work through the water phase is close to 56 mJ/m^2 . Thus, there is not a large difference in the tendency to contact the surfactant with the surfactant molecule and the surfactant with the Ber molecule through the water phase. However, the probability of the binding of Ber+ surfactant complexes through the water phase is smaller than that of surfactant molecules. Presumably for this reason, the CMC of ELP, RH40, and ELP + RH40 mixtures is higher in the presence of Ber than in its absence (Table 2). Based on these facts, it can be assumed that the micellization process of the surfactant mixture occurs as a result of connecting not only surfactant molecules but also surfactants with Ber molecules. Thus, it seems that the presence of Ber in the micelles of ELP, RH40, and their mixture is not due to the adsorption of Ber molecules on the micelles and its penetration into the micelles but rather by common aggregation. For mixed micelles of ELP + Ber (M1) and RH40 + Ber (M2), it is difficult to determine the mole fraction of surfactant and Ber in the micelles based on their CMC values. This possibility was based on the modified concept of Hua and Rosen (Equations (10)–(12)) [27,29]. The calculated mole fractions of ELP, RH40, and Ber showed that the mole fraction of Ber does not differ significantly from 0.5. This outcome indicated that the interactions of berberine + surfactant complexes through the water phase play a major role in the aggregation process. Indeed, the mole fraction of particular components of ELP + RH40 + Ber mixtures (M3) changes to a small extent as a function of temperature (Table 3). The change in the mole fractions of the mixture components, as well as the CMC value itself as a function of temperature, results, on the one hand, from the change in kinetic energy and, on the other hand, from the change in hydration degree, especially of the surfactant heads. A change in the configuration of the surfactant molecules can also have an effect.

Table 3. The values of the fraction of area occupied by a component in the micelles in mixture M3 (x^M), intermolecular interactions parameters for mixed micelle (β^M), activity coefficient (f^M), and the excess Gibbs energy of micelle formation per mole of the surfactant mixture (G^M) calculated from the Rosen and Hua concept (Equations (10)–(12), (24), (25) and (27)) at $T = 293, 303,$ and 313 K (1—ELP, 2—RH40, 3—Ber).

	$T = 293$ K	$T = 303$ K	$T = 313$ K
CMC	3.13×10^{-5}	2.81×10^{-5}	2.80×10^{-5}
C_1	2.50×10^{-5}	2.25×10^{-5}	2.24×10^{-5}
C_2	6.26×10^{-6}	5.63×10^{-6}	5.60×10^{-6}
C_3	1×10^{-4}	1×10^{-4}	1×10^{-4}
γ CMC	40.27	39.17	37.92
x_1^M	0.3954	0.4568	0.4508
x_2^M	0.2313	0.0418	0.0024
x_3^M	0.3733	0.5014	0.5467
$\beta_{(13)-2}^M$	−5.0834	0.3762	1.0993
$\beta_{(23)-1}^M$	−0.4159	−1.5256	−1.1598
f_{13}^M	0.7619	1.0007	1.0007
f_2^M	0.0496	1.4125	2.8469
f_{23}^M	0.9371	0.7273	0.7900
f_1^M	0.8590	0.6376	0.7048
$G_{(13)-2}^M$	−2.2018	0.0380	0.0682
$G_{(23)-1}^M$	−0.2422	−0.9536	−0.7472

The influence of these factors on the composition and size of micelles should be reflected in the parameter of intermolecular interactions. This parameter can be determined, among other ways, from Equation (27) [27,29]. Since Ber does not form micelles on its own, it was not possible to determine the interactions parameter between Ber and surfactants molecules in the micelles formed in the ELP + Ber and RH40 + Ber systems (M1 and M2). Considering the complexes of ELP + Ber and RH40 + Ber as individual compounds, it was possible to determine the interactions parameter (β^M) of Ber with ELP and RH40 in the mixed micelles of mixture M3 using the Hua and Rosen equation (Equation (27)). As follows from Table 3, the β^M parameter, calculated based on CMC determined from the surface tension measurements, is negative for the RH40 + Ber complex at each temperature but for ELP + Ber complex only at $T = 293$ K. A similar situation can be observed for the values of the excess Gibbs energy of micelle formation per mole of the surfactant mixture (G^M). In fact, the values of β^M depend on the temperature for both complexes. The negative β^M parameter suggests that there is synergism in the CMC. Unfortunately, this suggestion cannot be confirmed by the second condition for the existence of synergy for the abovementioned reason. It should also be noted that the values of the activity coefficient of ELP in the mixed micelles (Table 3) decrease, but for RH40, they increase with the T increase.

3.4. Thermodynamic Parameters of the Adsorption and Micellization

The standard Gibbs free energy, standard enthalpy, and entropy are useful to determine the tendency of the surfactants to adsorb at different interfaces and to form micelles, as well as the reason for this tendency. In the literature, there are many different methods used to determine the standard Gibbs free energy of adsorption (ΔG_{ads}^0) and micellization (ΔG_{mic}^0), the standard enthalpy of adsorption (ΔH_{ads}^0) and micellization (ΔH_{mic}^0), and the

standard entropy of adsorption (ΔS_{ads}^0) and micellization (ΔS_{mic}^0) of the single compounds. Regarding cases in which the mixed monolayer at the interfaces and mixed micelles is formed, it is difficult to find in the literature methods strictly connected with thermodynamics rules. Therefore, the criteria that should be fulfilled to calculate the real values of the thermodynamic parameters of adsorption and micellization are presented above. Unfortunately, it was impossible to determine the activity coefficients of the components in the mixed monolayer at the W-A interface based on the Hua and Rosen concept. Therefore, the ΔG_{ads}^0 values for Ber, ELP, and RH40 in the M1-M3 mixture was calculated from Equation (18), assuming the activity coefficients to be close to unity. The obtained results showed that, in the range of surfactants concentration at which they are present in the solution in the monomeric form, the ΔG_{ads}^0 values are almost constant (Table 4). At the surfactants concentration higher than CMC the ΔG_{ads}^0 values increase as a function of concentration. However, it should be mentioned that the surfactant molecules adsorb at the water-air interface only in the monomeric form. At surfactant concentrations higher than the CMC, their concentration in the monomeric form is constant. For this reason, the ΔG_{ads}^0 values are not real.

Table 4. Thermodynamic parameters of the adsorption process of ELP, RH40 and Ber (kJ/mol).

	T = 293 K			T = 303 K			T = 313 K		
	ΔG_{ads}^0	ΔH_{ads}^0	$T\Delta S_{ads}^0$	ΔG_{ads}^0	ΔH_{ads}^0	$T\Delta S_{ads}^0$	ΔG_{ads}^0	ΔH_{ads}^0	$T\Delta S_{ads}^0$
ELP	-46.91	-1.64	45.27	-47.97	-1.16	46.81	-50.00	-1.64	48.36
ELP from M1	-44.62	-0.23	44.39	-46.16	-0.26	45.90	-47.65	-0.23	47.42
ELP from M3	-43.64	2.65	46.29	-45.25	2.62	47.87	-46.80	2.65	49.45
RH40	-48.12	4.62	52.74	-50.11	4.43	54.54	-51.72	4.62	56.34
RH40 from M2	-45.69	2.54	48.23	-47.57	2.30	49.87	-48.98	2.54	51.52
RH40 from M3	-44.45	-8.85	35.6	-45.72	-8.91	36.81	46.88	84.91	38.03
Ber	-32.00	-1.97	30.03	-33.10	-2.04	31.06	-34.05	-1.97	32.08
Ber from M1	-31.63	-1.89	29.74	-32.62	-1.87	30.75	-43.66	-11.89	31.77
Ber from M2	-31.42	-3.15	28.27	-32.32	-3.08	29.24	-33.45	-3.25	30.20
Ber from M3	-31.02	-1.28	29.74	-32.02	-1.27	30.75	-32.95	-1.18	31.77

To compare the ΔG_{ads}^0 values obtained from Equation (18) to those determined using other methods, the calculations of ΔG_{ads}^0 were performed using the Langmuir equation modified by de Boer [29,43]. This equation has the following form:

$$\frac{A_i^0}{A_i - A_i^0} \exp \frac{A_i^0}{A_i - A_i^0} = \frac{C_i}{\omega} \exp \left(\frac{-\Delta G_{ads,i}^0}{RT} \right), \quad (39)$$

where A_i and A_i^0 are the areas occupied by one molecule of the i -th component of the mixture in the mixed monolayer and the limiting one.

The ΔG_{ads}^0 values calculated from Equation (39) based on the concentration of particular components in the mixed monolayer at the W-A interface, determined from the Frumkin equation (Figure S9) in the range of surfactant concentrations smaller than CMC, are similar to those obtained from Equation (18) (Table 4, Figures S9–S11). From the obtained ΔG_{ads}^0 values, it can be stated that the Ber presence decreases the ELP and RH40 tendency to adsorb at the W-A interface. This outcome confirms our suggestion that the surfactant + Ber molecule complexes can be adsorbed at this interface. As mentioned above, there are some differences in the hydration degree of the molecule complexes in comparison to the individual ones. In such cases, there is also a reduction in the difference between the tail-water and tail-air interface tension, which according to Equation (28) decreases ΔG_{ads}^0 . The standard

enthalpy of adsorption of particular components of the studied mixtures, determined based on Equations (20) and (21) in most cases, has a small absolute value except for the standard enthalpy value for RH40 adsorption at the W-A interface from the aqueous solution of mixture M3 (Table 4). The small absolute values of ΔH_{ads}^0 indicate that our suggestion about the adsorption of surfactant + berberine complexes is the most probable.

In many cases, the absolute values of the standard enthalpy of micellization are greater than those of the standard enthalpy of adsorption (Tables 4 and 5). In most studied systems, the ΔH_{mic}^0 is positive, indicating that some bonds are broken during the micellization process. In fact, it should refer to hydrogen bonds. There are some differences between the behavior of ELP and RH40. In solutions including RH40, the greatest changes of the standard enthalpy are observed in both adsorption and micellization processes compared to in the absence of RH40.

Table 5. Thermodynamic parameters of the micellization process of ELP, RH40, and Ber (kJ/mol).

	T = 293 K			T = 303 K			T = 313 K		
	ΔG_{mic}^0	ΔH_{mic}^0	$T\Delta S_{mic}^0$	ΔG_{mic}^0	ΔH_{mic}^0	$T\Delta S_{mic}^0$	ΔG_{mic}^0	ΔH_{mic}^0	$T\Delta S_{mic}^0$
ELP	−35.97	4.17	40.14	−37.33	4.18	41.51	−38.71	4.17	42.88
ELP from ELP + RH40	−35.81	6.68	42.49	−37.33	6.61	43.94	−38.71	6.68	45.39
ELP from M3	−32.96	1.47	34.43	−33.96	1.64	35.60	−35.31	1.47	36.78
RH40	−33.21	8.98	42.19	−36.80	6.83	43.63	−38.44	6.63	45.07
RH40 from RH40 + ELP	−36.19	−3.23	32.96	−36.80	−2.71	34.09	−38.44	−3.23	35.21
RH40 from M3	−31.28	16.92	48.20	39.88	89.72	49.84	−43.71	7.78	51.49
Ber from M3	−29.15	4.55	33.70	−31.57	3.28	34.85	−32.72	3.28	36.00

4. Materials and Methods

Kolliphor® ELP (ELP) (Cremophor® ELP, Polyoxyl 35 hydrogenated castor oil, polyoxyl-35 castor oil), Kolliphor® RH 40 (RH40) (Cremophor® RH 40, macrogolglycerol hydroxystearate, PEG-40 castor oil, polyoxyl 40 hydrogenated castor oil) (Sigma-Aldrich (St. Louis, MO, USA) and berberine chloride (Ber) (Alfa Aesar, Kandel, Germany) were used without further purification. The doubly distilled and deionized water used for the preparation of the aqueous solutions of ELP + Ber (M1), RH40 + Ber (M2), and ELP + RH40 + Ber mixture (M3, the mole fraction of ELP (α) in the bulk phase equal to 0.8) was obtained from a Destamat Bi18E distiller (Inkom Instruments, Warsaw, Poland). The surfactant solution concentration was from 1×10^{-6} to 1×10^{-2} mol/dm³, and the Ber concentration in the surfactant solutions was equal to 1×10^{-4} mol/dm³. Because Ber is poorly soluble in water, it was introduced into the aqueous solutions in the form of an ethanolic solution, similar to other research [44–46]. The concentration of ethanol in the aqueous solution was constant and equal to 1×10^{-3} mol/dm³.

The surface tension (γ_{LV}) measurements of the aqueous solutions of the M1, M2, and M3 mixtures were performed at temperatures of 293, 303, and 313 K using a Krüss K100 tensiometer (Krüss, Hamgurg, Germany), which was calibrated before the measurements, according to the platinum ring tensiometer method (du Nouy's method). The calibration was performed at 293 K using water and methanol, the surface tension values of which at this temperature were equal to 72.8 and 22.5 mN/m, respectively. The surface tension measurements for each concentration and composition of the studied solutions were repeated at least ten times. The standard deviation of the results obtained from the measurements was ± 0.1 mN/m, and the uncertainty was in the range of 0.3% to 0.9%.

Measurements of the advancing contact angle (θ) were performed using the sessile drop method with a DSA30 measuring system (Krüss, Germany) in a temperature-controlled chamber. For θ measurements on pressed Ber water (Destamat Bi18E), for-

mamide (>99.5%, Sigma-Aldrich (St. Louis, MO, USA) and diiodomethane (>99%, Sigma-Aldrich, St. Louis, MO, USA) were used. As previous studies showed, the value of the contact angle depends on the difference between the interface pressure and the hydrostatic pressure of the drop [47]. Therefore, in the contact angle measurements, the droplet sizes were different for diiodomethane, formamide, and water and equaled 4, 5, and 6 cm³, respectively. Ten drops for each studied system were used, and the standard deviation was in the range of 1 to 1.5°.

The conductivity measurements were performed using a Mettler Toledo™ Seven Multi with accuracy of ±0.5%.

The density of the studied solutions was measured with a U-tube densitometer (DMA 5000 Anton Paar). The precision of the density and temperature measurements given by the manufacturer is ±0.000005 g cm⁻³ and ±0.001 K. The uncertainty was calculated to be 0.01%. The densitometer was calibrated regularly with distilled and deionized water.

Steady-state fluorescence measurements were performed using a Hitachi F-2700 Fluorescence spectrometer. Fluorescence excitation was determined at 450 nm, and the emission spectra were recorded in the range of 350–650 nm at a scan speed of 300 nm/min. The excitation and emission slit widths were 2.5 nm.

5. Conclusions

The measurements and discussion of the obtained results based on the thermodynamic rules allow for drawing interesting conclusions. Berberine (Ber) is a bipolar compound, and its surface tension results from the Lifshitz–van der Waals and acid-base components. However, the contribution of the Lifshitz–van der Waals component is considerably larger than that of the acid-base one, indicating that Ber has poor solubility in water. In turn, the electron-acceptor-parameter of the acid-base component is considerably smaller than that of the electron-donor one.

Berberine reduces the water surface tension to a small extent, and its maximal Gibbs surface excess concentration is considerably smaller than those of ELP and RH40.

The minimal area occupied by one Ber molecule is close to its contactable area at a parallel orientation toward the water-air interface.

The components and parameters of the ELP and RH40 surface tension at the orientation of their molecules towards the air phase can be determined from their contact angle on the PTFE and PMMA surfaces. These components and parameters are similar to those of the TX165 surface tension at its orientation by the hydrophilic part towards the air phase.

The molecules of ELP and RH40 adsorbed at the water-air interface reduced only the LW component of the water surface tension.

The contribution of oxyethylene groups to the surface tension of ELP and RH40 is similar to that of Triton X-165.

The surface tension isotherm of the aqueous solution of Ber mixture with ELP, RH40, and ELP + RH40 can be described by the exponential function of the second order.

The LW components of the Ber, ELP, and RH40 tail surface tension, as well as the hydration degree of Ber molecules and the tail and head of ELP and RH40 molecules, are decisive regarding the concentration and composition of the mixed monolayer at the W-A interface.

The composition of the mixed monolayer at the W-A interface, determined based on the surface tension isotherm of aqueous solutions of Ber, ELP, and RH40, is close to that obtained from the Rosen and Rubingh equations. This composition allows for determining the surface concentration of particular components in the mixed monolayer, as well as their concentrations in the mixed monolayer at the W-A interface using the Frumkin equation.

At large concentrations of ELP, RH40, or the mixture of ELP + RH40, the mole fraction of Ber in the mixed monolayer is larger than in the bulk phase.

The concentration of the particular components in the mixed monolayer at the W-A interface for all studied mixtures is smaller than those of the individual components in the absence others.

The sum of the concentrations of Ber and the surfactant or of Ber and the ELP + RH40 mixture in the mixed surface monolayer is smaller than that of the surfactant or surfactant mixture in the absence of Ber.

The CMC values of the surfactant + Ber mixtures, determined from the surface tension isotherms, conductivity, density, and fluorescence emission spectroscopy, are different even for the same mixture.

The concentration of Ber in the mixed micelles is higher than in the bulk phase. This outcome indicates that the tendency of Ber toward solubilization in the micelles of ELP, RH40, and ELP + RH40 is greater than its tendency to adsorb at the water-air interface.

Using our thermodynamic considerations and the Hua and Rosen concept, it was possible to determine the standard thermodynamic parameters of adsorption and aggregation.

Supplementary Materials: The following supporting information can be downloaded at: <https://www.mdpi.com/article/10.3390/molecules28073115/s1>, Figure S1: A plot of the surface tension (γ_{LV}) of M1 (a), M2 (b), and M3 (c) aqueous solutions vs. the logarithms of ELP ($\log C_{ELP}$) and RH40 ($\log C_{RH40}$) and that of the sum of their concentrations ($\log(C_{ELP} + C_{RH40})$) at $T = 293$ K, 303 K, and 313 K. Figure S2: A plot of the constant y^0 (a), A_1 (b), A_2 (c), t_1 (d), and t_2 (e) in Equation (35) vs. the temperature (T). Figure S3: A plot of the mole fraction of ELP and Ber in M1 in the surface layer and in the bulk phase vs. the logarithm of ELP concentration ($\log C_{ELP}$) at $T = 293$ K, 303 K, and 313 K. Figure S4: A plot of the mole fraction of RH40 and Ber in M2 in the surface layer and in the bulk phase vs. the logarithm of RH40 concentration ($\log C_{RH40}$) at $T = 293$ K, 303 K, and 313 K. Figure S5: A plot of the mole fraction of ELP, RH40, and Ber in M3 in the surface layer and in the bulk phase vs. the logarithm of the sum of ELP and RH40 concentrations ($\log(C_{ELP} + C_{RH40})$) at $T = 293$ K, 303 K, and 313 K. Figure S6: A plot of the surface concentration (Γ) calculated from Equation (5) vs. the logarithm of ELP concentration ($\log C_{ELP}$) at $T = 293$ K, 303 K, and 313 K. Figure S7: A plot of the surface concentration (Γ) calculated from Equation (5) vs. the logarithm of RH40 concentration ($\log C_{RH40}$) at $T = 293$ K, 303 K, and 313 K. Figure S8: A plot of the surface concentration (Γ) of the M3 mixture components calculated from Equation (5) vs. the logarithm of the sum of ELP and RH40 concentrations ($\log(C_{ELP} + C_{RH40})$) at $T = 293$ K, 303 K, and 313 K. Figure S9: A plot of the Gibbs standard free energy of adsorption (ΔG_{ads}^0) calculated from Equation (39) vs. the logarithm of ELP concentration ($\log C_{ELP}$) at $T = 293$ K, 303 K, and 313 K. Figure S10: A plot of the Gibbs standard free energy of adsorption (ΔG_{ads}^0) calculated from Equation (39) vs. the logarithm of RH40 concentration ($\log C_{RH40}$) at $T = 293$ K, 303 K, and 313 K. Figure S11: A plot of the Gibbs standard free energy of adsorption (ΔG_{ads}^0) of the M3 mixture components calculated from Equation (39) vs. the logarithm of the sum of ELP and RH40 concentrations ($\log(C_{ELP} + C_{RH40})$) at $T = 293$ K, 303 K and 313 K.

Author Contributions: Conceptualization, M.S., K.S., A.Z. and B.J.; methodology, M.S. and K.S.; software, K.S.; validation, K.S., A.Z. and B.J.; formal analysis, K.S., A.Z. and B.J.; investigation, M.S. and K.S.; resources, K.S.; data curation, K.S., A.Z. and B.J.; writing—original draft preparation, K.S., A.Z. and B.J.; writing—review and editing, K.S., A.Z. and B.J.; visualization, K.S., A.Z. and B.J.; supervision, B.J.; project administration, K.S., A.Z. and B.J.; funding acquisition, B.J. All authors have read and agreed to the published version of the manuscript.

Funding: This research received no external funding.

Institutional Review Board Statement: Not applicable.

Informed Consent Statement: Not applicable.

Data Availability Statement: The data presented in this study are available in Supplementary Materials.

Conflicts of Interest: The authors declare no conflict of interest.

Sample Availability: Samples of the compounds are not available from the authors.

References

1. Zhang, X.; Dai, K.; Liu, C.; Hu, H.; Luo, F.; Qi, Q.; Wang, L.; Ye, F.; Jin, J.; Tang, J.; et al. Berberine-coated biomimetic composite microspheres for simultaneously hemostatic and antibacterial performance. *Polymers* **2021**, *13*, 360.
2. Patel, P. A bird's eye view on a therapeutically 'wonder molecule': Berberine. *Phytomed. Plus* **2021**, *1*, 100070. [[CrossRef](#)]

3. Pang, B.; Zhao, L.H.; Zhou, Q.; Zhao, T.Y.; Wang, H.; Gu, C.J.; Tong, X.-L. Application of berberine on treating type 2 diabetes mellitus. *Int. J. Endocrinol.* **2015**, *2015*, 905749. [[CrossRef](#)]
4. Xue, M.; Yang, M.-X.; Zhang, W.; Li, X.-M.; Gao, D.-H.; Ou, Z.-M.; Li, Z.-P.; Liu, S.-H.; Li, X.-J.; Yang, S.-Y. Characterization, pharmacokinetics, and hypoglycemic effect of berberine loaded solid lipid nanoparticles. *Int. J. Nanomed.* **2013**, *8*, 4677–4687. [[CrossRef](#)] [[PubMed](#)]
5. Younis, F.A.; Saleh, S.R.; Abd El-Rahman, S.S.; Newairy, A.-S.A.; El-Demellawy, M.A.; Ghareeb, D.A. Preparation, physicochemical characterization, and bioactivity evaluation of berberine-entrapped albumin nanoparticles. *Sci. Rep.* **2022**, *12*, 17431. [[CrossRef](#)]
6. Wang, L.; Ye, X.; Hua, Y.; Song, Y. Berberine alleviates adipose tissue fibrosis by inducing AMP-activated kinase signaling in high-fat diet-induced obese mice. *Biomed. Pharmacother.* **2018**, *105*, 121–129. [[CrossRef](#)]
7. Lee, Y.S.; Kim, W.S.; Kim, K.H.; Yoon, M.J.; Cho, H.J.; Shen, Y.; Ye, J.-M.; Lee, C.H.; Oh, W.K.; Kim, C.H.; et al. Berberine, a natural plant product, activates AMP-activated protein kinase with beneficial metabolic effects in diabetic and insulin resistant states. *Diabetes* **2006**, *55*, 2256–2264. [[CrossRef](#)]
8. Zhang, Y.; Li, X.; Zou, D.; Liu, W.; Yang, J.; Zhu, N.; Huo, L.; Wang, M.; Hong, J.; Wu, P.; et al. Treatment of type 2 diabetes and dyslipidemia with the natural plant alkaloid berberine. *J. Clin. Endocrinol. Metab.* **2008**, *93*, 2559–2565. [[CrossRef](#)]
9. Pirillo, A.; Catapano, A.L. Berberine, a plant alkaloid with lipid- and glucoselowering properties: From in vitro evidence to clinical studies. *Atherosclerosis* **2015**, *243*, 449–461. [[CrossRef](#)]
10. Wang, Y.; Huang, Y.; Lam, K.S.; Li, Y.; Wong, W.T.; Ye, H.; Lau, C.W.; Vanhoutte, P.M.; Xu, A. Berberine prevents hyperglycemia-induced endothelial injury and enhances vasodilatation via adenosine monophosphate-activated protein kinase and endothelial nitric oxide synthase. *Cardiovasc. Res.* **2009**, *82*, 484–492. [[CrossRef](#)]
11. Sahibzada, M.U.K.; Sadiq, A.; Faidah, H.S.; Khurram, M.; Amin, M.U.; Haseeb, A.; Kakar, M. Berberine nanoparticles with enhanced in vitro bioavailability: Characterization and antimicrobial activity. *Drug Des. Dev. Ther.* **2018**, *12*, 303–312. [[CrossRef](#)]
12. Behl, T.; Singh, S.; Sharma, N.; Zahoor, I.; Albarrati, A.; Albratty, M.; Meraya, A.M.; Najmi, A.; Bungau, S. Expatriating the pharmacological and nanotechnological aspects of the alkaloidal drug berberine: Current and future trends. *Molecules* **2022**, *27*, 3705. [[CrossRef](#)]
13. Guo, J.; Xia, Y.; Liu, Y.; Liu, S.; Zhang, L.; Li, B. Microscopic adsorption behaviors of ionic surfactants on lignite surface and its effect on the wettability of lignite: A simulation and experimental study. *J. Mol. Liq.* **2022**, *345*, 117851. [[CrossRef](#)]
14. Corona, R.R.B.; Sad, C.M.S.; da Silva, M.; Lopes, D.L.; Leite, J.S.D.; Viegas, G.M.D.F.; Gonçalves, G.R.; Figueiras, P.R.; de Castro, E.V.R. Adsorption of anionic surfactant in graphite oxide: A study for treatment of laundry wastewater. *J. Environ. Chem. Eng.* **2021**, *9*, 106858. [[CrossRef](#)]
15. Abu-Huwajir, R.; Al-Assaf, S.F.; Hamed, R. Recent exploration of nanoemulsions for drugs and cosmeceuticals delivery. *J. Cosmet. Dermatol.* **2022**, *21*, 3729–3740. [[CrossRef](#)]
16. Yu, F.; Miao, Y.; Wang, M.; Liu, G.; Yuan, L.; Geng, R.; Qiu, Q.; Ni, C.; Kay, M. Predicting nanoemulsion formulation and studying the synergism mechanism between surfactant and cosurfactant: A combined computational and experimental approach. *Int. J. Pharm.* **2022**, *615*, 121473. [[CrossRef](#)]
17. van Oss, C.J.; Constanzo, P.M. Adhesion of anionic surfactants to polymer surfaces and low-energy materials. *J. Adhes. Sci. Technol.* **1992**, *4*, 477–487. [[CrossRef](#)]
18. van Oss, C.J. *Interfacial Forces in Aqueous Media*; Marcel Dekker: New York, NY, USA, 1994.
19. van Oss, C.J.; Good, R.J. Surface tension and the solubility of polymers and biopolymers: The role of polar and apolar interfacial free energies. *J. Macromol. Sci. Chem.* **1989**, *26*, 1183–1203. [[CrossRef](#)]
20. van Oss, C.J.; Chaudhury, M.K.; Good, R.J. Monopolar surfaces. *Adv. Coll. Interface Sci.* **1987**, *28*, 35–64. [[CrossRef](#)]
21. Szymczyk, K.; Lewandowski, A.; Zdziennicka, A.; Szaniawska, M.; Jańczuk, B. Behavior of Auramine O in the aqueous solution of two Kolliphors and their mixture. *Molecules* **2022**, *27*, 8493. [[CrossRef](#)] [[PubMed](#)]
22. Szaniawska, M.; Szymczyk, K.; Zdziennicka, A.; Jańczuk, B. Adsorption properties and composition of binary Kolliphor mixtures at the water-air interface at different temperatures. *Molecules* **2022**, *27*, 877. [[CrossRef](#)]
23. Markarian, S.A.; Sargsyan, H.R.; Grigoryan, G.S.; Ghazoyan, H.H.; Chaban, V.V. Dimethyl sulfoxide fosters larger micelles of docusate sodium in the mixed solutions with water. *J. Mol. Liq.* **2023**, *369*, 120960. [[CrossRef](#)]
24. Lalthlengliani, J.; Gurung, J.; Pulikkal, A.K. Solubilization of aqueous-insoluble phenothiazine drug in TX-100 micellar solution and interactions of cationic/anionic surfactants with phenothiazine–TX-100 system. *J. Mol. Liq.* **2022**, *354*, 118823. [[CrossRef](#)]
25. Adamson, W.; Gast, A.P. *Physical Chemistry of Surfaces*, 6th ed.; Wiley Interscience: New York, NY, USA, 1997.
26. Atkins, P.; de Paula, J. *Atkins' Physical Chemistry*; Eighth Edition; Oxford University Press: New York, NY, USA, 2006.
27. Rosen, J.M.; Hua, X.Y. Surface concentrations and molecular interactions in binary mixtures of surfactants. *J. Colloid Interface Sci.* **1982**, *86*, 164–172. [[CrossRef](#)]
28. Rubingh, D.N. *Solution Chemistry of Surfactants*; Mittal, K.L., Ed.; Plenum Press: New York, NY, USA, 1979; Volume 3, pp. 337–354.
29. Rosen, M.J. *Surfactants and Interfacial Phenomena*, 3rd ed.; Wiley-Interscience: New York, NY, USA, 2004; pp. 34–178.
30. Butler, J.A.V. The Thermodynamics of the Surfaces of the Solutions. *Proc. Roy. Soc. Ser. A* **1932**, *138*, 348–375.
31. Jańczuk, B.; Méndez-Sierra, J.A.; González-Martin, M.L.; Bruque, J.M.; Wójcik, W. Properties of decylammonium chloride and cesium perfluorooctanoate at interfaces and standard free energy of their adsorption. *J. Colloid Interface Sci.* **1997**, *192*, 408–414. [[CrossRef](#)] [[PubMed](#)]

32. Zdziennicka, A.; Krawczyk, J.; Szymczyk, K.; Jańczuk, B. Macroscopic and microscopic properties of some surfactants and biosurfactants. *Int. J. Mol. Sci.* **2018**, *19*, 1934. [[CrossRef](#)]
33. Groszek, A.J. Selective adsorption at graphite/hydrocarbon interfaces. *Proc. R. Soc. Lond. A Math. Phys. Sci.* **1970**, *314*, 473–478.
34. Beyer, K. Phase structures, water binding, and molecular dynamics in liquid crystalline and frozen states of the system Triton X-100-D₂O: A deuteron and carbon NMR study. *J. Colloid Interface Sci.* **1982**, *86*, 73–89. [[CrossRef](#)]
35. Desai, T.R.; Dixit, S.G. Interaction and viscous properties of aqueous solutions of mixed cationic and nonionic surfactants. *J. Colloid Interface Sci.* **1996**, *177*, 471–477. [[CrossRef](#)]
36. Zdziennicka, A.; Szymczyk, K.; Krawczyk, J.; Jańczuk, B. Some remarks on the solid surface tension determination from contact angle measurements. *Appl. Surf. Sci.* **2017**, *405*, 88–101. [[CrossRef](#)]
37. Szymczyk, K.; Zdziennicka, A.; Jańczuk, B. Properties of some nonionic fluorocarbon surfactants and their mixtures with hydrocarbon ones. *Adv. Colloid Interface Sci.* **2021**, *292*, 102421. [[CrossRef](#)]
38. Bhadra, P.; Siu, S.W.I. Effect of concentration, chain length, hydrophobicity, and an external electric field on the growth of mixed alkanethiol self-assembled monolayers: A Molecular dynamics study. *Langmuir* **2021**, *37*, 1913–1924. [[CrossRef](#)]
39. Hubbe, M.A.; McLean, D.S.; Stack, K.R.; Lu, X.; Strand, A.; Sundberg, A. Self-assembly of alkyl chains of fatty acids in papermaking systems: A review of related pitch issues, hydrophobic sizing, and pH effects. *BioResources* **2020**, *15*, 4591–4635. [[CrossRef](#)]
40. Kloubek, J. Orientation of aliphatic hydrocarbons at the liquid-air interface. *Colloids Surfaces* **1990**, *48*, 323–335. [[CrossRef](#)]
41. Fowkes, F.M. Attractive forces at interfaces. *Ind. Eng. Chem.* **1964**, *56*, 40–52. [[CrossRef](#)]
42. Zdziennicka, A.; Szymczyk, K.; Krawczyk, J.; Jańczuk, B. Critical micelle concentration of some surfactants and thermodynamic parameters of their micellization. *Fluid Phase Equilibria* **2012**, *322–323*, 126–134. [[CrossRef](#)]
43. De Boer, J.H. *The Dynamic Character of Adsorption*; Oxford University: Oxford, UK, 1953.
44. Rathod, K.; Ahmed, H.; Gomte, S.S.; Chougule, S.; Prabakaran, A.; Dethé, M.R.; Patel, R.J.; Bharadwaj, D.; Alexander, A. Exploring the potential of anti-inflammatory activity of berberine chloride-loaded mesoporous silica nanoparticles in carrageenan-induced rat paw edema model. *J. Solid State Chem.* **2023**, *317*, 123639. [[CrossRef](#)]
45. Sailor, G.U.; Ramani, V.D.; Shah, N.; Parmar, G.R.; Gohil, D.; Balaram, R.; Seth, A. Design Of Experiment Approach Based Formulation Optimization Of Berberine Loaded Solid Lipid Nanoparticle For Antihyperlipidemic Activity. *Indian J. Pharm. Sci.* **2021**, *83*, 204–218. [[CrossRef](#)]
46. Xiong, W.; Sang, W.; Linghu, K.G.; Cheang, W.S.; Li, J.; Hu, Y.J.; Yu, H.; Wang, Y.T. Dual-functional Brij-S20-modified nanocrystal formulation enhances the intestinal transport and oral bioavailability of berberine. *Int. J. Nanomed.* **2018**, *13*, 3781–3793. [[CrossRef](#)]
47. Zdziennicka, A.; Szymczyk, K.; Jańczuk, B.; Longwic, R.; Sander, P. Adhesion of canola and diesel oils to some parts of diesel engine in the light of surface tension components and parameters of these substrates. *Int. J. Adhes. Adhes.* **2015**, *60*, 23–30. [[CrossRef](#)]

Disclaimer/Publisher's Note: The statements, opinions and data contained in all publications are solely those of the individual author(s) and contributor(s) and not of MDPI and/or the editor(s). MDPI and/or the editor(s) disclaim responsibility for any injury to people or property resulting from any ideas, methods, instructions or products referred to in the content.

ZAŁĄCZNIK 4a

MATERIAŁ UZUPEŁNIAJĄCY [SM4]

M. Szaniawska, K. Szymczyk*, A. Zdziennicka, B. Jańczuk, Thermodynamic parameters of berberine with Kolliphor mixtures adsorption and micellization, *Molecules*, 2023, 28(7), 3115

Supplementary Material

Thermodynamic parameters of berberine with Kolliphor mixtures adsorption and micellization

Magdalena Szaniawska, Katarzyna Szymczyk*, Anna Zdziennicka and Bronisław Jańczuk

Department of Interfacial Phenomena, Institute of Chemical Sciences, Faculty of Chemistry, Maria Curie-Skłodowska University in Lublin, Maria Curie-Skłodowska Sq. 3, 20-031 Lublin, Poland

*Correspondence: Katarzyna.szymczyk@mail.umcs.pl; Tel.: +48-81-537-55-38

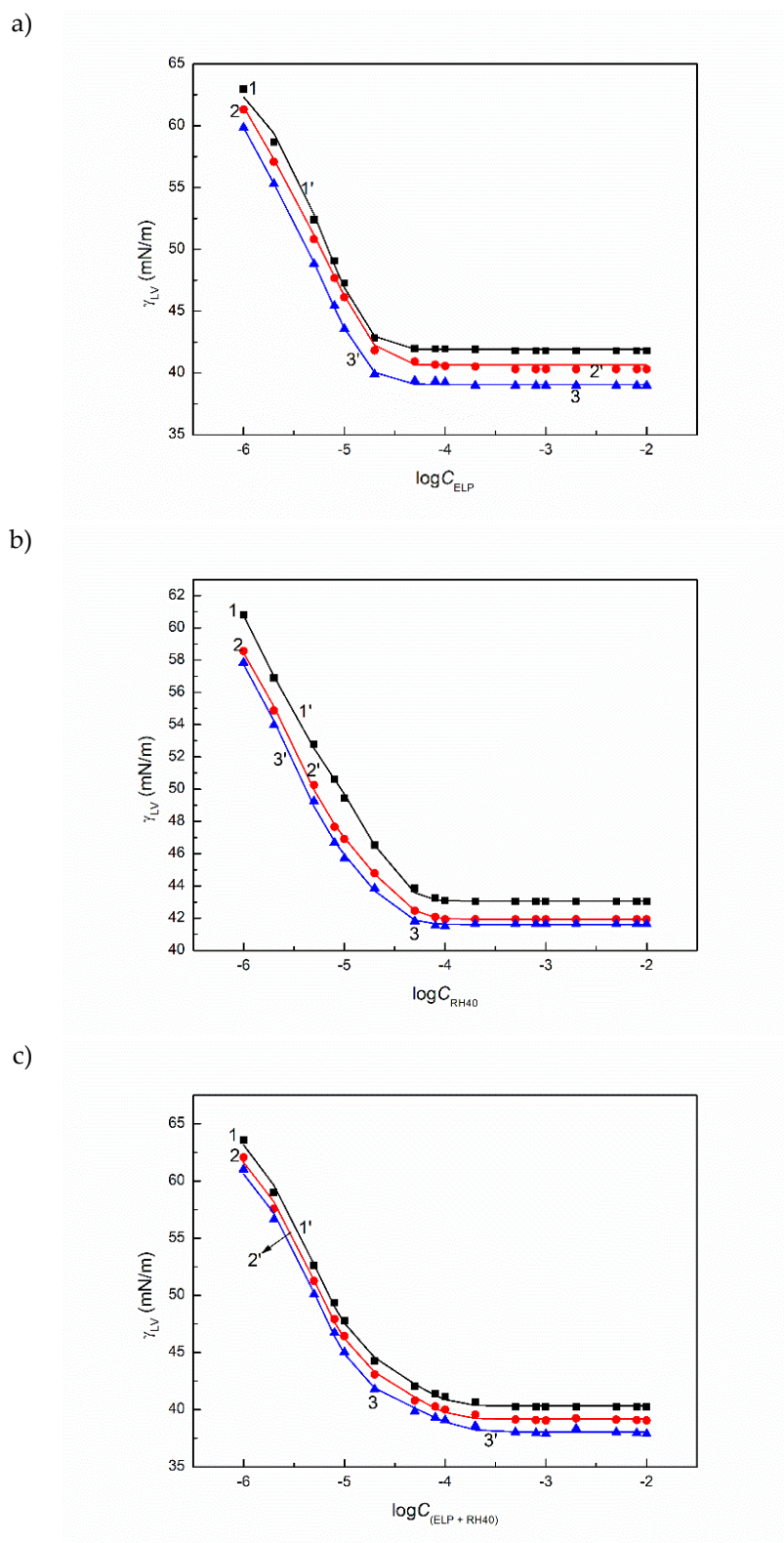


Figure S1. A plot of the surface tension (γ_{LV}) of M1 (a), M2 (b) and M3 (c) aqueous solutions vs. the logarithm of ELP ($\log C_{ELP}$), RH40 ($\log C_{RH40}$) and that of their concentration sum ($\log(C_{ELP} + C_{RH40})$) at the constant temperature equal 293 K (points 1 and curve 1'), 303 K (points 2 and curve 2') and 313 K (point 3 and curve 3'). Points 1 – 3 correspond to the measured values, curves 1', 2' and 3' to the values calculated from Eq. (35).

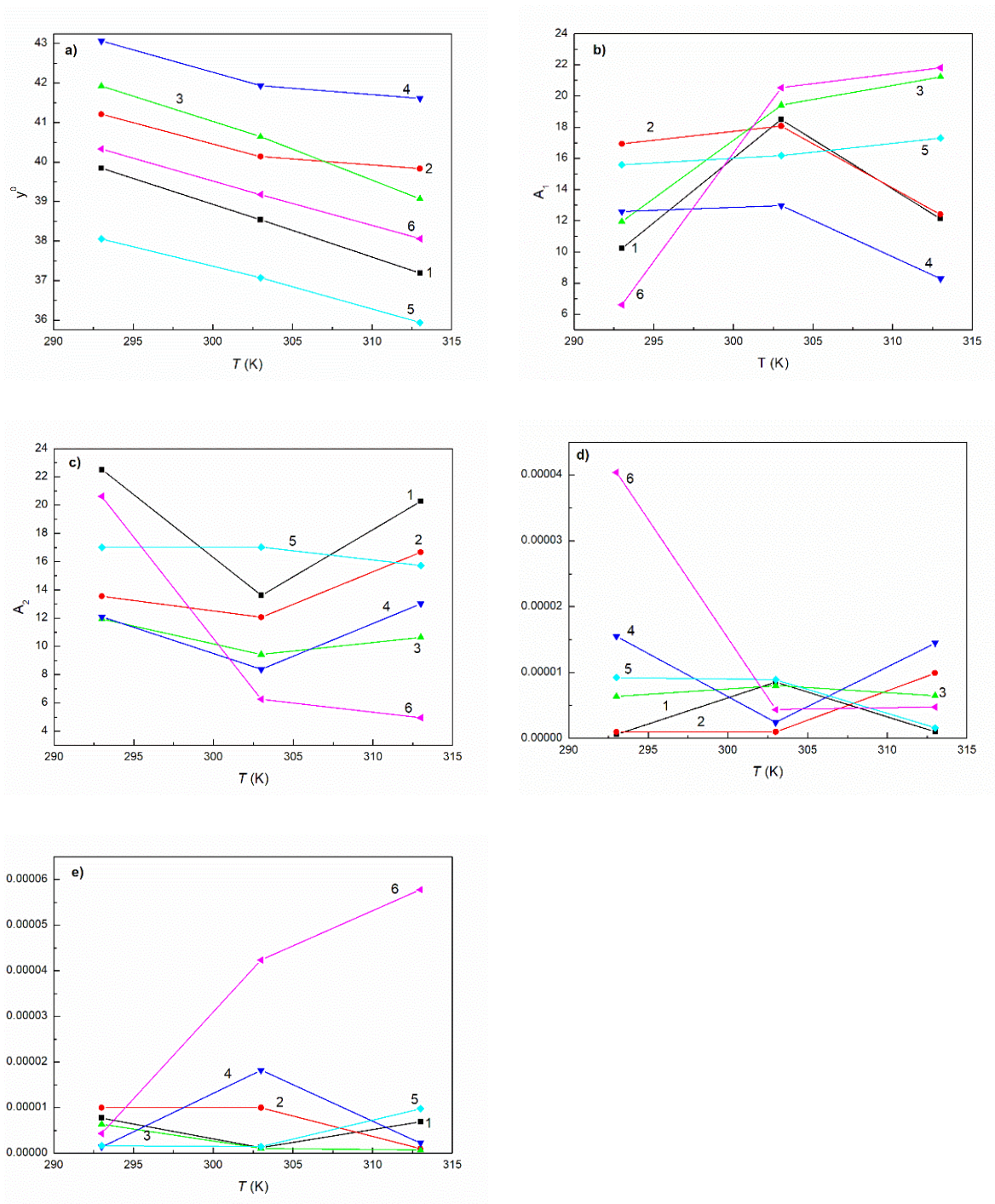


Figure S2. A plot of the constant y^0 (a), A_1 (b), A_2 (c), t_1 (d) and t_2 (e) in Eq. (35) vs. the temperature (T). Curves 1 – 6 correspond to the aqueous solutions of ELP, RH40, M1, M2, binary mixture of ELP and RH40 at the mole fraction of ELP in the bulk phase equal to 0.8 [22] and M3 mixtures, respectively.

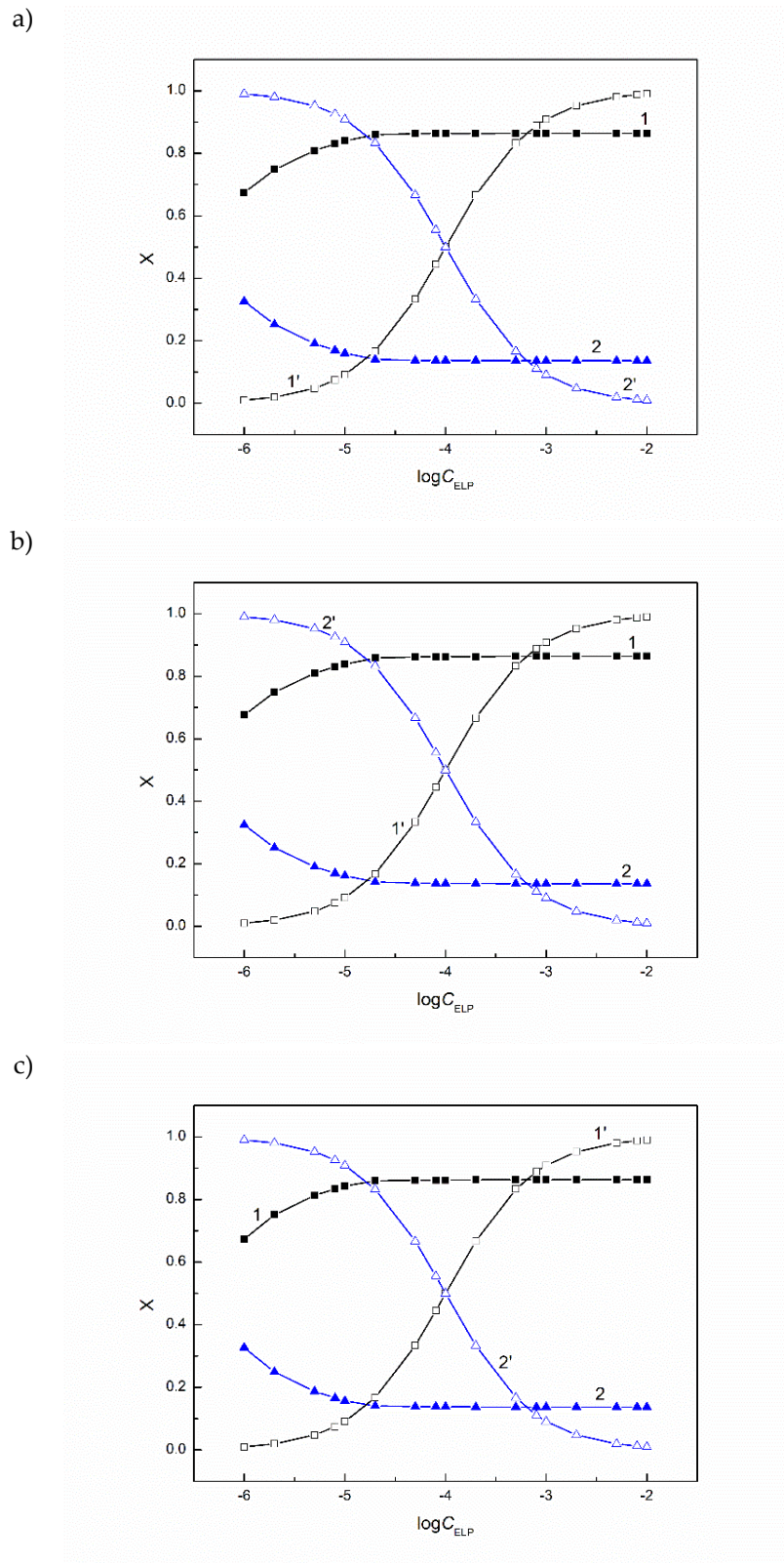


Figure S3. A plot of the mole fraction of ELP and Ber in M1 in the surface layer (curves 1 and 2) and in the bulk phase (curves 1' and 2') vs. the logarithm of ELP concentration ($\log C_{ELP}$) at the constant temperature equal 293 K (a), 303 K (b) and 313 K (c). Curves 1 and 1' correspond to ELP, curves 2 and 2' correspond to Ber.

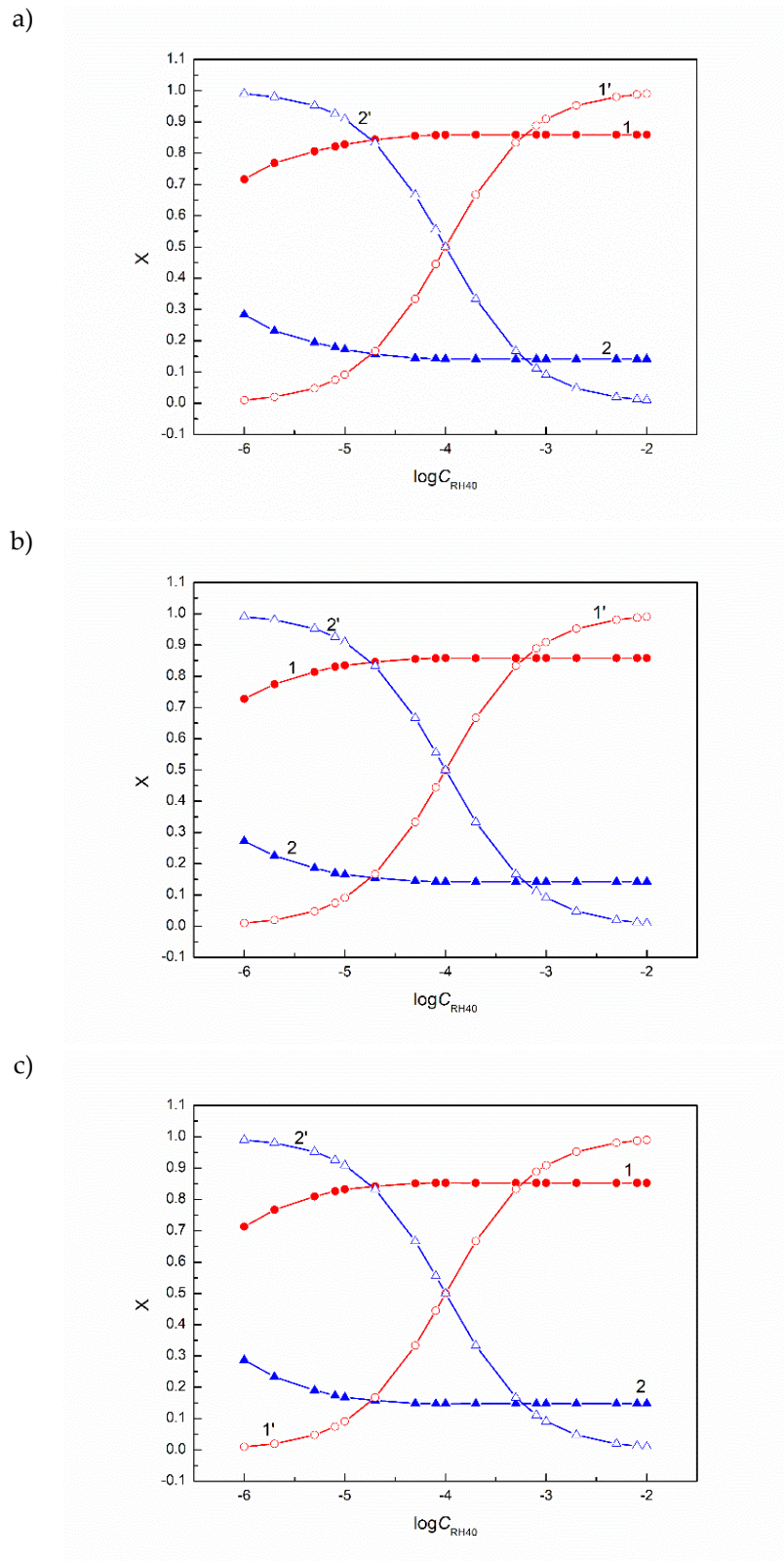


Figure S4. A plot of the mole fraction of RH40 and Ber in M2 in the surface layer (curves 1 and 2) and in the bulk phase (curves 1' and 2') vs. the logarithm of RH40 concentration ($\log C_{RH40}$) at the constant temperature equal 293 K (a), 303 K (b) and 313 K (c). Curves 1 and 1' correspond to RH40, curves 2 and 2' correspond to Ber.

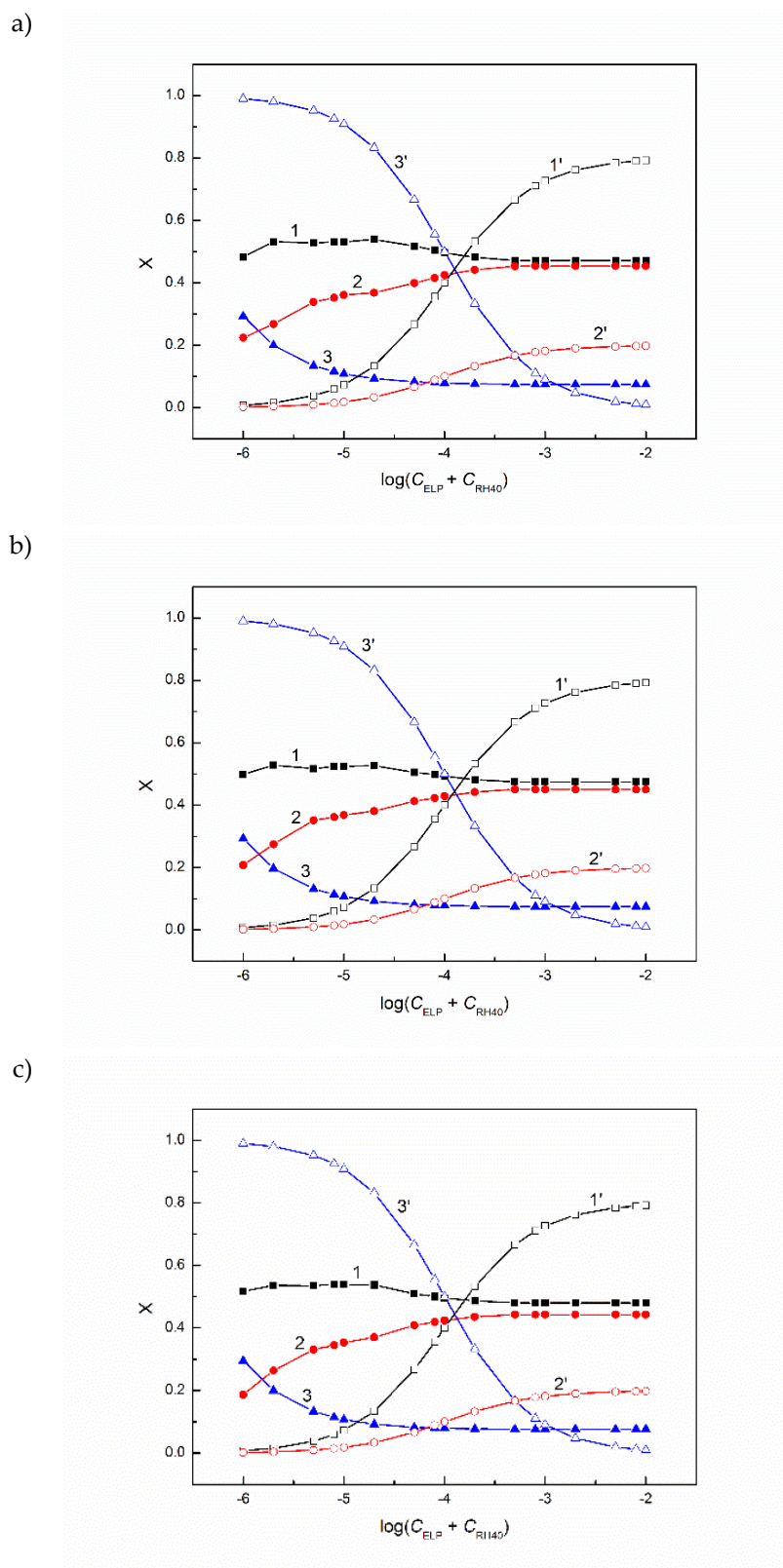


Figure S5. A plot of the mole fraction of ELP, RH40 and Ber in M3 in the surface layer (curves 1 -3) and in the bulk phase (curves 1 – 3') vs. the logarithm of the sum of ELP and RH40 concentration $\log(C_{\text{ELP}} + C_{\text{RH40}})$ at the constant temperature equal 293 K (a), 303 K (b) and 313 K (c). Curves 1 and 1' correspond to ELP, curves 2 and 2' correspond to RH40 and curves 3 and 3' correspond to Ber.

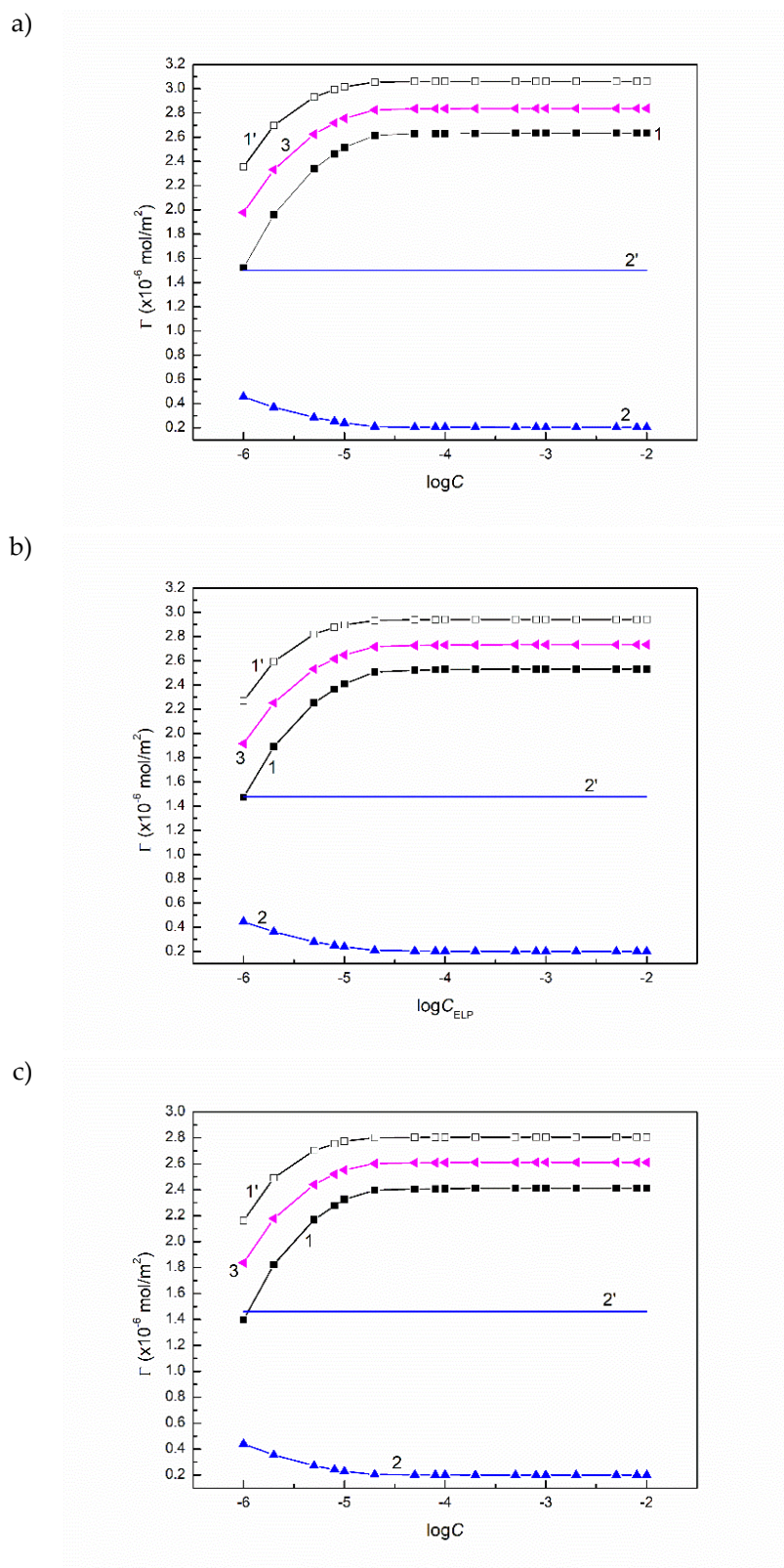


Figure S6. A plot of the surface concentration (Γ) calculated from Eq. (5) vs. the logarithm of ELP concentration ($\log C_{\text{ELP}}$) at the constant temperature equal 293 K (a), 303 K (b) and 313 K (c). Curves 1 and 2 correspond to the Γ values of ELP and Ber in M1 mixtures, curve 3 to their sum. Curves 1' and 2' correspond to the Γ values for ELP and Ber in their individual aqueous solutions.

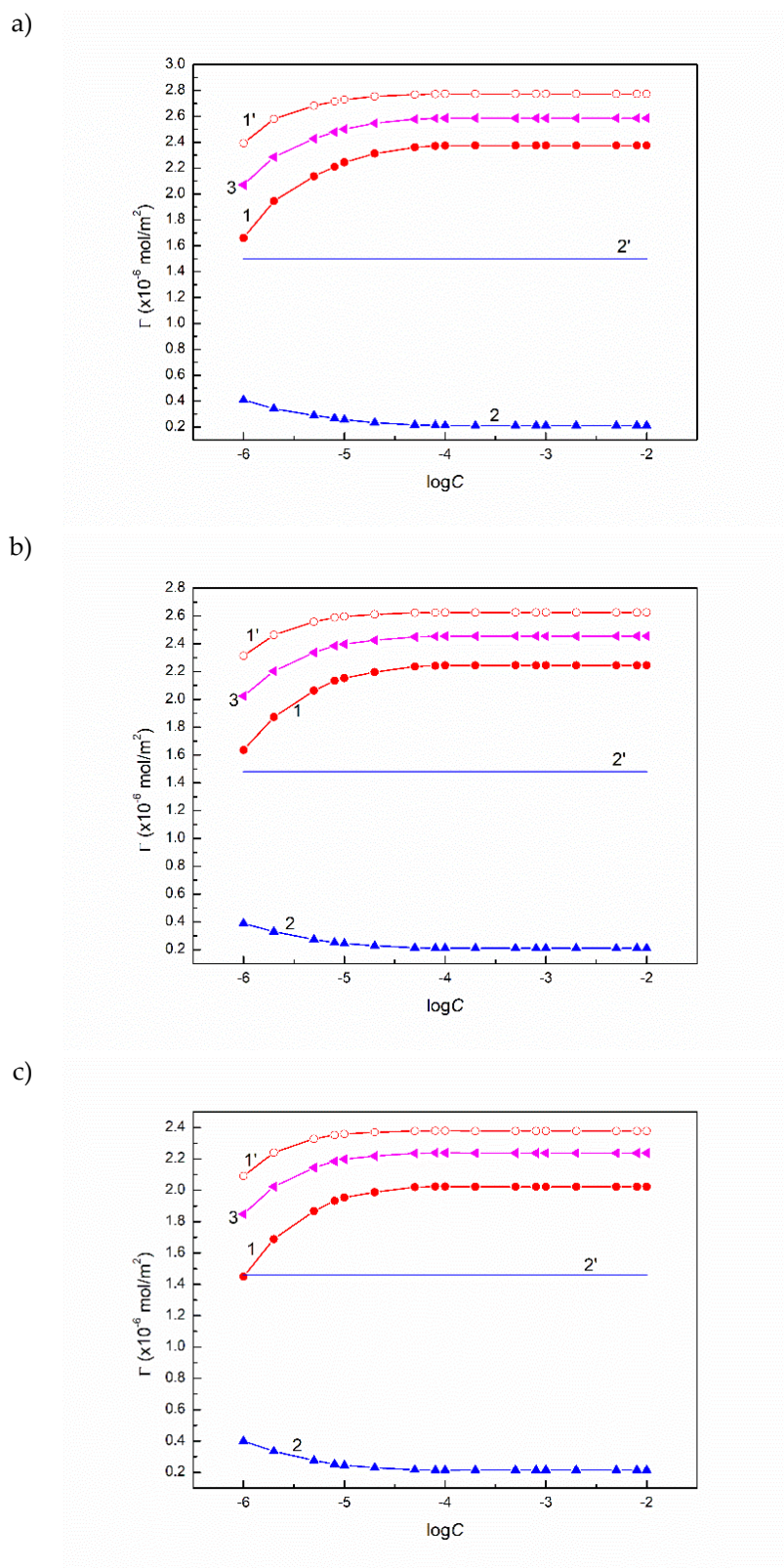


Figure S7. A plot of the surface concentration (Γ) calculated from Eq. (5) vs. the logarithm of RH40 concentration ($\log C_{\text{RH40}}$) at the constant temperature equal 293 K (a), 303 K (b) and 313 K (c). Curves 1 and 2 correspond to the Γ values of RH40 and Ber in M2 mixtures, curve 3 to their sum. Curves 1' and 2' correspond to the Γ values for RH40 and Ber in their individual aqueous solutions.

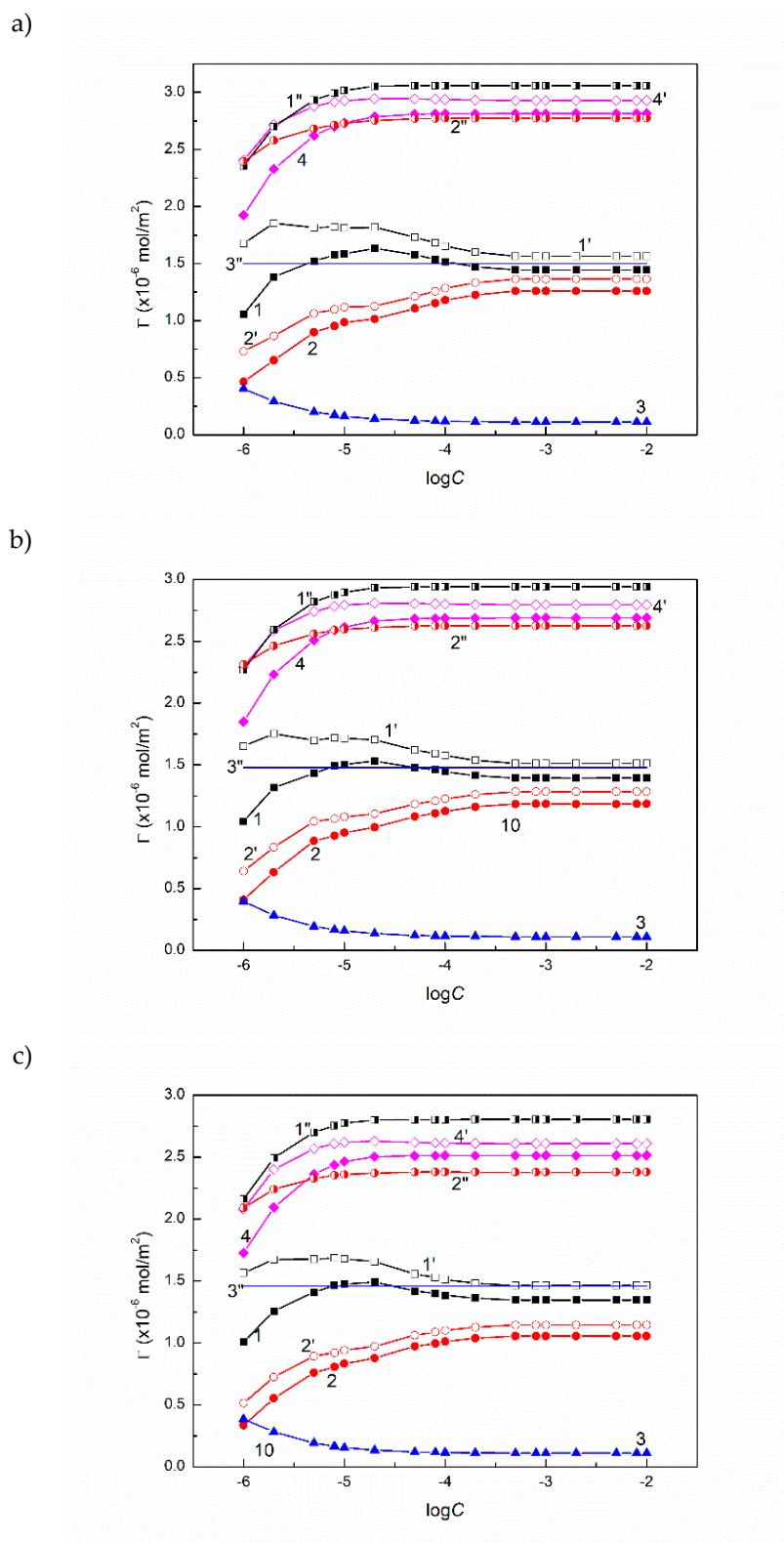


Figure S8. A plot of the surface concentration (Γ) calculated from Eq. (5) vs. the logarithm of concentration ($\log C$) at the constant temperature equal 293 K (a), 303 K (b) and 313 K (c). Curves 1 – 4 correspond to the Γ values for ELP, RH40 and Ber in M3 mixtures and their sum. Curves 1', 2' and 5 correspond to the Γ values for ELP and RH40 in the 0.8ELP + RH40 mixtures and their sum. Curves 1', 2' and 3' to the Γ values for ELP, RH40 and Ber in their individual aqueous solutions.

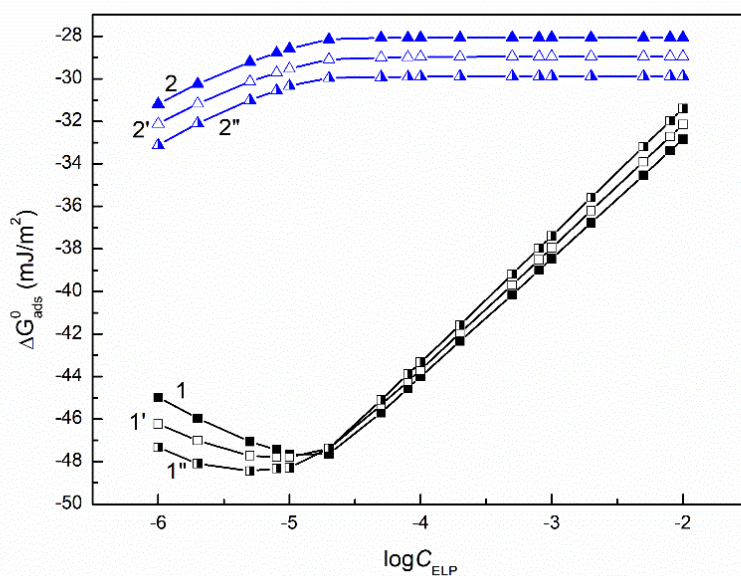


Figure S9. A plot of the Gibbs standard free energy of adsorption (ΔG_{ads}^0) calculated from Eq. (39) vs. the logarithm of ELP concentration ($\log C_{ELP}$) at the constant temperature equal 293 K (curves 1 and 2), 303 K (curves 1' and 2') and 313 K (curves 1'' and 2''). Curves 1, 1' and 1'' correspond to ELP, curves 2, 2' and 2'' to Ber in M1 mixtures.

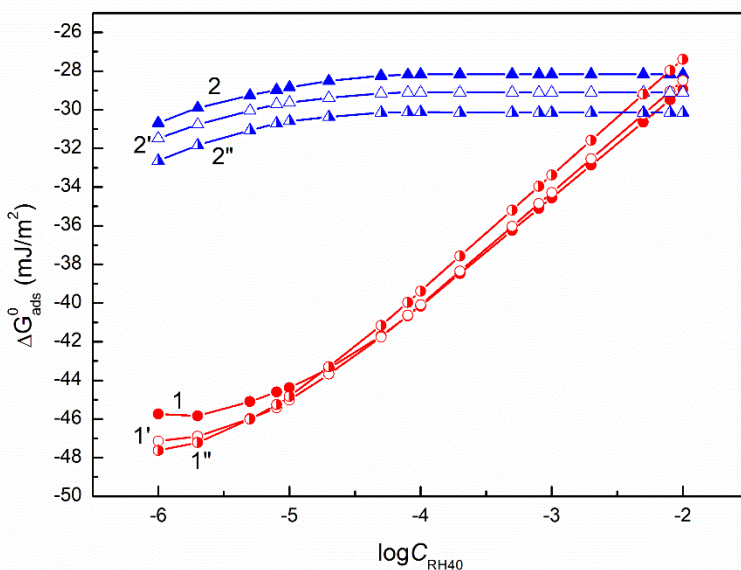


Figure S10. A plot of the Gibbs standard free energy of adsorption (ΔG_{ads}^0) calculated from Eq. (39) vs. the logarithm of RH40 concentration ($\log C_{RH40}$) at the constant temperature equal 293 K (curves 1 and 2), 303 K (curves 1' and 2') and 313 K (curves 1'' and 2''). Curves 1, 1' and 1'' correspond to RH40, curves 2, 2' and 2'' to Ber in M2 mixtures.

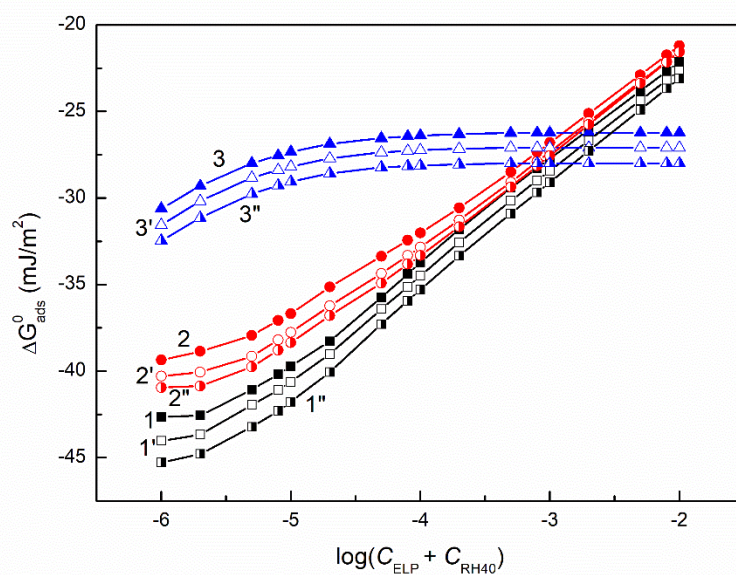


Figure S11. A plot of the Gibbs standard free energy of adsorption (ΔG_{ads}^0) calculated from Eq. (39) vs. the logarithm of the sum of ELP and RH40 concentration ($\log(C_{ELP} + C_{RH40})$) at the constant temperature equal 293 K (curves 1 – 3), 303 K (curves 1', 2' and 3') and 313 K (curves 1'', 2'' and 3''). Curves 1, 1' and 1'' correspond to ELP, curves 2, 2' and 2'' to RH40 and curves 3, 3' and 3'' to Ber in M3 mixtures.

ZAŁĄCZNIK 5

OŚWIADCZENIA AUTORÓW

dr hab. Katarzyna Szymczyk, prof. UMCS
Katedra Zjawisk Międzyfazowych
Instytut Nauk Chemicznych
Wydział Chemii UMCS
pl. M. Curie-Skłodowskiej 3
20-031 Lublin

Lublin, 06.06.2023

OŚWIADCZENIE

Oświadczam, że w pracy:

K. Szymczyk, M. Szaniawska, K. Terpiłowski, **Determination of Acoustical Parameters of Aqueous Solution of Kolliphors Binary Mixtures Using Density, Speed of Sound, Viscosity and Surface Tension Measurements**, *Journal of Surfactants and Detergents*, 2019, 22(5), 1163–1174, mój udział polegał na opracowaniu koncepcji artykułu, koordynowaniu merytorycznym badań, napisaniu oryginalnego maszynopisu pracy, opracowaniu i edycji wersji manuskryptu uwzględniającej uwagi recenzentów oraz współredagowaniu odpowiedzi na recenzje pracy.

K. Szymczyk, M. Szaniawska, J. Krawczyk, **Temperature Effect on the Adsorption and Volumetric Properties of Aqueous Solutions of Kolliphor®ELP**, *Molecules*, 2020, 25(3), 743, mój udział polegał na opracowaniu koncepcji artykułu, koordynowaniu merytorycznym badań, napisaniu oryginalnego maszynopisu pracy, opracowaniu i edycji wersji manuskryptu uwzględniającej uwagi recenzentów, współredagowaniu odpowiedzi na recenzje pracy oraz na prowadzeniu korespondencji z czasopismem.

M. Szaniawska, K. Szymczyk, A. Zdziennicka, B. Jańczuk, **Adsorption Properties and Composition of Binary Kolliphor Mixtures at the Water-Air Interface at Different Temperatures**, *Molecules*, 2022, 27(3), 877, mój udział polegał na opracowaniu koncepcji artykułu, koordynowaniu merytorycznym badań, napisaniu oryginalnego maszynopisu pracy, opracowaniu i edycji wersji manuskryptu uwzględniającej uwagi recenzentów oraz współredagowaniu odpowiedzi na recenzje pracy, wizualizacji danych eksperymentalnych.

M. Szaniawska, K. Szymczyk, A. Zdziennicka, B. Jańczuk, **Thermodynamic Parameters of Berberine with Kolliphor Mixtures Adsorption and Micellization**, *Molecules*, 2023, 28(7), 3115, mój udział polegał na opracowaniu koncepcji artykułu, koordynowaniu merytorycznym badań, napisaniu oryginalnego maszynopisu pracy, opracowaniu i edycji wersji manuskryptu uwzględniającej uwagi recenzentów oraz współredagowaniu odpowiedzi na recenzje pracy, wizualizacji danych eksperymentalnych oraz na prowadzeniu korespondencji z czasopismem.

Katarzyna Szymczyk

prof. dr hab. Anna Zdziennicka
Katedra Zjawisk Międzyfazowych
Instytut Nauk Chemicznych
Wydział Chemii UMCS
pl. M. Curie-Skłodowskiej 3
20-031 Lublin

Lublin, 06.06.2023

OŚWIADCZENIE

Oświadczam, że w pracy:

M. Szaniawska, K. Szymczyk, A. Zdziennicka, B. Jańczuk, **Adsorption Properties and Composition of Binary Kolliphor Mixtures at the Water-Air Interface at Different Temperatures**, *Molecules*, 2022, 27(3), 877, mój udział polegał na opracowaniu koncepcji artykułu, walidacji otrzymanych wyników, analizie danych, napisaniu oryginalnego maszynopisu pracy, opracowaniu i edycji wersji manuskryptu uwzględniającej uwagi recenzentów oraz współredagowaniu odpowiedzi na recenzje pracy oraz wizualizacji danych eksperymentalnych.

M. Szaniawska, K. Szymczyk, A. Zdziennicka, B. Jańczuk, **Thermodynamic Parameters of Berberine with Kolliphor Mixtures Adsorption and Micellization**, *Molecules*, 2023, 28(7), 3115, mój udział polegał na opracowaniu koncepcji artykułu, walidacji otrzymanych wyników, analizie danych, napisaniu oryginalnego maszynopisu pracy, opracowaniu i edycji wersji manuskryptu uwzględniającej uwagi recenzentów oraz współredagowaniu odpowiedzi na recenzje pracy, wizualizacji danych eksperymentalnych oraz na nadzorowaniu prac związanych z manuskrytem.

Anne Zdziennicka

prof. dr hab. Bronisław Jańczuk
Katedra Zjawisk Międzyfazowych
Instytut Nauk Chemicznych
Wydział Chemii UMCS
pl. M. Curie-Skłodowskiej 3
20-031 Lublin

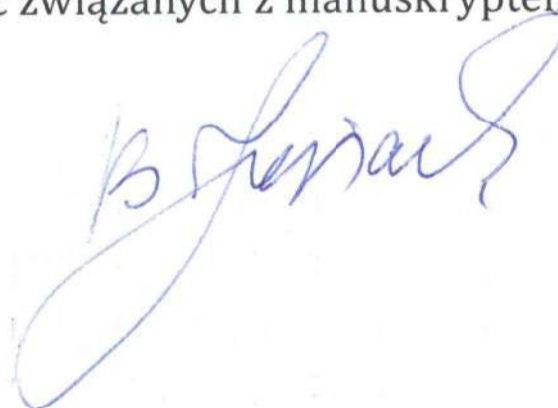
Lublin, 06.06.2023

OŚWIADCZENIE

Oświadczam, że w pracy:

M. Szaniawska, K. Szymczyk, A. Zdziennicka, B. Jańczuk, **Adsorption Properties and Composition of Binary Kolliphor Mixtures at the Water-Air Interface at Different Temperatures**, *Molecules*, 2022, 27(3), 877, mój udział polegał na opracowaniu koncepcji artykułu, walidacji otrzymanych wyników, analizie danych, napisaniu oryginalnego maszynopisu pracy, opracowaniu i edycji wersji manuskryptu uwzględniającej uwagi recenzentów oraz współredagowaniu odpowiedzi na recenzje pracy, wizualizacji danych eksperymentalnych, prowadzeniu korespondencji z czasopismem oraz na nadzorowaniu prac związanych z manuskrytem.

M. Szaniawska, K. Szymczyk, A. Zdziennicka, B. Jańczuk, **Thermodynamic Parameters of Berberine with Kolliphor Mixtures Adsorption and Micellization**, *Molecules*, 2023, 28(7), 3115, mój udział polegał na opracowaniu koncepcji artykułu, walidacji otrzymanych wyników, analizie danych, napisaniu oryginalnego maszynopisu pracy, opracowaniu i edycji wersji manuskryptu uwzględniającej uwagi recenzentów oraz współredagowaniu odpowiedzi na recenzje pracy, wizualizacji danych eksperymentalnych oraz na nadzorowaniu prac związanych z manuskrytem.



dr hab. Joanna Krawczyk
Katedra Zjawisk Międzyfazowych
Instytut Nauk Chemicznych
Wydział Chemii UMCS
pl. M. Curie-Skłodowskiej 3
20-031 Lublin

Lublin, 06.06.2023

OŚWIADCZENIE

Oświadczam, że w pracy:

K. Szymczyk, M. Szaniawska, J. Krawczyk, **Temperature Effect on the Adsorption and Volumetric Properties of Aqueous Solutions of Kolliphor®ELP**, *Molecules*, 2020, 25(3), 743, mój udział polegał na audycie oprogramowania oraz na nadzorowaniu prac związanych z manuskrypcem.

Joanna Krawczyk

dr hab. Konrad Terpiłowski, prof. UMCS
Katedra Zjawisk Międzyfazowych
Instytut Nauk Chemicznych
Wydział Chemii UMCS
pl. M. Curie-Skłodowskiej 3
20-031 Lublin

Lublin, 31.05.2023

OŚWIADCZENIE

Oświadczam, że w pracy:

K. Szymczyk, M. Szaniawska, K. Terpiłowski, **Determination of Acoustical Parameters of Aqueous Solution of Kolliphors Binary Mixtures Using Density, Speed of Sound, Viscosity and Surface Tension Measurements**, *Journal of Surfactants and Detergents*, 2019, 22(5), 1163–1174, mój udział polegał na opracowaniu koncepcji artykułu, współredagowaniu odpowiedzi na recenzje oraz korespondencji z czasopismem.

Konrad Terpiłowski